SYNTHESIS, CHARACTERIZATION AND ANTICANCER STUDIES OF MULTINUCLEAR RUTHENIUM(II) ARENE COMPLEXES BASED ON A DENDRITIC SCAFFOLD

Preshendren Govender

UNIVERSITY OF CAPE TOWN

2010

Synthesis, Characterization and Anticancer Studies of Multinuclear Ruthenium(II) Arene Complexes based on a Dendritic Scaffold

Preshendren Govender

A dissertation submitted in fulfilment of the requirements for the degree

Masters in Chemistry

University of Cape Town

Department of Chemistry

Supervisor: Dr Gregory S. Smith

August 2010

Declaration

I declare that "**Synthesis, Characterization and Anticancer Studies of Multinuclear Ruthenium(II) Arene Complexes based on a Dendritic Scaffold**" is my own work and to the best of my knowledge has never been reported or submitted for any degree or examination in any university. All sources of information used are cited, acknowledged and completely referenced at the end of each chapter.

I grant the University of Cape Town free license to reproduce the dissertation in whole or in-part for the purpose of research.

……..

Preshendren Govender

…../…../……..

Dedication

This dissertation is dedicated to my parents,
Dad and Ma, you both have given me everything to see me through this milestone in my life. Without your constant support and unconditional love it would not have been possible.

Acknowledgements

I would like to express my deepest appreciation and sincere gratitude to the following people, without whom this dissertation would not have been possible:

My supervisor Dr Gregory Smith, for his patience, guidance and constant encouragement throughout the project and a warm thank you to my co-supervisor Prof John Moss, who will always be remembered. I will also like to thank Mrs Deirdre Brooks for her constant administrative and academic support

The Swiss collaborators, Dr Bruno Therrien (University of Néuchatel) for the X-ray crystallography analysis and Prof Paul Dyson (Ecole Polytechnique Fédérale de Lausanne) for the *in vitro* anticancer testing and DNA binding experiments. The Japanese collaborators (Tokyo Institute of Technology), Prof Kohtaro Osakada and Prof Makoto Tanabe, for the MALDI-TOF experiments.

The analytical staff at the University of Cape Town, Mr Noel Hendricks and Mr Pete Roberts for running the spectroscopic data. Mr Gianpierro Benincasa for recording the elemental analysis data.

For financial support the Department of Chemistry: EDP Scholarship, NRF and UCT.

A heartfelt thank you to Prof Raymond Haines, Dr Subelia Botha, Dr David Khanye, Banothile and Prinessa for proof reading my dissertation. For the invaluable advice and encouragement, my colleagues, Tameryn, Tawfeeq and the Synthetic Organometallic and Bioorganometallic Research Group.

The European gentlemen, Johan and Michael, of whom I will always remember. My brothers from the Northern suburbs, Nick and Steven, of whom have listened and advised me throughout the difficult times, thank you boys.

And finally, to my family, Dad, Ma, Kirshia and Anja, I thank you for your unconditional support through out my academic career.

Table of Contents

Publications

Journal Article:

Published in *Journal of Organometallic Chemistry*,

P. Govender, N. C. Antonels, J. Mattsson, A. K. Renfrew, P. J. Dyson, J. R. Moss, B. Therrien and G. S. Smith, *Anticancer activity of multinuclear arene ruthenium complexes coordinated to dendritic polypyridyl scaffolds*, *J. Organomet. Chem.*, 2009, **694**, 3470.

Journal Article:

Published in *Dalton Transactions*,

P. Govender, A. K. Renfrew, C. M. Clavel, P. J. Dyson, B. Therrien and G. S. Smith, *Antiproliferative activity of chelating N,O- and N,N- ruthenium-arene functionalized poly(propyleneimine) dendrimer scaffolds, Dalton Trans.,* DOI:10.1039/C0DT00761G.

Conference Contributions

July 2009 - Poster Presentation:

Anticancer Activity of Multinuclear Arene Ruthenium Complexes Coordinated to Dendritic Polypyridyl Scaffolds, presented at **FIGIPAS 2009** - "FIGIPAS, 10th Meeting in Inorganic Chemistry" Palermo, Italy.

September 2009 - Poster Presentation:

Synthesis and Anticancer Activities of Multinuclear PGM Complexes Coordinated to Dendritic Polypyridyl Scaffolds, presented at **INORG 2009** - "South African Chemical Institute (SACI), primarily focusing on Inorganic Chemistry" Bloemfontein, South Africa.

November 2010 - Oral Presentation:

Synthesis, Characterization and Anticancer Studies of Multinuclear Ruthenium(II) Arene Complexes based on a Dendritic Scaffold, presented at **Young SACI 2010** - "SACI Student Symposium 25th November 2010" Rondebosch, South Africa.

Abstract

A series of monodentate (*N*-) and chelating bidentate (*N,N*-, *N,O*-), monomeric and dendritic ligands based on a poly(propyleneimine) dendrimer scaffold were synthesized via Schiff base condensation reactions of the relevant amine and appropriate aldehydes. These reactions yielded air- and moisture-stable oils or solids. These ligands contained pyridyl-imine moieties and salicylaldimine moieties. These compounds were isolated in good yields and characterized using standard spectroscopic and spectrometric, analytical techniques.

The monomeric and dendritic ligands were reacted with dimeric precursors of the type $[Ru(\eta^6\text{-arene})Cl_2]_2$ generating new ruthenium(II) arene complexes, consisting of neutral monodentate (*N*-), neutral chelating bidentate (*N,O*-) and cationic chelating bidentate (*N,N*-) compounds. These ruthenium(II) arene complexes were also isolated as air- and moisture-stable solids, in moderate to good yields, and were fully characterized using NMR and IR spectroscopies, as well as by elemental analysis and mass spectrometry. The molecular structures of the mononuclear ruthenium(II) arene complexes were determined using single crystal X-ray crystallography.

The cytotoxicities of the mononuclear and dendritic ruthenium(II) arene complexes were evaluated against the *cisplatin sensitive* (A2780) and *cisplatin resistant* (A2780cisR) human ovarian cancer cells. The chelating bidentate ruthenium(II) arene metallodendrimers showed superior biological activity over the monodentate ruthenium(II) arene analogues. The octanuclear cationic ruthenium(II) hexamethylbenzene complex was found to be the most active.

DNA interactions of the two most highly cytotoxic chelating bidentate ruthenium(II) arene complexes along with their mononuclear analogues were also investigated. This study showed a clear correlation between the size of the metallodendrimer, DNA damage and cytotoxicity.

Abbreviations

^{o}	degrees
^{o}C	degrees Celsius
Å	angstrom(s)
acac	acetylacetone
ar	aromatic
br	broad
$^{13}C\{^{1}H\}$-NMR	carbon nuclear magnetic resonance
calc	calculated
CDI	1,1'-carbonyldiimidazole
COSY	correlation spectroscopy
cye	cymene
d	doublet
DAB	1,4-diaminobutane poly(propyleneimine)
dapta	3,7-diacetyl-1,3,5-triaza-5-phosphabicyclo[3.3.1]nonane
DCM	dichloromethane
dendr	dendrimer
DMSO	dimethyl sulfoxide
DNA	deoxyribonucleic acid
dpk	2,2'-dipyridyl ketone
dpp	bis(2-pyridyl)pyrazine
EA	elemental analysis
en	ethylenediamine
EPR	enhanced permeability and retention
ESI-MS	electrospray ionization - mass spectrometry
EtOH	ethanol
Et_3N	triethylamine

Et_2O	diethyl ether
FT-IR	fourier transform infrared spectroscopy
FAB-MS	fast atom bombardment - mass spectrometry
g	gram(s)
GOF	goodness-of-fit
h	hour(s)
^{1}H-NMR	proton nuclear magnetic resonance
HMB	hexamethylbenzene
HMBC	heteronuclear multiple bond correlation
HPLC	high performance liquid chromatography
HSQC	heteronuclear single quantum correlation
Hz	hertz
IC_{50}	50 % inhibitory concentration
IR	infrared
J	coupling constant
μM	micromolar
m	multiplet (NMR); medium intensity (IR)
mal	3-oxy-2-methyl-4-pyrone
MALDI-TOF	matrix-assisted desorption/ionization - time of flight
Me	methyl
MeOH	methanol
MHz	megahertz
min	minute(s)
mL	millilitre(s)
mol	mole(s)
mmol	millimole(s)
MP	melting point

MS	mass spectrometry
m/z	mass to charge ratio
NMR	nuclear magnetic resonance
NOESY	nuclear overhauser effect spectroscopy
OC	open circular
ORTEP	Oak Ridge Thermal Ellipsoid Plot
p	para
PAMAM	poly(amidoamine)
PPh_3	triphenylphosphine
ppm	parts per million
Pr^i	isopropyl
pta	1,3,5-triaza-7-phosphaadamantane
pyr	pyridine
q	quartet
qn	quintet
RAPTA	ruthenium-arene PTA
RT	room temperature
s	singlet(NMR); strong intensity (IR)
SC	supercoiled
SEC	size exclusion chromatography
sep	septet
t	triplet
THF	tetrahydrofuran
w	weak intensity (IR)
WHO	World Health Organization

Chapter 1

Review of Ruthenium(II) Arene Multinuclear Dendritic Compounds, and their Applications in Medicinal Chemistry

1.1 Background

Cancer is a type of disease where cells within the body undergo cell division beyond the normal limits, invading adjacent tissues, and sometimes spreading to other locations of the body *via* blood or lymph.[1] These three malignant properties of cancers differentiate them from benign tumors, which are self-limited, and do not invade or metastasize.

Metastases takes place in many ways: through the lymphatic system, through the bloodstream, by spreading through spaces within the body, such as the bronchi or abdominal cavity, or through implantation. The most common way for cancer to spread is through the lymphatic system. The lymph system has its own channels that circulate throughout the body. These channels are very small and carry a tissue fluid called lymph throughout the body, an ideal pathway for the spread and growth of cancer.[1]

Most cancers form a tumor but some, like leukemia, do not. The branch of medicine concerned with the study, diagnosis, treatment, and prevention of cancer is oncology.

Cancer is one of the leading causes of death world wide, responsible for about 13 % of all human deaths in 2004.[2] According to the American Cancer Society, 7.6 million people died from cancer in the world during 2007.[3] The main types of cancer leading to overall cancer mortality each year are:

- lung (1.3 million deaths per year)
- stomach (803 000 deaths per year)
- colorectal (639 000 deaths per year)
- liver (610 000 deaths per year)
- breast (519 000 deaths per year)

The WHO (World Health Organization) has also reported that by 2030, deaths related to cancer may rise to 12 million per year.[2] Cancer may affect people of all ages, even foetuses, but the risk for most varieties increases with age (Fig. 1.1).[4]

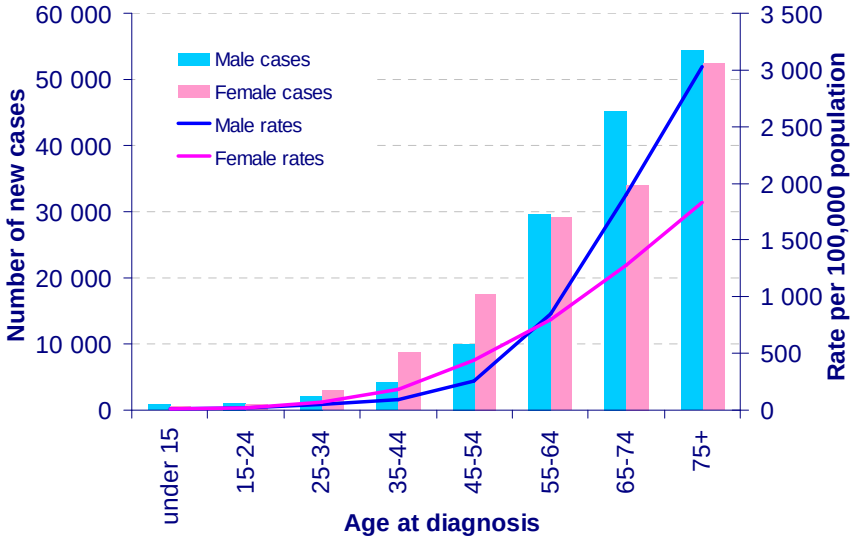

***Figure 1.1**: Number of new cases and rates, by age and sex, all malignant neoplasms, United Kingdom, 2006.[4]*

The increase in survival rates is due to better cancer treatment, thanks to the introduction of efficient anticancer drugs. Cancer treatment aims to cure, prolong and improve the quality of life for patients. Some of the most common cancer types, such as breast cancer, cervical cancer and colorectal cancer, have high cure rates when detected early and treated according to best practice. Currently, principal treatment methods are surgery, radiotherapy and chemotherapy. Fundamental for adequate treatment is an accurate diagnosis through imaging technology (ultrasound, endoscopy or radiography) and laboratory (pathology) investigations.[2]

1.2 Platinum based anticancer drugs

Reports on the earliest therapeutic use of metals or metal-containing drugs in cancer treatment were first reported in the 16th century. Hundreds of years of experience with inorganic anticancer agents was nearly forgotten until the mid to late 1960's, when the anticancer properties of *cis*-$[PtCl_2(NH_3)_2]$ (*cis*-diamminedichloro-

platinum(II)) was discovered by Barnett Rosenberg.[5] The various activities of metal ions in biology have stimulated the development of metal-based therapeutics, and thus the field of metal-based compounds in medicine has become very appealing to inorganic chemistry researchers.[6-8]

Metal complexes that fragment when introduced into the cell and retain their carrier ligands are important, as these non-leaving ligands can mediate the interaction with the target molecule (i.e. DNA) and provide selectivity and/or controlled activity. Examples of such complexes are the platinum(II) anticancer compounds (Fig. 1.2), which lose anionic ligands and form coordinate bonds with their targets.[9]

cis-$[PtCl_2(NH_3)_2]$ (Fig. 1.2) was first synthesized by Michele Peyrone in 1844 and was known as Peyrone's chloride. More than a century later it became the first metal-containing anticancer drug. Cisplatin is one of the leading metal-based drugs, used in treatment of a variety of cancers,[10] in particular, testicular[11,12] and ovarian cancers.[13,14] It is especially effective against squamous cell carcinoma and small cell lung carcinoma.[15]

Analogues of cisplatin, carboplatin and oxaliplatin (Fig. 1.2), have shown effectiveness as other second-generation chemotherapeutic agents for cancer.[15]

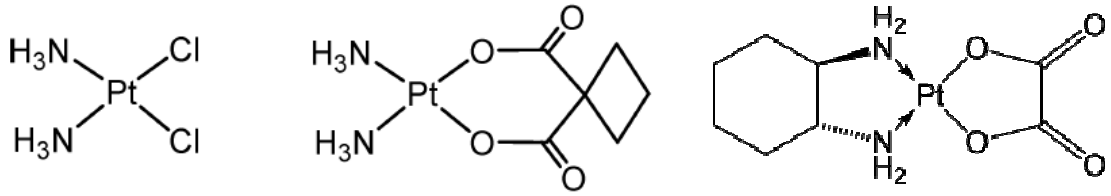

cisplatin carboplatin oxaliplatin

Figure 1.2: *Selected platinum compounds that are currently in clinical use.*

More recently, Farrell's group have had successes in synthesizing multiplatinum drugs.[16] The platinum-based trinuclear complex [*trans*, *trans*, *trans*-$(NH_3)_2Pt(Cl)NH_2(CH_2)_6NH_2Pt(NH_3)_2NH_2(CH_2)_6NH_2Pt$-$(NH_3)_2(Cl)][NO_3]_4$ (BBR3464) showed to have higher *in vitro* cytotoxicity than its mononuclear analogue and cisplatin, and has been claimed to be the first platinum based compound with a DNA binding mode different to that of cisplatin.[16,17] Though phase II trials of BBR3464

were not pursued further,[17] the concept of multinuclearity assisting in the improvement of the potency of potential anticancer drugs was established.

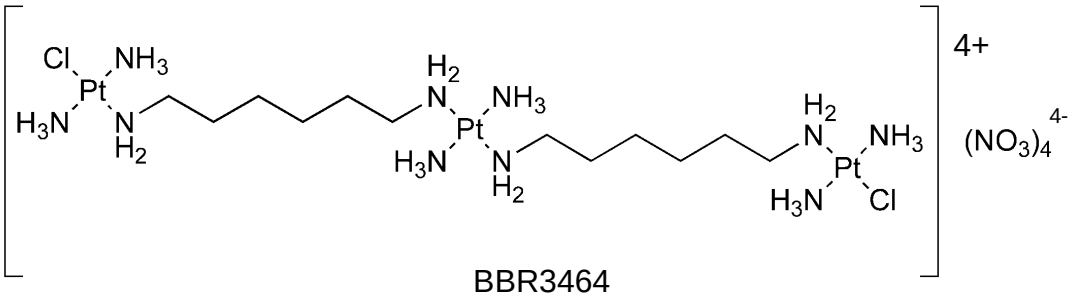

BBR3464

Figure 1.3: *An example of Farrell's multinuclear cationic trans-platinum(II) compound, BBR3464.*[17]

The clinical successes of cisplatin therapy are limited by severe toxic side effects and drug resistance, in particular nausea and vomiting, neuropathy, ototoxicity and nephrotoxicity.[18,19] To overcome limitations associated with platinum-based drugs, researchers have focused their attentions on compounds containing other metals.[20-22]

1.3 Ruthenium(III) compounds in cancer therapy

Ruthenium metal has proved to possess favourable properties, thus having the ability to replace platinum and form the basis for anticancer drug design.[15] Ruthenium is less toxic than platinum and its activity as an anticancer agent may reside in its ability to mimic the behaviour of iron, and bind to several biomolecules, such as human serum albumin and transferrin.[24] A variety of ruthenium complexes with 2+ or 3+ oxidation states have shown activity against metastatic cancers.[25,26] Two ruthenium(III) complexes, NAMI-A (imidazolium [*trans*-tetrachloro(dimethylsulfoxide)-imidazoleruthenate(III)])[27] and KP1019 (indazolium [*trans*-tetrachlorobis (1H-indazole)ruthenate(III)])[28,29] (Fig. 1.4) have successfully completed phase I clinical trials and are currently undergoing phase II clinical trials.[30]

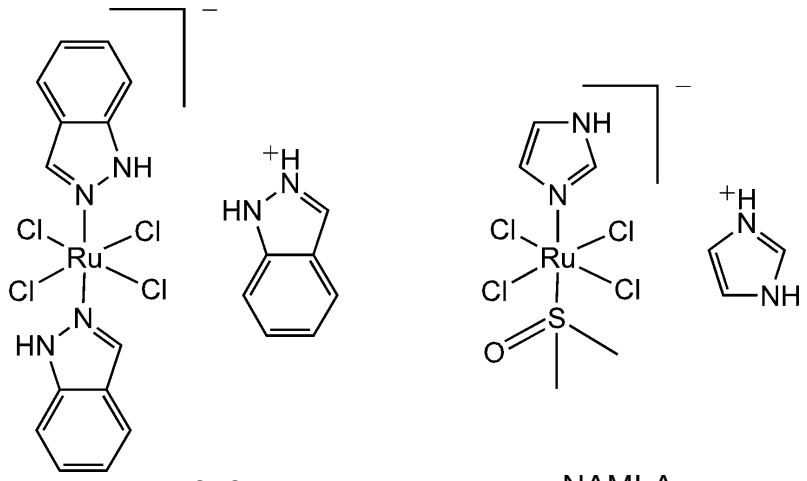

Figure 1.4: *Ruthenium(III) drugs which have completed phase I clinical trials, KP1019 and NAMI-A.*[30]

NAMI-A was the first ruthenium anticancer agent to undergo clinical trials. The drug was developed by Sava *et al*. and is a negatively charged complex containing an octahedral ruthenium(III) centre bound to a single imidazole ligand, with a *trans* positioned dimethyl sulfoxide (DMSO) ligand and four chloride ligands.[31] They showed that the drug was not very active against cancer cell lines, which is usually the initial screen for potential activity as antitumor agents. However, the drug showed enhanced activity against metastases and appears to inhibit cancer growth as a result of a delayed process of metastasis, but has little impact on primary tumours in animal models.[32,33]

KP1019 was the second ruthenium anticancer agent to undergo clinical trials. The drug was synthesized by the Keppler group in 1989.[28] Both cisplatin and KP1019 are administered intravenously and therefore, proteins are the first binding partners in the blood stream. It is thought that the binding of platinum complexes to serum proteins leads to the side effects, while KP1019 binds to transferrin, and seems to be an important step in the mode of action.[34] Despite the similarities between NAMI-A and KP1019, the drug was found to be a cytotoxin, active against primary tumours and being investigated for activity against colorectal cancers.

In recent years interest has shifted from ruthenium(III) compounds to ruthenium(II) complexes, in particular ruthenium(II) arene anticancer agents, some of which show

antimetastatic activity similar to that of NAMI-A. It has been suggested that ruthenium(III) complexes are 'activated' by undergoing reduction *in vivo* to ruthenium(II), which coordinates more rapidly to biomolecules.[25,26] There is a lower oxygen content and more acidic pH within tumours than in normal tissue and so the production of ruthenium(II) relative to ruthenium(III) should be favoured in tumours.[25]

1.4 Ruthenium(II) anticancer complexes

The majority of ruthenium compounds which have been evaluated for anticancer activity are coordination compounds with the ruthenium in the 3+ oxidation state. It has been proposed that in this oxidation state ruthenium is less biologically active and is reduced *in vivo* to more biologically active ruthenium(II) complexes, a process less favoured in the hypoxic environment of a tumour.[35] However, it should be noted that ruthenium(II) compounds exhibit a low general toxicity and since cancer cells can also become oxidized at certain stages of their growth cycle, oxidation of the ruthenium cannot be excluded.[36]

1.4.1 Ruthenium(II) arenes: An alternative to classic ruthenium anticancer agents

Similar to ruthenium(III) complexes, organometallic ruthenium(II) arene complexes of the type [(η^6-arene)Ru(ZY)X] (ZY = chelating ligand and/or two monodentate ligands, X typically a halide), where ZY are nitrogen or oxygen donor ligands (*NN*-, *NO*-, *OO*-) have also been studied extensively (Scheme 1.1), as potential anticancer agents.

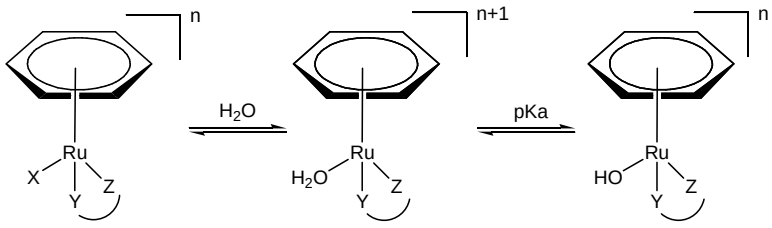

Scheme 1.1: *Aquation of a ruthenium(II) arene compound.*

These complexes all have the η^6-arene ring occupying one coordination site, and depending on the nature of the chelating ligand, the complexes can either be neutral

or cationic (isolated as salts). The presence of the η^6-arene ring stabilises and protects the metal centre, preventing rapid oxidation to ruthenium(III).[36]

The structural and electronic features of metal-arene bonding have been thoroughly reviewed.[37,38] The η^6-arene is considered as a π-acid/π-acceptor ligand towards ruthenium. Evidence comes from the ^{1}H-NMR spectrum, upon arene coordination to the ruthenium centre, the proton-resonance shifts to a lower frequency due to increased electron density.[39,40]

Generally ruthenium-arene bonds are stable towards hydrolysis although recently there have been reports that photochemical displacement of the arene can occur in aqueous solution for dinuclear complexes such as $\{(\eta^6\text{-indan})RuCl\}_2(\mu\text{-2,3-dpp})](PF_6)_2$ (where indan = arene and μ-2,3-dpp = 2,3-bis(2-pyridyl)pyrazine).[41] Arene lability can be induced by the presence of strong π-acceptor ligands bonded elsewhere in the complex.

There are presently two types of ruthenium(II) arene anticancer classes which are widely developed, one class developed by Sadler and the other by Dyson (Fig. 1.5).[42,43]

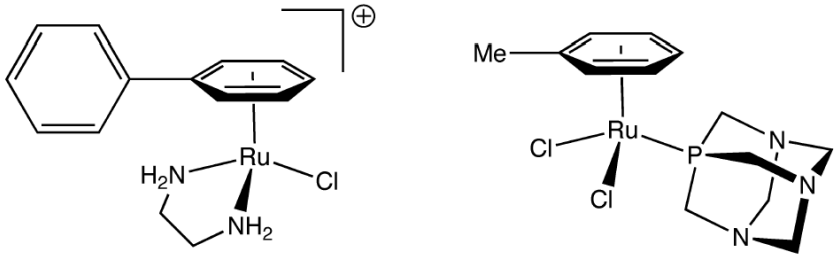

Figure 1.5: *Two classes of ruthenium(II) arene anticancer agents, ruthenium(II) agents of Sadler (left)[42] and RAPTA agents of Dyson (right).[43]*

The first class was synthesized by Sadler's group, a three-legged 'piano-stool' conformation, consisting of an aryl group coordinated to the ruthenium metal, which is coordinated to a bidentate ethylenediamine and a chloride ligand. Sadler's group showed that this type of arene ruthenium complex is as potent as cisplatin and carboplatin in primary cell lines, and was also active against some cell lines which have formed a resistance to cisplatin.[42] They also showed that by replacing the simple aryl group to more extended aryl systems (e.g. biphenyls,

tetrahydroanthracene) the anticancer activity was increased. On the other hand, changing the *N*-donor ligands to a more bulky ligand (e.g. *N, N, N', N'*-tetramethylethylenediamine) reduced the anticancer activity.[44]

The second class of ruthenium(II) arene anticancer agents was synthesized by Dyson's group. These were termed RAPTA (Ruthenium-Arene PTA) anticancer agents, similar in structure to the first class synthesized by Sadler's group, but instead the three remaining coordination sites are occupied by two chloride ligands and a mono-dentate PTA (1,3,5-triaza-7-phosphaadamantane) ligand. Similar to that of NAMI-A, these agents were found to be inactive against primary tumours, but were found to be very active *in vivo* against lung metastases in CBA mice.[45] RAPTA compounds were found to be less toxic (in mice) than NAMI-A and thus could be administrated in high doses.[43]

1.4.2 Proposed mechanism of cytotoxic action of Ru(II) arene complexes

The mechanism of action of ruthenium(II) arenes is generally thought to involve hydrolysis of the Ru-X bond resulting in an active Ru-OH_2 species (aquation), while the arene-Ru bond is robust. This species can exist over a range of pH values, but above the pH = *p*Ka value (the pH at which 50 % of the species exists as Ru-OH_2 and Ru-OH through deprotonation of the H_2O ligand) the hydroxo Ru-OH species formed by deprotonation will be predominant (Scheme 1.1). This complex is usually considered to be a less reactive species as hydroxide is a less labile ligand than water and will not be easily displaced by biomolecule targets. Thus, ideally *p*Ka values of ca. pH > 7 for aqua adducts should ensure that the active species predominates at physiological pH (7.2 - 7.4). The rate of hydrolysis is therefore important. If the complexes hydrolyze too fast, they may not reach the target site.[46]

Hydrolysis can be suppressed extracellularly due to high chloride concentration (*ca.* 0.1 M) but this becomes impossible after the complex enters the cells due to lower chloride concentrations (*ca.* 4 - 25 mM) typically found intracellularly, thus obtaining selective attraction inside the cell. The primary cellular target for ruthenium(II) arenes, as with many metal-based drugs, is thought to be DNA.[47] Therefore, factors affecting DNA binding such as rate, extent of binding and non-

covalent interactions such as hydrogen bonding and DNA intercalation become important.[46]

1.4.3 Ruthenium(II) arene anticancer complexes: Structure versus activity

One of the earliest examples of a ruthenium(II) arene complexes investigated as an anticancer drug candidate was $[(\eta^6\text{-}C_6H_6)Ru(DMSO)Cl_2]$.[48] It has been suggested by the authors that the DMSO derivative strongly inhibits topoisomerase (II) activity by cleavage complex formation *via* interaction with DNA and crosslink formation with topoisomerase (II).

Morris and co-workers synthesized a series of ruthenium(II) arene complexes with three mono-dentate ligands [(*p*-cymene)Ru(X)(Y)(Z)], where X, Y or Z = halide, acetonitrile or isonicotinamide.[49] The ruthenium(II) arene complexes proved inactive (IC_{50}, the dose which inhibits cell growth by 50 % of the cells, > 50 μM) towards the human ovarian cells (A2780) *in vitro*. The authors suggested that the complexes may be too reactive with components of the cell culture medium and/or the cells, and are deactivated by biomolecules before reaching their target sites.

To avoid this problem, the authors decided to keep the ligand constant and vary the arene ring.[50] They obtained reproducible cytotoxicity against the A2780 cell line, for chelated diamine complexes of the type $[(\eta^6\text{-arene})Ru(N,N)(X)]^+$ where *N,N*- is typically ethylenediamine, and X is chloride (Fig. 1.6).

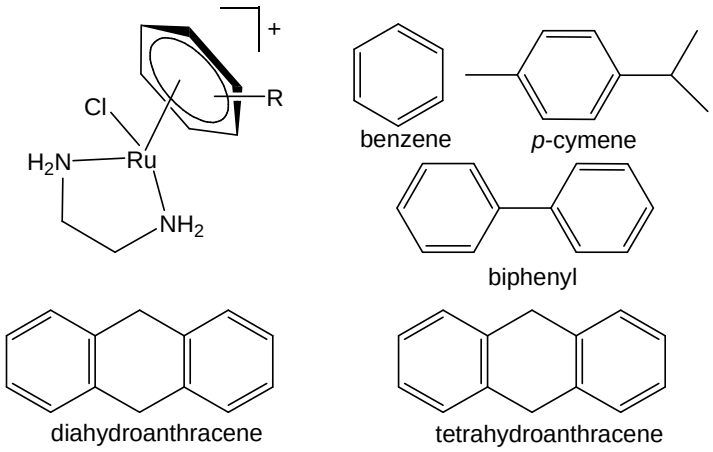

Figure 1.6: *Five $[(\eta^6\text{-arene})Ru(en)Cl]^+$ complexes (arenes shown separately) which show activity against the A2780 cell lined.[50]*

Cells were incubated with the particular ruthenium(II) arene complex for 24 hours, washed, and then cell numbers determined after growth on fresh medium for a further three days. Activity was found to increase with the size of the coordinated arene (Table 1.1): benzene < *p*-cymene < biphenyl < dihydroanthracene < tetrahydroanthracene, such that, the biphenyl complex has similar cytotoxicity to the anticancer drug carboplatin (IC_{50} = 6 μM) and while the tetrahydroanthracene complex is as active as cisplatin (IC_{50} = 0.6 μM).

Table 1.1: *IC_{50} values for ruthenium(II) arene complexes [(η^6-arene)Ru(X)(Y)(Cl)]A (A= PF_6^- for positively-charged complexes) in the A2780 cell line after 24 hour drug exposure, and comparison with carboplatin and cisplatin.*[50]

Arene/Pt complex	X	Y	IC_{50} (μM)
p-cymene	CH_3CN	CH_3CN	> 100
p-cymene	Cl	isonicotinamide	> 100
$C_6H_5CO_2CH_3$	$H_2NCH_2CH_2NH_2$		56
benzene	$H_2NCH_2CH_2NH_2$		17
p-cymene	$H_2NCH_2CH_2NH_2$		10
carboplatin	-		6
$C_6H_5C_6H_5$	$H_2NCH_2CH_2NH(Et)$		6
$C_6H_5C_6H_5$	$H_2NCH_2CH_2NH_2$		5
dihydroanthracene	$H_2NCH_2CH_2NH_2$		2
cisplatin	-		0.6
tetrahydroanthracene	$H_2NCH_2CH_2NH_2$		0.5

On the other hand, it appears that extended ligand groups, such as biphenyl and tetrahydroanthracene, improve the cytotoxicity of the drug, whilst the introduction of an electron withdrawing group at the arene moiety (such as CO_2CH_3) results in complexes with poor cytotoxicity. Compared to (*p*-cymene)RuCl(en)]PF_6 (where en = ethylenediamine) (IC_{50} = 9 μM) (Fig. 1.7), the cationic complex [(η^6-$C_6H_5CO_2CH_3$)RuCl(en)]PF_6

(IC_{50} = 55 μM) (Fig. 1.7), showed a moderate activity on the A2780 cell line, due to the presence of an electron-withdrawing group on the arene ligand, reducing the activity of the complex.[49]

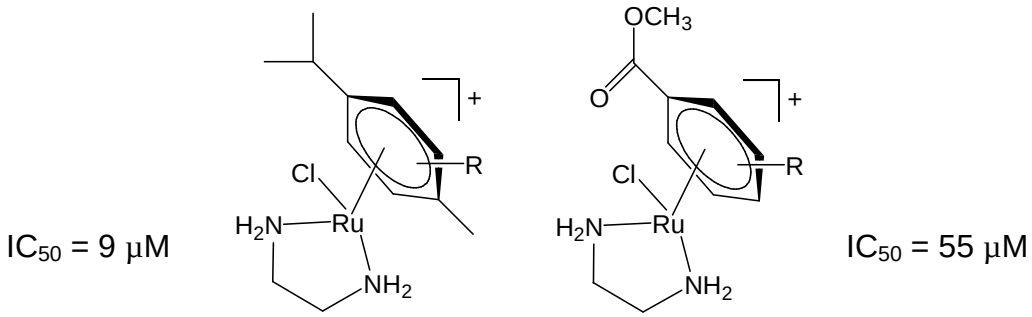

Figure 1.7: *Two ruthenium(II) arene complexes, (p-cymene)RuCl(en)]PF_6 (left) and [(η^6-$C_6H_5CO_2CH_3$)RuCl(en)]PF_6 (right), complexes of which biological activity against A2780 cells vary with particular arene moiety.*[49]

Recently, a new series of organometallic ruthenium(II) arene complexes with potential hydrogen-bonding groups attached to the pendant arm of the arene ligand have been prepared and studied for their cytotoxicity as potential anticancer agents.[51] The pta (1,3,5-triaza-7-phosphaadamantane) and dapta (3,7-diacetyl-1,3,5-triaza-5-phosphabicyclo[3.3.1]nonane) ligands were used to obtain the neutral and cationic mononuclear ruthenium(II) arene complexes shown (Fig. 1.8). The cytotoxicity of these functionalized ruthenium(II) arene complexes showed no enhancement of biological activity towards the cancer cells screened, as compared to the analogous ruthenium(II) arene complexes without hydrogen-bonding substituents, namely toluene, *p*-cymene, hexamethylbenzene.[51]

Whilst the presence of hydrogen bonding substituents can potentially hydrogen bond to DNA, in a similar manner titanocene-type drugs containing hydrogen bonding groups, showed an increase in cytotoxicity.[52] In the case of these ruthenium(II) arene complexes the effect of the hydrogen-bonding function is actually the opposite. The origin of this unexpected effect was not clearly identified.

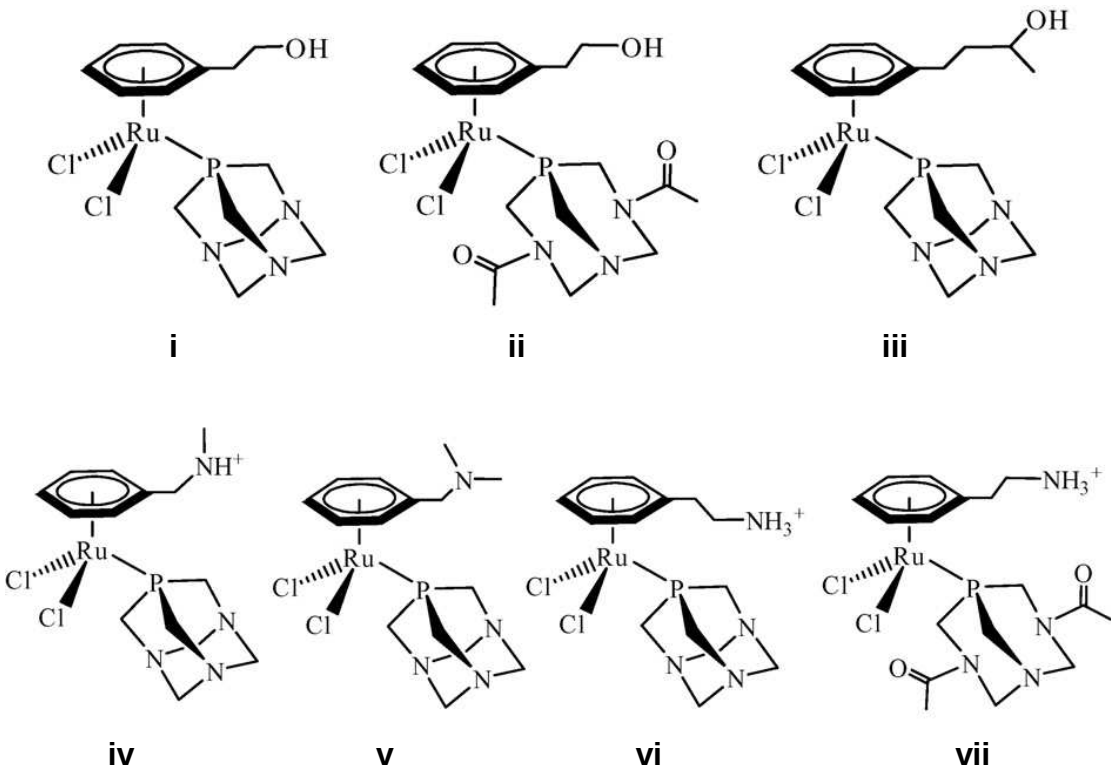

Figure 1.8: *Seven [(η^6-arene)Ru(X)Cl_2]$^+$ complexes, where X = pta or dapta, with potential hydrogen bonding groups.*[51]

Ruthenium(II) arene complexes appear to have a wide spectrum of cytotoxicity towards cancer cells. For example, the complexes [(η^6-biphenyl)Ru(en)Cl]PF_6 and [(η^6-dihydroantracene)Ru(en)Cl]PF_6 are not only active against A2780 human ovarian cancer cells, but also HT29 colon, Panc-1 pancreatic and NX02 lung cancer cells with IC_{50} values in the range 1 - 13 μM.[53]

1.4.4 Multinuclear ruthenium(II) arene complexes as anticancer agents

In contrast to multinuclear platinum complexes, analogous multinuclear organometallic ruthenium compounds have been rarely studied for their anticancer properties, with just a few examples to be found in the literature.[23,54-58]

Keppler and co-workers have reported on the development of dinuclear ruthenium arene compounds (Scheme 1.2)[59,60] with high *in vitro* anticancer activity (Table 1.2), whereas the mononuclear maltolato complex ([(η^6-*p*-cymene)Ru(mal)Cl], were mal = 3-oxy-2-methyl-4-pyrone) was found to be inactive.[61,62]

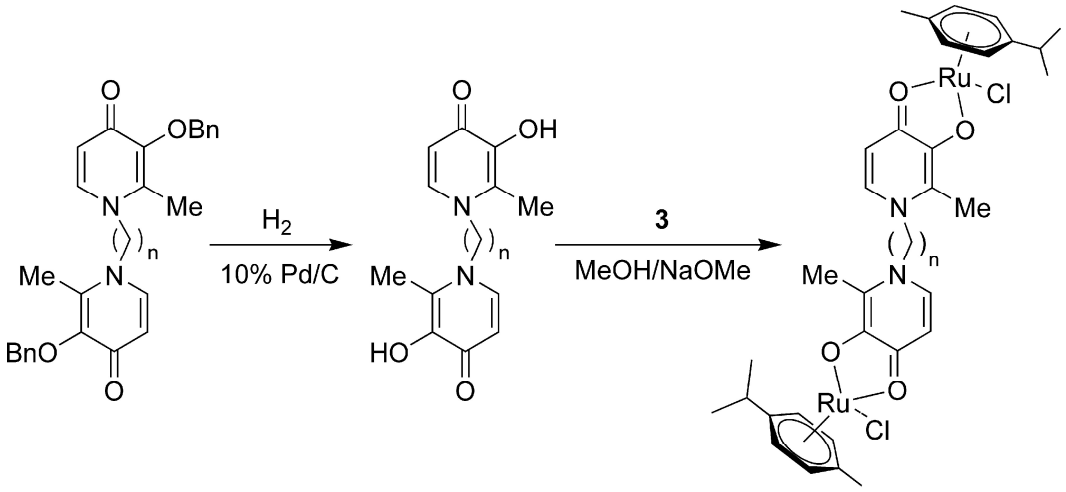

Scheme 1.2: *Synthesis of the dinuclear ruthenium complexes (a, n=3; b, n=6; c, n=12).*[59]

Table 1.2: *IC_{50} values of the complexes a - c in A2780 and SW480 cells, comparing cisplatin, oxaliplatin, carboplatin, BBR3464, the ruthenium(III) compound KP1019 and the mononuclear maltolato complex.*[59]

	IC_{50} (µM)	
Compound	**A2780**	**SW480**
a	25 ± 2	62 ± 14
b	30 ± 6	26 ± 8
c	1.5 ± 0.3	0.29 ± 0.05
Mononuclear maltolato	> 100	> 100
Cisplatin	0.33 ± 0.04	4.5 ± 1.7
Carboplatin	-	61 ± 10
Oxaliplatin	0.40 ± 0.12	0.30 ± 0.08
BBR3464	0.01	-
KP1019	-	49 ± 11

In addition, they have synthesized a series of mono-, di- and tri-nuclear ruthenium(II) arene complexes, and investigated their anticancer activity.[63] The *in vitro* anticancer activity of the dinuclear, its closest mononuclear analogue, and the trinuclear complex (Fig. 1.9) was compared.

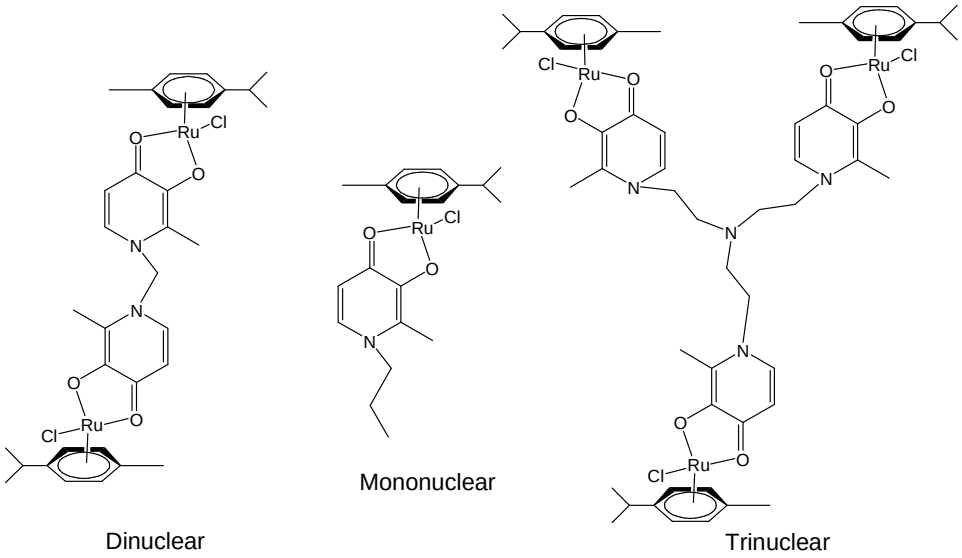

Figure 1.9: *Dinuclear, mononuclear and trinuclear ruthenium(II) arene anticancer compounds.*[63]

In both SW480 and A2780 cells, the dinuclear complex was identified as the most active species, while there is no meaningful difference between the mono- and the tri-nuclear complex (Table 1.3). When comparing the hydrophilicity of the three complexes (i.e. their solubility in water), the mononuclear complex is the most soluble, followed by the tri- and di-nuclear derivatives (Table 1.3).

Table 1.3: *Water solubility and IC_{50} values of ruthenium(II) arene complexes in human SW480 and A2780 cells.*[63]

		IC_{50} (μM)	
Compound	**Solubility (mM)**	**SW480**	**A2780**
Dinuclear	3.9	26 ± 8	30 ± 6
Mononuclear	10.3	42 ± 1	88 ± 12
Trinuclear	7.4	59 ± 18	80 ± 7

Keppler and co-workers also showed that the dinuclear compound represents a good balance between solubility and hydrophilicity necessary for cellular uptake. They concluded that the modification of the compound to link a higher number of ruthenium moieties improved the water solubility; but, showed a decrease in biological activity.

In contrast, Therrien and co-workers showed that an increase in nuclearity results in an increase in biological activity. They reported the synthesis of water-soluble metallaprisms which are capable of encapsulating planar aromatic molecules (e.g. pyrene, coronene),[64] or metal complexes (e.g. $[Pd(acac)_2]$, $[Pt(acac)_2]$).[58] These "complex-in-a-complex" systems showed high cytotoxicity toward the human ovarian cancer cell line, A2780.[58] More recently, this group synthesized tetranuclear metallarectangles (Fig. 1.10)[65] of the general formula $[Ru_4(arene)_4(N\cap N)_2(OO\cap OO)_2]^{4+}$ (arene = *p*-cymene or hexamethylbenzene; *OO∩OO* = 2,5-dihydroxy-1,4-benzoquinonato, 2,5-dichloro-1,4-benzoquinonato; *N∩N* = pyrazine, 4,4'-bipyridine or 1,2-bis(4-pyridyl)ethylene), prepared from a particular dinuclear ruthenium(II) arene complex (Fig. 1.11).[58,64]

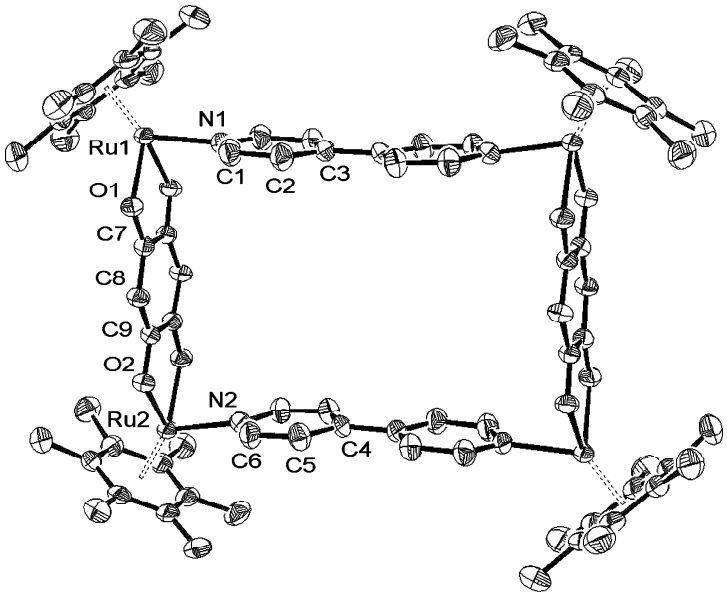

Figure 1.10: *ORTEP representation of ruthenium(II) hexamethylbenzene tetranuclear metallarectangle.[65] (Permission obtained from authors to reproduce structure).*

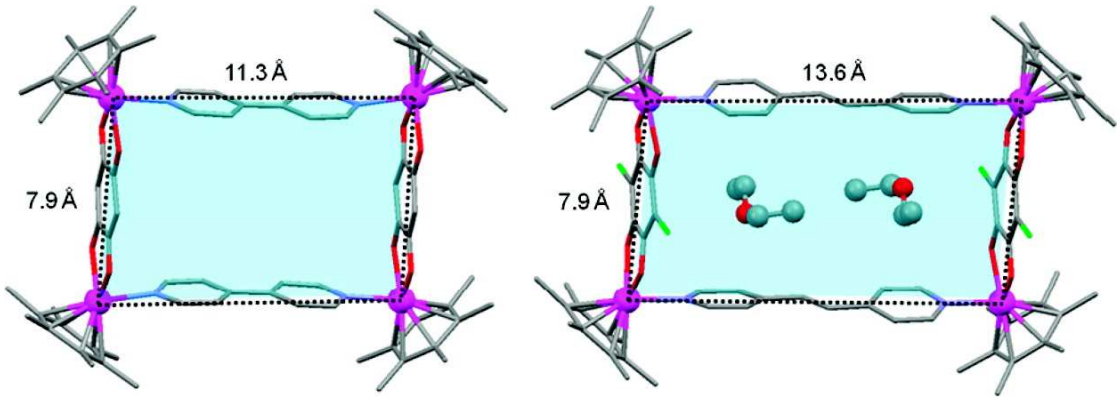

Figure 1.11: *Capped stick representations of ruthenium(II) hexamethylbenzene tetranuclear metallarectangle (left) and diethyl ether encapsulated by ruthenium(II) hexamethylbenzene tetranuclear metallarectangle (right).*[65] *(Permission obtained from authors to reproduce structure).*

The authors evaluated the activity of the water-soluble complexes against the A2780 ovarian cancer cell line. All the complexes showed moderate to excellent activity with IC_{50} values in the range 4 - 66 μM. It is likely that these large rectangular complexes would be taken up more efficiently by tumor cells,[66] which are permeable to large, non-natural molecules, whereas healthy cells are less able to take up such structures, which should provide a degree of selectivity and ultimately lead to reduced drug side effects.

There is a clear enhancement in biological activity between mononuclear and multinuclear ruthenium(II) arene compounds, hence functionalizing the ruthenium-arene moiety on the periphery of a dendritic scaffold might be a viable option.

1.5. Metallodendrimers

Dendrimers are complex molecules, built around a central core, having a well defined molecular structure.[67] The term ‘dendrimer’ is built from two Greek words “dendros” meaning “tree” or “branch”, and “meros” meaning “part”. These compounds can be obtained by a series of reaction steps. Both regular and highly branched types exist (Fig. 1.12).[68] They are represented in a symmetrical fashion with all tiers pointing outwards. These macromolecules can have a wide range of functionalities located on the periphery. Functionalization of the periphery with transition metals, gives the complex several advantages in the field of catalysis, such as enhanced catalytic

activity when compared to other mononuclear analogues.[69,70] These metal containing branched macromolecules are known as metallodendrimers.

1.5.1 Synthesis, characterization and properties

The divergent route and convergent route are two synthetic strategies used for the formation of various dendrimers. Both approaches involve a repetition of steps, with each yielding an additional generation. Each route has its own characteristics and therefore, to obtain the desired dendritic product, care has to be taken when choosing the synthetic approach.

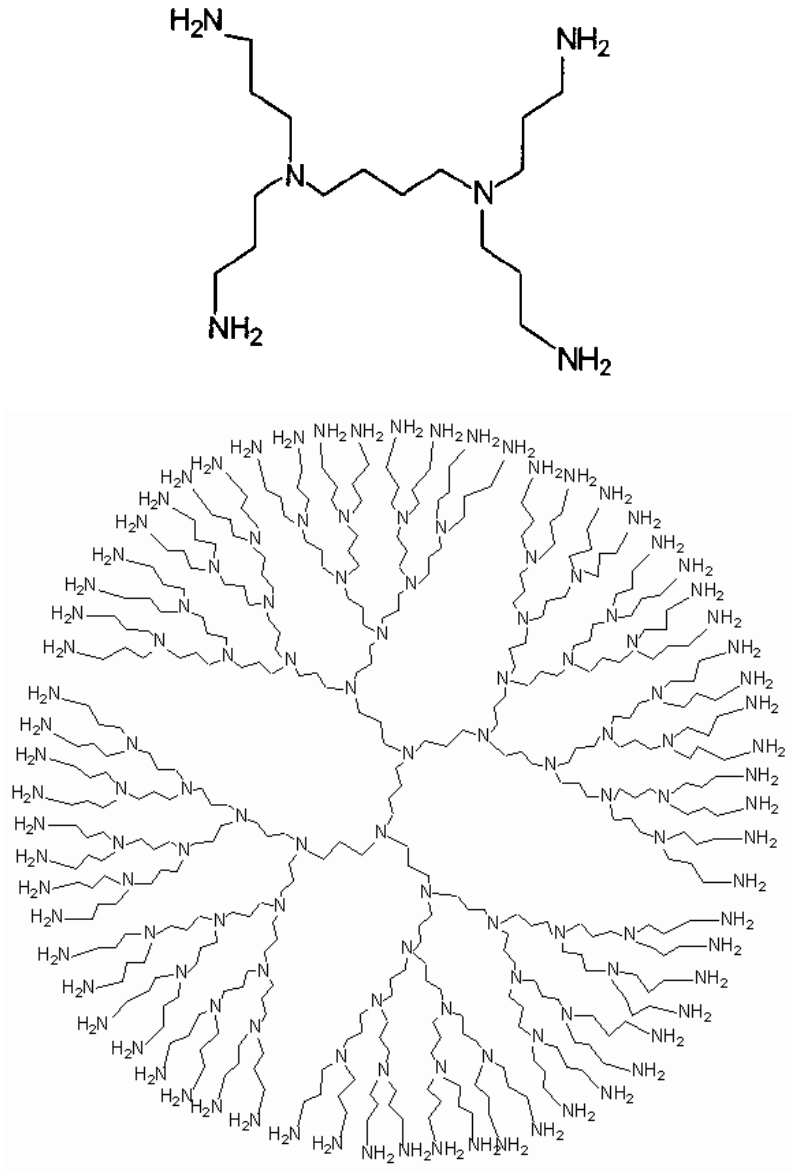

Figure 1.12: *Regular dendrimer (top) and a highly branched dendrimer (bottom).*[68]

The divergent route involves starting the synthesis with a multifunctional core molecule and extending it to the periphery in a stepwise manner.[68] In such a manner, the poly(propyleneimine) dendrimers are synthesized with the polyalkylamine core (Fig. 1.13). The nitrogen atoms serve as branch points which are reacted with acrylonitrile *via* a "Michael addition" to give a branched alkyl chain structure. The end-group is reduced yielding a new set of primary amines. The process can be repeated for further branching.[71] This approach is sometimes troublesome because as the generations increase, so do the number of structural defects, making purification difficult.

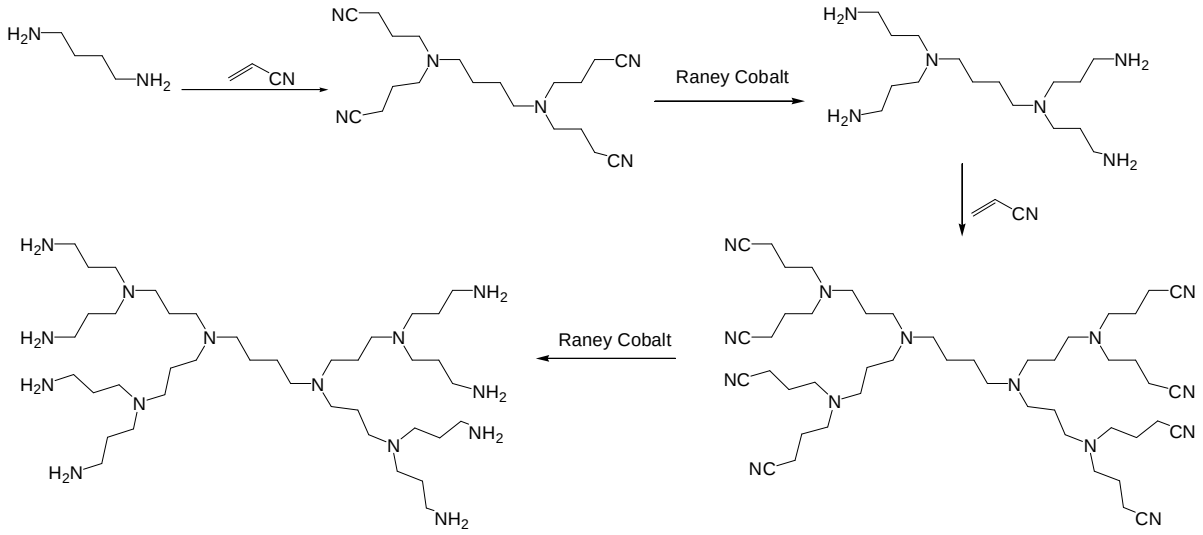

Figure 1.13: *Poly(propylene imine) dendrimer synthesis via the divergent approach.*[71]

Hence, a second approach is required. The convergent approach (sometimes known as the "defect-free" method) entails making dendrons (a dendritic wedge without a core) and reacting them to a core molecule in the last step of a synthesis. The large "molecular difference" between the reactant and the product facilitates ease of purification.

Early dendritic structures were synthesized using the divergent route, which have been thoroughly investigated by Tomalia[72] and Newkome,[73] for poly(amidoamine) (PAMAM) dendrimers and arboral systems respectively. In 1978, Buhleier reported the first synthesis of the poly(propylene imine) dendrimers, which were also prepared by the divergent route.[74] The convergent approach was introduced by Hawker and

Fréchet, where synthesis started at the periphery and extended towards the core (Fig. 1.14).[75]

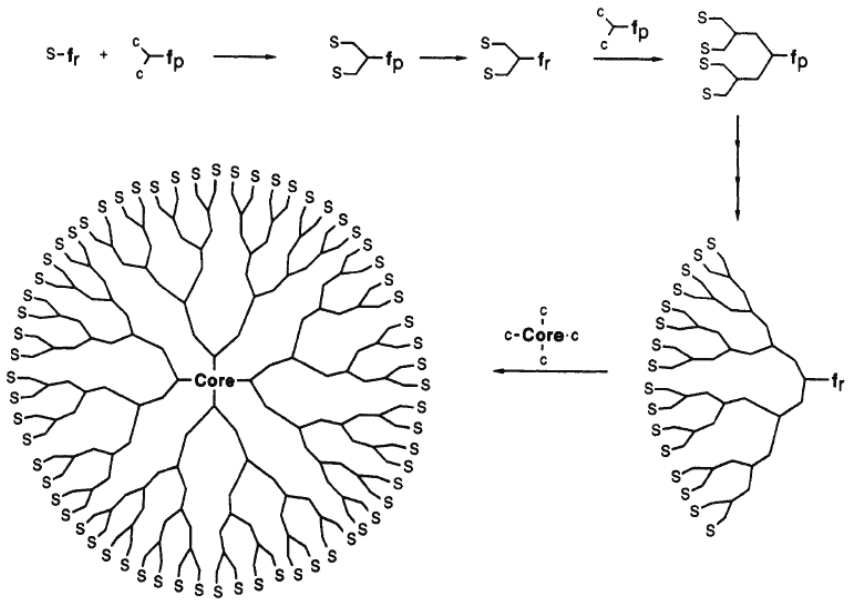

Figure 1.14: *Convergent approach, making use of wedges that can be connected to a core in the last step of a reaction by Hawker and Fréchet.*[75]

The last type of dendrimer is a convergently produced phenylacetylene dendrimer synthesized by Xu and Moore (Fig. 1.15).[76]

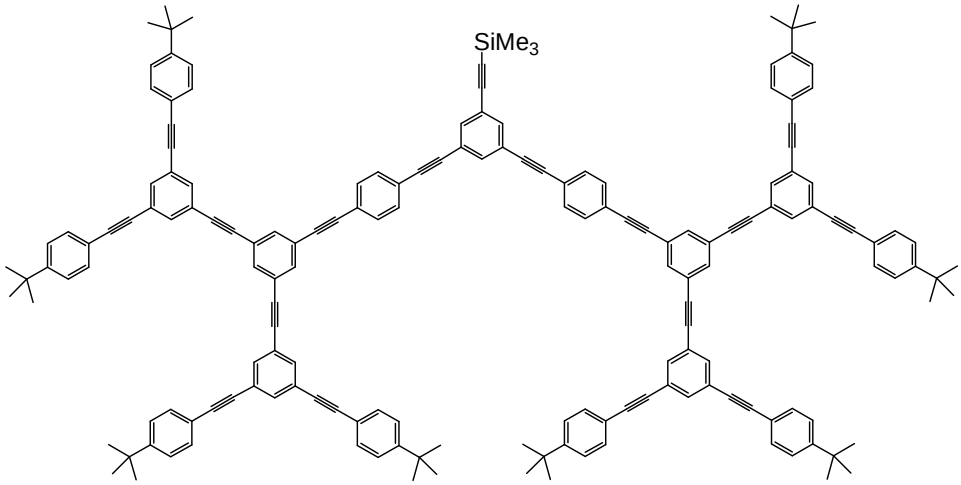

Figure 1.15: *Convergently synthesized phenylacytylene dendrimer by Xu and Moore.*[76]

Characterisation of dendrimers is complex, due to the shear size and symmetry of the macromolecules. A number of techniques can be used to fully characterise the dendritic complexes, such as NMR spectroscopy (^{1}H, $^{13}C\{^{1}H\}$, ^{15}N, ^{31}P), elemental analysis and chromatography techniques (HPLC and SEC).[77] Softer analytical

methods such as ESI (electrospray ionization) and MALDI-TOF (matrix-assisted laser desorption ionization-time of flight) mass spectrometry allow for in-depth analysis of macromolecules by giving the molecular ion of the dendrimer.[78]

1.5.2 General applications of metallodendrimers

Early work of Tomalia and Newkome mainly focused on the synthesis and characterisation of dendrimers.[72,73] More recently, the focus has shifted, to areas of functionality and applications of dendrimers. Such areas include medicinal chemistry,[79] host-guest chemistry[80] and catalysis.[81]

A high density of functional groups on the periphery attracted researchers to the area of medicinal chemistry. Functionalization of the periphery with identical biologically active groups showed enhanced activities.[82] Roy and co-workers investigated the activity of glycodendrimers, having an L-lysine core with various carbohydrates substituted on the periphery, compared to the monofunctional residue (Fig. 1.16).[83] As a biological catalyst, the glycodendrimer showed enhanced binding properties compared to the monofunctional residue.[83]

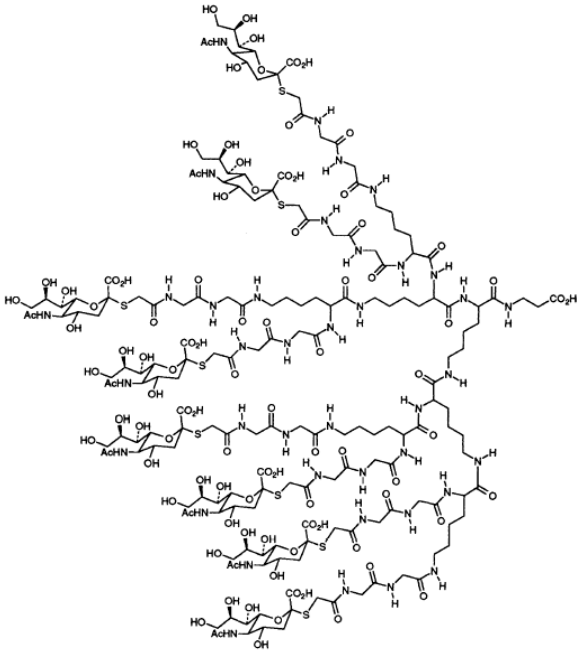

Figure 1.16: *A glycodendrimer with an L-lysine core and various carbohydrates on the periphery, synthesized by Roy and co-workers.*[83]

It has been shown that dendrimers can possess cavities within their macromolecular structure that can be used to accommodate guest molecules.[84] Therefore, research is focusing on this property for the development of sophisticated drug-delivery systems (Fig. 1.17).

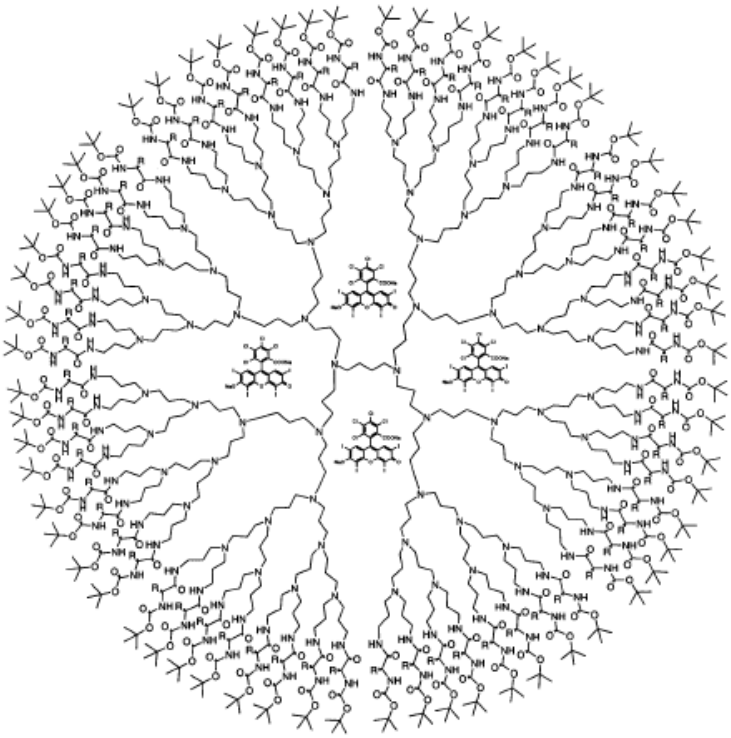

Figure 1.17: *Dendritic box synthesized by Jansen and co-workers, used as a drug delivery agent.*[84]

Functionalization of the dendrimer arms with various transition-metals showed promise in medicine and catalysis. Metallodendrimers used in medicine and catalysis can have the active metal centre located at the core or on the periphery (Fig. 1.18).

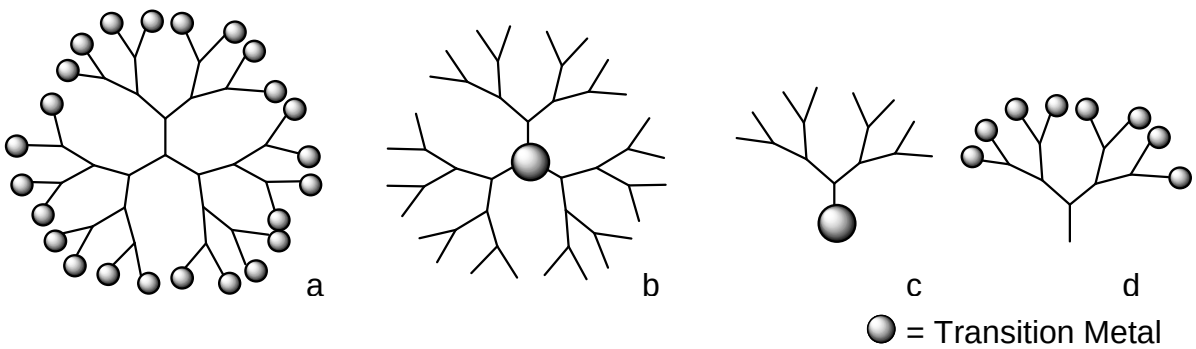

Figure 1.18: *Catalytically active transition-metal complexes can be attached to the periphery (a), the core (b), at the focal point of a wedge (c), and at the periphery of a wedge (d).*[67]

An example of a multinuclear metallodendrimer synthesized by Smith and co-workers is the poly(propyleneimine)pyridyliminepalladium dendrimer (Fig. 1.19), which was used in ethylene polymerisation studies.[85] The dendritic palladium complex also shows high activity and efficiency in Heck cross-coupling reactions in the coupling of an aryl halide with electron-deficient or electron-rich olefins.[85]

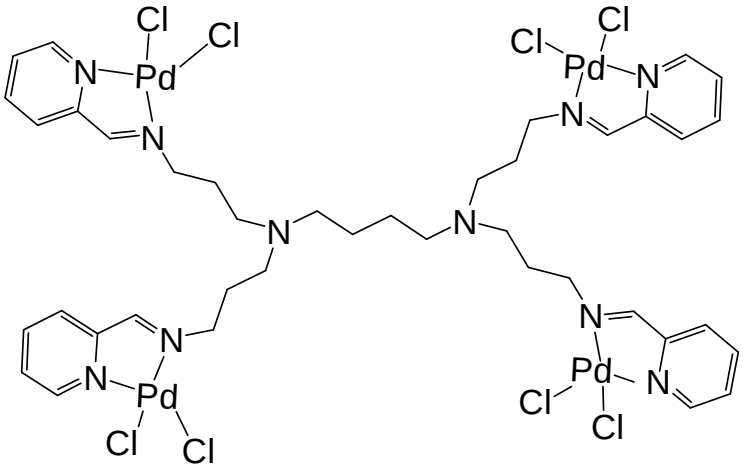

Figure 1.19: *Poly(propylene imine)pyridyliminepalladium metallodendrimer.*[85]

1.5.3 Enhanced permeability and retention (EPR) effect

The EPR effect is a phenomenon in which macromolecules (such as polymers and dendrimers) can accumulate at the tumour site due to an increase in blood vessel permeability within the cancerous tissues over normal tissues (Fig. 1.20).[86] The normal endothelial layer surrounding the blood vessels feeding healthy tissues, restricts the size of molecules that can diffuse from the blood stream. In contrast, the endothelial layer of blood vessels in cancerous tissues is more porous, providing access to the surrounding tissue. Furthermore, diseased tissues do not usually have a lymphatic drainage system. Therefore, once macromolecules have entered the tissue they are retained and show increased bio-availability. A tetraruthenium cluster was found to be highly active against the polio virus without damaging the host cells, thereby offering the potential of developing highly selective drugs.[87]

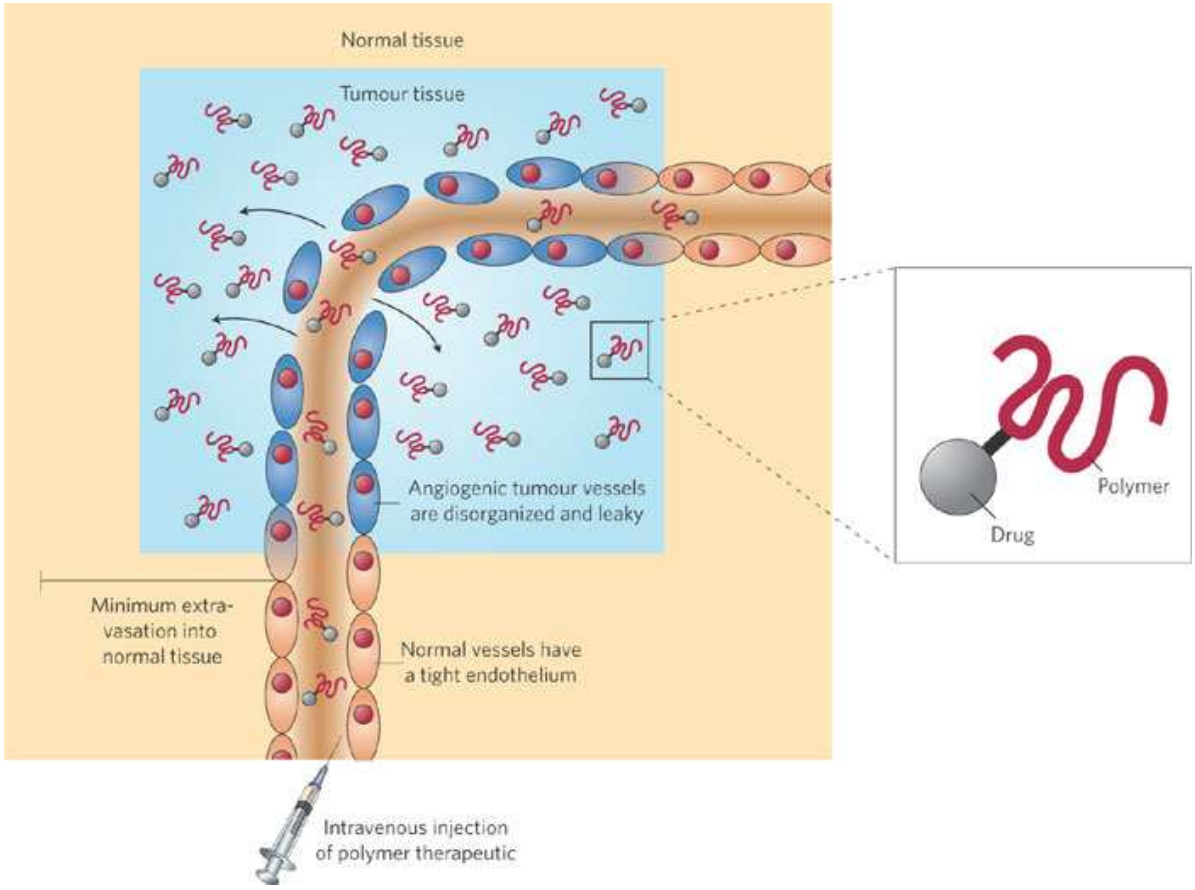

Figure 1.20: *Diagram representing the enhanced permeability and retention (EPR) effect.*[86]

1.5.4 Metallodendrimers used as anticancer agents

More recently it has been shown that polynuclear platinum complexes are a very important group of antitumor active compounds. A different toxicity profile and slight different mode of action was observed compared to cisplatin. They cross-link the DNA differently, in a 1→4 base pair pattern rather than the 1→2 base pair pattern of cisplatin.[88]

It was shown that synthesis of polymeric platinates is another means to increase platinum solubility, reduce toxicity and localise more drug in the tumour *via* the enhanced permeability and retention effect, to partially overcome mechanisms of resistance.[89,90]

The study done by Kapp and co-workers focused their attention to the design of drugs with increased selectivity for breast tumors.[91] They coupled the DAB

(1,4-diaminobutane poly(propyleneimine)) polyamine dendrimer with the well-known [1,2-bis(4-flurophenyl)ethylenediamine]platinum(II) complex (Fig. 1.21).[92] It was concluded that the platinum functionalized dendrimer operates as a carrier for the shuttling of platinum into the cell nuclei of the cancerous cell, with no cytotoxic effects seen.

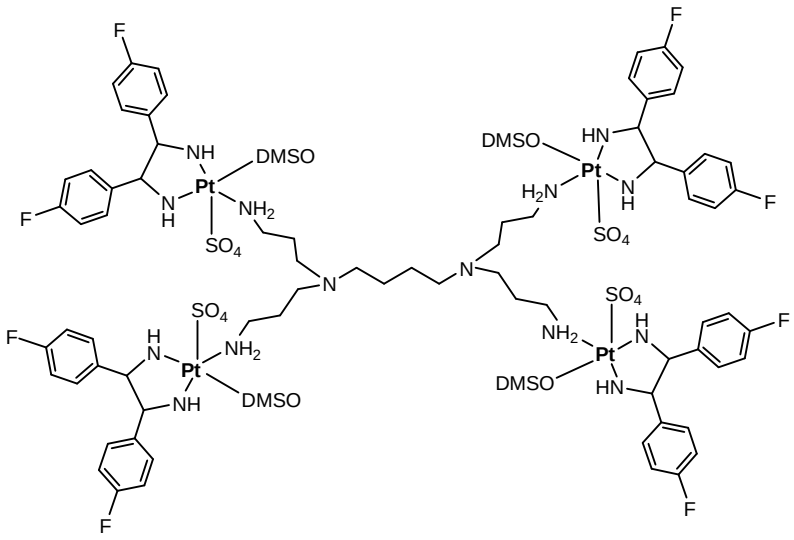

Figure 1.21: *A platinum functionalized metallodendrimer synthesized by Kapp and co-workers.*[91]

To overcome cisplatin resistance Jansen and co-workers coupled the $DAB(PA)_4$ polyamine dendrimer with cisplatin to render the tetranuclear platinum ($DAB(PA\text{-}tPt\text{-}Cl)_4$) compound (Fig. 1.22).[93] The compound was designed to overcome two problems associated with cisplatin, deactivation of cisplatin by intracellular thiolates and improved repair of crosslinks with DNA. The tetranuclear platinum compound showed moderate cytotoxicity (IC_{50} = 12.4 μM) against L1210 mouse leukemia cells and less cytotoxicity in resistant cell lines. The low cytotoxicity of the tetranuclear platinum complex was attributed to the high charge of the species at physiological pH. The high charge makes diffusion through the cell membrane (apolar) unlikely.

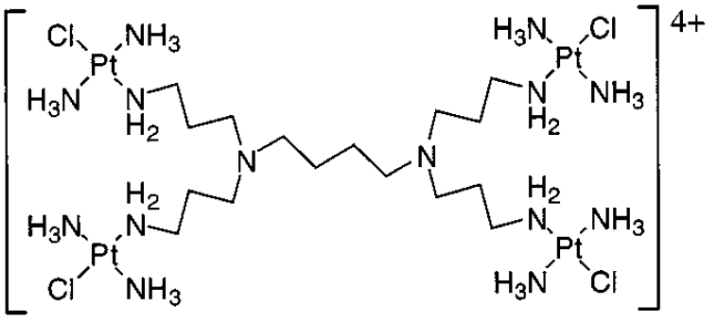

Figure 1.22: *The first generation tetranuclear platinum complex DAB(PA-tPt-Cl)$_4$.* [93]

Malik and co-workers synthesized a dendrimer-platinate with a sodium carboxylate surface (Fig. 1.23), by conjugating the polyamidoamine (PAMAM) dendrimer (generation 3.5) with cisplatin, which was highly water soluble and released platinum slowly *in vivo.*[94] Whilst *in vivo*, the dendrimer-Pt complex and cisplatin were equi-active against L1210 (mouse lymphocytic leukemia) cell line. At high concentration of the dendrimer-Pt, the dendrimer killed B16F10 (mouse melanoma) cells whilst cisplatin did not. Additionally, the dendrimer-Pt was used to treat a palpable B16F10 melanoma and showed antitumour activity whereas cisplatin was inactive. Thus, this approach showed potential as a novel antitumor approach.

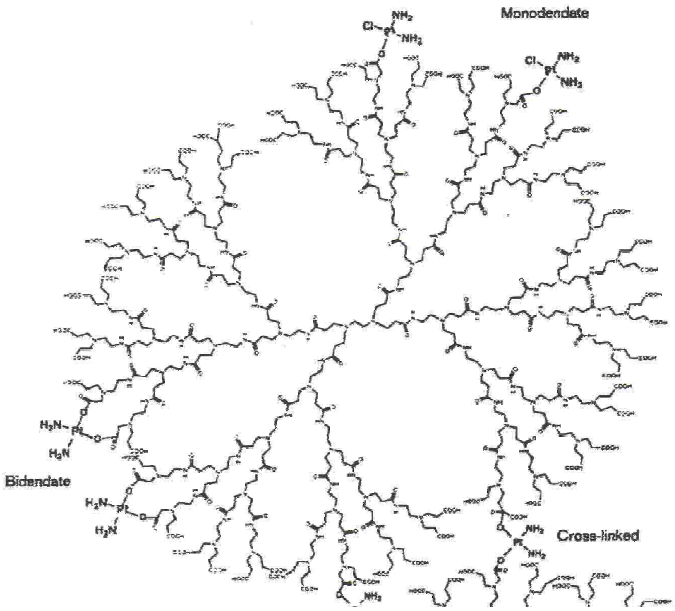

Figure 1.23: *Proposed structure of generation 3.5 PAMAM dendrimer-Pt with the three possible binding sites: monodentate, bidentate and cross-linked.*[94]

In 2009 Zhao *et al.* reported synthesis of a multinuclear chloropyridyliminecopper(II) complex. The dendritic complex contained seven copper(II) centers (Fig. 1.24).[95]

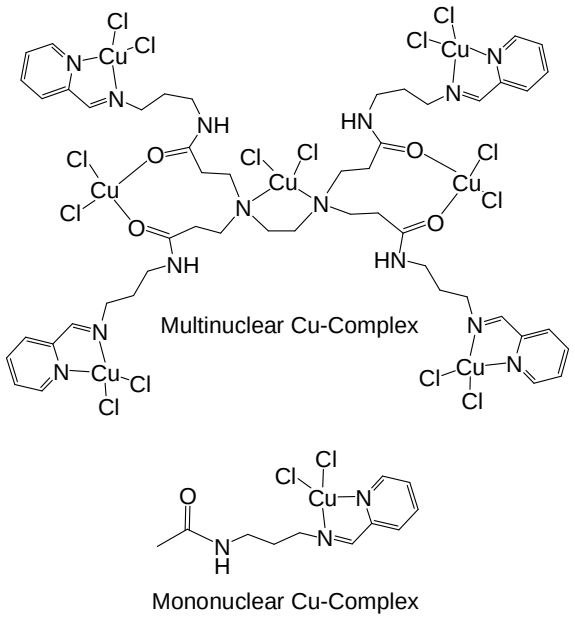

Figure 1.24: *A multinuclear (top) and mononuclear copper complex (bottom) synthesized by Zhao and co-workers.*[95]

They investigated the biological activity of these complexes as potential anticancer agents, which to their surprise showed enhanced *in vitro* cytotoxicity. The copper(II) complexes were studied against leukemia cells (MOLT-4), breast cancer cells (MCF-7), and Chang Liver cells (Table 1.4).

Table 1.4: *IC_{50} values of multinuclear and mononuclear Cu-complexes versus cisplatin.*[95]

	IC_{50} (μM)		
Compound	**MOLT-4**	**MCF-7**	**Chang liver**
Cisplatin	15.5 ± 4.2	-	73.5 ± 3.7
Multinuclear Cu-complex	11.1 ± 0.6	10.2 ± 1.5	8.7 ± 0.7
Mononuclear Cu-complex	24.7 ± 2.4	73.1 ± 4.9	-

In comparison with the mononuclear copper derivative, the authors showed an enhanced improvement in cytotoxicity. Furthermore, the multinuclear copper complex

demonstrated enhanced cytotoxicity compared to cisplatin, against MOLT-4 and cisplatin-resistance MCF-7.

1.5.5 Ruthenium(II) arene metallodendrimers

Functionalized metallodendrimers with ruthenium arene moieties on the periphery are rare in the literature. A ruthenium arene functionalized metallodendrimer was recently synthesized by Pettirossi and co-workers.[96] They synthesized the multicationic ruthenium arene metallodendrimer (Fig. 1.25) by coupling of [(η^6-*p*-cymene)Ru(κ^3-dpk-OCH_2CH_2OH)]X (dpk = 2,2'-dipyridyl ketone, X=PF_6) with the $DAB(PA)_4$ polyamine dendrimer mediated by 1,1'-carbonyldiimidazole (CDI). The metallodendrimers were characterised with multidimensional and multinuclear NMR techniques (^{1}H, ^{13}C, ^{1}H-COSY, ^{1}H-NOESY, ^{1}H,^{13}C-HSQC NMR, and ^{1}H,^{13}C-HMBC NMR spectroscopy). The authors showed that the attachment of an organometallic moiety to a dendritic structure neither alters the relative anion–cation orientation nor does it cause a significant spatial proximity of two metal centers. The solvophobicity of the metallodendrimers is much higher than that of neutral dendrimers and increases with the generation.

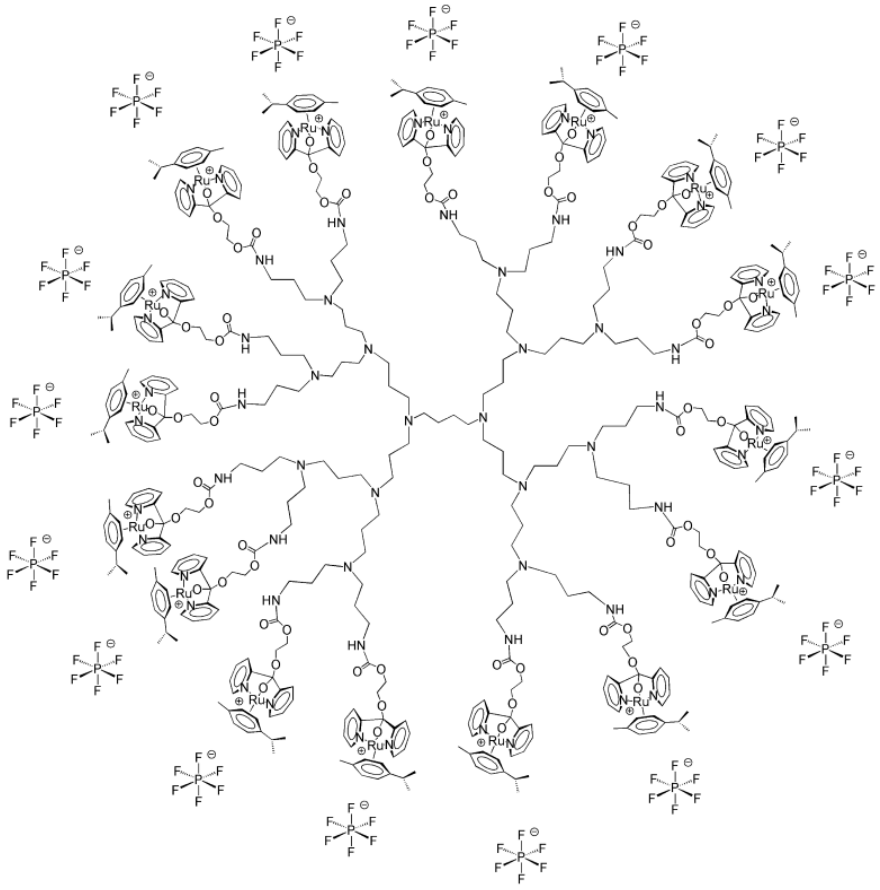

Figure 1.25: *First ruthenium arene metallodendrimer synthesized by Pettirossi and co-workers.*[96]

The use of functionalized metallodendrimers combined with ruthenium arene moieties on the periphery as anticancer agents are few and rare, which further gives motivation for the present study.

1.6 General conclusions

Severe side effects, high toxicity and drug resistance of platinum-based therapies have over shadowed the clinical successes of these compounds. Thus, researchers have focused their attention on compounds incorporating ruthenium metal. Arene ruthenium chemistry has shown to be an attractive alternate to platinum-based therapies. These compounds are stable and have shown high antiproliferative activity to a variety of carcinomas. However, whilst the field of ruthenium arene chemistry is growing, exploration into functionalized ruthenium arene metallodendrimers is in its infancy.

As a result, the development of ruthenium arene metallodendrimers and their uses as biological agents have not been studied. Coupling the stability and cytotoxicity of the ruthenium arene moiety with the ‘enhanced permeability and retention’ (EPR) effect of dendrimers prompts further investigation into this field.

1.7 Aims and objectives of the dissertation

1.7.1 General aims

In light of the past and recent developments in the field of ruthenium-arene chemistry, interest towards the use of these types of compounds as potential biological agents is rife. Therefore, the aim of this project is to synthesize and characterize a range of highly functionalized multinuclear monodentate and chelating bidentate ruthenium(II) arene metallodendrimers, and to evaluate their biological activity as potential anticancer agents.

1.7.2 Specific objectives

The specific objectives of the Dissertation are to:

- Synthesize and characterize a range of Schiff-Base end-group modified first and second generation poly(propyleneimine) dendrimers (Fig. 1.26).

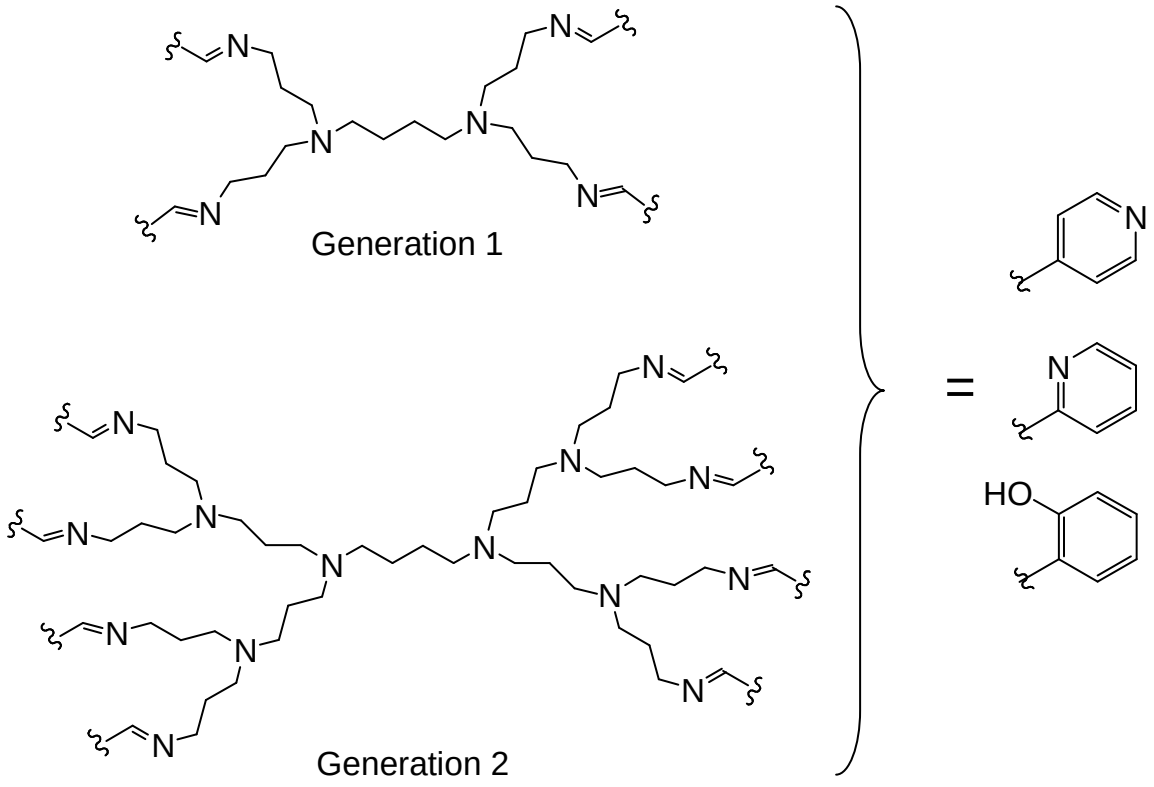

Figure 1.26: *1st and 2nd generation Schiff-Base end group modified poly(propyleneimine) dendrimers.*

- Complex ruthenium-arene precursors such as **[Ru(η^6-p-Pr^{i}C$_6$H$_4$Me)Cl$_2$]** [97] and **[Ru(η^6-C$_6$Me$_6$)Cl$_2$]$_2$** [98] (Fig. 1.27) with the appropriate poly(propyleneimine) dendritic ligands.

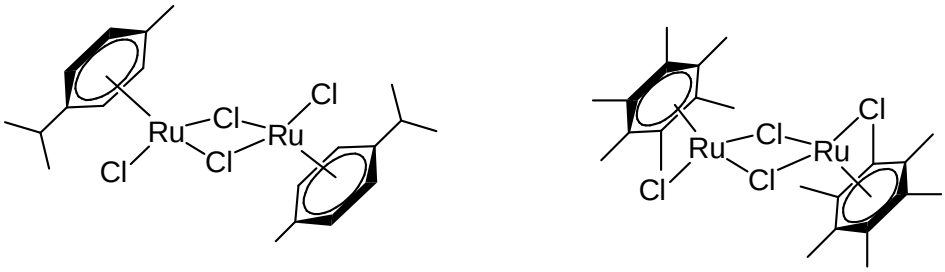

Figure 1.27: *Ruthenium arene dimers,* ***[Ru(η^6-p-Pr^{i}C$_6$H$_4$Me)Cl$_2$]$_2$*** *(left),*[97] *and* ***[Ru(η^6-C$_6$Me$_6$)Cl$_2$]$_2$*** *(right).*[98]

- Synthesize ruthenium(II) arene mononuclear analogues to compare their biological activities with those of the multinuclear derivatives.

- Evaluate the antiproliferative activity of the mononuclear and dendritic ruthenium(II) arene complexes, against the A2780 and A2780cisR human ovarian cell lines.

- Conduct DNA binding experiments on the most biologically active ruthenium(II) arene dendritic complexes

All compounds are characterized by a variety of analytical and spectroscopic techniques, which include NMR and IR spectroscopy, elemental analysis and mass spectrometry.

1.8 References

1) Health Castle.com, *Metastases: How does Cancer Spread?*, http://www.healthcastle.com/cancer_general_mets.shtml, (accessed 16 August 2010)
2) World Health Organization, *Cancer*, http://www.who.int/mediacentre/factsheets/fs297/en/, (accessed 16 August 2010).
3) American Cancer Society, *Report sees 7.6 million global 2007 cancer deaths.*, http://www.reuters.com/article/idUSN1633064920071217, (accessed 16 August 2010).
4) Cancer Research UK, *UK cancer incidence statistics by age*., http://info.cancerresearchuk.org/cancerstats/incidence/age/, (accessed 16 August 2010).
5) B. Rosenberg, L. Van Camp, J. E. Trosko and V. H. Mansour, *Nature*, 1969, **222**, 385.
6) N. J. Farrer, L. Salassa and P. J. Sadler, *Dalton Trans*., 2009, **48**, 10690.
7) C. A. Puckett, R. J. Ernst and J. K. Barton, *Dalton Trans.*, 2009, **39**, 1159.
8) P. C. A. Bruijnincx and P. J. Sadler, *Current Opin. Chem. Biol.*, 2008, **12**, 197.
9) T. W. Hambley, *Dalton Trans.*, 2007, **43**, 4929.
10) C. X. Zhang and S. J. Lippard, *Curr. Opin. Chem. Bio.,* 2003, **7**, 481.
11) D. J. Higby, H. J. Jr. Wallace, D. Albert and J. F. Holland, *J. Urol.*, 1974, **112**, 100.
12) A. Horwich, *Br. J. Cancer*, 1989, **59**, 156.
13) E. Wiltshaw and T. Carr, *Rec. Res. Cancer Res.*, 1974, **48**, 178.
14) J. P. Neijt, W. W. ten Bokkel Huinink, M. E. van der Berg, A. T. van Oosterom, P. H. Vermorken, A. C. van Lindert, A. P. Heintz, E. Aartsen, M. van Lent, *et al.*, *Eur. J. Cancer*, 1991, **27**, 1367.
15) M. Gordon and S. Hollander, *J. Med.*, 1993, **24**, 209.
16) C. Billecke, S. Finniss, L. Tahash, C. Miller, T. Mikkelsen, N. P. Farrell and O. Bogler, *Neuro-Ocology*, 2006, **8**, 215.

17) D. I. Jodrell, T. R. J. Evans, W. Steward, D. Cameron, J. Prendiville, C. Aschele, C. Noberasco, M. Lind, J. Carmichael, N. Dobbs, G. Camboni, B. Gatti and F. De Braud, *Eur. J. Cancer*, 2004, **40**, 1872.

18) E. Wong and C. M. Giandomenico, *Chem. Rev.*, 1999, **99**, 2451.

19) M. Galanski, M. A. Jakupec and B. K. Keppler, *Curr. Med. Chem.,* 2005, **12**, 2075.

20) M. Frezza, C. N. Verani, D. Chen and Q. Ping Dou, *Lett. Drug Des. Discov.*, 2007, **4**, 311.

21) A. C. F. Caires, *Anti-Cancer Agents Med. Chem.*, 2007, **7**, 484.

22) I. Kostova, *Curr. Med. Chem.*, 2006, **13**, 1085.

23) B. Therrien, W. H. Ang, F. Chérioux, L. Vieille-Petit, L. Juillerat-Jeanneret, G. Süss-Fink and P. J. Dyson, *J. Clust. Sci.*, 2007, **18**, 741.

24) M. Pongratz, P. Schluga, M. A. Jakupec, V. B. Arion, C. G. Hartinger, G. Allmaier and B. K. Keppler, *J. Anal. At. Spectrom.*, 2004, **19**, 46.

25) M. J. Clarke, *Coord. Chem.*, 2003, **236**, 209.

26) C. G. Hartinger and P. J. Dyson, *Chem. Soc. Rev.*, 2009, **38**, 391.

27) G. Sava, R. Gagliardi, A. Bergamo, E. Alessio and G. Mestroni, *Anticancer Res.*, 1999, **19**, 969.

28) B. K. Keppler, M. Henn, U. M. Juhl, M. R. Berger, R. Niebl and F. E. Wagner, *Prog. Clin. Biochem. Med.,*1989, **10**, 41.

29) C. G. Hartinger, M. A. Jakupec, S. Zorbas-Seifried, M. Groessl, A. Egger, W. Berger, H. Zorbas, P. J. Dyson and B. K. Keppler, *Chem. Biodiversity*, 2008, **5**, 2140.

30) M. J. Hannon, *Pure Appl. Chem.*, 2007, **79**, 2243.

31) E. Alessio, G. Mestroni, A. Bergamo and G. Sava, *Curr. Top. Med. Chem.*, 2004, **4**, 1525.

32) E. Alessio, G. Mestroni, A. Bergamo and G. Sava, *Metal Ions Biol. Sys.*, 2004, **42**, 323.

33) G. Sava, S. Zorzet, C. Turrin, F. Vita, M. R. Soranzo, G. Zabucchi, M. Cocchietto, A. Bergamo, S. DiGiovone, G. Pezzoni, L. Sartor and S. Garbisa, *Clin. Cancer Res.*, 2003, **9**, 1898.

34) A. R. Timerbaev, C. G. Hartinger, S. S. Aleksenko and B. K. Keppler, *Chem. Rev.*, 2006, **106**, 2224.

35) M. J. Clarke, S. Bitler, D. Rennert, M. Buchbinder, A. D. Kelman, *J. Inorg. Biochem.*, 1980, **12**, 79.

36) P. J. Dyson and G. Sava, *Dalton Trans.*, 2006, **16**, 1929.

37) E. L. Muetterties, J. R. Bleeke, E. J. Wucherer and T. Albright, *Chem. Rev.*, 1982, **82**, 499.

38) B. Therrien, *Coord. Chem. Rev.*, 2009, **253**, 493.

39) M. Stebler-Roethlisberger, W. Hummel, P. A. Pittet, H. B. Buergi, A. Lundi, A. E. Merbach, *Inorg. Chem.*, 1988, **27**, 1358.

40) Y. Hung, W.-J. Kung and H. Taube, *Inorg. Chem.*, 1981, **20**, 457.

41) S. W. Magennis, A. Habtemariam, O. Novakova, J. B. Henry, S. Meier, S. Parsons, I. D. H. Oswald, V. Brabec and P. J. Sadler, *Inorg. Chem.*, 2007, **46**, 5059.

42) Y. K. Yan, M. Melchart, A. Habtemariam and P. J. Sadler, *Chem. Commun.*, 2005, **38**, 4764.

43) W. H. Ang and P. J. Dyson, *Eur. J. Inorg. Chem.*, 2006, **20**, 4003.

44) V. Brabec and O. Novakova, *Drug Resist. Updates*, 2006, **9**, 111.

45) P. J. Dyson, *Chimia*, 2007, **61**, 698.

46) S. J. Dougan and P. J. Sadler, *Chimia*, 2007, **61**, 704.

47) X. Zhang and S. J. Lippard, *Curr. Opin. Chem. Biol.*, 2003, **7**, 481.

48) Y. N. V. Gopal, D. Jayaraju and A. K. Kondapi, *Biochemistry*, 1999, **38**, 4382.

49) R. E. Morris, R. E. Aird, P. S. Murdoch, H. Chen, J. Cummings, N. D. Hughes, S. Parsons, A. Parkin, G. Boyd, D. I. Jodrell and P. J. Sadler, *J. Med. Chem.*, 2001, **44**, 3616.

50) R. E. Aird, J. Cummings, A. A. Ritchie, M. Muir, R. E. Morris, H. Chen, P. J. Sadler and D. I. Jodrell, *Br. J. Cancer*, 2002, **86**, 1652.

51) C. Scolaro, T. J. Geldbach , S. Rochat, A. Dorcier, C. Gossens, A. Bergamo, M. Cocchietto, I. Tavernelli, G. Sava, U. Rothlisberger and P. J. Dyson, *Organometallics*, 2006, **25**, 756.

52) F. –J. K. Rehmann, L. P. Cuffe, O. Mendoza, D. K. Rai, N. Sweeney, K. Strohfeldt, W. M. Gallagher and M. Tacke, *Appl. Organomet. Chem.*, 2005, **19**, 293.

53) A. Habtemariam, R. Fernández, M. Melchart, H. Chen, E. P. L. Van der Geer, R. E. Aird, D. I. Jodrell and P. J. Sadler, unpublished results.

54) L. A. Huxham, E. L. S. Cheu, B. O. Patrick and B. R. James, *Inorg. Chim. Acta*, 2003, **352**, 238.

55) H. Chen, J. A. Parkinson, O. Novakova, J. Bella, F. Wang, A. Dawson, R. Gould, S. Parsons, V. Brabec and P. J. Sadler, *Proc. Natl. Acad. Sci. U. S. A.*, 2003, **100**, 14623.

56) F. Schmitt, P. Govindaswamy, G. Suess-Fink, W. H. Ang, P. J. Dyson, L. Juillerat-Jeanneret and B. Therrien, *J. Med. Chem.*, 2008, **51**, 1811.

57) M. Auzias, B. Therrien, G. Suess-Fink, P. Stepnicka, W. H. Ang and P. J. Dyson, *Inorg. Chem. Int. Ed.*, 2008, **47**, 578.

58) B. Therrien, G. Suess-Fink, P. Govindaswamy, A. K. Renfrew and P. J. Dyson, *Angew. Chem. Int. Ed.*, 2008, **47**, 3773.

59) M. G. Mendoza-Ferri, C. G. Hartinger, R. E. Eichinger, N. Stolyarova, M. A. Jakupec, A. A. Nazarov, K. Severin and B. K. Keppler, *Organometallics*, 2008, **27**, 2405.

60) M. G. Mendoza-Ferri, C. G. Hartinger, A. A. Nazarov, W. Kandioller, K. Severin and B. K. Keppler, *Appl. Organomet. Chem.*, 2008, **22**, 326.

61) A. F. A. Peacock, M. Melchart, R. J. Deeth, A. Habtemariam, S. Parsons and P. J. Sadler, *Chem. Eur. J.*, 2007, **13**, 2601.

62) W. Kandioller, C. G. Hartinger, A. A. Nazarov, M. L. Kuznetsov, R. O. John, C. Bartel, M. A. Jakupec, V. B. Arion and B. K. Keppler, *Organometallics*, 2009, **28**, 4249.

63) M. G. Mendoza-Ferri, C. G. Hartinger, A. A. Nazarov, R. E. Eichinger, M. A. Jakupec, K. Severin and B. K. Keppler, *Organometallics.*, 2009, **28**, 6260.

64) J. Mattsson, P. Govindaswamy, J. Furrer, Y. Sei, K. Yamaguchi, G. Suess-Fink and B. Therrien, *Organometallics*, 2008, **27**, 4346.

65) J. Mattsson, P. Govindaswamy, A. K. Renfrew, P. J. Dyson, P. Stepnicka, G. Suess-Fink and B. Therrien, *Organometallics*, 2009, **28**, 4350.

66) S. Modi, J. P. Jain, A. J. Domb and N. Kumar, *Curr. Pharm. Des.*, 2006, **12**, 4785.

67) G. E. Oosterom, J. N. H. Reek, P. C. J. Kamer and P. W. N. M. van Leeuwen, *Angew. Chem. Int. Ed.*, 2001, **40**, 1828.

68) A. W. Bosman, H. M. Janssen and E. W. Meijer, *Chem. Rev.*, 1999, **99**, 1665.

69) M. T. Reetz, G. Lohmer and R. Schwickardi, *Angew. Chem. Int. Ed. Engl.*, 1997, **36**, 1526.

70) M. T. Reetz, *Top. Catal.*, 1998, **4**, 187.

71) E. M. M. de Brabander-van den Berg and E. W. Meijer, *Angew. Chem.*, 1993, **105**, 1370.

72) D. A. Tomalia, H. Baker, J. R. Dewald, M. Hall, G. Kallos, S. Martin, J. Roeck, J. Ryder and P. Smith, *Macromolecules,* 1986, **19**, 2466.

73) G. R. Newkome, Z. Yao, G. R. Baker and V. K. Gupta, *Org. Chem.*, 1985, **50**, 2003.

74) E. Buhleier, W. Wehner and F. Voegtle, *Synthesis*, 1978, **2**, 155.

75) C. J. Hawker and J. M. J. Fréchet, *J. Am. Chem. Soc.,* 1990, **112**, 7638.

76) Z. Xu and J. S. Moore, *Angew. Chem. Int. Ed. Engl*., 1993, **32**, 246.

77) D. J. Pesak, J. S. Moore and T. E. Wheat, *Macromolecules*, 1997, **30**, 6467.

78) J. C. Hummelen, J. L. J. van Dongen and E. W. Meijer, *Chem. Eur. J*., 1997, **3**, 1489.

79) H. Yang and W. J. Kao, *J. Biomater. Sci. Polymer Edn.*, 2006, **17**, 3.

80) R. E. Bauer, C. G. Clark, Jr. and K. Müllen, *New J. Chem.*, 2007, **31**, 1275.

81) D. Astruc, *Pure Appl. Chem.*, 2003, **75**, 461.

82) M. Mammen, S.-K. Choi and G. M. Whitesides, *Angew. Chem. Int. Ed.,* 1998, **37**, 2755.

83) R. Roy, D. Zanini, S. J. Meunier and A. Romanowska, *J. Chem. Soc. Chem. Commun*., 1993, **24**, 1869.

84) J. F. G. A. Jansen, E. M. M. de Barbander-van den Berg and E. W. Meijer, *Science*, 1994, **266**, 1226.

85) G. Smith, R. Chen and S. Mapolie, *J. Organomet. Chem.*, 2003, **673**, 111.

86) D. F. Baban and L. W. Seymour, *Adv. Drug Delivery Rev.*,1998, **34**, 109.

87) C. S. Allardyce, P. J. Dyson, D. J. Ellis, P. A. Salter and R. Scopelliti, *J. Organomet. Chem.*, 2003, **668**, 35.

88) C. Manzotti, G. Pratesi, E. Menta, R. D. Domenico, E. Cavalletti, H. H. Fiebig. L. R. Kelland, N. Farrell, D. Polizzi, R. Supino, G. Pezzoni, and F. Zunino, *Clin. Cancer Res.*, 2000, **6**, 2626.

89) Y. Matsumura and H. Maeda, *Cancer Res.*, 1986, **6**, 6387.

90) L. W. Seymour, K. Ulbrich, P. S. Steyger, M. Brereton, V. Subr, J. Strohalm and R. Duncan, *Br. J. Cancer*, 1994, **70**, 636.

91) T. Kapp, A. Dullin and R. Gust, *J. Med. Chem.*, 2006, **49**, 1182.

92) R. Müller, R. Gust, M. Jennerwein, H. Reile, R. Laske, W. Krischke, G. Bernhardt, T. Spruss, J. Engel and H. Schönenberger, *Eur. J. Med. Chem.*, 1989, **24**, 341.

93) B. A. J. Jansen, J. van der Zwan, J. Reedijk, H. Den Dulk and J. Brouwer, *Eur. J. Inorg. Chem.*, 1999, 1429.

94) N. Malik, E. G. Evagorou and R. Duncan, *Anti-Cancer Drugs*, 1999, **10**, 767.

95) X. Zhao, S.-C. J. Loo, P. P.-F. Lee, T. T. Y. Tan and C. K. Chu, *J. Inorg. Biochem.*, 2010, **104**, 105.

96) S. Pettirossi, G. Bellachioma, G. Ciancaleoni, C. Zuccaccia, D. Zuccaccia and A. Macchioni, *Chem. Eur. J.*, 2009, **15**, 5337.

97) M. A. Bennett and A. K. Smith, *J. Chem. Soc. Dalton Trans.*, 1974, **2**, 233.

98) M. A. Bennett, T. W. Matheson, G. B. Robertson, A. K. Smith, and P. A. Tucker, *Inorg. Chem.*, 1980, **19**, 1014.

Chapter 2

Synthesis and Characterisation of Dendritic and Monomeric Pyridyl-imine and Salicylaldimine Ligands

2.1 Introduction

In order to exploit size selective uptake of drugs into tumour cells effectively, large compounds are required. In recent years, dendrimers have found potential as molecular tools in biological applications,[1-3] especially as nano-carriers,[4,5] diagnostic agents[6] and as chemotherapeutics.[7-9] Moreover, another advantage of dendrimers is their multivalency, which leads to increased interaction between a dendrimer-drug conjugate and target bearing multiple receptors, further improving selectivity to cancer cells.

As part of a study towards the synthesis of ruthenium(II) arene complexes, a series of pyridylimine- and salicylaldimine-functionalised ligands were prepared. The dendritic scaffolds of interest are based on the poly(propyleneimine) dendrimer, the 1,4-diaminobutane poly(propyleneimine) tetraamine (DAB-*dendr*-$(NH_2)_4$-**G1**) and 1,4-diaminobutane poly(propyleneimine) octaamine (DAB-*dendr*-$(NH_2)_8$-**G2**) (Fig. 2.1).

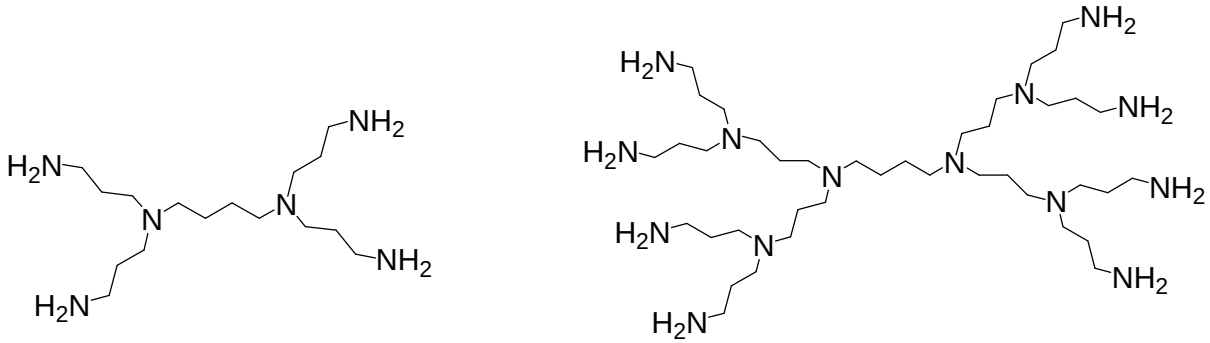

Figure 2.1: *Diagram of dendritic scaffolds chosen, DAB-dendr-$(NH_2)_4$-**G1** (left) and DAB-dendr-$(NH_2)_8$-**G2** (right).*

The periphery of the dendritic scaffolds has been modified with iminopyridyl and salicylaldimine moieties *via* a condensation reaction, by reacting the dendritic

scaffold (amine) with the appropriate aldehyde, with aims to synthesize mono- and bidentate dendritic ligands (Scheme 2.1).

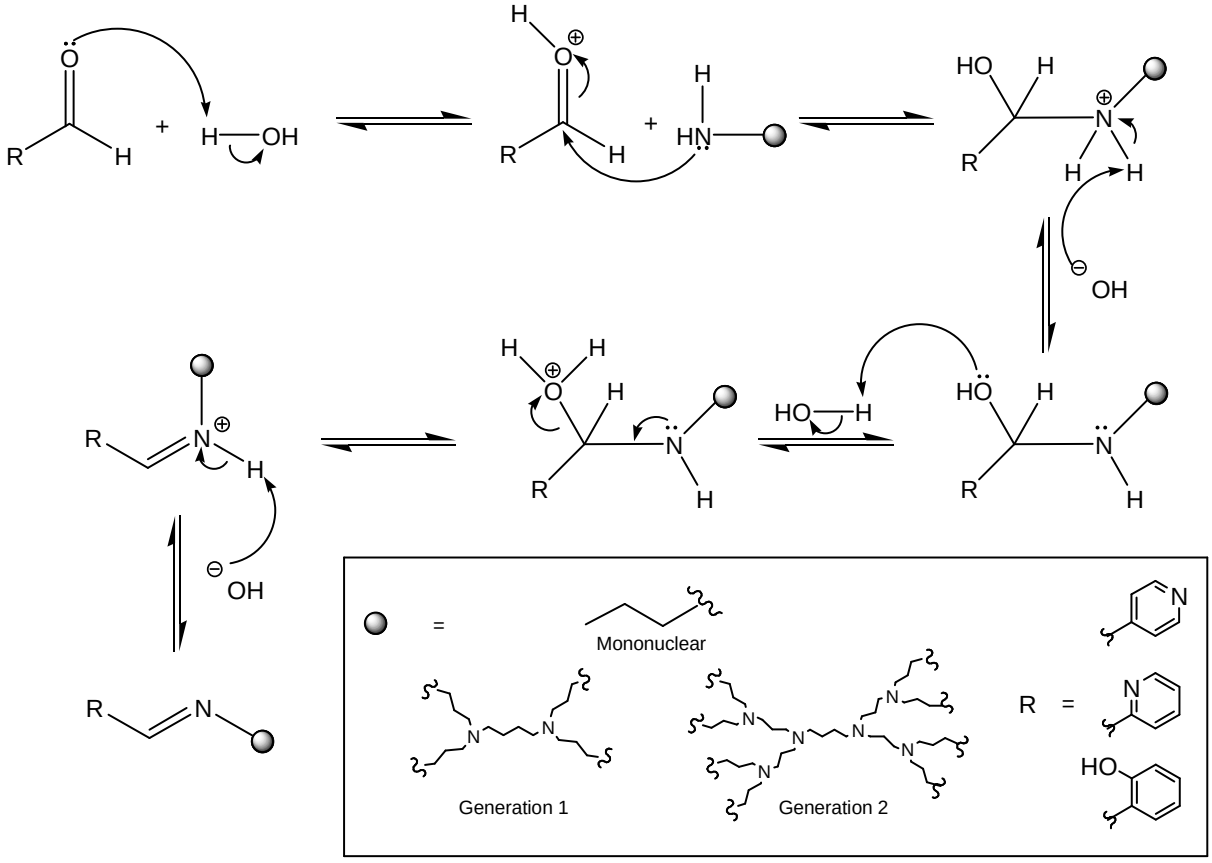

Scheme 2.1: *Mechanistic outline of a Schiff-base condensation reaction.*

This chapter describes the synthesis and characterisation of a series of monodentate and chelating bidentate ligands containing pyridyl-imine and salicylaldimine moieties. These compounds were characterized using a range of spectroscopic and analytical techniques, which include ^{1}H-NMR, ^{13}C{^{1}H}-NMR and infrared (IR) spectroscopy, mass spectrometry and elemental analysis.

2.2 Synthesis of 4-pyridyl-imine and 2-pyridyl-imine monomeric ligands (L1, L2)

Monomeric pyridylimine-functionalised ligands **L1** and **L2** were synthesized by reacting either the commercially available 4-pyridinecarboxaldehyde or the 2-pyridinecarboxaldehyde with *n*-propylamine (Scheme 2.2). The reactions were

stirred for 24 hours in the presence of anhydrous magnesium sulfate in dry diethyl ether. Isolation of the air stable organic products afforded pale-yellow (**L1**) and yellow (**L2**) oils, with yields of 71 % and 35 % respectively. The oils were soluble in most organic solvents such as dichloromethane, chloroform, methanol, toluene, diethyl ether, tetrahydrofuran, acetonitrile and dimethylsulfoxide.

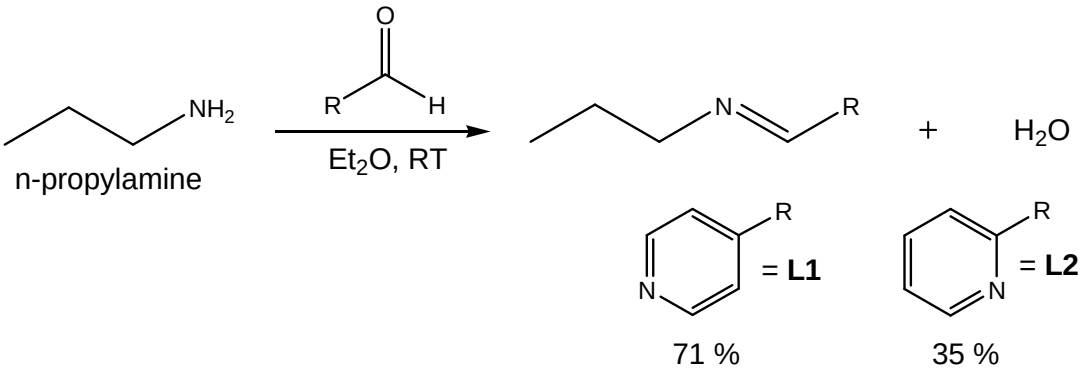

Scheme 2.2 *Outline for the synthesis of monomeric ligands (**L1** and **L2**).*

2.2.1 ^{1}H-NMR and ^{13}C{^{1}H}-NMR spectroscopy

The two monomeric ligands **L1** and **L2** were characterized by ^{1}H- and ^{13}C{^{1}H}-NMR spectroscopy and detailed chemical shifts were listed in Chapter 5. Evidence of the condensation reaction is clearly reflected by the ^{1}H-NMR spectrum (Fig. 2.2) of both **L1** and **L2**, which shows the disappearance of the NH_2 singlet around 0.90 ppm and the appearance of the $(CH)_{imine}$ singlet around 8.09 ppm for **L1** and around 8.36 ppm for **L2**. Further evidence is the shift of the triplet assigned to the CH_2 group adjacent to the nitrogen atom from 2.52 ppm (*n*-propylamine) to 3.73 ppm for **L1** and to 3.63 ppm for **L2**. The downfield shift of this signal is due to the electron withdrawing effects of the imine bond. Aromatic protons for the 4- and 2-pyridyl rings are seen in the ^{1}H-NMR spectra (Fig. 2.2) and showed typical chemical shifts for aromatic protons between 7 ppm and 9 ppm.

The ^{13}C{^{1}H}-NMR spectra for ligands **L1** and **L2** showed similar shifts for the aliphatic carbons in the region of 12-63 ppm with differences only observed in the shifts of the aromatic carbon signals. The 4-pyridyl-imine and 2-pyridyl-imine ligands showed aromatic signals between 121-159 ppm. The characteristic singlet observed for the

imine carbon at ~160 ppm confirms the Schiff-base condensation reaction, and the presence of the imine bond, for both ligands **L1** and **L2**.

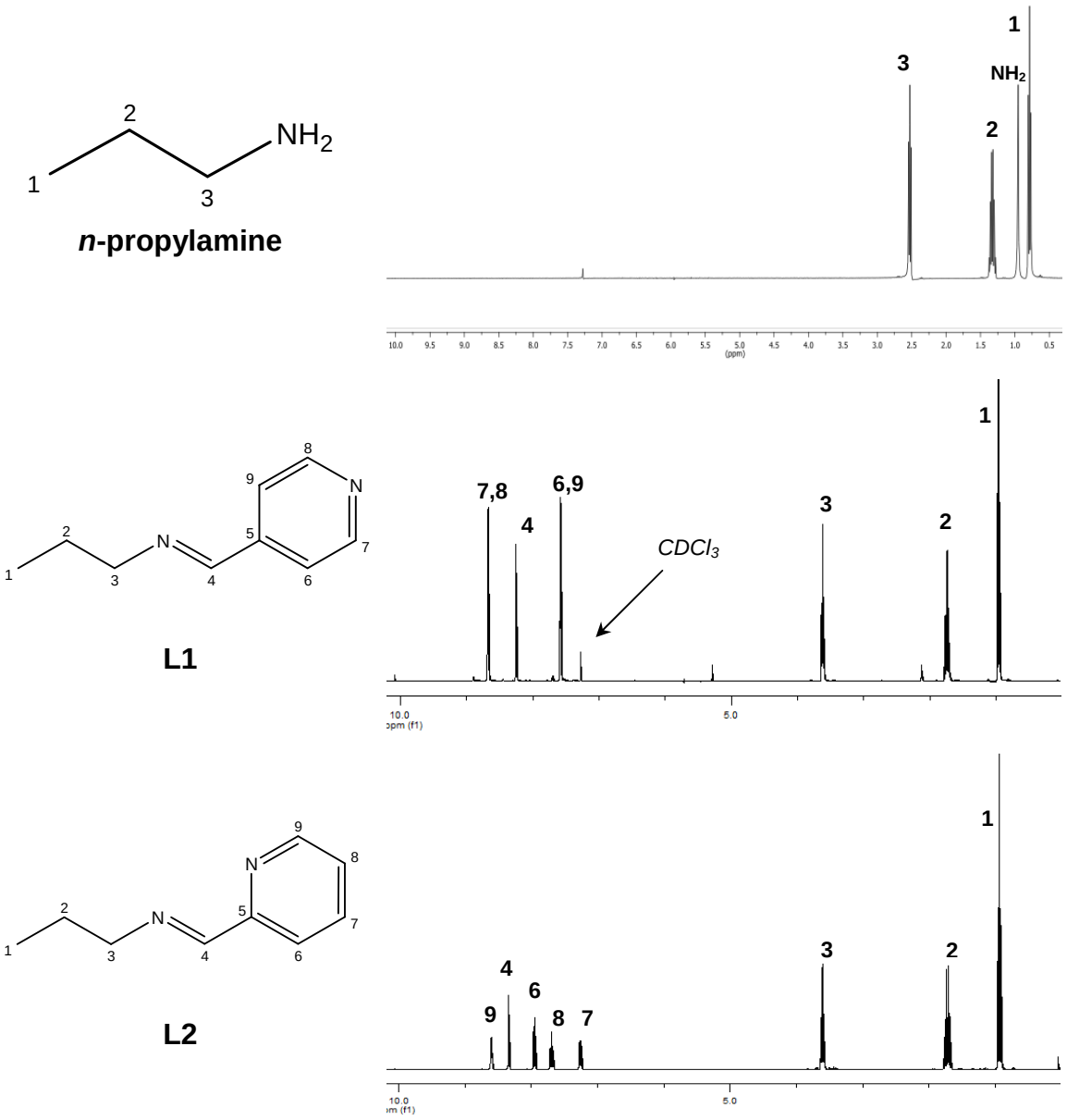

Figure 2.2: *^{1}H-NMR spectra of n-propylamine (top), ligand **L1** (middle) and ligand **L2** (bottom).*

2.2.2 Infrared (IR) spectroscopy

Infrared spectroscopy was also used as a diagnostic tool to show the formation of the imine bond of the iminopyridyl ligands **L1** and **L2**. The IR spectra of the two ligands **L1** and **L2** were recorded in dichloromethane using NaCl solution cells. In both cases, two strong absorption bands are observed around 1650 and 1590 cm^{-1}. These

which were assigned to the $(C=N)_{imine}$ stretching vibration and $(C=N)_{pyridyl}$ stretching vibration respectively.

2.2.3 Elemental analysis and mass spectrometry

Elemental analyses of the monomeric oils (**L1**, **L2**) were found to correlate with calculated results. The ^{1}H- , $^{13}C\{^{1}H\}$-NMR and IR spectral data was supported by ESI-MS data, which showed a molecular ion peak in the spectrum of each ligand at *m/z* 149 $[M+H]^+$ and 130 $[M-CH_3H_2]^+$ for ligand **L1** and **L2**, respectively.

2.3 Synthesis of 4-pyridyl-imine dendritic ligands (L3, L4)

The new 4-pyridyl-imine-functionalised dendritic ligands **L3** and **L4** were first synthesized in 2009.[10] In the formation of *N*- donor, monodentate ligands, dendritic ligands **L3** and **L4** were synthesized by reacting 4-pyridinecarboxaldehyde with DAB-*dendr*-$(NH_2)_n$ (n = 4, 8 for **L3**, **L4** respectively) (Scheme 2.3). The starting materials were stirred with anhydrous magnesium sulfate in toluene for 24 hours. The crude product was isolated and washed with copious amounts of distilled water to remove any unreacted aldehyde. With higher generations of dendrimers, the 'arms' of the dendrimer have the ability to fold-in towards the core, trapping unreacted aldehyde. Thus, washings were increased from 6 to 8 times with distilled water. This occurrence has also been observed with other poly(propyleneimine) dendrimers functionalised at the periphery with organic groups.[15] The organic products were isolated as a dark-orange oil for **L3** and an orange-yellow oil for **L4**, with yields ranging between 68-84 %. The dendrimers are soluble in most organic solvents such as dichloromethane, chloroform, methanol, diethyl ether and tetrahydrofuran.

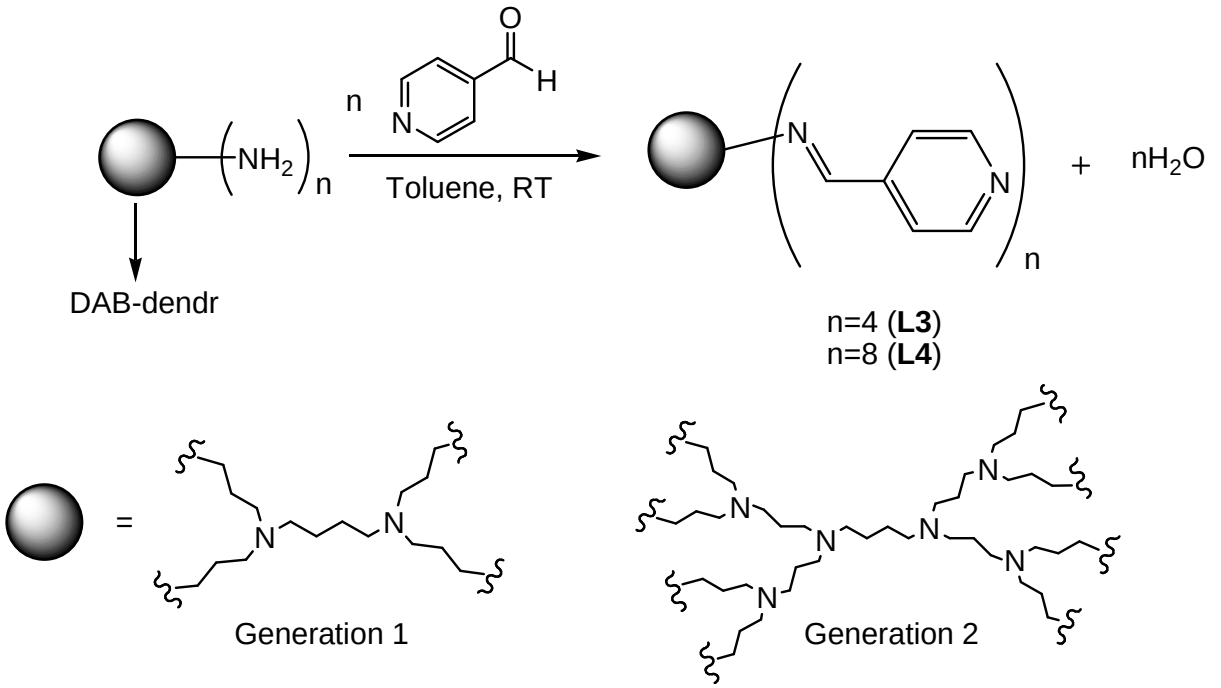

Scheme 2.3 *Outline for the synthesis of dendritic ligands (**L3** and **L4**).*

2.3.1 ^{1}H-NMR and ^{13}C{^{1}H}-NMR spectroscopy

The dendritic ligands **L3** and **L4** were characterized in deuterated chloroform using ^{1}H- and ^{13}C{^{1}H}-NMR spectroscopy. The chemical shifts are listed in Chapter 5 for both ligands **L3** and **L4**. The condensation reaction can be confirmed with the shift in the CH_2 signal, adjacent to the NH_2 of the starting 1st generation dendrimer, to around 3.63 ppm, in the ^{1}H-NMR spectrum of **L3** (Fig. 2.3). Two distinct doublets, typical of a para substituted aromatic ring, are seen with coupling constants (^{3}J~ 6.0 Hz) typical of vicinal protons, and assigned to the aromatic protons on the pyridyl rings. Further verification of the reaction is the appearance of a singlet at 8.23 ppm assigned to the imine proton. For the higher generation dendritic ligand **L4**, the ^{1}H-NMR spectrum shows a singlet assigned to the imine proton at around 8.17 ppm.

Both ligands **L3** and **L4** show complex ^{1}H-NMR spectra upon increasing dendrimer generation. The reason for this is the dendritic framework has a distinct set of aliphatic segments separated by nitrogen atoms. Confirmations of the higher generation aliphatic systems were made using 2D ^{1}H-NMR, by performing 2D-COSY

experiments on the ligands. Thus with the use of these experiments and other related publications,[11-14] spectra were assigned appropriately.

$^{13}C\{^{1}H\}$-NMR spectra for both ligands **L3** and **L4** showed similar spectra. Signals assigned to the aliphatic carbons were seen in the region of 25-60 ppm and aromatic carbons in the region of 121-150 ppm for both generations. As expected for both ligands, the imine-carbon was the most deshielded signal at 159 ppm.

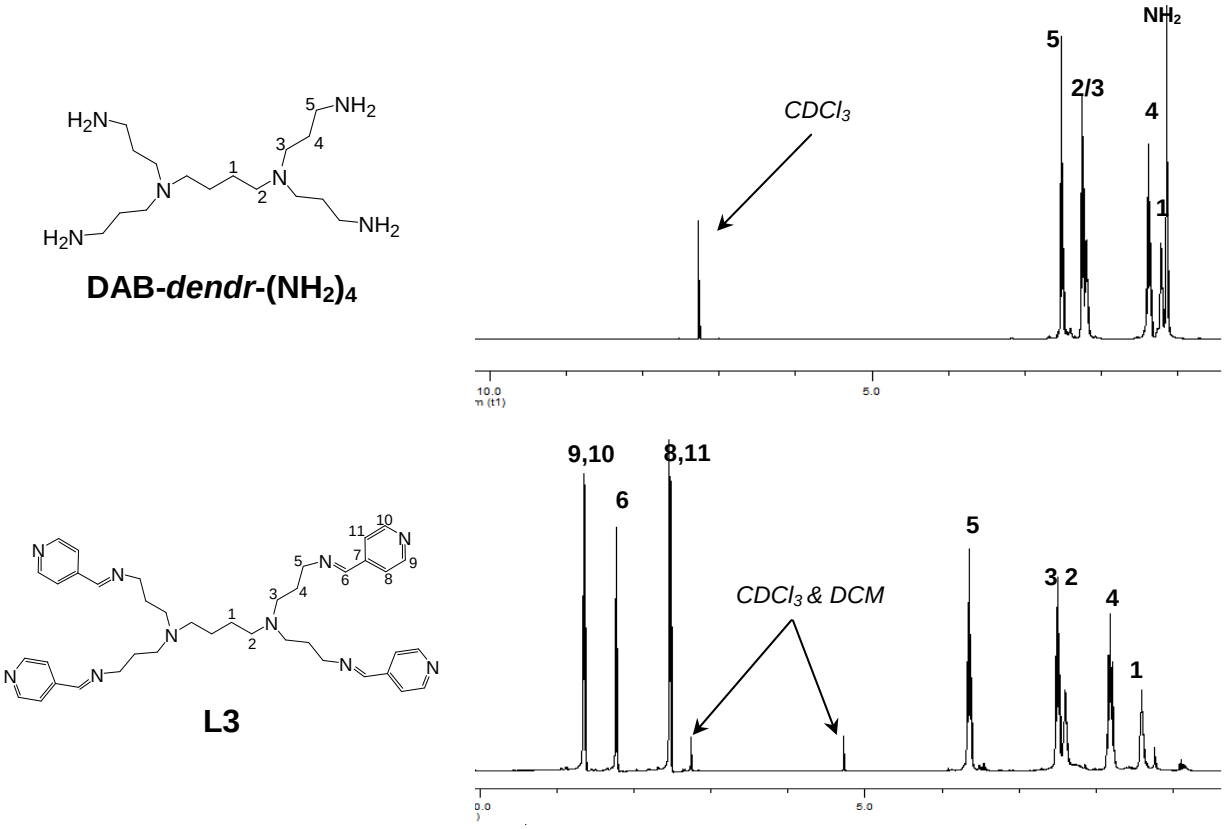

Figure 2.3: *^{1}H-NMR spectra of* ***DAB-dendr-(NH$_2$)$_4$*** *(top) and dendritic ligand* ***L3*** *(bottom).*

2.3.2 Infrared (IR) spectroscopy

Infrared spectroscopy was used to give a qualitative description of the end-group moiety, illustrating the presence of the imine bond in ligands **L3** and **L4**. The dendritic ligands (**L3**, **L4**) were recorded in dichloromethane utilising NaCl solution cells. Similar to the monomeric ligand **L1**, two strong absorption bands appeared at ~1647 cm^{-1} and 1599 cm^{-1} and were assigned the $(C=N)_{imine}$ vibration and $(C=N)_{pyridyl}$ vibrations.

2.3.3 Elemental analysis and mass spectrometry

Elemental analysis results showed percentages of which were outside acceptable limits. As mentioned before, dendrimers have the ability to trap solvent molecules or excess aldehyde within the dendritic framework. Evidence of this can be seen in the ^{1}H-NMR spectra of **L3**, where a strong dichloromethane peak can be noted at 5.25 ppm and a small peak at around 10 ppm for the aldehyde moiety. Thus, with the inclusion of solvent molecules, the recalculated values were found to be in acceptable limits to the values found by elemental analysis. This is also the case for the higher generation **L4**.

The ^{1}H-NMR, ^{13}C{^{1}H}-NMR and IR spectral data were supported by FAB-MS data, which showed the molecular ion peak in the spectrum of each ligand at *m/z* 673 $[M]^{+}$ and 1485 $[M]^{+}$ for ligand **L3** and **L4** respectively.

2.4 Synthesis of 2-pyridyl-imine dendritic ligands (L5, L6)

A series of *N,N*- chelating, bidentate, dendritic ligands **L5** and **L6** were synthesized *via* a condensation reaction, by a route similarly used by Smith and co-workers (Scheme 2.4).[12,13] The dendritic starting material was stirred with 2-pyridinecaboxaldehyde and anhydrous magnesium sulfate in toluene for 24 hours. The crude products were isolated by filtration and rotatory evaporation of the reaction solution. The purification method used was similar to that of dendritic ligands **L3** and **L4**. Drying of the products under reduced pressure yielded a yellow-brown oil and an orange-yellow oil for ligands **L5** and **L6** respectively, in relatively good yields of 61 % and 74 % respectively. The oils were found to be soluble in most organic solvents such as dichloromethane, chloroform, methanol, toluene, diethyl ether, tetrahydrofuran, acetonitrile and dimethylsulfoxide.

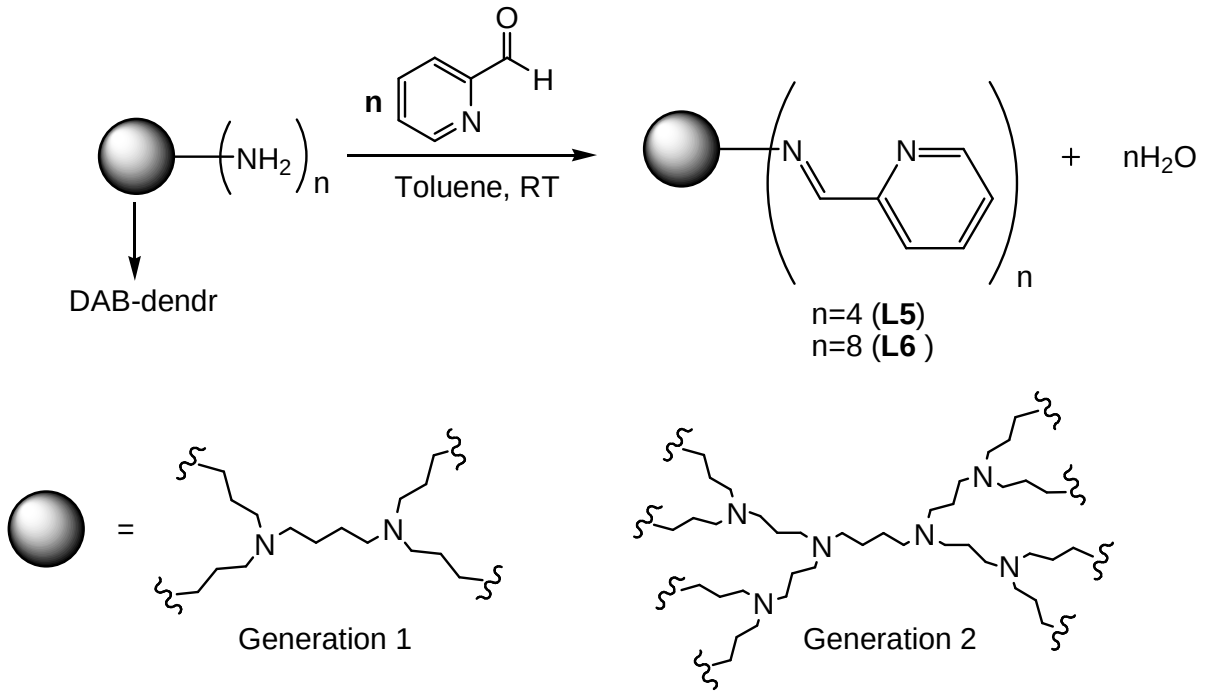

Scheme 2.4 *Outline for the synthesis of dendritic ligands (**L5** and **L6**).*

2.4.1 ^{1}H- NMR and ^{13}C{^{1}H}-NMR spectroscopy

The successful reaction of the aldehyde with the DAB dendrimers (**DAB-*dendr*-$(NH_2)_4$** or **DAB-*dendr*-$(NH_2)_8$**) was confirmed from the ^{1}H- and ^{13}C{^{1}H}-NMR spectra (Chapter 6) of oils **L5** and **L6** (Fig. 2.4). Evidence for the formation of 2-pyridylimine dendrimers **L5** and **L6** (similar to **L3** and **L4**), is supported by the downfield shift of the triplet assigned for the CH_2 moiety adjacent to the imine bond. Other evidence is the singlet corresponding to the imine proton at 8.35 ppm for **L5** and 8.33 ppm for **L6**. The aromatic protons of the pyridyl rings for both the first and second generations showed similar resonance to their monomeric analogue **L2**. As mentioned earlier, the higher generations of dendrimer showed slightly more complex ^{1}H-NMR spectra, resulting in the overlap of signals for the aliphatic protons.

^{13}C{^{1}H}-NMR spectra for both ligands **L5** and **L6** were similar. Signals for the aliphatic carbons were observed in the region of 22-60 ppm and aromatic carbons in the region of 121-155 ppm for both generations (**L5** and **L6**). As seen for the 4-pyridylimine-functionalised ligands, the imine-carbon was the most deshielded signal at 159 ppm and 162 ppm for **L5** and **L6** respectively.

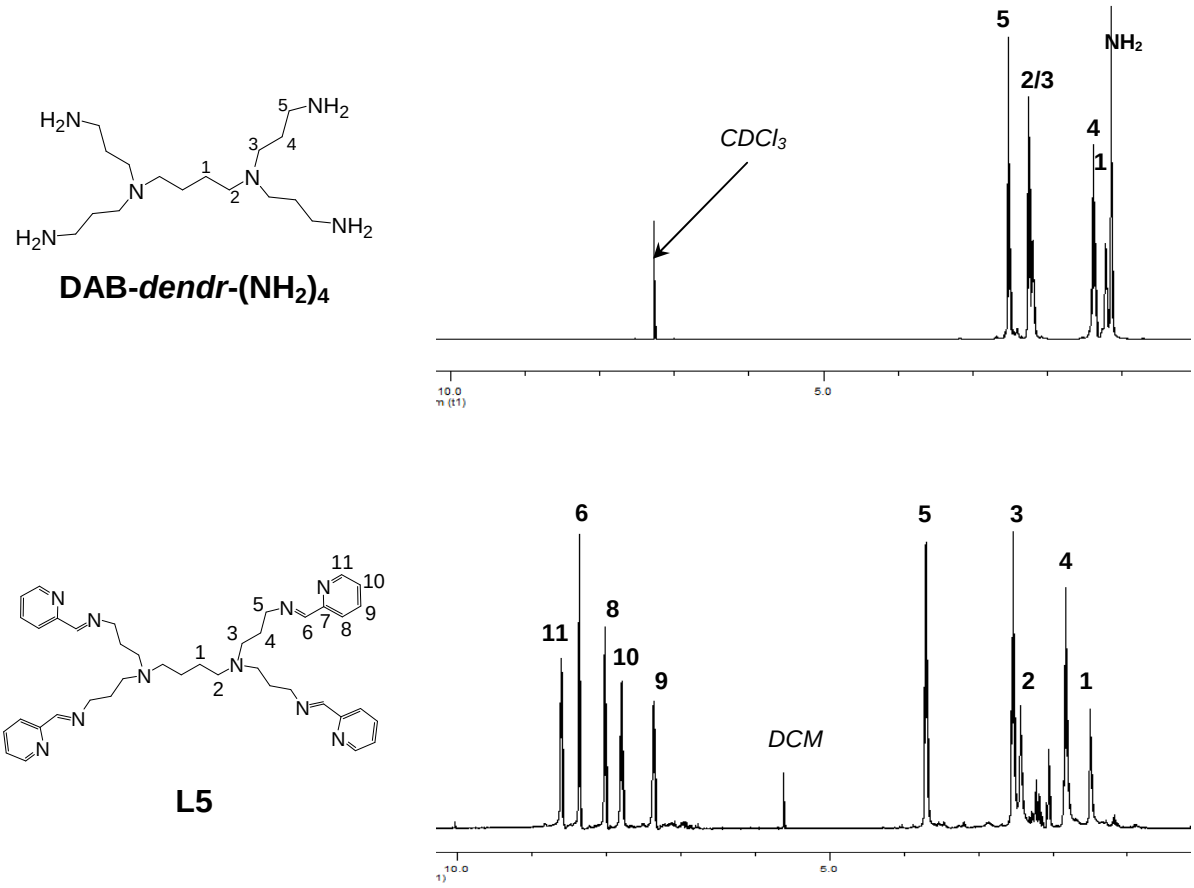

Figure 2.4: *^{1}H-NMR spectra of* ***DAB-dendr-(NH$_2$)$_4$*** *(top) and dendritic ligand* ***L5*** *(bottom).*

2.4.2 Infrared (IR) spectroscopy

To confirm that the Schiff-base condensation and the formation of the imine bond had occurred, the infrared spectra of ligands **L5** and **L6** were recorded on NaCl solution cells in dichloromethane. Similar to the monomeric equivalent **L2**, strong absorption bands are seen in the regions of 1649 cm^{-1} and 1588 cm^{-1} and were assigned to the $(C=N)_{imine}$ and $(C=N)_{pyridyl}$ vibrations.

2.4.3 Elemental analysis and mass spectrometry

Elemental analysis was obtained on both the 1st and 2nd generation dendritic ligands (**L5**, **L6**). The purification procedures were similar to that of the 4-pyridylimine-functionalised ligands, using dichloromethane. The higher generations showed percentages outside acceptable limits, this can ascribed to possible solvent inclusion, and also seen in the ^{1}H-NMR spectrum of **L5** and **L6**. Recalculation of the

percentages with the inclusion of half a molecule of dichloromethane gave percentages within acceptable limits. The phenomenon is also observed in other poly(propyleneimine) dendrimers functionalised at the periphery with organic groups.[15] The ^{1}H-, ^{13}C{^{1}H}-NMR and IR spectral data was supported by FAB-MS data, which showed the molecular ion peak in the spectrum of each ligand at *m/z* 673 $[M]^{+}$ and 1485 $[M]^{+}$ for ligand **L5** and **L6** respectively.

2.5 Synthesis of salicylaldimine monomeric ligand (L7)

Prior to the synthesis of the dendritic *N,O*- chelating , bidentate ligands, the monomeric salicylaldimine ligand **L7** was synthesized using a similar method to that of the monomeric ligands **L1** and **L2**, *via* a Schiff-base condensation reaction. The commercially available starting materials, salicyldehyde and *n*-propylamine, were reacted in the presence of anhydrous magnesium sulfate, and stirred at room temperature in ethanol for 5 hours (Scheme 2.5). The crude product was isolated and purified by washing with copious amounts of distilled water. The purified ligand was isolated as an orange-yellow oil in 72 % yield. The oil was soluble in most organic solvents such as dichloromethane, chloroform, methanol, toluene, diethyl ether, tetrahydrofuran, acetonitrile and dimethylsulfoxide.

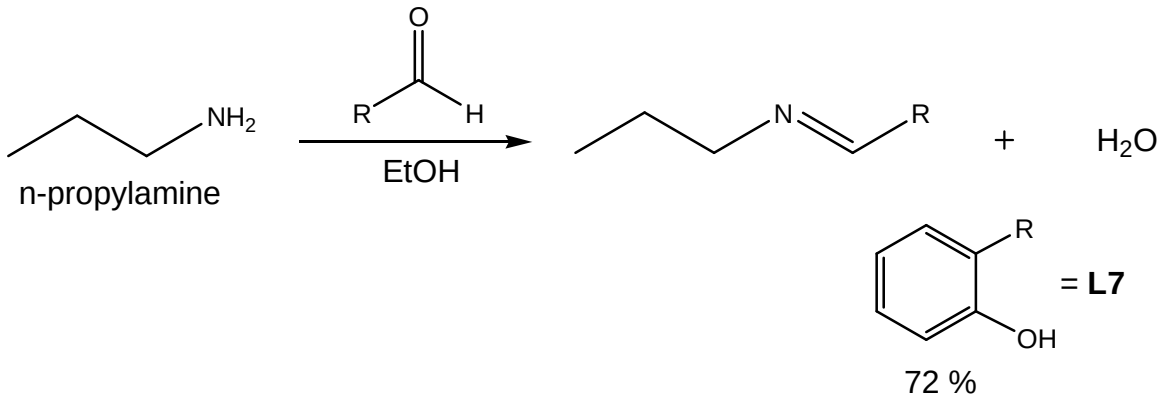

Scheme 2.5 *Outline for the synthesis of monomeric ligand (**L7**).*

2.5.1 ^{1}H-NMR and ^{13}C{^{1}H}-NMR spectroscopy

The reaction between *n*-propylamine and salicyldehyde resulted in the formation of monomeric ligand **L7**, and can be confirmed from ^{1}H- and ^{13}C{^{1}H}-NMR spectroscopy. ^{1}H- and ^{13}C{^{1}H}-NMR spectra were recorded in deuterated chloroform. In the ^{1}H-NMR spectrum of the ligand **L7**, the characteristic shift of the CH_2 group (adjacent to the newly formed imine bond) was observed from 2.52 ppm to 3.56 ppm (Fig. 2.5). This is an expected shift due to the electron withdrawing effect of the imine group. The peaks assigned to the aromatic protons appear between 6.00 ppm and 8.00 ppm. Further confirmation can be seen in the appearance of the singlet assigned to the imine proton at 8.32 ppm. A broad signal was observed at 13.66 ppm, which was assigned to the proton on the hydroxyl group.

The ^{13}C{^{1}H}-NMR spectrum of the monomeric ligand **L7** showed 3 signals upfield, assigned to the aliphatic carbons in the aliphatic region. Signals assigned to the carbons of the aromatic ring were seen between 117 ppm and 132 ppm. The signal assigned to the carbon of the imine group appeared at 164 ppm.

2.5.2 Infrared (IR) spectroscopy

The infra-red spectrum of the monomeric ligand **L7** was recorded using a NaCl solution cell in dichloromethane, to assist in confirming the formation of the imine bond. A strong sharp absorption band was seen at 1635 cm^{-1} which was assigned to the $(C=N)_{imine}$ stretching frequency.

2.5.3 Elemental analysis and mass spectrometry

The microanalysis of **L7** was found to be within acceptable limits, confirming the integrity of the proposed structure. Further complementing our proposed structure was the ESI-MS data, which showed a molecular ion peak at *m/z* 164 $[M+H]^{+}$.

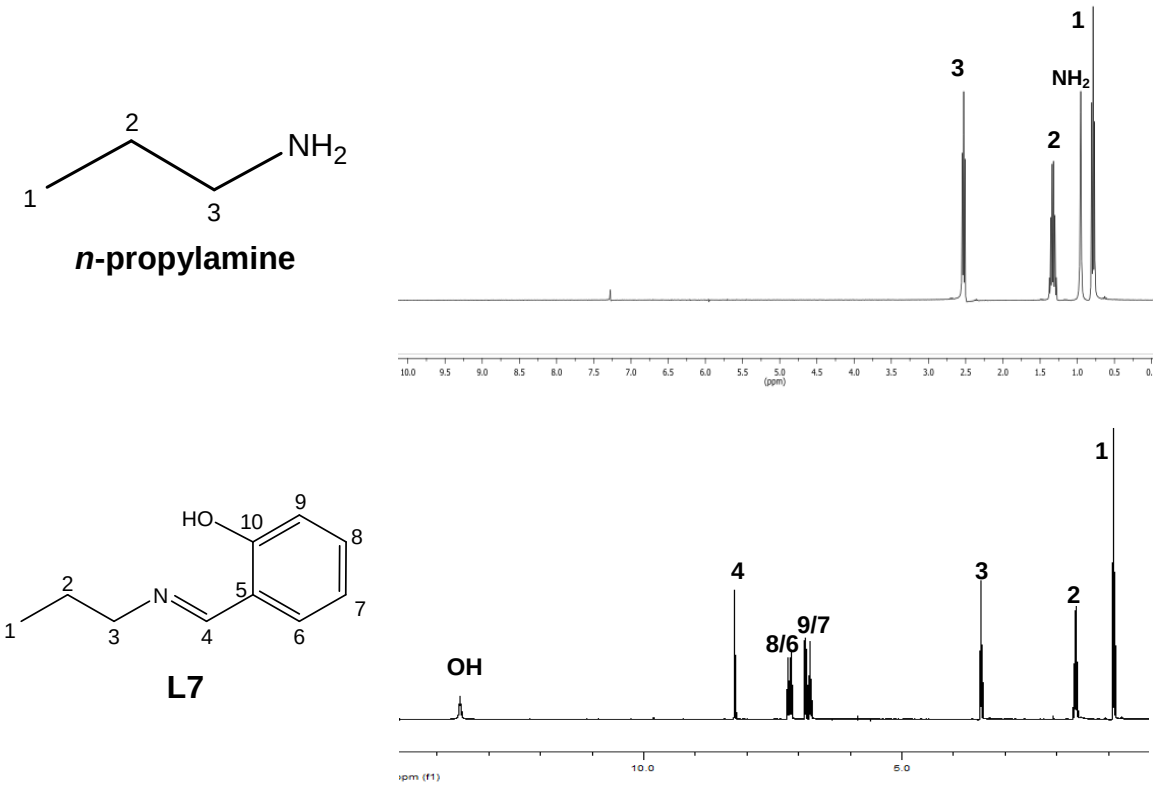

Figure 2.5: *^{1}H-NMR spectra of n-propylamine (top) and ligand **L7** (bottom).*

2.6 Synthesis of salicylaldimine dendritic ligands (L8, L9)

The salicylaldimine dendritic ligands **L8** and **L9** were formed using the method reported by Malgas and co-workers.[16] Salicyldehyde was added to a solution of the DAB-*dendr*-$(NH_2)_n$ (n = 4, 8 for **L8**, **L9** respectively) in toluene (Scheme 2.6). The reaction was stirred at 40 ^{o}C overnight. A crude oil was isolated. Once purified the 1st generation ligand **L8** was isolated as a bright yellow solid in 51 % yield. The 2nd generation ligand **L9** was isolated as an orange oil in 92 % yield. The dendritic ligands **L8** and **L9** are soluble in most organic solvents such as dichloromethane, chloroform, methanol, diethyl ether and tetrahydrofuran.

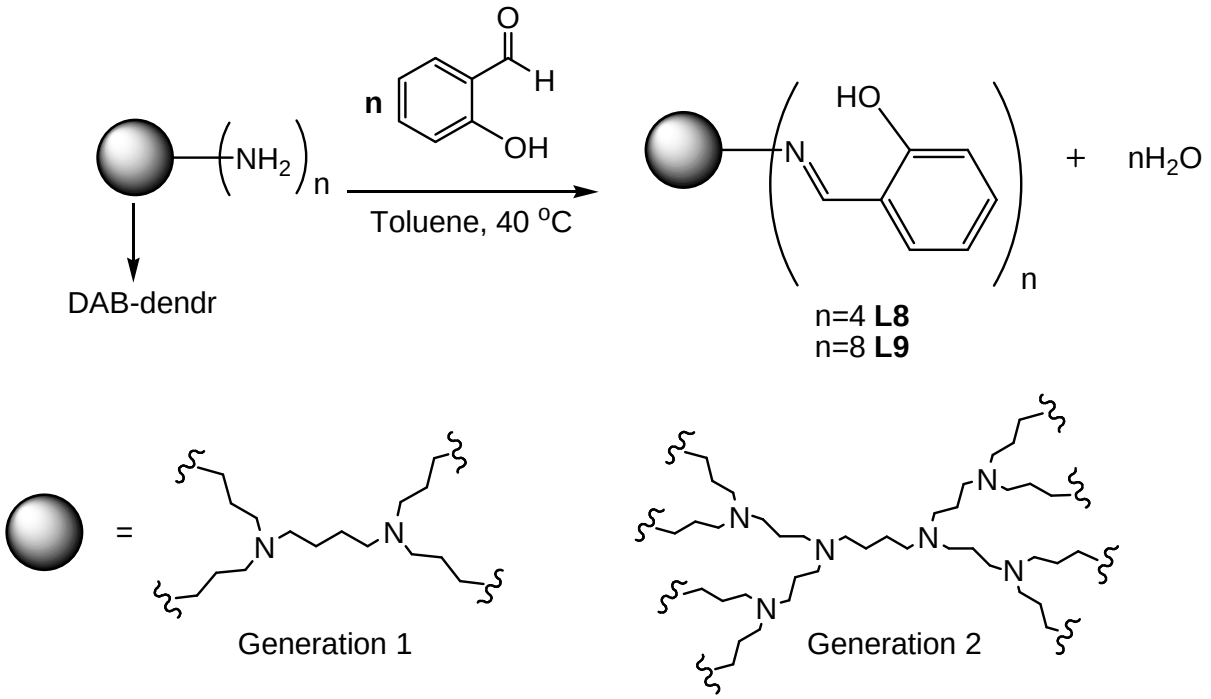

Scheme 2.6: *Outline for the synthesis of dendritic ligands (**L8** and **L9**).*

2.6.1 ^{1}H-NMR and ^{13}C{^{1}H}-NMR spectroscopy

The ^{1}H- NMR and ^{13}C{^{1}H}-NMR spectra of ligands **L8** and **L9** was recorded in deuterated chloroform. The ^{1}H-NMR spectra of the dendritic ligands showed a distinct shift in the signal assigned to CH_2 group adjacent to the imine nitrogen from 2.52 ppm to 3.60 ppm for **L8** and 3.58 ppm for **L9** (Fig. 2.6). The shift in the signal is expected due to the electron withdrawing effects experienced by the imine group. The aliphatic protons of the core and of the branches of the dendritic ligand **L8** appear between 1.40 ppm and 3.60 ppm. The higher generation dendritic ligand **L9** showed a more complex ^{1}H-NMR spectrum, resulting in the overlap of signals for the aliphatic protons. The aromatic protons resonate in a similar range to the monomeric ligand **L7**, between 6.82 ppm and 7.27 ppm for both dendritic ligands **L8** and **L9**. The imine and hydroxyl protons were observed around 8.30 ppm and 13.50 ppm respectively for both dendritic ligands.

^{13}C{^{1}H}-NMR spectra for both dendritic ligands **L8** and **L9** showed similar pattern. Signals for the aliphatic carbons were seen in the region of 24-57 ppm and aromatic carbons in the region of 117-132 ppm for both generations. Similar to the

pyridylimine-functionalised ligands the signal assigned to the imine-carbon was the most deshielded signal at 165 ppm for both dendritic ligands **L8** and **L9**.

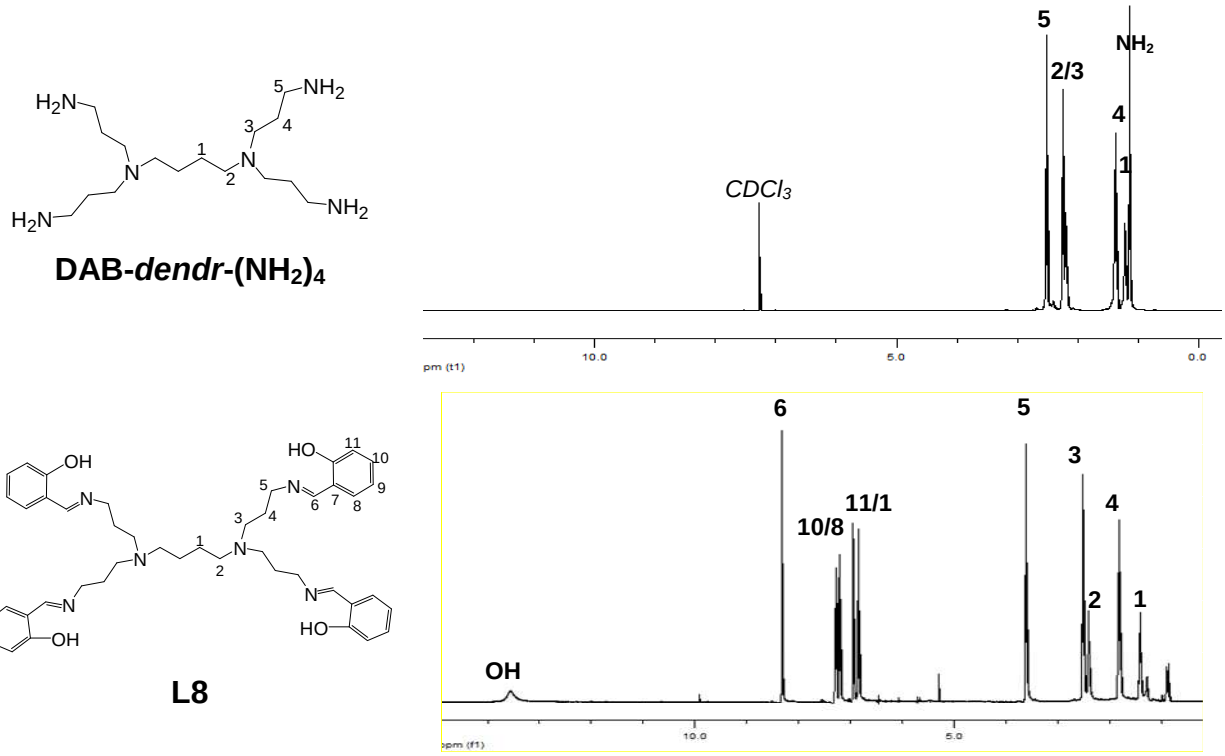

Figure 2.6: *^{1}H-NMR spectra of **DAB-dendr-(NH$_2$)$_4$** (top) and dendritic ligand **L8** (bottom).*

2.6.2 Infrared (IR) spectroscopy

Infrared spectra were used to give a qualitative characterisation of the end group functionalized moiety. The dendritic ligands **L8** and **L9** were recorded in dichloromethane in NaCl solution cells. Similar to the monomeric ligand **L7**, a strong sharp absorption band appears at ~1631 cm^{-1} for ligand **L8** and 1635 cm^{-1} for ligand **L9**, assigned to the $(C=N)_{imine}$ vibration.

2.6.3 Elemental analysis and mass spectrometry

The elemental analysis data was found to be within acceptable limits and confirms the proposed structures for both dendritic ligands **L8** and **L9**, without the presence of solvent inclusions.

Formation of **L7** and **L8** was further supported by FAB-MS data, which showed molecular ion peak in the spectrum of each ligand at *m/z* 733 $[M]^+$ and 1607 $[M]^+$ for dendritic ligands **L8** and **L9** respectively.

2.7 Conclusions

A range of *N*- (**L1**, **L3**, **L4**), *N,N*- (**L2**, **L5**, **L6**) and *N,O*- (**L7**, **L8**, **L9**) donor monodentate and chelating bidentate ligands were prepared. The synthesized compounds were characterized using a range of spectroscopic and analytical techniques, namely ^{1}H-, ^{13}C{^{1}H}- NMR and IR spectroscopy; and mass spectrometry and elemental analysis.

2.8 References

1) U. Boas, J. B. Christensen and P. M. H. Heegaard, in *Dendrimers in Medicine and Biotechnology: New Molecular Tools*, RSC Publishing, 2006.
2) C. C. Lee, J. A. MacKay, J. M. J. Fréchet and F. C. Szoka, *Nature Biotech.*, 2005, **23**, 1517.
3) D. A. Tomalia, L. A. Reyna and S. Svenson, *Biochem. Soc. Trans.*, 2007, **35**, 61.
4) F. Aulenta, W. Hayes and S. Rannard, *Eur. Polym. J.*, 2003, **39**, 1741.
5) Y. Cheng, J. Wang, T. Rao, X. He and T. Xu, *Front. Biosci.*, 2008, **13**, 1447.
6) J. B. Wolinsky and M. W. Grinstaff, *Adv. Drug Deliv. Rev.*, 2008, **60**, 1037.
7) A. Agarwal, S. Saraf, A. Asthana, U. Gupta, V. Gajbhiye and N. K. Jain, *Int. J. Pharm.*, 2008, **350**, 3.
8) E. R. Gillies and J. M. J. Fréchet, *Drug Discov. Today*, 2005, **10**, 35.
9) S.-G. Sampathkumar, and K. J. Yarema, in *Nanomaterials for Cancer Diagnosis*, Ed. C. S. S. R. Kumar , Wiley-VCH, 2007, vol. 7.
10) P. Govender, N. C. Antonels, J. Mattsson, A. K. Renfrew, P. J. Dyson, J. R. Moss, B. Therrien and G. S. Smith, *J. Organomet. Chem.*, 2009, **694**, 3470.
11) P. Di Bernardo, P. L. Zanonato, S. Tamburini, P. A. Vigato, *Inorg. Chim. Acta*, 2007, **360**, 1083.
12) G. Smith, R. Chen and S. Mapolie, *J. Organomet. Chem.*, 2003, **673**, 111.
13) G. S. Smith and S. F. Mapolie, *J. Mol. Catal. A: Chem.*, 2004, **213**, 187.
14) J. Cloete and S. F. Mapolie, *J. Mol. Catal. A: Chem.*, 2006, **243**, 221.
15) J. F. G. A. Jansen, E. M. M. de Brabander-van den Berg and E. W. Meijer, *Science*, 1994, **266**, 1226.

Chapter 3

Synthesis and Characterization of Multinuclear Ruthenium(II) Arene Complexes of Pyridyl-imine and Salicylaldimine Ligands

3.1 Introduction

Ruthenium(II) arene complexes are reported to have a wide range of applications in the fields of catalysis,[1] supramolecular self assemblies[2] and in the field of medicinal chemistry, displaying antiviral,[3] antibiotic[4,5] and anticancer activities.[6] The ruthenium(II) arene complexes have the typical half-sandwich geometry known as the "three-legged piano stool" complexes (Fig. 3.1), with a pseudo-tetrahedral geometry around the ruthenium centre. The arene ring occupies one coordination site (the seat) and the ligands occupy the remaining three sites (the legs). The arene π system stabilizes the +2 oxidation state and prevents rapid oxidation into the +3 oxidation state.

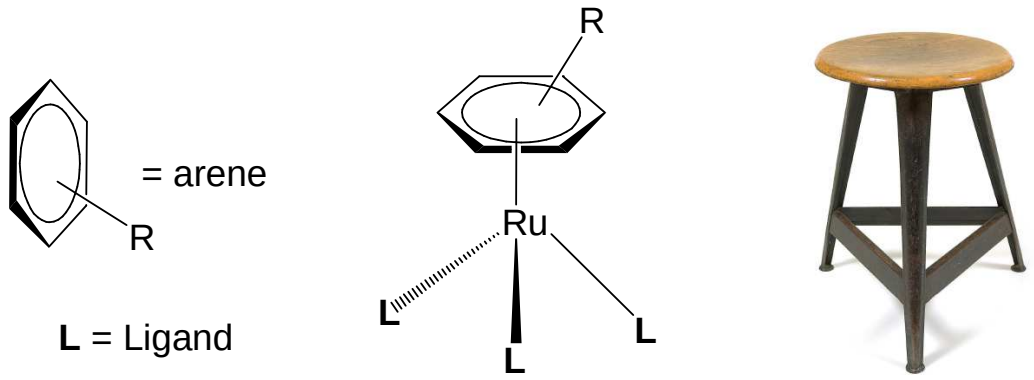

Figure 3.1: *Line drawing of a ruthenium(II) arene compound, illustrating the 'three-legged piano stool" structure.*

In synthesizing ruthenium(II) arene complexes, ruthenium-arene dimers are synthesized by reacting the ruthenium(III) salt (**$RuCl_3.nH_2O$**) with a diene to give rise to a ruthenium-arene dimer. The ruthenium-arene dimers or precursors (**$[Ru(\eta^6\text{-}p\text{-}Pr^iC_6H_4Me)Cl_2]_2$** and **$[Ru(\eta^6\text{-}C_6Me_6)Cl_2]_2$**) were synthesized *via* two routes. The most common route involves reacting the ruthenium salt (**$RuCl_3.nH_2O$**) with a cyclohexadiene ligand in methanol or ethanol (Scheme 3.1-Route **A**).[7] The second

route involves the exchange of the π ligand at elevated temperatures (Scheme 3.2-Route **B**).[8]

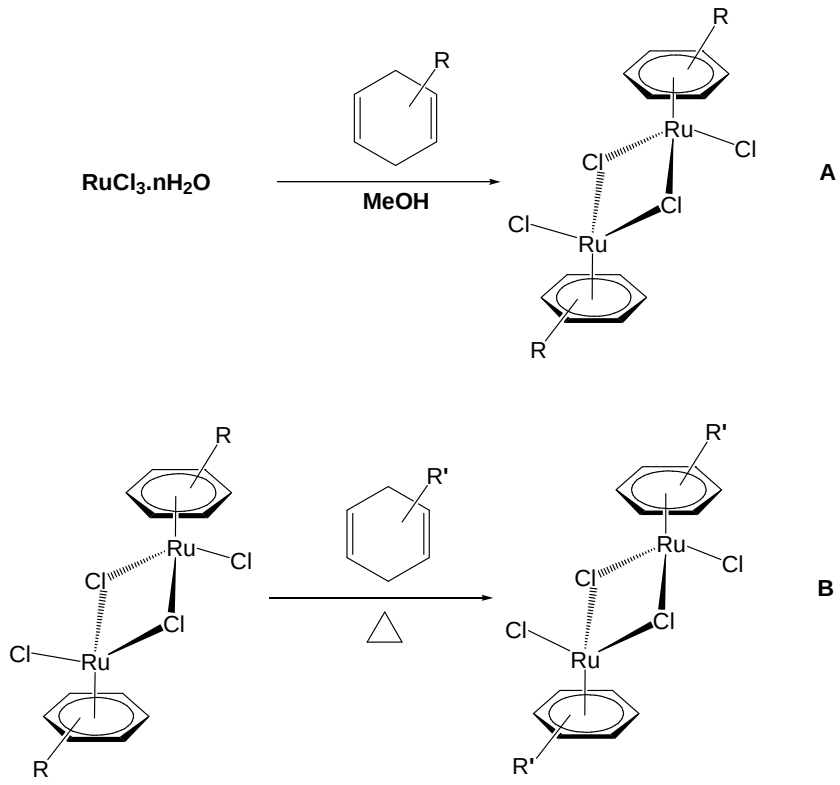

Scheme 3.1: *General synthesis of ruthenium(II) arene precursors.*

Reactions involving the chloro-bridged dimers with a range of ligands, generally afford half sandwich ruthenium(II) arene complexes. This chapter describes the synthesis and characterisation of a series of half sandwich ruthenium(II) arene monodentate and chelating bidentate, neutral and cationic, mononuclear and multinuclear complexes. These dendritic compounds were characterized using a range of spectroscopic and analytical techniques, including ^{1}H-NMR, ^{13}C{^{1}H}-NMR and infrared (IR) spectroscopy, mass spectrometry, and elemental analysis.

3.2 Synthesis of neutral 4-pyridyl-imine mononuclear and dendritic ruthenium(II) arene complexes (1 - 6)

The general method of complexation involved stirring a solution of the ligand (**L1**, **L3**, **L4**) and the dimer (**[Ru(η^6-*p*-Pr^{i}C$_6$H$_4$Me)Cl$_2$]** or **[Ru(η^6-C$_6$Me$_6$)Cl$_2$]$_2$**) in dichloromethane at room temperature. The reactions were generally allowed to

proceed for 24 hours with the mononuclear reaction proceeding for a shorter period. The complexation reactions yielded two new mononuclear complexes (**1**, **2**) and four new dendritic complexes (**3** - **6**).

The 4-pyridyl-imine ligands **L1**, **L3** and **L4** yield neutral monodentate complexes, such that coordination of the ruthenium metal occurs only at the pyridyl nitrogen atom. The rationale for the synthesis of the mononuclear complexes (**1**, **2**), was to help investigate properties, assist in characterisation and optimize methodology before synthesising the larger more complex metallodendrimers (**3** - **6**).

In the synthesis of complexes **1** - **6**, m equivalents (where m = 2 for **1** and **2**; m = 0.5 for **3** and **4**; m = 0.25 for **5** and **6**) of the ligand (**L1** for **1** and **2**, **L3** for **3** and **4**, **L4** for **5** and **6**) were added to a solution of the ruthenium dimer (**[Ru(η^6-*p*-Pr^{i}C$_6$H$_4$Me)Cl$_2$]** for **1**, **3**, **5**; **[Ru(η^6-C$_6$Me$_6$)Cl$_2$]$_2$** for **2**, **4**, **6**) in dichloromethane (Scheme 3.2).

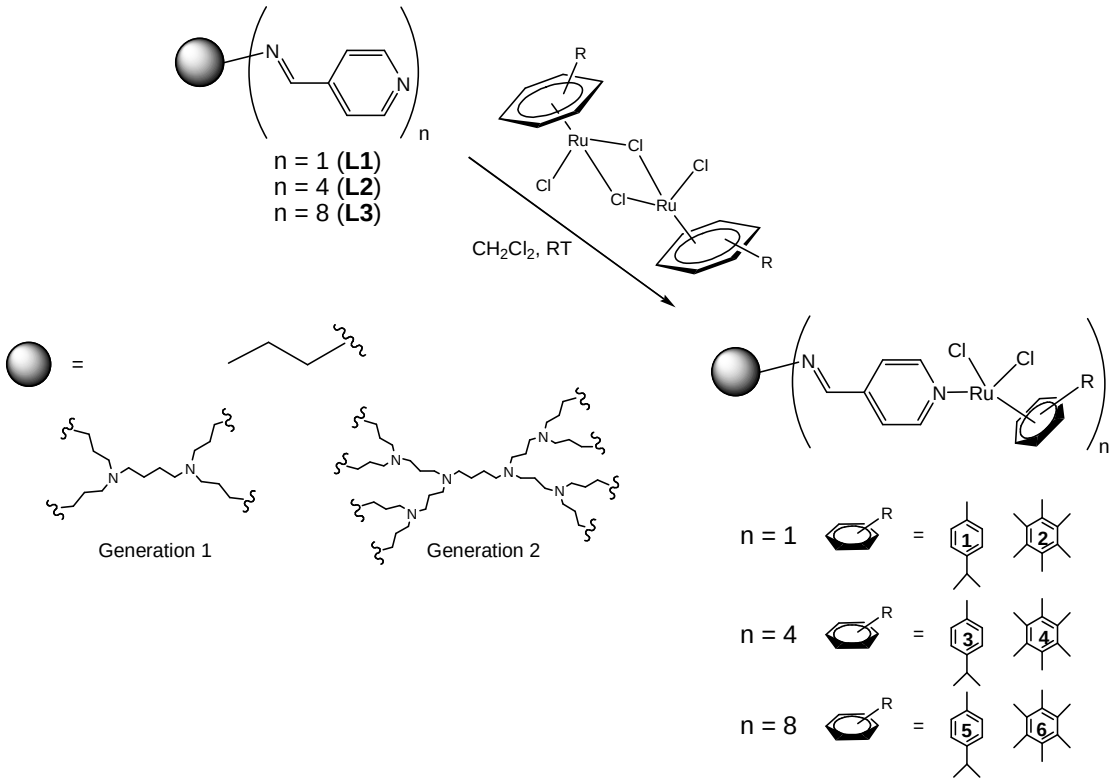

Scheme 3.2: *Outline synthesis of neutral ruthenium(II) arene complexes (**1** - **6**).*

The reaction was stirred overnight and the solvent reduced. The product was precipitated from solution with petroleum ether and further washed with the same solvent.

3.2.1 Physical properties

The complexes were dried under vacuum and were isolated as yellow solids in moderate to high yields, and were found to be thermally stable (Table 3.1).

***Table 3.1**: Physical appearance, percentage yield and melting points for complexes **1** - **6**.*

Complex	Physical Appearance	Yield (%)	Melting Point (^{o}C)
1	Mustard- yellow solid	46	163 - 166
2	Yellow-orange solid	50	139[a]
3	Mustard- yellow solid	79	165[a]
4	Yellow solid	87	188[a]
5	Mustard- yellow solid	98	214[a]
6	Yellow solid	92	194[a]

[a]*Decompose without melting into a black solid*

Ruthenium(II) arene complexes **1** - **6** are non-hygroscopic, air-stable and soluble in most organic solvents, such as dichloromethane, chloroform, ethanol, dimethylsulfoxide, acetone and acetonitrile, and insoluble in diethyl ether, petroleum ether and tetrahydrofuran.

3.2.2 ^{1}H-NMR and ^{13}C{^{1}H}-NMR spectroscopy

Coordination of the ruthenium-arene moiety to the pyridyl nitrogen was confirmed by ^{1}H-NMR spectroscopy in chloroform-*d*. The ^{1}H-NMR spectrum (Fig. 3.2) of complex **1** and **2** showed the presence of peaks associated with the complexation of ligand **L1** and the ruthenium dimer (**[Ru(η^6-*p*-Pr^{i}C$_6$H$_4$Me)Cl$_2$]** or **[Ru(η^6-C$_6$Me$_6$)Cl$_2$]$_2$**).

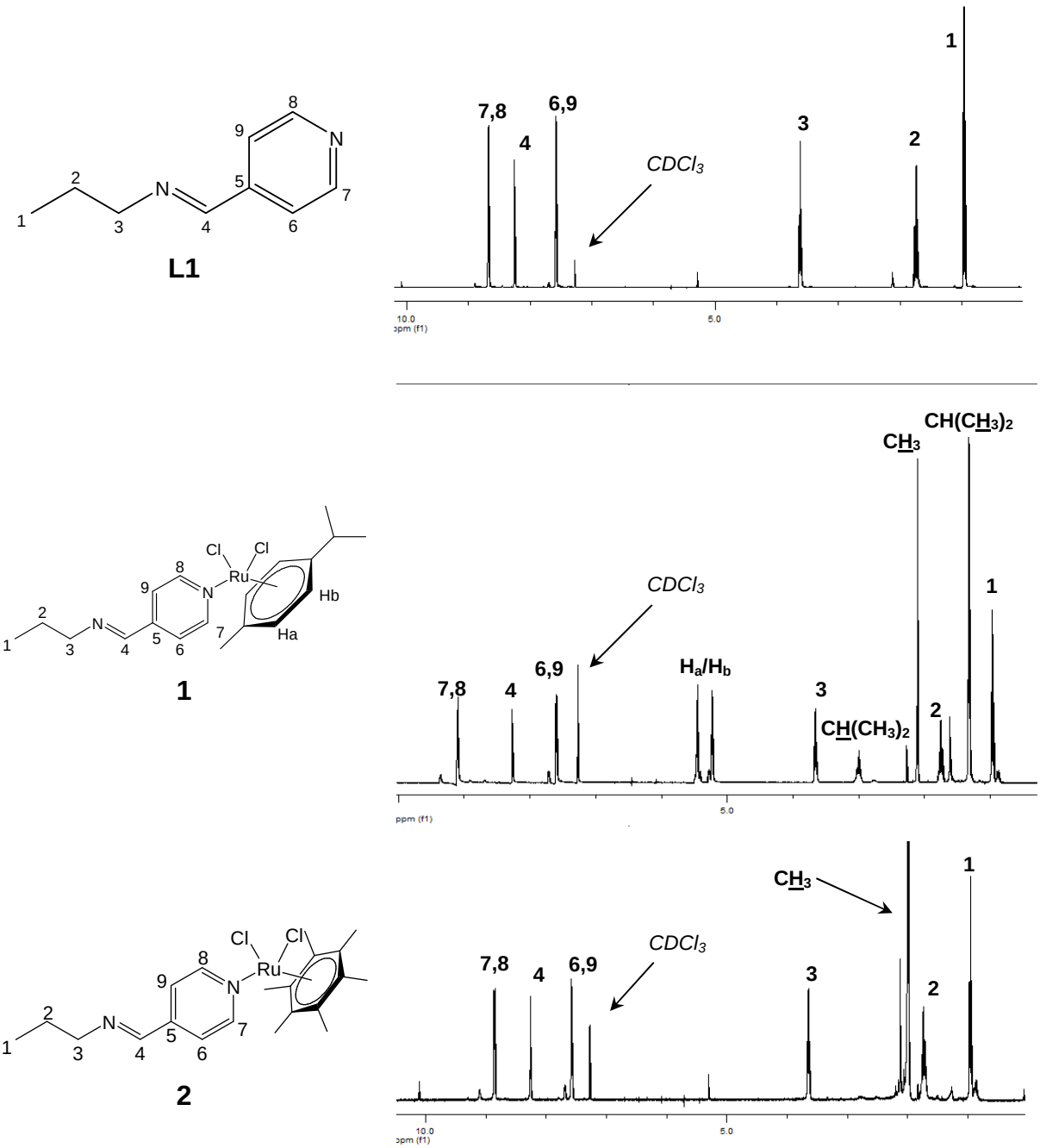

Figure 3.2: *^{1}H-NMR spectra of 4-pyridyl-imine ligand **L1** (top) and mononuclear complexes **1** (middle) and **2** (bottom).*

A similar pattern was observed in the ^{1}H-NMR spectra of the tetranuclear complexes (**3**, **4)** (Fig. 3.3) and the octanuclear complexes (**5**, **6**). The coordination of the ruthenium metal centre to the pyridyl nitrogen atom (and not the imine nitrogen atom) was evidenced by a downfield shift of the doublet (assigned the protons ortho-substituted to the pyridyl nitrogen atom) from ~8.7 ppm (in the ligand) to ~8.9 ppm (Table 3.2). This is due to the electron-withdrawing effects of the coordinated metal.

***Table 3.2**: Selected ^{1}H-NMR data for complexes **1** - **6**.*

Complex	Imine Proton(s) (ppm)	Pyridyl Protons (ppm)	Arene Ring (ppm)
1	8.27	7.60; 9.10	1.32; 2.11; 3.00 5.2-5.5
2	8.23	7.54; 8.78	1.99
3	8.20	7.49; 9.06	1.30; 2.09; 2.97 5.3-5.7
4	8.23	7.51; 8.78	1.97
5	8.19	7.49; 9.05	1.32; 2.09; 2.97 5.3-5.5
6	8.26	7.57; 8.86	2.03

This is the characteristic splitting pattern seen for aromatic rings with different groups para-positioned on the ring. A single doublet, integrating for two protons, was observed downfield and another doublet (integrating for two protons) is observed upfield (Fig. 3.4). The aliphatic protons of the dendritic core and side arms of the dendritic complexes (**3** - **6**) occur at similar shifts to those of the dendritic ligands **L3** and **L4**. The imine proton remains constant at ~8.2 ppm further confirming coordination at the pyridyl nitrogen only.

*p-Cymene complexes (**1**, **3**, **5**)*

The methyl protons of the isopropyl group appear as a doublet in the ^{1}H-NMR spectra for all the *p*-cymene complexes (**1**, **3**, **5***)* and the multiplet at ~ 3 ppm was assigned to the single proton of the isopropyl groups. Two doublets in the range between 5.2 - 5.7 ppm were assigned to the aromatic protons of the *p*-cymene ring and the singlet at ~ 3 ppm assigned to the single methyl group for the *p*-cymene complexes (**1**, **3**, **5**).

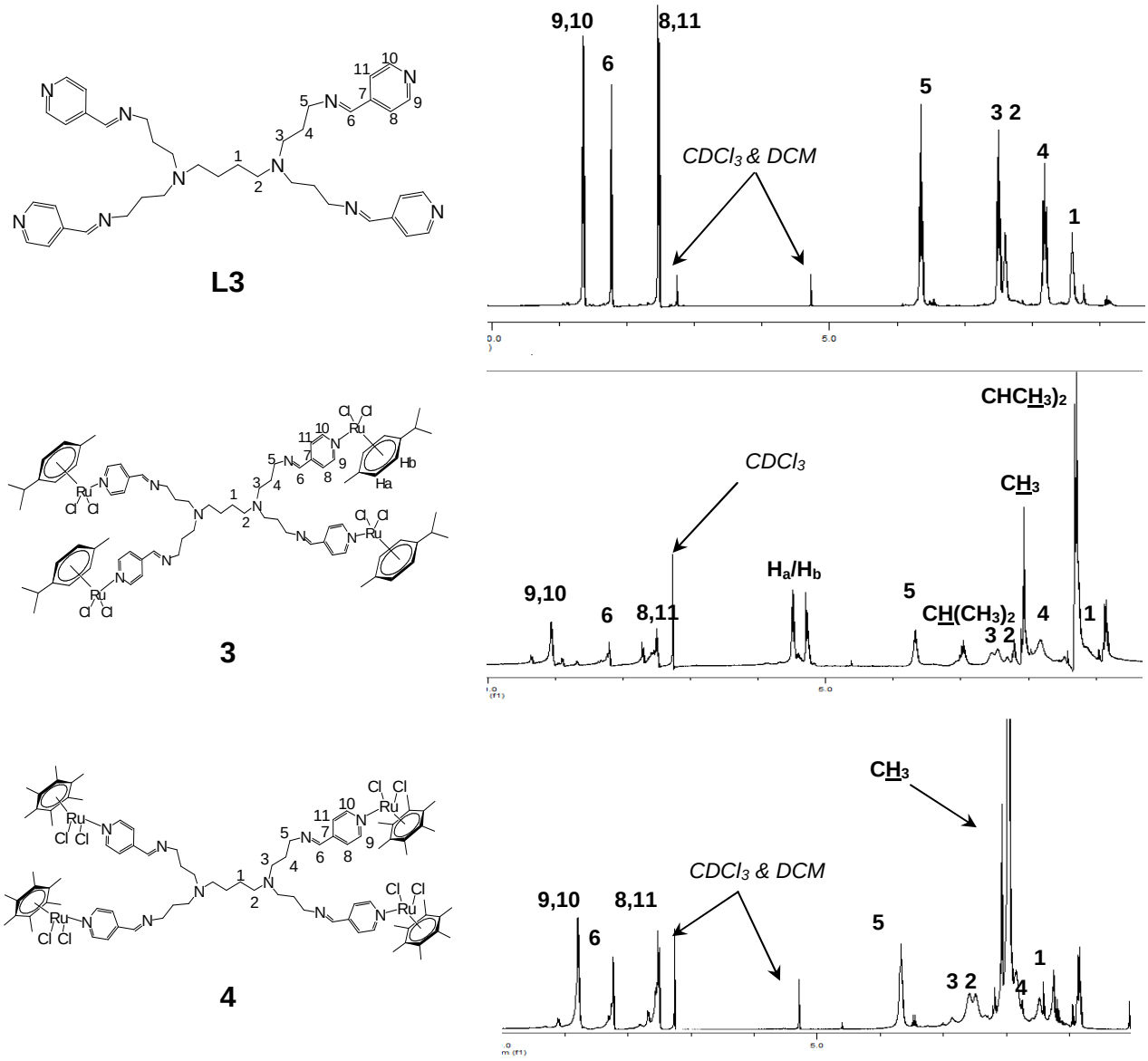

***Figure 3.3**: [1]H-NMR spectra of 4-pyridyl-imine dendritic ligand **L3** (top) and dendritic complexes **3** (middle) and **4** (bottom).*

*Hexamethylbenzene (**2**, **4**, **6**)*

The appearance of the singlet (~ 2 ppm), which was assigned to the protons of the CH_3 groups on the arene ring, showed the presence of the arene ring for the mononuclear complex (**2**). Similarly a singlet at the same chemical shift confirmed the presence of the desired dendritic complex (**4**, **6**), and was assigned to the methyl protons of the arene ring.

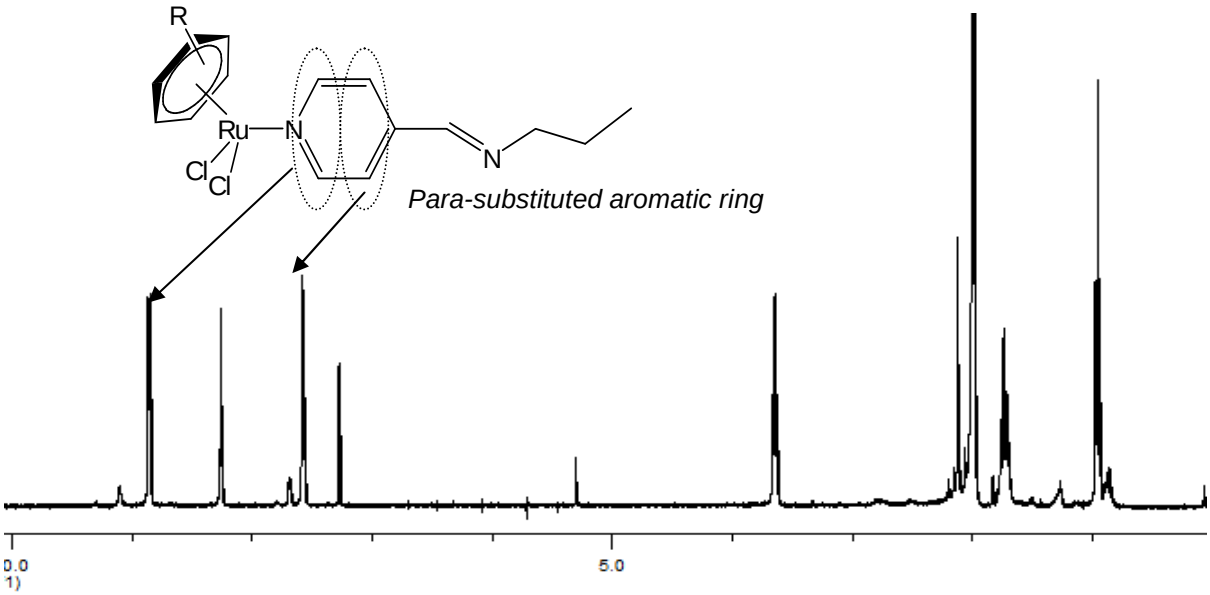

***Figure 3.4**: [1]H-NMR spectrum of a mononuclear complex, illustrating the characteristic splitting pattern observed for para-substituted aromatic rings.*

The ^{1}H-NMR spectra of the 1st generation dendritic complexes (**3**, **4**) show broadened peaks (Fig. 3.3). After extensive washing with a non-polar solvent (petroleum ether), peaks of small intensity could still be seen on the baseline, which are assigned to solvent inclusions or other inorganic material. This is attributed to a phenomenon, where the fluxional arms of the dendrimer can trap solvent molecules and/or molecules of starting material.[10] The ^{1}H-NMR spectrum of the second generation complexes (**5**, **6**) showed similar shifts to the first generation complexes **3** and **4** respectively. Once again, broad overlaps of signals are seen, these were assigned to the aliphatic protons of the side arms of the dendrimer.

^{13}C{^{1}H}-NMR spectra of the mononuclear complexes (**1**, **2**) were similar to that of the monomeric ligand **L1** with differences only in the chemical shifts of the pyridyl carbons (Table 3.3), due to coordination of the ruthenium metal centre. ^{13}C{^{1}H}-NMR spectra for dendritic complexes (**3** - **6**) were similar with only extra signals seen in the ^{13}C{^{1}H}-NMR spectrum of the second generation complexes (**5**, **6**) (Table 3.3). These were assigned to the carbons of the aliphatic side arms of the dendrimers.

***Table 3.3**: Selected $^{13}C\{^{1}H\}$-NMR data for complexes **1** - **6**.*

Complex	Imine Carbon(s) (ppm)	Pyridyl Carbons (ppm)	Arene Ring (ppm)
1	157	123-145	18-22; 31-104
2	158	123-144	15; 91
3	158	123-140	18-22; 31-103
4	159	123-144	15; 91
5	158	123-144	18-22; 31-103
6	159	123-144	15; 91

$^{13}C\{^{1}H\}$-NMR spectra of the neutral monodentate complexes **1** - **6** show chemical shifts of its pyridyl carbons in the range of 123-144 ppm. The *p*-cymene derivatives (**1**, **3**, **4**) showed signals in two ranges (18-22 ppm and 31-104 ppm), which are assigned to the carbons of the arene ring. The hexamethylbenzene ring of complexes **2**, **5** and **6**, show two signals, one at 15 ppm and another at 91 ppm, and were assigned to the methyl carbons and the aromatic carbons respectively. A singlet ~159 ppm was assigned to the imine carbons of complexes **1 - 6**.

3.2.3 Infrared (IR) spectroscopy

Infrared studies were employed on all neutral monodentate complexes (**1** - **6)** using a NaCl solution cell in dichloromethane, to qualitatively show coordination of the ruthenium metal centre to the aromatic nitrogen. Shifts in the $(C=N)_{imine}$ and the $(C=N)_{pyridyl}$ bands verified the mode of coordination of the metal to one or both nitrogen sites. The dendritic complexes (**3** - **6**) showed a similar pattern as their mononuclear analogues (**1**, **2**) (Table 3.4).

A shift in the $(C=N)_{pyridyl}$ band, for all monodentate complexes (**1** - **6**), was observed from a lower frequency around 1599 cm^{-1} (in the ligand) to a higher frequency around 1614 cm^{-1} in the IR spectrum. This confirms coordination of the ruthenium metal to the pyridyl nitrogen atom only. The characteristic free $(C=N)_{imine}$ band around 1647 cm^{-1} remains unchanged and confirms no coordination occurred at this site.

***Table 3.4**: Selected IR absorption bands for complexes **1** - **6**.*

Complex	$(C=N)_{imine}$ (cm^{-1})	$(C=N)_{pyridyl}$ (cm^{-1})
1	1647	1615
2	1646	1614
3	1646	1615
4	1646	1614
5	1646	1614
6	1646	1613

3.2.4 Elemental analysis and mass spectrometry

Elemental analysis results of the new mononuclear complexes (**1**, **2**) were found to correlate with the calculated values. However, the ruthenium(II) arene functionalised metallodendrimers (**3**, **6**) were precipitated as solids, with the inclusion of solvent trapped between the dendritic arms. The dendritic arms often tend to fold back on one-another which results in the entrapment of solvent molecules. The elemental analysis data correlates with the inclusion of 2 and 4 molecules of dichloromethane for the *p*-cymene dendritic complexes **3** and **5** respectively. The calculations correlate well with the inclusion of 1 molecule (**4**) and 2 molecules (**6**) of dichloromethane for the hexamethylbenzene dendritic complexes.

Along with elemental analysis the ESI-mass spectrometry results further confirmed the proposed structures for complexes **1** - **6** (Table 3.5).

***Table 3.5**: Mass spectrometry data for complexes **1** - **6**.*

Complex	Calculated Molecular Mass (g/mol)	Molecular Fragment (m/z)	Assignment
1	454.1	419	$[M\text{-}Cl]^{+}$
2	482.5	447	$[M\text{-}Cl]^{+}$
3	1897.7	565	$[M+4H+4CH_2Cl_2+H_2O]^{4+}$
4	2009.9	635	$[M\text{-}3Cl]^{3+}$
5	3935.7	569	$[M\text{-}7Cl+3CH_2Cl_2+CH_3CN]^{7+}$
6	4160.0	631	$[M\text{-}7Cl+5CH_2Cl_2+2CH_3CN]^{7+}$

3.2.5 X-ray crystallography

The molecular structures were established of the neutral mononuclear complexes **1** and **2** were confirmed by single crystal X-ray diffraction. The crystals were grown by slow diffusion of hexane into a concentrated dichloromethane solution of the complexes. Complexes **1** and **2** both crystallize in the monoclinic space groups $P2_1/c$ and $P2_1$. The structure analysis shows the ruthenium atom possessing the well documented "three-leg piano-stool", pseudo-tetrahedral geometry.[11] The arene ring represents the "seat" and, the ligand bound by the pyridyl-nitrogen and chlorido ligand, are the "legs". ORTEP drawings of the mononuclear complexes **1** and **2** are shown (Fig. 3.5), with the crystallographic data listed in Table 3.6 and selected bond lengths and angles tabulated in Table 3.7.

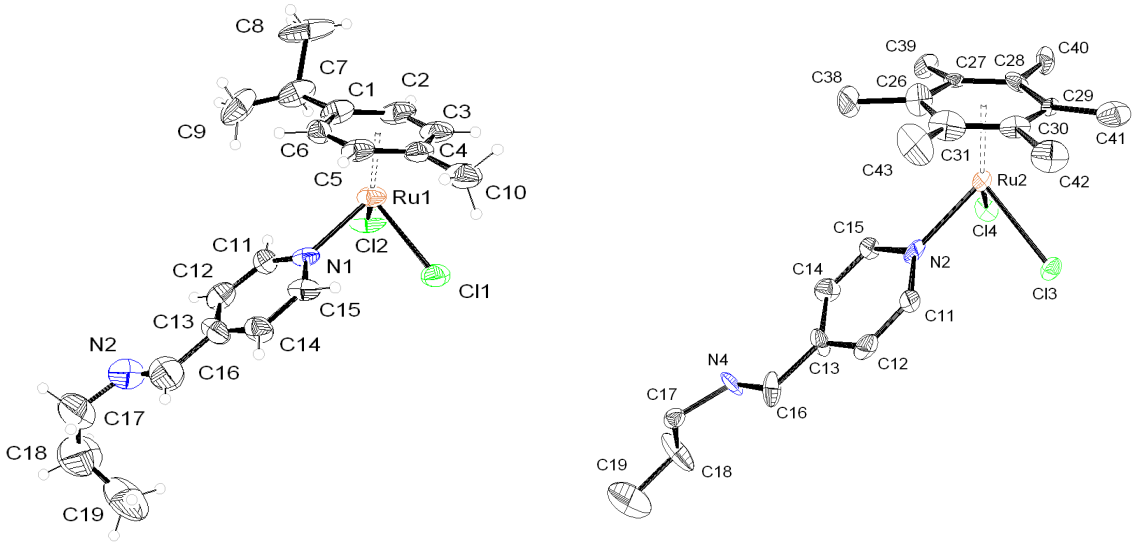

***Figure 3.5**: The ORTEP structures of the neutral mononuclear complexes **1** (left) and **2** (right).*

***Table 3.6**: Crystallographic and structure refinement parameters for neutral complexes **1** and **2**.*

Complex	1	2
Chemical formula	$C_{19}H_{26}Cl_2N_2Ru$	$C_{21}H_{30}Cl_2N_2Ru$
Formula weight (g /mol)	454.39	482.44
Crystal system	Monoclinic	Monoclinic
Space group	$P\ 2_1/c$	$P2_1$
a (Å)	18.246(3)	15.005(3)
b (Å)	15.057(2)	8.100(2)
c (Å)	7.3464(11)	19.185(4)
α (^{o})	90.00	90.00
β (^{o})	101.360(14)	112.03(3)
γ (^{o})	90.00	90.00
V (Å^3)	1978.7(5)	2161.5(8)
Z	4	4
T (K)	293(2)	293(2)
Wavelength λ (Å)	0.71073	0.71073
Density D_X (g /cm^3)	1.525	1.483
Absorption coefficient μ (mm^{-1})	1.065	0.980
F(000)	928	992
Scan range (^{o})	$1.14 < \theta < 25.26$	$2.17 < \theta < 26.04$
Unique reflections	12695	12997
Reflections used [$I > 2\sigma(I)$]	3530	7781
R_{int}	0.2154	0.1150
Final R indices [$I > 2\sigma(I)$][a]	0.0650, wR_2 0.1515	0.1037, wR_2 0.2687
R indices (all data)	0.1632, wR_2 0.1830	0.1442, wR_2 0.2839
Goodness-of-fit (GOF)	0.755	1.031
Maximum, Minimum $\Delta\rho$ (e Å^{-3})	0.504, -0.991	4.646, -1.864

[a] Structures were refined on F_0^2: $wR_2 = [\Sigma[w(F_0^2 - F_c^2)^2] / \Sigma\, w(F_0^2)^2]^{1/2}$, where $w^{-1} = [\Sigma\,(F_0^2) + (aP)^2 + bP]$ and $P = [max(F_0^2, 0) + 2F_c^2]/3$.

***Table 3.7**: Selected bond lengths (Å) and angles (°) for neutral complexes **1** and **2**.*

1		**2**	
Distances (Å)		*Distances (Å)*	
Ru(1)-C(1)	2.216(12)	Ru(2)-C(26)	2.180(2)
Ru(1)-C(2)	2.171(12)	Ru(2)-C(27)	2.250(2)
Ru(1)-C(3)	2.188(13)	Ru(2)-C(28)	2.150(2)
Ru(1)-C(4)	2.206(13)	Ru(2)-C(29)	2.221(16)
Ru(1)-C(5)	2.181(10)	Ru(2)-C(30)	2.213(14)
Ru(1)-C(6)	2.151(11)	Ru(2)-C(31)	2.202(17)
Ru(1)-Cl(1)	2.406(3)	Ru(2)-Cl(3)	2.423(5)
Ru(1)-Cl(2)	2.405(3)	Ru(2)-Cl(4)	2.427(5)
Ru(1)-N(1)	2.128(9)	Ru(2)-N(2)	2.123(15)
N(2)-C(16)	1.340(3)	N(4)-C(16)	1.220(3)
N(2)-C(17)	1.490(3)	N(4)-C(17)	1.650(3)
C(13)-C(16)	1.540(2)	C(13)-C(16)	1.490(3)
Angles (°)		*Angles (°)*	
N(1)-Ru(1)-Cl(1)	87.0(2)	N(2)-Ru(2)-Cl(3)	87.90(5)
N(1)-Ru(1)-Cl(2)	84.8(2)	N(2)-Ru(2)-Cl(4)	84.40(4)
Cl(1)-Ru(1)-Cl(2)	87.65(12)	Cl(3)-Ru(2)-Cl(4)	87.33(19)

The bond distance of the Ru-N_{pyr} of complexes **1** (2.128(9) Å) and **2** (2.123(15) Å) are comparable to the bond distances of the Ru-N_{pyr} of the *p*-cymene derivative recently published (2.130(2) Å) by Keppler and co-workers.[9] Similarly, the bond angles of N_{pyr}-Ru-Cl and Cl-Ru-Cl of complexes **1** (84.8(2) ° and 87.65(12) °) and **2** (84.40(4) ° and 87.33(19) °) are also comparable to the bond angles of the *p*-cymene derivative N_{pyr}-Ru-Cl and Cl-Ru-Cl (84.50(6) ° and 87.00(2) °) synthesized by Keppler.[9] The crystal analysis thus further confirms mode of coordination at the pyridyl nitrogen atom.

3.3 Synthesis of cationic 2-pyridyl-imine mononuclear and dendritic ruthenium(II) arene salts (7 - 12)

The *N,N*- donor ligands (**L2**, **L5**, **L6**) were complexed with two ruthenium precursors (**[Ru(η^6-*p*-Pr^{i}C$_6$H$_4$Me)Cl$_2$]**) and (**[Ru(η^6-C$_6$Me$_6$)Cl$_2$]$_2$**). For complexes **7** - **12**, m equivalents (where m = 2 for **7** and **8**; m = 0.5 for **9** and **10**; m = 0.25 for **11** and **12**) of the ligand (**L2** for **7** and **8**; **L5** for **9** and **10**; **L6** for **11** and **12**) were added to a solution of the ruthenium dimer (**[Ru(η^6-*p*-Pr^{i}C$_6$H$_4$Me)Cl$_2$]** for **7**, **9**, **11**; **[Ru(η^6-C$_6$Me$_6$)Cl$_2$]$_2$** for **8**, **10**, **12**) in ethanol or methanol (Scheme 3.3). As seen for similar chelating systems,[12-14] 2-pyridyl-imine ligands have the ability to coordinate to the metal centre in a cationic bidentate fashion *via* the imine and pyridyl nitrogen atoms. Coordination of the ligand (**L2**, **L5**, **L6**) to the ruthenium metal centre splits the dimer, displacing a chloride ion (as the counter-ion), and generate a cationic metal complex.

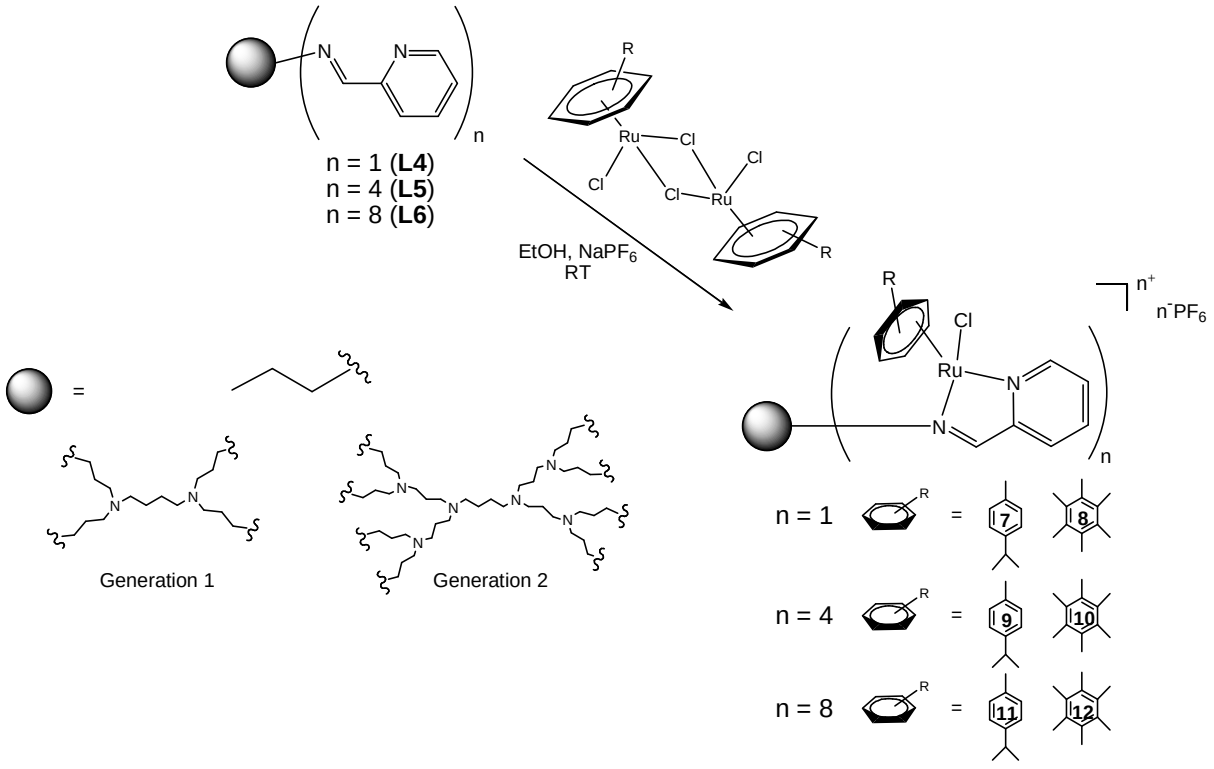

Scheme 3.3: *Outline synthesis of cationic ruthenium(II) arene complexes (**7** - **12**).*

However, isolation and purification of the complexes (**7** - **12**) as chloride salts proved to be a major challenge, as these compounds were found to be very hygroscopic. Due to the large nature of the complexes the chlorido anion was not a suitable

counter-ion for the complex, which could have aided in difficulty in isolating the complexes. A metathesis reaction was preformed, using the sodium hexafluorophosphate salt to assist in the exchange (Scheme 3.3). The bulky nature of this anion is said to stabilise the overall complex. The products precipitated out of solution and were isolated by filtration, and dried under vacuum. The complexation reactions yielded two new mononuclear salts **7** and **8**, and four new dendritic ruthenium(II) arene salts **9** - **12**.

3.3.1 Physical properties

The complexes (**7** - **12**) were dried and isolated as dark yellow-red solids in moderate yields, and were found to be thermally stable (Table 3.8).

Table 3.8*: Physical appearance, percentage yield and melting points for complexes* ***7*** *-* ***12****.*

Complex	Physical Appearance	Yield (%)	Melting Point (^{o}C)
7	Yellow solid	38	186-187
8	Orange solid	51	239-241
9	Yellow-brown solid	48	169-172
10	Red-brown solid	66	232-236
11	Yellow-brown solid	40	175-179
12	Red-brown solid	48	210-212

The cationic salts **7** - **12** were non-hygroscopic, air-stable and soluble in dimethylsulfoxide, acetone, acetonitrile and insoluble in methanol, diethyl ether, hexane and tetrahydrofuran.

3.3.2 ^{1}H-NMR and ^{13}C{^{1}H}-NMR spectroscopy

^{1}H-NMR spectroscopy was used to assist in providing evidence for the coordination of the ruthenium-arene moiety to both the imine and pyridyl nitrogen atoms. The ^{1}H-NMR spectra (Fig. 3.6) of complexes **7** and **8** were run in acetone-d_6 and showed all the relevant peaks for a combination of the ligand **L2** and the ruthenium dimer (**[Ru(η^6-*p*-Pr^{i}C$_6$H$_4$Me)Cl$_2$]** or **[Ru(η^6-C$_6$Me$_6$)Cl$_2$]$_2$**).

A similar pattern is seen in the ^{1}H-NMR spectra (Fig. 3.7) of the dendritic complexes **9** - **12**. The ^{1}H-NMR spectra for the dendritic salts showed broadened peaks, with many of the peaks overlapping and/or coalescing, due to the multinuclear nature of these complexes.

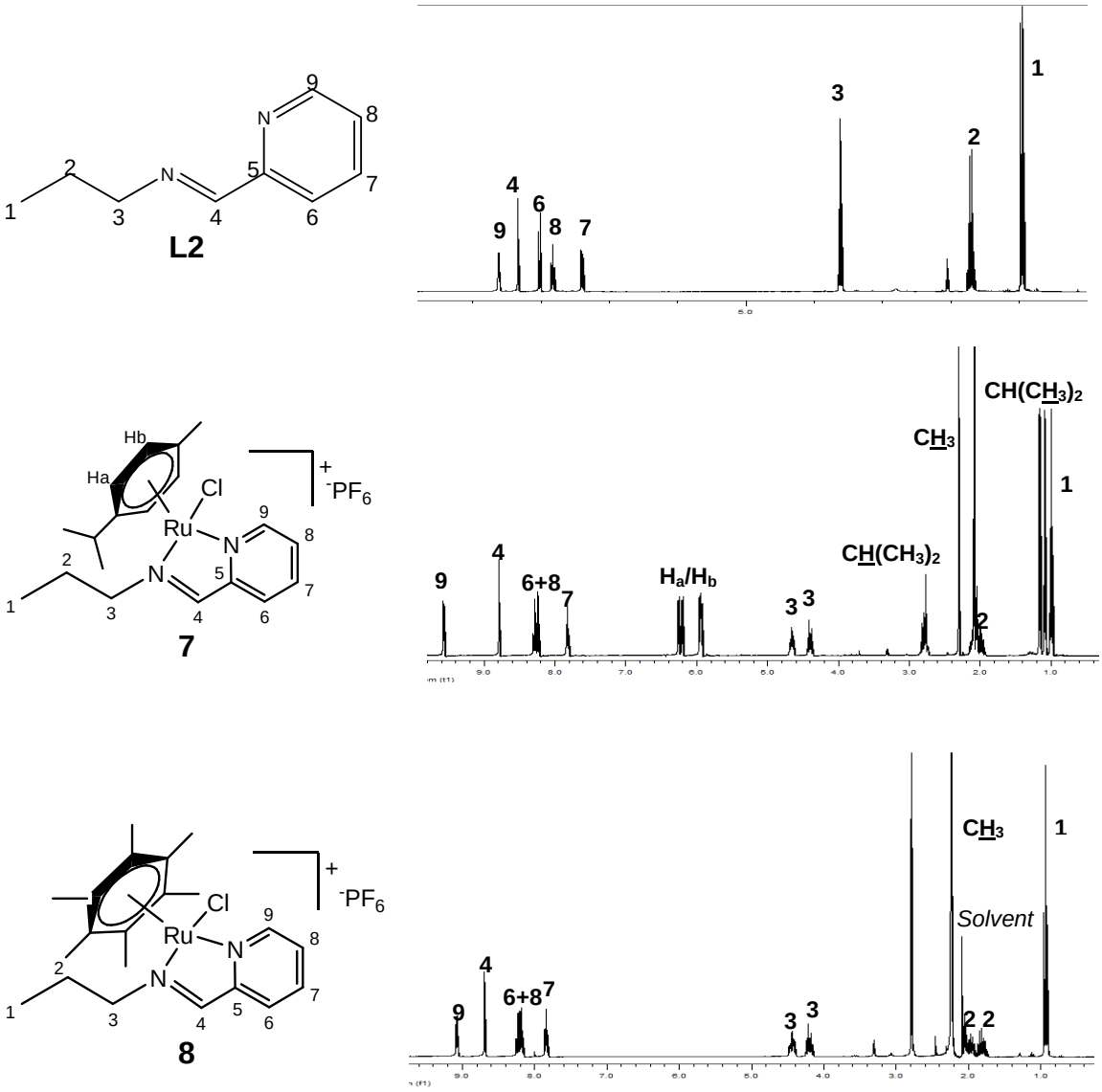

Figure 3.6: *^{1}H-NMR spectra of 2-pyridyl-imine ligand **L2** (top), mononuclear salts **7** (middle) and **8** (bottom) recorded in acetone-d_6.*

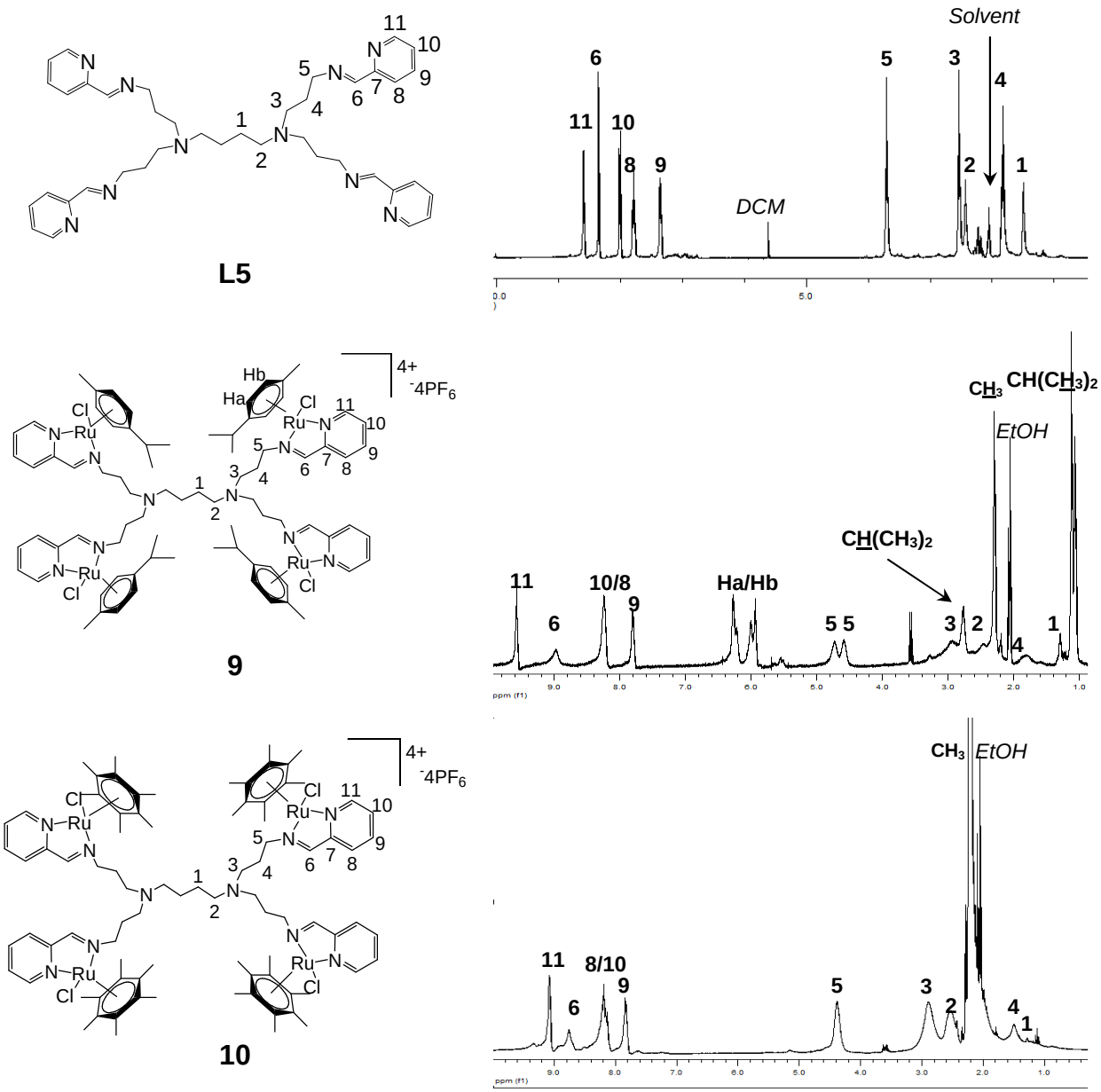

Figure 3.7: *^{1}H-NMR spectra of 2-pyridyl-imine dendritic ligand **L5** (top), dendritic salts **9** (middle) and **10** (bottom) recorded in acetone-d_6.*

As a result of the ruthenium-arene moiety coordinating to both the imine and pyridyl nitrogen atom, there is a shift in both the imine proton and protons on the pyridyl ring, for all complexes **7** - **12**. All cationic salts showed a general shift of signals downfield due to the cationic nature of the complex. Upon coordination of the ruthenium-arene moiety to the ligand, the ruthenium metal centre becomes chiral. The newly formed chiral centre is due to the coordination of four different groups on the ruthenium metal centre. The diastereotopic nature of the protons on carbon 3 of the mononuclear complexes **7** and **8** further confirm the formation of the chiral centre. Both sets of

diastereotopic protons, on each carbon, show two sets of multiplets in the ranges of 2.0 - 2.1 ppm and 4.4 - 4.7 ppm for complexes **7** and **8**. The diastereotopic protons on the dendritic arms of complexes (**9** - **12**), adjacent to the imine nitrogen, show the same effect as to their mononuclear counterparts. Two broad multiplets for the first generation complexes (**9** and **10**), between 4.6 - 4.7 ppm are seen and a very broad multiplet for the second generation complexes (**11** and **12**) between 4.6 - 4.8 ppm is also noted.

*p-Cymene salts (**7**, **9**, **11**)*

There is a lack of rotation around the *p*-cymene ring due to the bulky nature of the isopropyl group. This in turn results in the methyl protons of the isopropyl group exhibiting two sets of doublets (~1.1 ppm) in the ^{1}H-NMR spectrum of the mononuclear complex **7**. Two broad multiplets were observed for the dendritic complexes at ~1.1 ppm (**9** and **11**) and were assigned to the methyl protons of the isopropyl group. A septet (**7**) and a broad multiplet (**9** and **11**) were observed at 2.5 ppm and were assigned to the single proton of the isopropyl group (Table 3.9). The triplet and the doublet-of-doublets observed at 5.9 ppm and 6.2 ppm respectively (**7**), correspond to the aromatic protons of the *p*-cymene ring. The dendritic salts (**9** and **11**) show two multiplets assigned to the aromatic protons of the *p*-cymene ring. The splitting pattern can be explained as a result of the long range coupling with the isopropyl protons (Table 3.9).

*Hexamethylbenzene salts (**8**, **10**, **12**)*

A strong singlet is seen in the ^{1}H-NMR spectrum of complex **8** at 2.2 ppm, and was assigned the methyl protons of the hexamethylbenzene ring (Table 3.9). Similarly the dendritic salts (**10** and **12**) show a singlet at 2.2 ppm assigned to the methyl protons of the hexamethylbenzene ring (Table 3.9).

***Table 3.9**: Selected ^{1}H-NMR data for cationic salts **7** - **12**.*

Complex	Imine Proton(s) (ppm)	Pyridyl Protons (ppm)	Arene Ring (ppm)
7	8.79	7.8-8.3; 9.57	1.11; 2.3-2.8; 5.9-6.2
8	8.70	7.8-8.2; 9.07	2.24
9	8.98	7.8-8.2; 9.57	1.11; 2.3-2.8; 6.0-6.3
10	8.76	7.8-8.2; 9.08	2.21
11	9.13	7.8-8.3; 9.58	1.09; 2.3-2.8; 6.0-6.3
12	8.70	7.8-8.2; 9.07	2.20

The aromatic protons of the arene ring (*p*-cymene or hexamethylbenzene) are observed more downfield compared to the starting ruthenium precursors (**[Ru(η^6-*p*-Pr^{i}C$_6$H$_4$Me)Cl$_2$]$_2$** or **[Ru(η^6-C$_6$Me$_6$)Cl$_2$]$_2$**) due to the cationic nature of the complex.

^{13}C{^{1}H}-NMR spectra of the mononuclear complexes **7** and **8** were run in acetone-d_6 and were found to be similar to that of the monomeric ligand **L2**, with a downfield shift seen in the signals assigned to the imine and pyridyl carbons as a result of coordination to the ruthenium metal centre (Table 3.10). ^{13}C{^{1}H}-NMR spectra of the dendritic complexes **9** and **10** were similar to the second generation complexes **11** and **12**, with only extra signals seen in the ^{13}C{^{1}H}-NMR spectra, assigned to the carbons of the aliphatic side arms (Table 3.10).

***Table 3.10**: Selected ^{13}C{^{1}H}-NMR data for cationic salts **7** - **12**.*

Complex	Imine Carbon(s) (ppm)	Pyridyl Carbons (ppm)	Arene Ring (ppm)
7	167	129-155	21-23; 31-106
8	167	128-155	15; 97
9	166	129-155	19-22; 31-106
10	167	128-155	15; 97
11	169	129-155	19-22; 31-106
12	167	128-155	15; 97

$^{13}C\{^{1}H\}$-NMR spectra of the cationic salts (**7** - **12**) showed chemical shifts of signals assigned to its pyridyl carbons in the range of 128 - 155 ppm, and peaks for the imine carbons at ~168 ppm. The $^{13}C\{^{1}H\}$-NMR spectra of the *p*-cymene complexes (**7, 9**, **11**) showed a range of signals between 19 - 22 ppm and between 31 - 106 ppm. The $^{13}C\{^{1}H\}$-NMR spectra of the hexamethylbenzene complexes (**8**, **10**, **12**) showed signals at 15 and 97 ppm, assigned to the sp^3 and sp^2 hybridized carbons of the arene ring.

3.3.3 Infrared (IR) spectroscopy

The IR spectrum for the mononuclear complexes (**7** and **8**) showed shifts of the two bands assigned to the $(C=N)_{pyridyl}$ and $(C=N)_{imine}$ stretching frequencies, which suggests coordination of the ruthenium metal to these systems. Similarly, shifts in the $(C=N)_{pyridyl}$ and $(C=N)_{imine}$ stretching frequencies for the dendritic salts (**9** - **12**) were also seen. The $(C=N)_{pyridyl}$ stretching frequency shifted from around ~1590 cm^{-1} to a higher frequency of ~1600 cm^{-1} for all of the cationic salts **7** - **12** (Table 3.11), whilst the $(C=N)_{imine}$ stretching frequency shifted from around ~1650 cm^{-1} to a lower frequency of ~1623 cm^{-1} for the same complexes (Table 3.11).

Table 3.11*: Selected IR absorption bands for cationic salts **7** - **12**.*

Complex	$(C=N)_{imine}$ (cm^{-1})	$(C=N)_{pyridyl}$ (cm^{-1})
7	1623	1599
8	1625	1600
9	1625	1599
10	1624	1598
11	1623	1598
12	1621	1597

These shifts can be explained by the synergic effect.[15] The $(C=N)_{imine}$ experiences electron-withdrawing effects from the coordinated metal and the pyridyl ring, which in-turn weakens the $(C=N)_{imine}$ bond and pushes the stretching frequency to a lower frequency. The shift of the $(C=N)_{pyridyl}$ is brought about by the synergic effect (Fig. 3.8). Back-donation of electron density from the electron rich metal centre into the

empty anti-bonding (π^*) orbitals, strengthening the $(C=N)_{pyridyl}$ bond, thus pushing the stretching-frequency to a higher frequency.

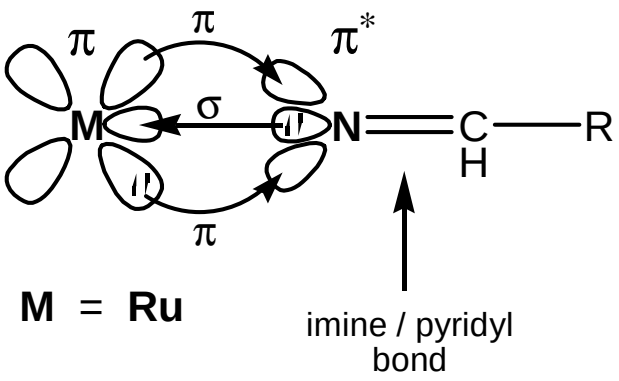

***Figure 3.8**: Molecular orbital diagram illustrating the synergic effect.*

3.3.4 Elemental analysis and mass spectrometry

The values for cationic salt **7**, correlated with the calculated values. When comparing the observed values for cationic salt **8** with the calculated values, they were found to be outside acceptable limits. With the possibility of solvent inclusions, calculated values were recalculated to include half a molecule of methanol. This brought the observed values in direct correlation with calculated values. Elemental analysis for the cationic dendritic complexes **9** - **12** were found to correlate with calculated values.

Further complementing spectroscopic and analytical data, were the MALDI-TOF mass spectrometry data for the cationic salts **9**, **10** and **12**, which showed the molecular ion base peak with one-less a PF_6 molecule as the highest molecular weight fragment, but, cationic salt **11** gave the molecular ion base peak as the highest molecular weight fragment (Table 3.12).

***Table 3.12**: Mass spectrometry data for **7** - **12**.*

Complex	Calculated Molecular Mass (g/mol)	Molecular Fragment (m/z)	Assignment
7	563.9	419	$[M\text{-}PF_6]^+$
8	592.0	447	$[M\text{-}PF_6]^+$
9	2335.8	2192	$[M\text{-}PF_6]^+$
10	2448.0	2304	$[M\text{-}PF_6]^+$
11	4811.8	4811	$[M]^+$
12	5036.2	4891	$[M\text{-}PF_6]^+$

3.3.5 X-ray crystallography

The proposed structures of the mononuclear cationic salts **7** and **8** were confirmed by single crystal X-ray diffraction. The crystals were grown by slow diffusion of hexane into a concentrated acetone solution of the salts. The complexes **7** and **8** crystallize in the triclinic and orthorhombic space groups *P* -1 and *P* $2_12_12_1$ respectively. The crystal analysis shows the ruthenium atom possess the "three-leg piano-stool", pseudo-tetrahedral geometry in both structures.[11] Similar to the neutral mononuclear complexes (**1**, **2**), the arene ring (*p*-cymene or hexamethylbenzene) represents the "seat" and, coordinated to the metal centre are the pyridyl-nitrogen, imine- nitrogen atoms and single chlorido atom, which are the "legs". ORTEP drawings of the mononuclear cationic salts **7** and **8** are shown (Fig. 3.9), with the crystallographic data listed (Table 3.13) and selected bond lengths and angles tabulated (Table 3.14).

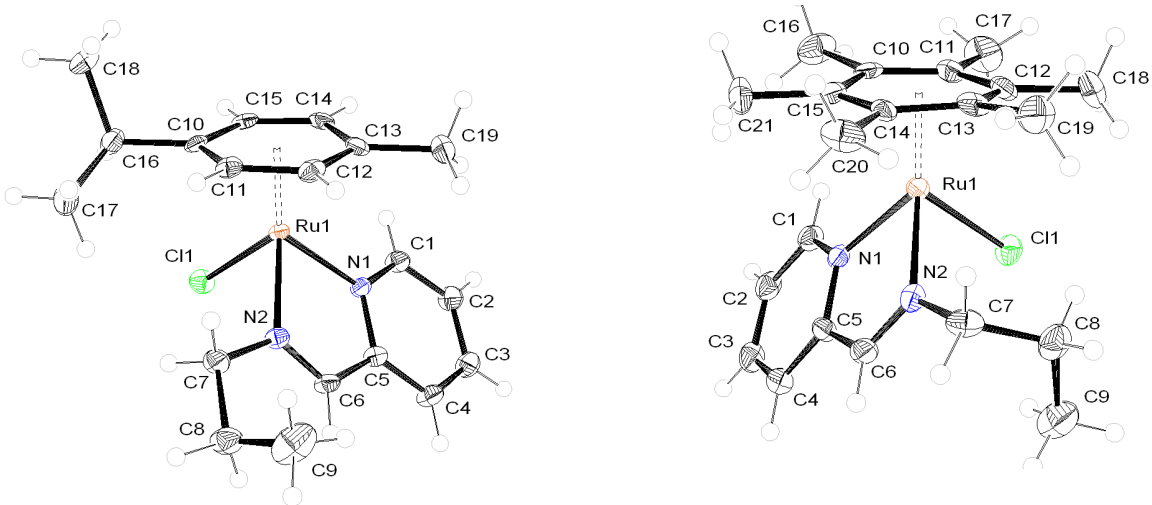

***Figure 3.9**: The ORTEP structures of the cationic salts **7** (left) and **8** (right), counter-ions (PF_6) have been omitted for clarity.*

Table 3.13**: Crystallographic and structure refinement parameters for mononuclear cationic salts **7** and **8.

Complex	7	8
Chemical formula	$C_{19}H_{26}ClF_6N_2PRu$	$C_{21}H_{30}ClF_6N_2PRu$
Formula weight (g /mol)	563.91	591.96
Crystal colour and shape	Orange block	Orange block
Crystal size (mm)	0.26 x 0.23 x 0.18	0.24 x 0.21 x 0.16
Crystal system	Triclinic	Orthorhombic
Space group	*P* -1	*P* $2_12_12_1$
a (Å)	9.1490(9)	12.4312(10)
b (Å)	9.8468(9)	13.1480(12)
c (Å)	12.2766(12)	14.1942(10)
α (^{o})	81.583(11)	90.00
β (^{o})	79.178(11)	90.00
γ (^{o})	83.705(11)	90.00
V (Å^3)	1070.76(18)	2320.0(3)
Z	2	4
T (K)	293(2)	293(2)
Wavelength *λ* (Å)	0.71073	0.71073
Density D_X (g /cm^3)	1.749	1.695
Absorption coefficient *μ* (mm^{-1})	0.992	0.920
F(000)	568	1200
Scan range (^{o})	2.27 < *θ* < 26.05	2.11 < *θ* < 26.18
Unique reflections	7931	12015
Reflections used [$I > 2\sigma(I)$]	3927	4563
R_{int}	0.0244	0.0501
Final *R* indices [$I > 2\sigma(I)$][a]	0.0238, wR_2 0.0589	0.0335, wR_2 0.0617
R indices (all data)	0.0305, wR_2 0.0725	0.0525, wR_2 0.0671
Goodness-of-fit (GOF)	1.152	0.929
Maximum, Minimum *Δρ* (e Å^{-3})	0.641, -0.673	0.710, -1.485

[a] Structures were refined on F_0^2: $wR_2 = [\Sigma[w(F_0^2 - F_c^2)^2] / \Sigma w(F_0^2)^2]^{1/2}$, where $w^{-1} = [\Sigma (F_0^2) + (aP)^2 + bP]$ and $P = [max(F_0^2, 0) + 2F_c^2]/3$.

***Table 3.14**: Selected bond lengths (Å) and angles (°) for cationic complexes **7** and **8**.*

Complex	7	8
		Distances (Å)
Ru(1)-C(10)	2.228(3)	2.260(4)
Ru(1)-C(11)	2.209(3)	2.230(4)
Ru(1)-C(12)	2.176(3)	2.208(4)
Ru(1)-C(13)	2.197(3)	2.255(4)
Ru(1)-C(14)	2.212(3)	2.198(4)
Ru(1)-C(15)	2.193(3)	2.206(4)
Ru(1)-Cl(1)	2.3910(7)	2.3979(10)
Ru(1)-N(1)	2.079(2)	2.097(4)
Ru(1)-N(2)	2.076(2)	2.089(4)
N(2)-C(7)	1.464(4)	1.465(6)
N(2)-C(6)	1.283(4)	1.277(6)
C(6)-C(5)	1.444(4)	1.433(6)
		Angles (°)
N(1)-Ru(1)-N(2)	76.50(14)	77.00(9)
N(1)-Ru(1)-Cl(1)	82.76(10)	86.42(6)
N(2)-Ru(1)-Cl(1)	88.00(10)	85.67(6)

The bond distances of the Ru-N_{pyr} and Ru-N_{imine} of complex **7** (2.079(2) Å and 2.076(2) Å) are comparable to the bond distances of the Ru-N_{pyr} and Ru-N_{imine} of the hexamethylbenzene derivative of complex **8** (2.097(4) Å and 2.089(4) Å). Similarly the bond angles of N_{pyr}-Ru-N_{imine}, N_{pyr}-Ru-Cl and N_{imine}-Ru-Cl of complex **7** (76.50(14) °, 82.76(10) ° and 88.00(10) °) are comparable to the bond angles of N_{pyr}-Ru-N_{imine}, N_{pyr}-Ru-Cl and N_{imine}-Ru-Cl of complex **8** (71.09(9) °, 86.42(6) ° and 85.67(6) °). The bond distance and angles of both complexes **7** and **8** are comparable to similar known cationic complexes synthesized by the Kollipara group.[12-14] The crystal analysis thus confirms mode of coordination of the ruthenium metal centre.

A hydrogen bond is observed in the crystal packing of the cationic salt **8**, between the CH_{imine} group and the chloride atom of an adjacent molecule (Fig. 3.10). The

hydrogen bonding gives rise to infinite one-dimensional chains in the crystal. In the cationic salt **8** the C···Cl distance is 3.697(5) Å and the C-H···Cl angle 153.6 °. However, this was not observed in the crystal packing of cationic salt **7**, with the CH_{imine} group slightly protected by the propyl chain. The chloride atom (cationic salt **7**) interacts weakly with a CH group of the arene ring (adjacent molecule), whilst the CH_{imine} group interacts with two fluorine atoms of the PF_6 counter-ion.

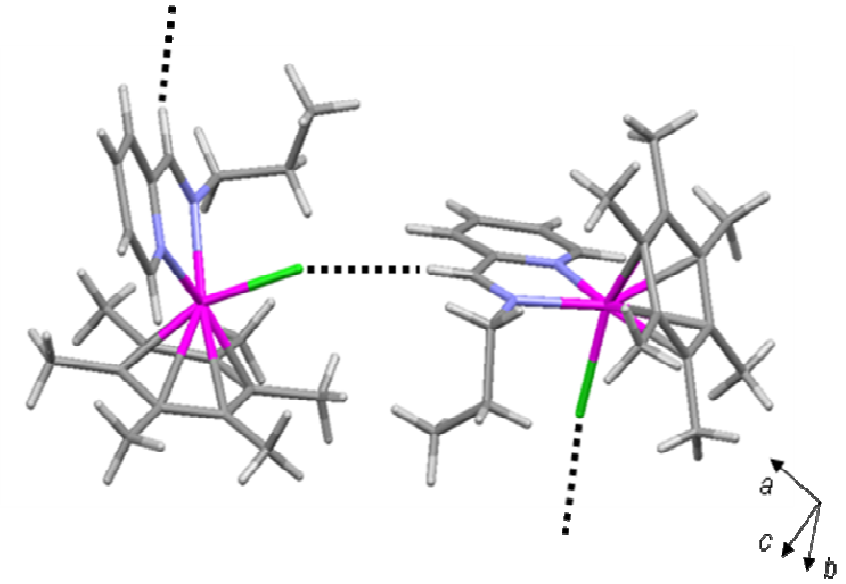

Figure 3.10: *Crystal packing of cationic salt **8** illustrating the infinite one-dimensional chains.*

3.4 Synthesis of neutral salicylaldimine mononuclear and dendritic ruthenium(II) arene complexes (13 -18)

In synthesizing new neutral chelating bidentate ruthenium(II) arene complexes, salicylaldimine *N,O*- ligands **L7**, **L8** and **L9** were complexed with the particular ruthenium dimer (**[Ru(η^6-*p*-Pr^{i}C$_6$H$_4$Me)Cl$_2$]$_2$** or **[Ru(η^6-C$_6$Me$_6$)Cl$_2$]$_2$**). The method of complexation involved the stirring of a solution of the ligand (**L7**, **L8**, **L9**), with a weak base (Et_3N), to assist in deprotonation of the ligand. Deprotonation of the ligand was followed by the addition of the ruthenium dimer in ethanol at room temperature. The reactions involving the dendrimers were generally allowed to proceed for 15 hours (with second generations proceeding overnight) and the mononuclear reactions proceeding for a shorter period (Scheme 3.4). In the synthesis of complexes **13** - **18**, m equivalents (where m = 2 for **13** and **14**; m = 0.5 for **15** and **16**; m = 0.25 for **17**

and **18**) of the ligand (**L2** for **13** and **14**; **L5** for **15** and **16**; **L6** for **17** and **18**) were added to a solution of the ruthenium dimer (**[Ru(η^6-*p*-Pr^{i}C$_6$H$_4$Me)Cl$_2$]** for **13**, **15**, **17**; **[Ru(η^6-C$_6$Me$_6$)Cl$_2$]$_2$** for **14**, **16**, **18**) in ethanol or tetrahydrofuran (Scheme 3.4).

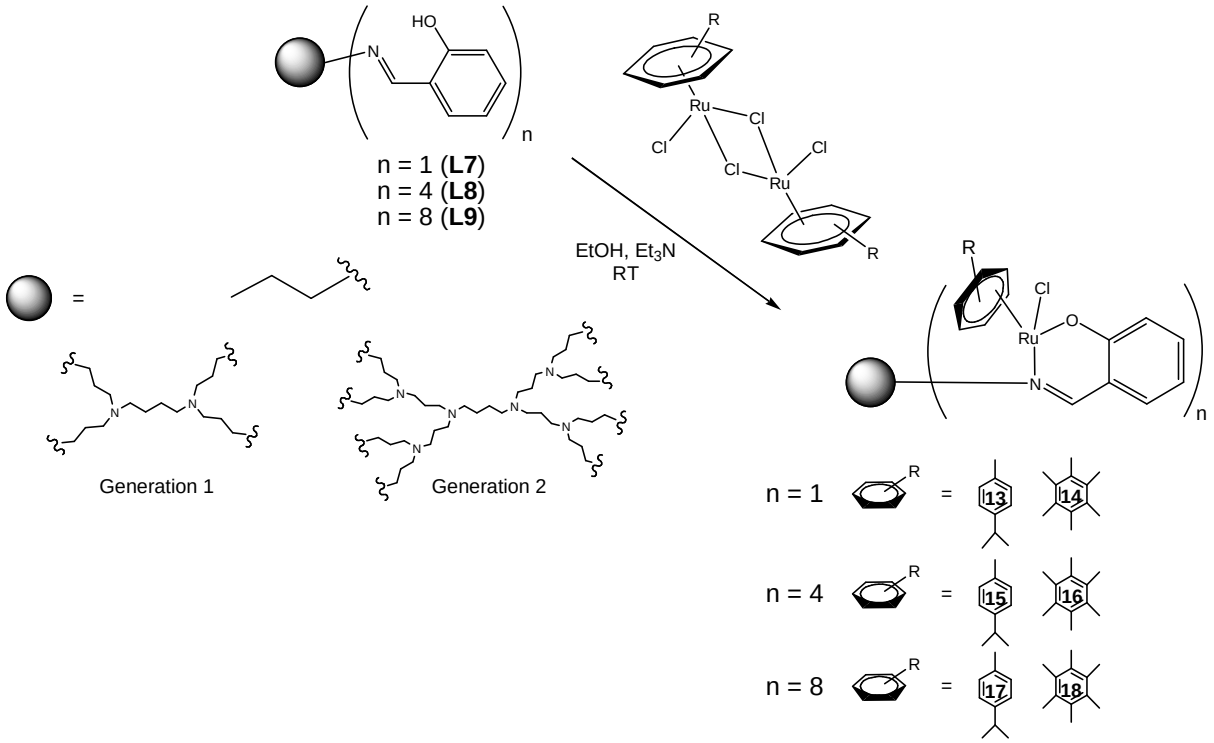

Scheme 3.4: *Outline synthesis of neutral ruthenium(II) arene complexes (**13** - **18**).*

This complexation was first carried out without the addition of the base. The starting material was stirred in ethanol at room temperature and then in a separate reaction, at an elevated temperature, with both reactions yielding no product. A weak base (Et_3N) was then added to promote the reaction, with the base removing the phenolic proton from the aromatic ring (Scheme 3.5).

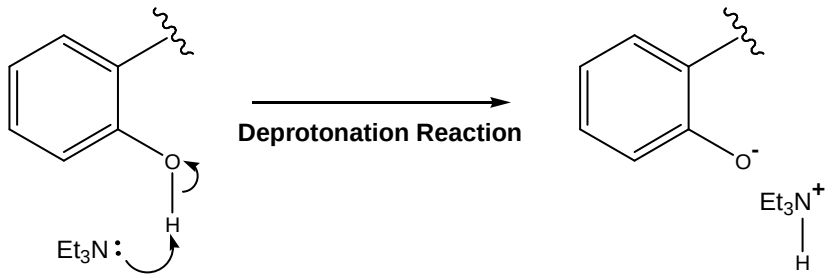

Scheme 3.5: *Mechanism of the deprotonation of a phenolic proton.*

The complexation reactions yielded two new mononuclear (**13**, **14**) and four new multinuclear (**15** - **18**) ruthenium(II) arene complexes. The salicylaldimine ligands (**L7** - **L8**) chelate to the ruthenium metal centre, *via* the *N*- and *O*- donor atoms, yielding a neutral 6-membered ring complex.

3.4.1 Physical properties

The complexes were dried and isolated as dark orange solids in moderate yields, and were found to be thermally stable (Table 3.15).

Table 3.15*: Physical appearance, percentage yield and melting points for complexes* ***10 - 15****.*

Complex	Physical Appearance	Yield (%)	Melting Point (^{o}C)
10	Red-brown solid	43	150-152
11	Red-orange	74	205-208
12	Orange-brown solid	88	161-164
13	Dark orange solid	87	186-188
14	Red-orange solid	60	172[a]
15	Mustard-yellow solid	66	177[a]

[a]*Decompose without melting into a black solid*

The chelating *N,O*- ruthenium(II) arene complexes **13** - **18** are non-hygroscopic, air-stable and soluble in dimethylsulfoxide, acetone, acetonitrile, tetrahydrofuran, dichloromethane, chloroform, toluene, ethanol, methanol and insoluble in diethyl ether and hexane.

3.4.2 ^{1}H-NMR and ^{13}C{^{1}H}-NMR spectroscopy

The proposed chelation of the ruthenium metal centre to the *N*- and *O*- atoms were confirmed by ^{1}H-NMR spectroscopy. The ^{1}H-NMR spectra (Fig. 3.11) of mononuclear complexes **13** and **14** were run in chloroform-*d* and showed characteristic peaks for the coordination of the ligand **L7** and the ruthenium precursor (**[Ru(η^6-*p*-Pr^{i}C$_6$H$_4$Me)Cl$_2$]** or **[Ru(η^6-C$_6$Me$_6$)Cl$_2$]$_2$**).

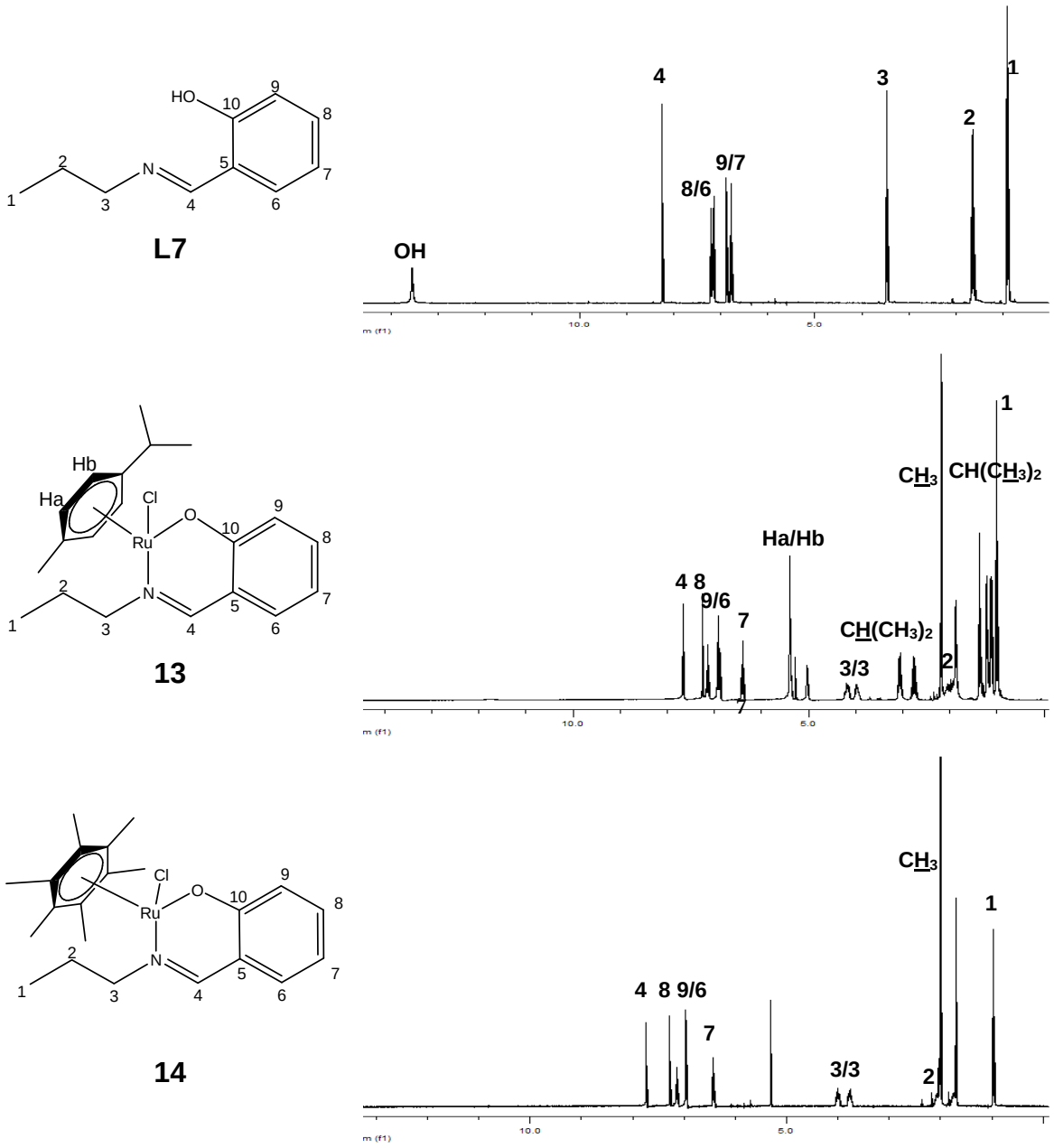

***Figure 3.11**: [1]H-NMR spectra of salicylaldimine ligand **L7** (top), mononuclear complexes **13** (middle) and **14** (bottom).*

A similar pattern is seen in the [1]H-NMR spectra (Fig. 3.12) of the dendritic complexes **15** - **18**. The [1]H-NMR spectra of the dendritic complexes showed broadened peaks (similar to that of the previously mentioned dendritic complexes), with many of the peaks overlapping and/or coalescing, due to the multinuclear nature of these complexes.

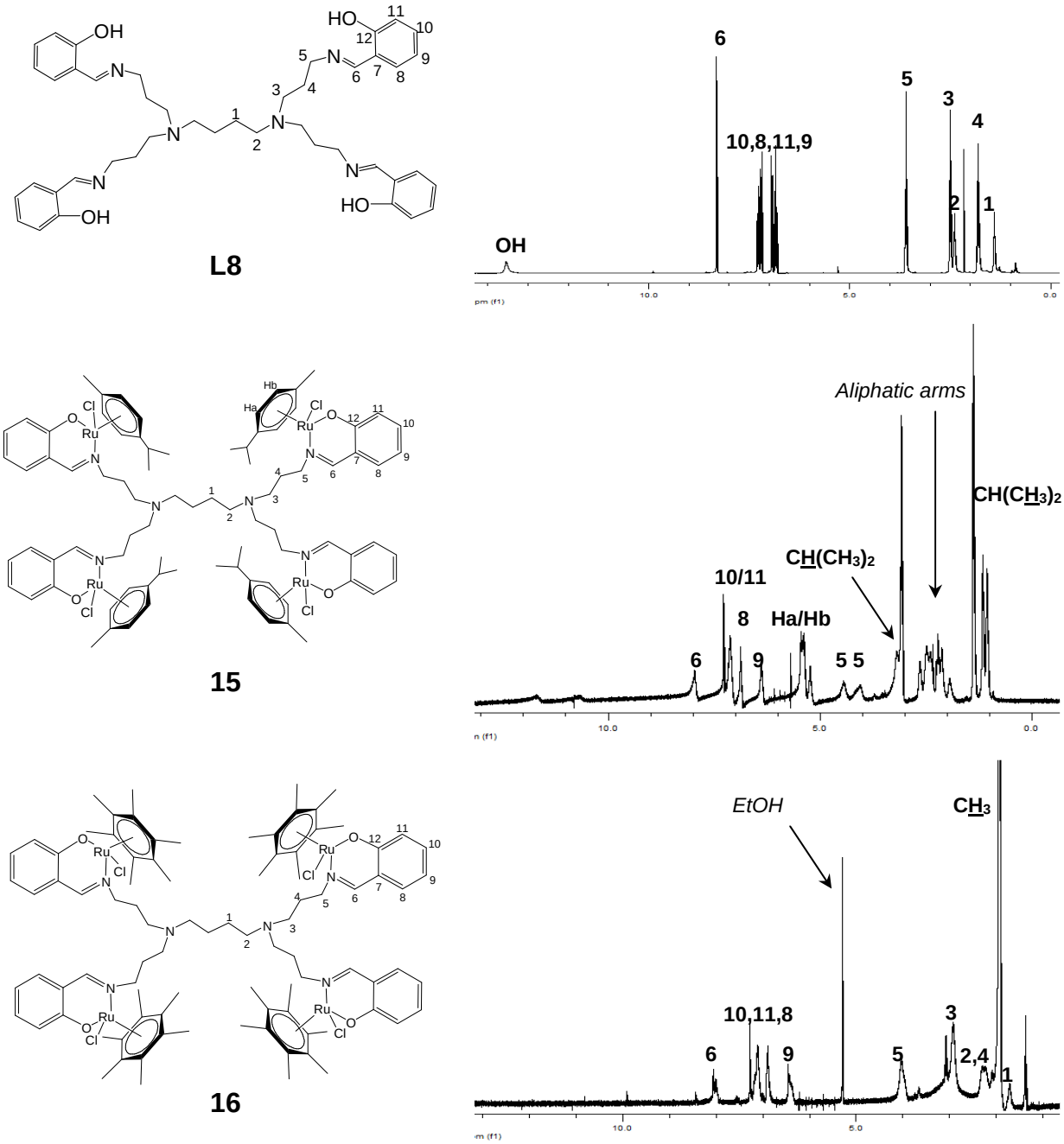

***Figure 3.12**: [1]H-NMR spectra of salicylaldimine dendritic ligand **L8** (top), dendritic complexes **15** (middle) and **16** (bottom).*

As a result of the ruthenium-arene moiety coordinating to both the imine and oxygen atom, there is a shift in both the imine proton and protons on the aromatic ring for all complexes **13** - **18**. Similar to the cationic salts, upon coordination of the ruthenium-arene moiety to the ligand, the ruthenium metal centre becomes chiral. The newly formed chiral centre is due to the coordination of four different groups on the ruthenium metal centre. The diastereotopic nature of the protons on the aliphatic

chain of the mononuclear complexes **13** and **14** further confirms the presence of the chiral centre. Both sets of diastereotopic protons, on each carbon (carbon 2 and 3), show two sets of multiplets in the ranges 1.6 - 2.1 ppm and 3.7 - 4.2 ppm for complexes **13** and **14**. The diastereotopic protons on the dendritic arms of complexes (**15** - **18**), adjacent to the imine nitrogen, show the same effect as their mononuclear counterparts. Two broad multiplets for the first generation complexes (**15** and **16**), between 4.0 - 4.5 ppm are seen and a very broad multiplet for the second generation complexes (**17** and **18**) between 4.0 - 4.5 ppm is also noted.

*p-Cymene complexes (**13**, **15**, **17**)*

In the ^{1}H-NMR spectrum of complex **13**, the methyl protons on the isopropyl group (on the *p*-cymene ring), exhibit one doublet per methyl group, each of the doublets integrated for three protons. This could be due to the lack of rotation of the *p*-cymene ring, similar to that of the cationic salts previously mentioned. Two broad multiplets were observed for the dendritic complexes (**15** and **17**) at ~1.0 ppm and ~1.1 ppm and were assigned the diastereotopic methyl protons of the isopropyl group.

A multiplet for complex (**13**) and a broader multiplet for complexes (**15** and **17**) were observed between 3.0 - 3.3 ppm and were assigned to the single proton of the isopropyl group (Table 3.16).

The doublet and the multiplet observed at 5.0 ppm and 5.4 ppm respectively (**10**), correspond to the aromatic protons of the *p*-cymene ring. The dendritic complexes (**15** and **17**) show two doublets assigned to the aromatic protons of the *p*-cymene ring. Similar to the cationic salts, the splitting pattern can be explained due to the long range coupling with the isopropyl protons (Table 3.16).

*Hexamethylbenzene complexes (**14**, **16**, **18**)*

A singlet, integrating for 18 protons, is seen in the ^{1}H-NMR spectrum of complex **14** at 2.0 ppm, and was assigned to the methyl protons of the hexamethylbenzene ring (Table 3.16). Similarly, the dendritic complexes (**16** and **18**) show a singlet peak at 1.7 ppm and 1.9 ppm respectively, and were assigned to the methyl protons of the hexamethylbenzene ring (Table 3.16).

***Table 3.16**: Selected ^{1}H-NMR data for complexes **13** - **18**.*

Complex	Imine Proton(s) (ppm)	Aromatic Protons (ppm)	Arene Ring (ppm)
13	7.7	6.4-7.1	1.17; 1.9-2.8; 5.0-5.4
14	7.7	6.4-7.1	1.96
15	8.0	6.4-7.1	1.12; 2.2-3.2; 5.2-5.4
16	8.1	6.4-7.1	1.71
17	8.1	6.4-7.2	1.10; 2.2-3.3; 5.3-5.5
18	8.1	6.4-7.2	1.94

The ^{1}H-NMR spectrum showed upfield shifts of the imine and aromatic protons, due to coordination of the ruthenium metal. The disappearance of the broad peak (~ 13.5 ppm) assigned to the hydroxyl proton of the free ligand (**L7**, **L8**, **L9**), confirms coordination of the ruthenium metal to both imine nitrogen and the phenolic oxygen.

^{13}C{^{1}H}-NMR spectra of the neutral chelating complexes (**13** - **18**) were run in chloroform-*d* and were found to be very similar, with extra signals seen in the ^{13}C{^{1}H}-NMR spectra, these were assigned to the carbons of the aliphatic side arms (Table 3.17). The ^{13}C{^{1}H}-NMR spectrum of the mononuclear complexes (**13** and **14**) is similar to the ^{13}C{^{1}H}-NMR spectrum of the monomeric ligand **L2**, with shifts seen in the signals that were assigned to the imine and pyridyl carbons, as a result of coordination to the ruthenium metal centre (Table 3.17).

***Table 3.17**: Selected ^{13}C{^{1}H}-NMR data for complexes **13** - **18**.*

Complex	Imine Carbon(s) (ppm)	Aromatic Carbons (ppm)	Arene Ring (ppm)
13	164	114-165	19-23; 31-102
14	165	114-166	16; 91
15	165	114-165	19-23; 31-100
16	165	114-166	16; 91
17	165	114-165	19-23; 31-100
18	165	114-166	16; 91

$^{13}C\{^{1}H\}$-NMR spectra of the neutral chelating complexes (**13** - **18**) showed chemical shifts of its aromatic carbons in the range of 114 - 165 ppm. The $^{13}C\{^{1}H\}$-NMR spectra of the *p*-cymene complexes (**13**, **15**, **17**) showed a range of signals between 19 - 23 ppm and 31 - 102 ppm. The $^{13}C\{^{1}H\}$-NMR spectra of the hexamethylbenzene complexes (**14**, **16**, **18**) showed signals at 16 and 91 ppm.

3.4.3 Infrared (IR) spectroscopy

Further confirmation for the coordination of the ruthenium metal centre can be seen from the IR spectra of the complexes (**13** - **18**). A distinct shift in the imine stretching frequency from ~1635 cm^{-1} (for the ligand) to ~1620 cm^{-1} for the complexes (**13** - **18**) is seen (Table 3.18).

***Table 3.18**: Selected IR absorption bands for complexes **13** - **18**.*

Complex	$(C=N)_{imine}$ (cm^{-1})
13	1624
14	1624
15	1621
16	1618
17	1621
18	1618

3.4.4 Elemental analysis and mass spectrometry

Elemental analysis data of the new mononuclear neutral chelating complexes **13** and **14** were found to correlate with the calculated values. The dendritic complexes were found to be inconsistent with theoretical values. Thus, calculated values were recalculated with the inclusion of solvent molecules (dichloromethane). This brought the found values in direct correlation with calculated values.

Due to the various sizes of the complexes, mononuclear complexes were sent for electron spray mass spectrometry, whilst the larger dendritic complexes were sent for MALDI-TOF mass spectrometry. Mass spectrometry data further supported elemental analysis data for the neutral chelating complexes (**14** - **18**), which showed

$[M\text{-}Cl]^+$ as the highest molecular weight fragment but mononuclear complex **13** gave $[C_{20}H_{23}NRuClO]^+$ as the highest molecular weight fragment (Table 3.19).

***Table 3.19**: Mass spectrometry data for **13** - **18**.*

Complex	Calculated Molecular Mass (g/mol)	Molecular Fragment (m/z)	Assignment
13	433.0	430	$[C_{20}H_{23}NRuClO]^+$
14	461.0	426	$[M\text{-}Cl]^+$
15	1812.5	1777	$[M\text{-}Cl]^+$
16	1923.5	1888	$[M\text{-}Cl]^+$
17	3800.5	3765	$[M\text{-}Cl]^+$
18	3990.5	3955	$[M\text{-}Cl]^+$

3.4.5 X-ray crystallography

The neutral mononuclear chelating complex **14** was structurally characterized by single crystal X-ray crystallography. The crystals were grown by slow diffusion of diethyl ether into a concentrated dichloromethane/methanol (5:1) solution of complex **14**. Crystals of complex **14** were isolated as orange crystalline plates, in the monoclinic space group $P\ 2_1/c$. The ruthenium centre of the mononuclear structure shows the typical “three-leg piano-stool”, pseudo-tetrahedral geometry.[11] Similar to the cationic mononuclear complexes **7** and **8**, the arene ring (hexamethylbenzene) represent the “seat” and, bound by the oxygen and imine- nitrogen are the bidentate and single chlorido ligands, which are the “legs”. The ORTEP drawing of the neutral mononuclear complex **14** is shown (Fig. 3.13), with the crystallographic data listed (Table 3.20) and selected bond lengths and angles tabulated in Table 3.21.

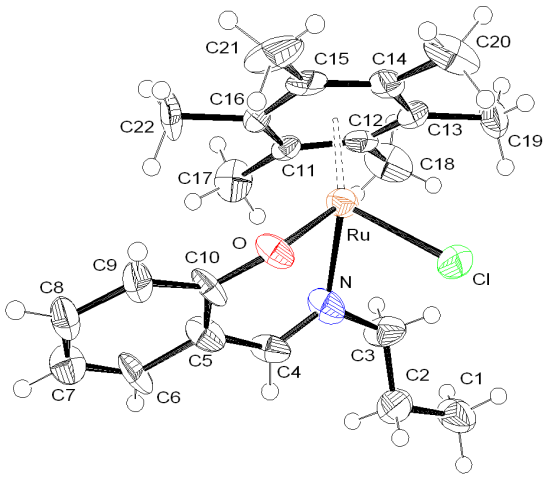

***Figure 3.13**: The ORTEP structure of the mononuclear salicylaldimine complex **14**.*

The salicylaldimine mononuclear complex **14** is essentially a planar molecule, with the arene moiety being the only substituent out of the plane. Complex **14** has bond distances of the Ru-N_{imine} and Ru-O being 2.078(15) and 2.085(10) Å respectively. The ruthenium atom is π bonded to the hexamethylbenzene ligand with Ru-C distances ranging from 2.160(14) to 2.236(13) Å. The Ru-Cl distance in complex **14** (2.429(5) Å) is slightly longer than the cationic salts **7** (2.3910(7)) and **8** (2.3979(1) Å). The bond distances and angles of complex **14** are comparable to similar known *N,O*- complexes.[16,17] The crystal analysis confirmed the mode of coordination of the ruthenium metal centre.

As seen for the cationic salt **8**, the mononuclear complex **14** showed a hydrogen bond between the CH_{imine} group and the chloride atom of a neighbouring molecule; giving rise to infinite one-dimensional chains (Fig. 3.14). In complex **14**, the hydrogen bond C-H···Cl distance is 3.557(17) Å with a C-H···Cl angle of 135.5°.

***Table 3.20**: Crystallographic and structure refinement parameters for mononuclear salicylaldimine complex **14**.*

Complex	14
Chemical formula	$C_{22}H_{30}ClNORu$
Formula weight (g /mol)	460.99
Crystal colour and shape	Orange plate
Crystal size (mm)	0.18 x 0.15 x 0.07
Crystal system	Monoclinic
Space group	$P\ 2_1/c$
a (Å)	7.620(2)
b (Å)	21.340(4)
c (Å)	12.830(3)
α (°)	-
β (°)	99.67(3)
γ (°)	-
V (Å^3)	2056.7(8)
Z	4
T (K)	173(2)
Wavelength λ (Å)	0.71073
Density D_X (g /cm^3)	1.489
Absorption coefficient μ (mm^{-1})	0.903
F(000)	952
Scan range (°)	1.37 < θ < 26.63
Unique reflections	5350
Reflections used [$I > 2\sigma(I)$]	1814
R_{int}	0.3647
Final R indices [$I > 2\sigma(I)$][a]	0.1373, wR_2 0.3016
R indices (all data)	0.2884, wR_2 0.3898
Goodness-of-fit (GOF)	0.937
Maximum, Minimum $\Delta\rho$ (e Å^{-3})	1.620, -1.563

[a] Structures were refined on F_0^2: $wR_2 = [\Sigma[w(F_0^2 - F_c^2)^2] / \Sigma\, w(F_0^2)^2]^{1/2}$, where $w^{-1} = [\Sigma\,(F_0^2) + (aP)^2 + bP]$ and $P = [\max(F_0^2, 0) + 2F_c^2]/3$.

***Table 3.21**: Selected bond lengths (Å) and angles (°) for mononuclear salicylaldimine complex **14**.*

Complex	14
Distances (Å)	
Ru(1)-C(11)	2.160(14)
Ru(1)-C(12)	2.236(13)
Ru(1)-C(13)	2.225(13)
Ru(1)-C(14)	2.175(12)
Ru(1)-C(15)	2.195(13)
Ru(1)-C(16)	2.192(13)
Ru(1)-Cl(1)	2.429(5)
Ru(1)-N(1)	2.078(15)
Ru(1)-O(1)	2.085(10)
N(1)-C(4)	1.295(16)
C(4)-C(5)	1.410(19)
Angles (°)	
N(1)-Ru(1)-Cl(1)	86.4(5)
O(1)-Ru(1)-Cl(1)	85.2(4)
O(1)-Ru(1)-N(1)	84.5(5)

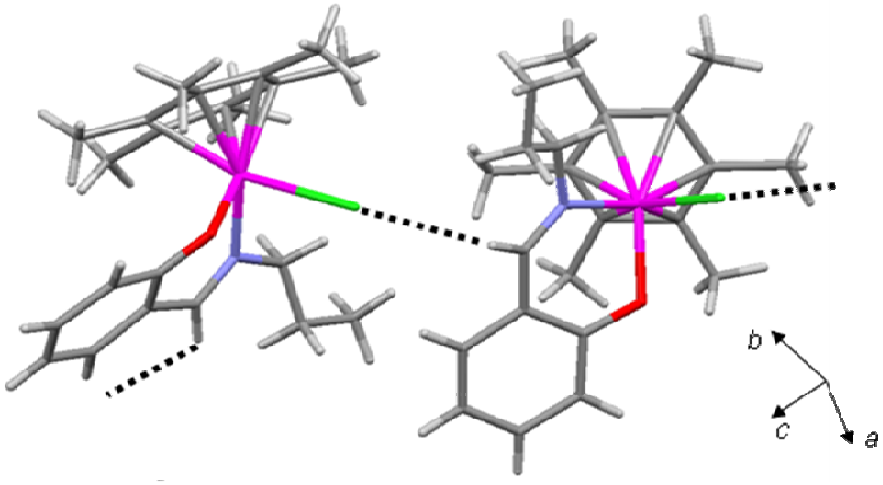

***Figure 3.14:** Crystal packing of mononuclear complex **14** illustrating the infinite one-dimensional chains. The hydrogen atoms are omitted for clarity.*

3.5 Conclusions

In the pursuit of synthesizing new multinuclear dendritic ruthenium(II) arene complexes, a series of air-stable monodentate *N*- donor and chelating, bidentate *N,N*- and *N,O*- donor ruthenium(II) arene metallodendrimers were prepared. These new dendritic complexes were fully characterized using spectroscopic and analytical techniques, namely ^{1}H-NMR, ^{13}C{^{1}H}-NMR, IR spectroscopy, and elemental analysis and mass spectrometry. X-ray crystallography experiments were employed on the mononuclear complexes to further confirm the mode of coordination of the ruthenium-arene moiety and proposed structures.

3.6 References

1) M. Fujita, M. Tominaga, A. Hori and B. Therrien, *Acc. Chem. Res.,* 2005, **38**, 369.
2) M. A. Bennett, *Coord. Chem. Rev.*, 1997, **166**, 225.
3) C. S. Allardyce, P. J. Dyson, D. J. Ellis, P. A. Salter and R. Scopelliti, *J. Organomet. Chem.*, 2003, **668**, 35.
4) L. Mishra, A. Kumar Yadaw, S. Srivastava and A. Bahadur Patel, *New J. Chem.*, 2000, **24**, 505.
5) M. Melchart and P. J. Sadler, in Bioorganometallics, Ed. G. Jaouen, Wiley-VCH, Weinheim, 1st Edn., 2006, vol. 1, ch. 2, pp. 39–62.
6) G. Süss-Fink, *Dalton Trans.*, 2010, **39**, 1673.
7) M. A. Bennett and A. K. Smith, *J. Chem. Soc. Dalton Trans.*, 1974, **2**, 233.
8) M. A. Bennett, T. W. Matheson, G. B. Robertson, A. K. Smith, and P. A. Tucker, *Inorg. Chem.*, 1980, **19**, 1014.
9) S. Grgurić-Šipka, I. Ivanović, G. Rakić, N. Todorović, N. Gligorijević, S. Radulović, V. B. Arion, B. K. Keppler and Ž. Lj. Tešić, *Eur. J. Med. Chem.*, 2010, **45**, 1051.
10) J. F. G. A. Jansen, E. M. M. de Brabander-van den Berg and E. W. Meijer, *Science*, 1994, **266**, 1226.
11) B. Therrien, *Coord. Chem. Rev.*, 2009, **253**, 493.
12) R. Lalrempuia, M. R. Kollipara and P. J. Carroll, *Polyhedron*, 2003, **22**, 605.
13) P. Govindaswamy, Y. A. Mozharivskyj and M. R. Kollipara, *J. Organomet. Chem.*, 2004, **689**, 3265.
14) P. Govindaswamy, P. J. Carroll, C. Sinha and M. R. Kollipara, *J. Coord. Chem.*, 2007, **60**, 97.
15) Ch. Elschenbroich and A. Salzer, *Organometallics - A concise Introduction*, VCH Publishers Inc., New York, 2nd Edn., 1992.
16) P. Govindaswamy, B. Therrien, G. Süss-Fink, P. Štěpnička and J. Ludvík, *J. Organomet. Chem.*, 2007, **692**, 1661.
17) T.-T. Thai, B. Therrien and G. Süss-Fink, *J. Organomet. Chem.*, 2009, **694**, 3973.

Chapter 4

In Vitro Biological Evaluation of Multinuclear Ruthenium(II) Arene Complexes of Pyridyl-imine and Salicylaldimine Dendritic Ligands

4.1 Introduction

It is believed that organometallic complexes are known for their toxicity and instability, decomposing when exposed to air and/or water. This observation has been misinterpreted, as there are an increasing number of air-stable and water-soluble complexes in the literature, and ruthenium(II) arene complexes are such examples.[1] Despite the fact that ruthenium(II) arene compounds have a low general toxicity and have a high selectivity for cancer cells, the main reason for their design are the amphiphilic properties of the arene-ruthenium unit, in the form of the hydrophobic arene ligand and the hydrophilic ruthenium metal centre. The arene ring is said to stabilize the metal oxidation state and gives the complex a lipophilic property, whilst the halide ligand is labile and undergoes hydrolysis in aqueous media. Aquation is believed to be the key aspect in the biological activity of the $[(\eta^6\text{-arene})Ru(en)Cl]^+$ (en = ethylenediamine) complex (Fig. 4.1).[2]

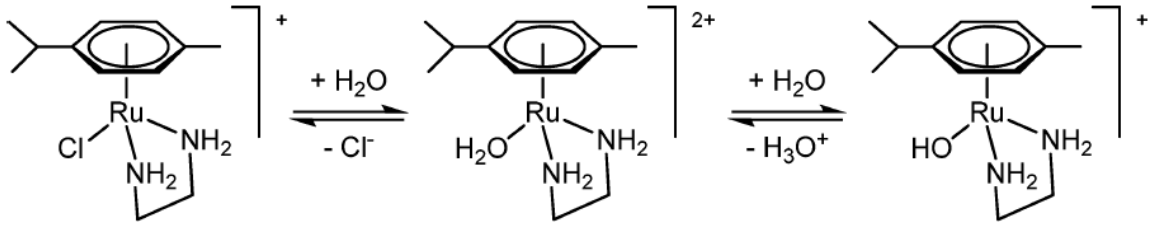

Figure 4.1: *Hydrolysis of $[(\eta^6\text{-}p\text{-}Pr^iC_6H_4Me)Ru(en)Cl]^+$ (en = ethylenediamine) in water at a 10 μM concentration.*

The mechanism of action of arene-ruthenium complexes is generally thought to involve hydrolysis of the Ru-X bond resulting in an active $Ru\text{-}OH_2$ species.[3] Ruthenium(II) arene complexes provide an excellent substrate for the coupling of organic drugs to the ruthenium moiety in targeted chemotherapy.

The development of multinuclear complexes as anticancer agents has recently also generated tremendous interest. The platinum-based trinuclear complex [*trans*, *trans*, *trans*-$(NH_3)_2Pt(Cl)NH_2(CH_2)_6NH_2Pt(NH_3)_2NH_2(CH_2)_6NH_2Pt$-$(NH_3)_2(Cl)][NO_3]_4$ (BBR3464, Fig. 4.2) showed higher *in vitro* cytotoxicity than its mononuclear analogue and cisplatin.[4] Though phase II trials of BBR3464 were not pursued further,[5] the concept that multinuclearity could assist in the improvement of the potency of potential anticancer drugs was established.

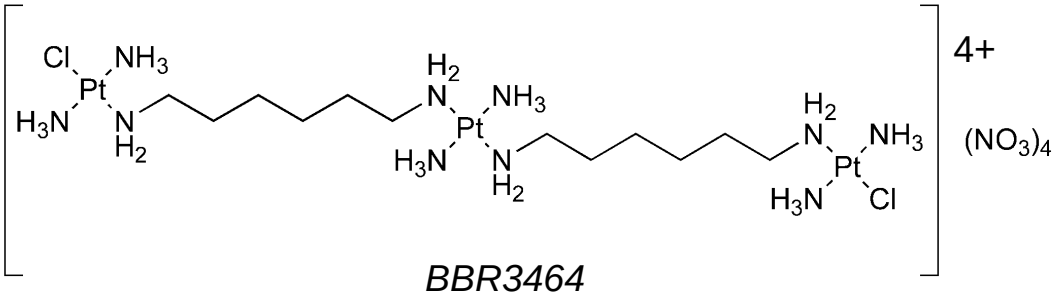

BBR3464

Figure 4.2: *The trans-platinum(II)-based trinuclear complex (BBR3464)*.

Compared to multinuclear platinum complexes, analogous multinuclear organometallic ruthenium compounds have been less studied for their anticancer properties, with just a few examples to be found in the literature.[6-9]

More recently, the *in vitro* anticancer activity of a series of mono-, di- and trinuclear ruthenium(II) *p*-cymene complexes has been investigated on SW480 and A2780 cell lines, with the dinuclear complex proving to be the most active, probably by cross-linking biomacromolecules (Fig. 4.3).[10,11]

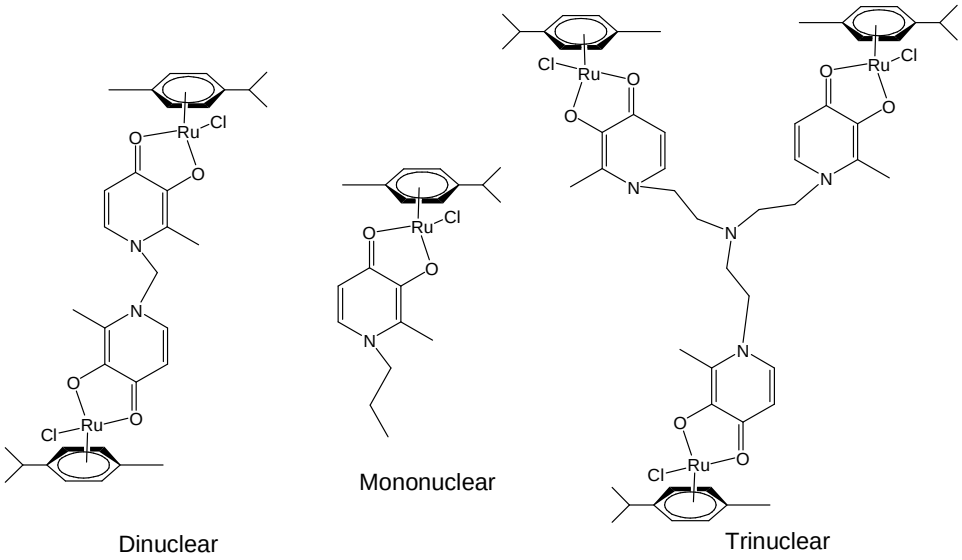

Figure 4.3: *Dinuclear, mononuclear and trinuclear ruthenium(II) arene anticancer compounds.*

The relative size of metallodendrimers implies that they may exploit the 'enhanced permeability and retention' (EPR) effect, a phenomenon in which macromolecules accumulate at the tumour site due to an increase in blood vessel permeability within diseased tissues compared to normal tissues.[12] The increase in the local concentration of transition metals in the metallodendrimer endows them with several advantages in the field of catalysis such as, enhanced catalytic activity compared to their mononuclear analogues.[13-15] With these two aspects in mind, the *in vitro* biological activity of the synthesized ruthenium(II) arene complexes (**1** - **18**) (Fig. 4.4) in the A2780 cell line were investigated, and selected complexes were tested in the cisplatin resistant (A2780cisR) cell line.

This chapter describes the biological activity, of the synthesized mononuclear and multinuclear ruthenium(II) arene complexes, against the cisplatin sensitive (A2780) and cisplatin resistant (A2780cisR) human ovarian cancer cells. Interactions of the two most highly cytotoxic ruthenium(II) arene complexes with DNA were also investigated, in the form of DNA binding experiments.

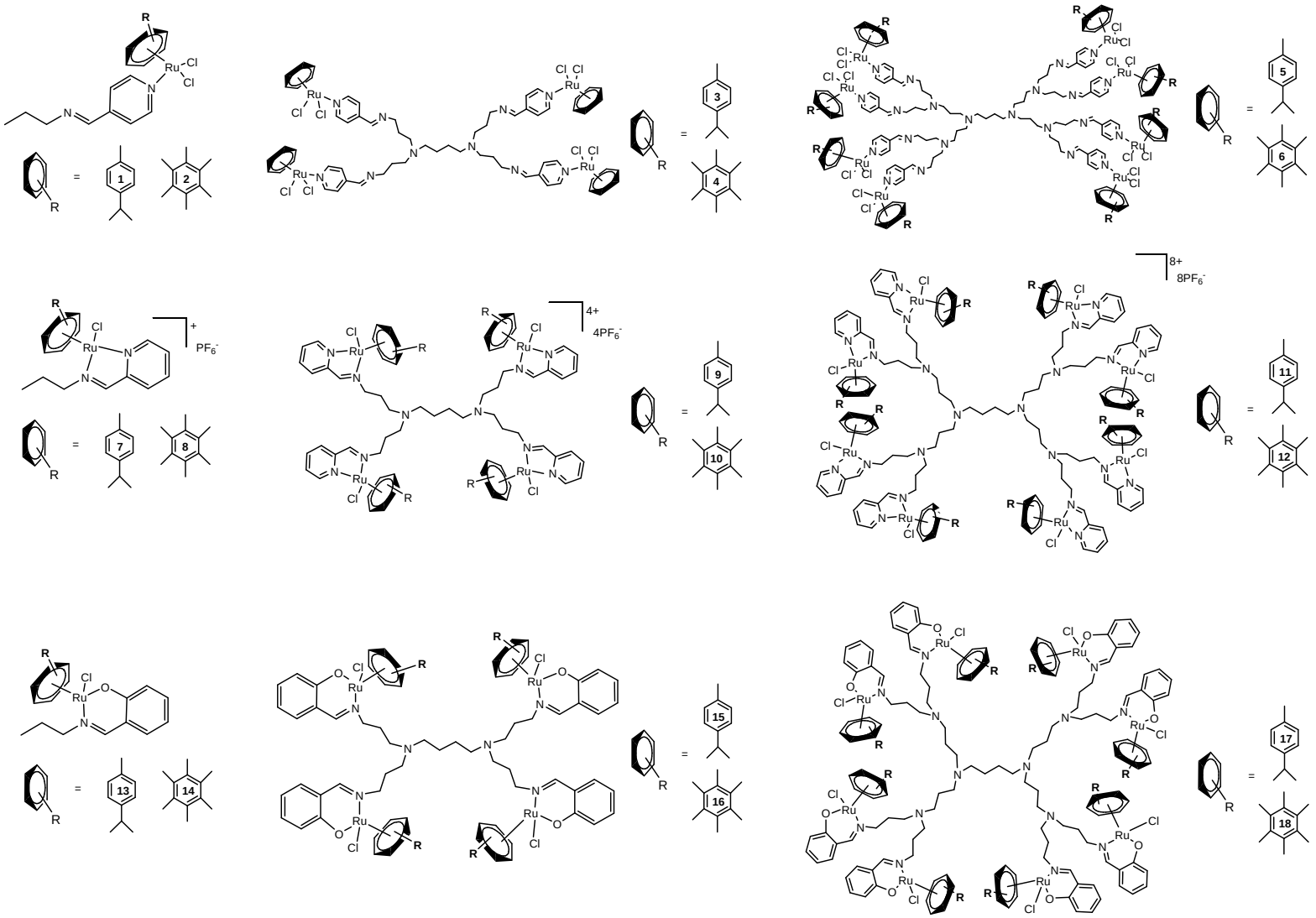

Figure 4.4: *Synthesized ruthenium(II) arene complexes (**1** - **18**).*

4.2 Influence of the number of ruthenium centres: mono- vs. tetra- vs. octanuclear

The poly(propyleneimine) dendritic scaffolds (**L3** - **L6**, **L8**, **L9**) were chosen to exploit the number of metal sites, on one substrate, entering the cancerous cell. The 1st and 2nd generation derivatives (**3** - **6**) and their mononuclear analogues (**1**, **2**) of the monodentate 4-pyridyl-imine series were compared, following their biological evaluation in the A2780 cell line (Table 4.1). These findings have been recently published.[16]

Table 4.1: *IC_{50} values of synthesized monodentate 4-pyridyl-imine ruthenium(II) complexes tested against A2780 human ovarian cancer cells.*

Compound	n[a]	Arene	(IC_{50}, μM)
			A2780
4-Pyridyl-imine			
1	1	*p*-CYE	98 ± 5.0
2	1	HMB	94 ± 5.0
3	4	*p*-CYE	43 ± 5.0
4	4	HMB	40 ± 5.0
5	8	*p*-CYE	21 ± 5.0
6	8	HMB	20 ± 5.0
Cisplatin	1	-	1.5

[a] *Number of metals within the compound*

The second generation derivatives (**5**, **6**) with 8 arene-ruthenium moieties within the complex show the greatest activity (IC_{50} ~ 20 μM), followed by the first generation derivatives (**3**, **4**) with 4 arene-ruthenium moieties (IC_{50} ~ 41 μM). The mononuclear derivatives (**1**, **2**) with only 1 arene-ruthenium moiety showed no remarkable activity (IC_{50} > 90 μM). The trend seen within the 4-pyridyl series confirms the hypothesis that functionalization with the ruthenium-arene moiety and increasing the metal content of higher dendritic generations will lead to an increase in the biological activity of the complexes.

The bidentate chelating ruthenium(II) arene *N,N*- series (**12**) and *N,O*- series (**17**, **18**) show the best activity of the ruthenium(II) dendritic series (Table 4.2). The biological activity of the mononuclear ruthenium(II) arene analogues (**1**, **2**, **7**, **8**, **13**, **14**) are lower and drop further with the tetranuclear derivatives (**3**, **4**, **9**, **10**, **15**, **16**), when comparing them to the activity of the octanuclear complexes (**5**, **6**, **11**, **12**, **17**, **18**) (Table 4.2).

Table 4.2: *IC_{50} values of synthesized bidentate 2-pyridyl-imine and salicylaldimine ruthenium(II) complexes on A2780 human ovarian cancer cells.*

Ru(II) Compound	n[a]	Arene	(IC_{50}, µM)	
			A2780	A2780cisR
2-Pyridyl-imine (*N,N*-)				
7	1	*p*-CYE	> 200	> 200
8	1	HMB	> 200	> 200
9	4	*p*-CYE	> 200	> 200
10	4	HMB	32 ± 1.6	42 ± 5.1
11	8	*p*-CYE	23 ± 2.1	76 ± 9.4
12	8	HMB	4 ± 1.3	4 ± 0.3
Salicylaldimine (*N,O*-)				
13	1	*p*-CYE	49 ± 2.3	47 ± 0.8
14	1	HMB	19 ± 1.8	18 ± 0.8
15	4	*p*-CYE	50 ± 1.4	52 ± 0.8
16	4	HMB	27 ± 1.3	25 ± 1.3
17	8	*p*-CYE	22 ± 1.2	15 ± 1.4
18	8	HMB	10 ± 0.3	9 ± 0.3
Cisplatin	1	-	1.5	25

[a] *Number of metals within the compound*

The IC_{50} values of the bidentate chelating *N,N*- and *N,O*- ruthenium(II) arene complexes were also evaluated against the cisplatin resistant cell line (Table 4.2). A similar trend is seen to the non-cisplatin resistant cell line, however, the higher generations (8 arene-ruthenium metal centres) displayed the greatest activity. A more interesting observation are the results of the octanuclear complexes (**11**, **12**,

17, **18**) when comparing them to cisplatin, a platinum based drug currently used to fight most carcinomas. In the A2780 cell line, the second generation ruthenium(II) arene complexes (**12**: IC_{50} = 4 μM, **18**: IC_{50} = 10 μM) were approximately 3 folds lower in biological activity compared to that of cisplatin (IC_{50} = 1.5 μM). However, the biological activity of the second generation ruthenium(II) arene complexes (**12**: IC_{50} = 4 μM, **17**: IC_{50} = 15 μM, **18**: IC_{50} = 9 μM) against the A2780cisR cell line, showed more potency than cisplatin (IC_{50} = 25 μM). The octanuclear *N,O*- bidentate complexes (**17**, **18**) were found to show high cytotoxicity compared to similar mononuclear *N,O*- bidentate complexes reported by Grgurić-Šipka *et al.*[17]

Analysis of the biological results obtained for each cell line (A2780 vs. A2780cisR) showed another trend. Comparing the biological values of the synthesized ruthenium(II) arene complexes (**7** - **18**) for each cell line (A2780 & A2780cisR), It was found that very similar values were obtained. This suggests that the mechanism of action followed by the mononuclear (**7**, **8**, **13**, **14**) and dendritic (**9** - **12**, **15** - **18**) ruthenium(II) arene complexes is different to that of the mechanism of action followed by cisplatin.

4.3 Influence of the arene ring: *p*-cymene vs. hexamethylbenzene

In the synthesis of the ruthenium(II) arene complexes, two types of arene ring systems, *p*-cymene and hexamethylbenzene, were used. Their antiproliferative activity as a function of the arene ring was investigated (Table 4.3).

Table 4.3: *IC_{50} values of synthesized ruthenium(II) complexes against the A2780 human ovarian cancer cell line.*

Ru(II) Compound	n[a]	Arene	(IC_{50}, µM) A2780
4-Pyridyl-imine			
1	1	*p*-CYE	98 ± 5.0
2	1	HMB	94 ± 5.0
3	4	*p*-CYE	43 ± 5.0
4	4	HMB	40 ± 5.0
5	8	*p*-CYE	21 ± 5.0
6	8	HMB	20 ± 5.0
2-Pyridyl-imine (*N,N*-)			
7	1	*p*-CYE	> 200
8	1	HMB	> 200
9	4	*p*-CYE	> 200
10	4	HMB	32 ± 1.6
11	8	*p*-CYE	23 ± 2.1
12	8	HMB	4 ± 1.3
Salicylaldimine (*N,O*-)			
13	1	*p*-CYE	49 ± 2.3
14	1	HMB	19 ± 1.8
15	4	*p*-CYE	50 ± 1.4
16	4	HMB	27 ± 1.3
17	8	*p*-CYE	22 ± 1.2
18	8	HMB	10 ± 0.3
Cisplatin	1	-	1.5

[a] *Number of metals within the compound*

The arene ring system is another structural feature that is suggested to play an important role in the mode of action of ruthenium(II) arene complexes.[2,18] In order to increase the π- electron density of the ring system of the arene ligand, the *p*-cymene ligand was replaced with hexamethylbenzene, which in turn results in a more lipophilic complex.

All synthesized ruthenium(II) complexes showed a moderate to high biological activity. In the ligand systems (*N,N*- & *N,O*-) the ruthenium(II) complexes containing the hexamethylbenzene arene ring exhibit a lower IC_{50} value than their *p*-cymene analogues. Literature suggests that the higher activity observed in hexamethylbenzene derivatives are due to the increased uptake of the hexamethylbenzene complexes due to the greater lipophilicity of the arene ring.

Such an effect is also seen with the metallarectangles synthesized by Therrien and co-workers (Fig. 4.5).[19] The *p*-cymene metallarectangles showed a higher IC_{50} value (A2780 cell line) than their hexamethylbenzene metallarectangles, suggesting greater lipophilicity of the hexamethylbenzene derivatives.[1]

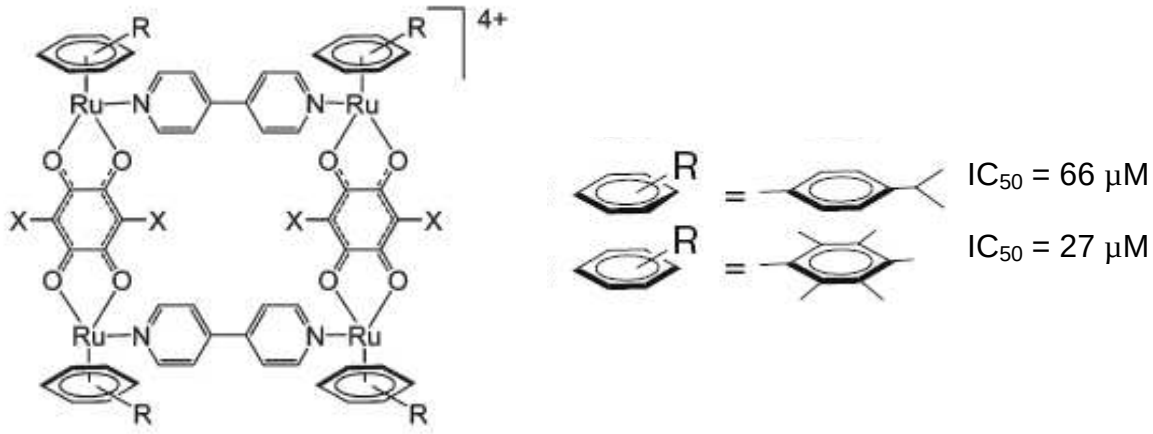

***Figure 4.5**: Molecular structure and IC_{50} values of ruthenium(II) arene metallarectangles.*

A similar effect was seen with their ruthenium(II) arene complexes containing the 2-(pyridine-2-yl)thiazole *N,N*- chelating ligand (Fig. 4.6), with the hexamethylbenzene derivatives showing high antiproliferative activity against the A2780 cell line.[20]

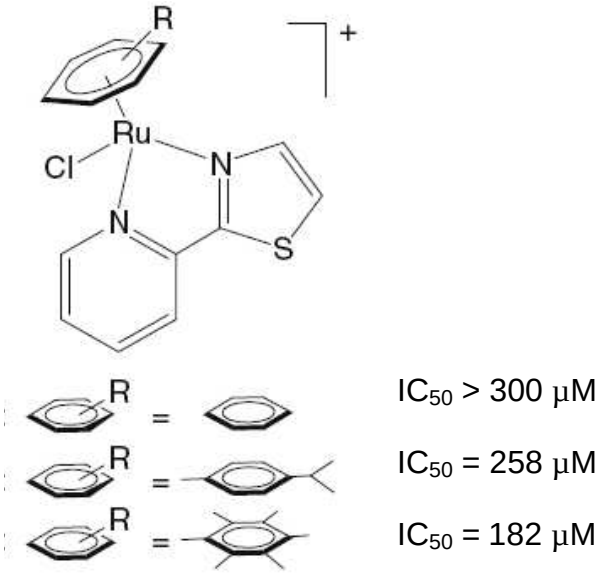

***Figure 4.6**: Molecular structure and IC_{50} values of ruthenium(II) arene complexes containing the 2-(pyridine-2-yl)thiazole N,N- chelating ligand.*

4.4 Influence of the ligand: monodentate vs. bidentate ligand system

Currently there are a few structure-activity relationship studies with ruthenium(II) arene complexes. Dyson and co-workers have shown that variation in the arene ligand system and/or the monodentate or bidentate ligand does influence the antiproliferative activity of these complexes.[21] In comparing the two systems, the 4-pyridyl-imine (monodentate) and the *N,N*- and *N,O*- (bidentate) systems, the bidentate systems show higher biological activity (Table 4.3). The second generation bidentate derivatives (**12**: IC_{50} = 4 μM, **18**: IC_{50} = 10 μM) show a higher activity over the second generation monodentate derivatives (**6**: IC_{50} = 20 μM, **5**: IC_{50} = 21 μM).

Variation on the bidentate chelating (*N,N*- vs. *N,O*-) system generated cationic (**7** - **12**) and neutral (**13** - **18**) complexes. The effects on the biological activity of the complexes were evaluated on the A2780 and A2780cisR cell lines (Table 4.6). The mononuclear cationic salts (**7**, **8**: IC_{50} > 200 μM) show no activity in comparison to the mononuclear *N,O*- complexes (**13**: IC_{50} = 49 μM, **14**: IC_{50} = 19 μM). The cationic dendritic salts (**10**, **11**) show moderate antiproliferative activity compared to the salicylaldimine dendritic complexes (**15** - **17**), however the octanuclear cationic salt (**12**: IC_{50} = 4 μM) showed a much lower IC_{50} value than the neutral octanuclear complex (**18**: IC_{50} = 10 μM) for both cell lines.

The low activity of the mono- (**7**, **8**) and tetranuclear (**9**, **10**) complexes, could be due to the poor solubility of the cationic complexes (**7** - **12**). The PF_6 counterion of these cationic complexes is believed to give these compounds very poor solubility in the aqueous medium, for both the mononuclear (**7**, **8**) and dendritic complexes (**9** - **12**).

Table 4.6: *IC_{50} values of synthesized N,N- (cationic) and N,O- (neutral) complexes on A2780 and A2780cisR human ovarian cancer cells.*

Ru(II) Compound	n[a]	Arene	(IC_{50}, μM)	
			A2780	A2780cisR
2-Pyridyl-imine (*N,N*-)				
7	1	*p*-CYE	> 200	> 200
8	1	HMB	> 200	> 200
9	4	*p*-CYE	> 200	> 200
10	4	HMB	32 ± 1.6	42 ± 5.1
11	8	*p*-CYE	23 ± 2.1	76 ± 9.4
12	8	HMB	4 ± 1.3	4 ± 0.3
Salicylaldimine (*N,O*-)				
13	1	*p*-CYE	49 ± 2.3	47 ± 0.8
14	1	HMB	19 ± 1.8	18 ± 0.8
15	4	*p*-CYE	50 ± 1.4	52 ± 0.8
16	4	HMB	27 ± 1.3	25 ± 1.3
17	8	*p*-CYE	22 ± 1.2	15 ± 1.4
18	8	HMB	10 ± 0.3	9 ± 0.3
Cisplatin	1	-	1.5	25

[a] *Number of metals within the compound*

4.5 DNA binding studies

The second generation, cationic octanuclear *N,N*- bidentate complex (**12**: IC_{50} = 4 μM) and the second generation neutral octanuclear *N,O*- complex (**18**: IC_{50} = 10 μM) showed the highest biological activity of all the synthesized complexes against the A2780 human ovarian cancer cell line. As DNA is suggested to be a potential target for arene-ruthenium drugs, the interactions of these two highly cytotoxic octanuclear complexes **12** and **18** with DNA were investigated.

Gel electrophoresis was employed for the DNA binding studies. It is a technique used to separate DNA based on its mobility in an electric field. Mobility of the DNA is primarily based on size. Thus, the larger the DNA fragment, the smaller the migration band down the gel matrix (agarose gel). Typically, the metal complex is incubated with the plasmid DNA and then separated by electrophoresis (Fig. 4.7). The process involved the connection of opposite ends of the gel plate to a power source whish is used to initiate migration of the DNA. Following electrophoresis, the gel is stained with a staining agent (ethidium bromide) and the bands analysed with an ultraviolet gel scanner. Incubation of the DNA with the metal complex may result in DNA damage which will alter the pattern of migration (i.e. retardation of the band).

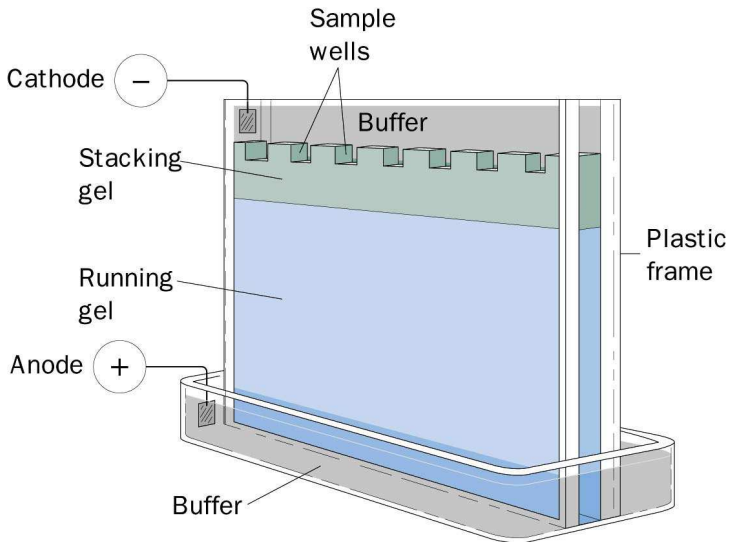

Figure 4.7: *Illustration showing a general setup of gel electrophoresis*

DNA binding studies were performed by incubating plasmid DNA in the presence of the ruthenium (II) arene complexes (**12**, **18**) and cisplatin for 24 hours at 37℃ at different metal center/DNA base pair ratios (r = 0.5, 0.25 and 0.125). The mononuclear ruthenium(II) arene complexes (**8**, **14**) were also investigated for a comparison between the mononuclear and octanuclear analogues. The resulting mixtures were separated by gel electrophoresis and the resulting gels are shown in Fig. 4.8.

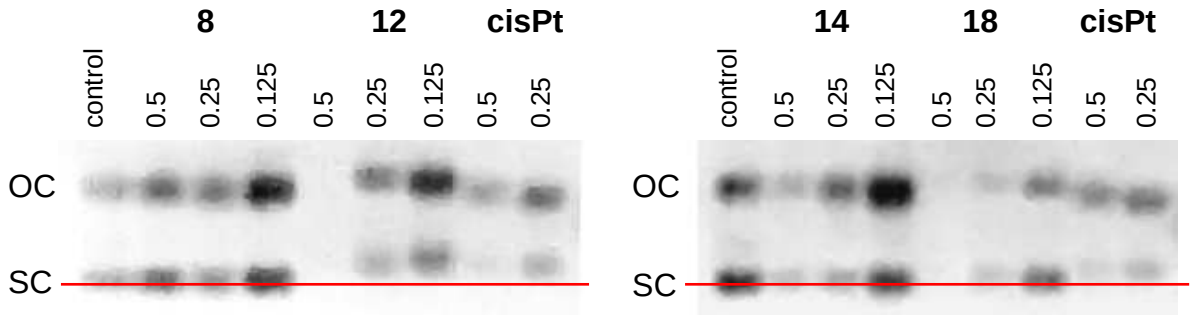

Figure 4.8: *Gel electrophoresis of pBR322 plasmid DNA incubated in presence of (from left to right on each gel) the N,N- cationic mononuclear complex **8** and octanuclear equivalent **12**, the N,O- neutral mononuclear complex **14** and the octanuclear equivalent **18** and cisplatin (cisPt) for 24 h at different metal cente to :DNA base pair ratios (r = 0.5, 0.25 and 0.125).*

Using a metal centre to DNA base pair ratio allows the effect of metallodendrimer on DNA binding to be compared directly (i.e. the octanuclear complexes (**12**, **18**) are 8 times less concentrated than their mononuclear analogues (**8**, **14**) and cisplatin). The control lane (no metal complex present) shows the migration of unmodified free plasmid DNA, which consist of about 5 % open circular (OC) DNA and 95 % supercoiled (SC) DNA. The darker the band, the more plasmid DNA present at that particular band.

The mononuclear analogues (**8**, **14**) show no visible movement of the DNA species, as the plasmid DNA migrates to the same point as the control, suggesting that there is no interaction under these conditions. These findings correlate with the low biological activity of the mononuclear complexes (**8**, **14**). At r = 0.125 concentration (i.e. the metal centre to DNA base pair ratio), the bands were very dark for the mononuclear complexes (**8**, **14**), suggesting that the plasmid DNA is binding more

readily with the staining agent over the mononuclear complexes (**8**, **14**). Hence, there is no interaction between the mononuclear complexes (**8**, **14**) and the plasmid DNA.

At r = 0.5, no bands were visible for both the octanuclear complexes (**12**, **18**). It could be that at this concentration and above, the octanuclear complexes (**12**, **18**) are competing with the staining agent. For all concentrations (r = 0.5, 0.25 and 0.125), the octanuclear complexes (**12**, **18**) show a smaller migration of the plasmid DNA relative to the control, which suggests some interaction between the complex (**12**, **18**) and DNA species. The cationic *N,N*- octanuclear complex **12** shows a greater interaction with the plasmid DNA over the neutral *N,O*- octanuclear complex (**18**). These findings further correlate with the IC_{50} values of these two complexes (**12**: IC_{50} = 4 μM, **18**: IC_{50} = 10 μM). Cisplatin is known to interact with DNA readily, so the retarded migrations of cisplatin bands are expected. The cationic octanuclear complex (**12**) at r = 0.125 shows a smaller migration than cisplatin at r = 0.25. Therefore, the cationic octanuclear complex (**12**), the most cytotoxic complex of the series, interacts more efficiently with the plasmid DNA than cisplatin, while the neutral octanuclear complex (**18**) exhibits a moderate DNA binding activity.

The reason for ready interaction of the cationic *N,N*- chelating bidentate octanuclear complex (**12**) with the plasmid DNA is not known. Two possible reasons for this interaction is therefore proposed; firstly there exists negatively charged phosphate groups on the surface of the DNA helix, which in turn allows electrostatic interactions between these groups and the cationic octanuclear complex (**12**). Secondly, the dendritic scaffold of the cationic octanuclear complex (**12**) resembles that of naturally occurring polyamines, which are known for their biological activity.[22] Naturally occurring polyamines such as spermidine and putrescine have the ability to interact with nucleic acids of DNA and inhibit DNA replication.[23] Moreover, there could be a cooperative effect between these two possible suggestions, resulting in the high cytotoxicity and DNA binding of the cationic *N,N*- octanuclear complex (**12**).

4.6 Conclusions

Following the synthesis of a series of new dendritic ruthenium(II) arene complexes (**1** -**18**), their cytotoxicities against A2780 and A2780cisR human ovarian cell lines were evaluated. As proposed the second generation cationic *N,N*- chelating bidentate octanuclear complex (**12**) and neutral *N,O*- chelating bidentate octanuclear complex (**18**) showed the highest antiproliferative activity against both cell lines. In the human ovarian cisplatin resistant cell line (A2780cisR), the cationic *N,N*- chelating bidentate octanuclear complex (**12**) showed encouraging results as this compound displayed higher cytotoxicity than the mononuclear platinum based drug, cisplatin.

As a result of an increased lipophilicity of the hexamethylbenzene ruthenium(II) arene derivatives, these showed lower IC_{50} values in comparison with their *p*-cymene analogues. The chelating bidentate complexes displayed a higher biological activity over the monodentate derivatives. Nevertheless, some ruthenium compounds were shown to have low *in vitro* activity, but have shown in a number of cases to have good antitumor properties against animal models (*in vivo* studies).[24]

The interaction of plasmid DNA and the two most cytotoxic octanuclear complexes (**12**, **18**), their mononuclear analogues (**8**, **14**) and cisplatin were investigated in the form of DNA binding experiments. The cationic *N,N*- chelating bidentate octanuclear complex (**12**) was found to interact more efficiently with plasmid DNA than cisplatin, with the neutral *N,O*- chelating bidentate octanuclear complex (**18**) displaying moderate interaction. Furthermore, the findings from the DNA binding experiments supplement the high cytotoxic data found for these complexes. In addition, these experiments showed that the new metallodendrimers appear to operate *via* a different mechanism to that of cisplatin.

4.7 References

1) G. Süss-Fink, *Dalton Trans.*, 2010, **39**, 1673.
2) R. E. Morris, R. E. Aird, P. del Socorro Murdoch, H. Chen, J. Cummings, N. D. Hughes, S. Parsons, A. Parkin, G. Boyd, D. I. Jodrell and P. J. Sadler, *J. Med. Chem.*, 2001, **44**, 3616.
3) S. J. Dougan and P. J. Sadler, *Chimia*, 2007, **61**, 704.
4) C. Billecke, S. Finniss, L. Tahash, C. Miller, T. Mikkelsen, N. P. Farrell and O. Bogler, *Neuro-Oncology*, 2006, **8**, 215.
5) D. I. Jodrell, T. R. J. Evans, W. Steward, D. Cameron, J. Prendiville, C. Aschele, C. Noberasco, M. Lind, J. Carmichael, N. Dobbs, G. Camboni, B. Gatti, and F. De Braud, *Eur. J. Cancer*, 2004, **40**, 1872.
6) E. Corral, A. C. G. Hotze, H. den Dulk, A. Leczkowska, A. Rodger, M. J. Hannon and J. Reedijk, *J. Biol. Inorg. Chem.*, 2009, **14**, 439.
7) F. Linares, M. A. Galindo, S. Galli, M. Angustias Romero, J. A. R. Navarro and E. Barea, *Inorg. Chem.*, 2009, **48**, 7413.
8) G. Ribeiro, M. Benadiba, D. de Oliveira Silva and A. Colquhoun, *Cell Biochem. Funct.*, 2010, **28**, 15.
9) T. Gianferrara, A. Bergamo, I. Bratsos, B. Milani, C. Spagnul, G. Sava and E. Alessio, *J. Med. Chem.*, 2010, **53**, 4678.
10) M. G. Mendoza-Ferri, C. G. Hartinger, A. A. Nazarov, R. E. Eichinger, M. A. Jakupec, K. Severin and B. K. Keppler, *Organometallics*, 2009, **28**, 6260.
11) O. Novakova, A. A. Nazarov, C. G. Hartinger, B. K. Keppler and V. Brabec, *Biochem. Pharmacol.*, 2009, **77**, 364.
12) D. F. Baban and L. W. Seymour, *Adv. Drug Delivery Rev*., 1998, **34**, 109.
13) A. W. Bosman, H. M. Janssen and E. W. Meijer, *Chem. Rev.*, 1999, **99**, 1665.
14) M. T. Reetz, G. Lohmer and R. Schwickardi, *Angew. Chem. Int. Ed. Engl.*, 1997, **36**, 1526.
15) M. T. Reetz, *Top. Catal.*, 1998, **4**, 187.
16) P. Govender, N. C. Antonels, J. Mattsson, A. K. Renfrew, P. J. Dyson, J. R. Moss, B. Therrien and G. S. Smith, *J. Organomet. Chem.*, 2009, **694**, 3470.

17) S. Grgurić-Šipka, I. Ivanović, G. Rakić, N. Todorović, N. Gligorijević, S. Radulović, V. B. Arion, B. K. Keppler and Ž. Lj. Tešić, *Eur. J. Med. Chem.*, 2010, **45**, 1051.

18) H. Chen, J. A. Parkinson, S. Parsons, R. A. Coxall, R. O. Gould and P. J. Sadler, *J. Am. Chem. Soc.*, 2002, **124**, 3064.

19) J. Mattsson, P. Govindaswamy, A. K. Renfrew, P. J. Dyson, P. Štěpnička, G. Süss-Fink and B. Therrien, *Organometallics*, 2009, **28**, 4350.

20) M. Gras, B. Therrien, G. Süss-Fink, A. Casini, F. Edafe and P. J. Dyson, *J. Organomet. Chem.*, 2010, **695**, 1119.

21) C. A. Vock, A. K. Renfrew, R. Scopelliti, L. Juillerat-Jeanneret and P. J. Dyson, *Eur. J. Inorg. Chem.*, 2008, 1661.

22) G. Karigiannis and D. Papaioannou, *Eur. J. Org. Chem.*, 2000, 1841.

23) R. A. Casero Jr. and P. M. Woster, *J. Med. Chem.*, 2009, **52**, 4551.

24) I. Kostova, *Curr. Med. Chem.*, 2006, **13**, 1085.

Chapter 5
Overall Summary and Future Outlook

5.1 Overall summary

A series of first- and second- generation end-group modified monodentate and chelating bidentate poly(pyridylimine) dendritic ligands were prepared. These dendritic ligands were fully characterized using a range of spectroscopic and analytical techniques.

The synthesized dendritic ligands were coupled with ruthenium(II) arene precursors to afford air-stable monodentate *N*- donor and chelating, bidentate *N,N*- and *N,O*- donor ruthenium(II) arene multinuclear metallodendrimers, which were characterised using analytical and spectroscopic methods.

Mononuclear analogues of the ruthenium(II) arene metallodendrimers were synthesized and characterized. The molecular structures of the mononuclear ruthenium(II) arene complexes were determined using single crystal X-ray crystallography.

Subsequent to the synthesis of the ruthenium(II) arene metallodendrimers, their cytotoxicities against A2780 and A2780cisR human ovarian cell lines were evaluated. The second generation cationic *N,N*- and neutral *N,O*- chelating bidentate octanuclear hexamethylbenzene complexes showed the highest antiproliferative activity against both cell lines. The cationic *N,N*- chelating bidentate octanuclear hexamethylbenzene metallodendrimer displayed higher cytotoxicity than cisplatin in the cisplatin resistant cell line (A2780cisR).

The two most cytotoxic octanuclear metallodendrimers, their mononuclear analogues and cisplatin were further investigated in the form of DNA binding experiments. The cationic *N,N*- chelating bidentate octanuclear hexamethylbenzene metallodendrimer was found to interact well with plasmid DNA over cisplatin. Additionally, the DNA binding experiments have supplemented the high antiproliferative data shown for

these metallodendrimers and that these new metallodendrimers operate *via* a different mechanism to that of cisplatin. Hence, this study has shown a definite correlation between the size of the metallodendrimer, DNA damage and cytotoxicity.

5.2 Future outlook

The project has shown great scope in the field of ruthenium-arene metallodendrimers as biological agents. Functionalizing higher generations of the poly(pyridylimine) dendritic scaffold with the ruthenium(II) arene moiety may in turn show enhanced biological activity. Moreover, the introduction of a water soluble dendritic scaffold may play a role in increasing the antiproliferative activity of these complexes, such as replacing the DAB dendritic scaffold with the PAMAM dendritic scaffold.[1]

Introducing water soluble ligands to the ruthenium-arene moiety, such as replacing the chlorido ligand with a water soluble phosphine ligand (e.g. PPh_3 or PTA), may increase the water solubility of these complexes which in turn may result in lower IC_{50} values.[2] One of the more obvious alterations to the ruthenium-arene moiety is changing the arene ring to a more extended ring, such as introducing the tetrahydroanthracene ring which has shown to have good antiproliferative activity,[3] or the biphenyl ring which has shown to improve lipophilicity.[3]

Further biological experiments need to be achieved to clearly confirm possible drug targets for these ruthenium(II) arene metallodendrimers. Such biological experiments may include cell uptake studies, cell fractionation or imaging studies (ruthenium distribution).[4]

5.3 References

1) X. Zhao, S.-C. J. Loo, P. P.-F. Lee, T. T. Y. Tan and C. K. Chu, *J. Inorg. Biochem.*, 2010, **104**, 105.
2) C. Scolaro, T. J. Geldbach , S. Rochat, A. Dorcier, C. Gossens, A. Bergamo, M. Cocchietto, I. Tavernelli, G. Sava, U. Rothlisberger and P. J. Dyson, *Organometallics*, 2006, **25**, 756.
3) R. E. Aird, J. Cummings, A. A. Ritchie, M. Muir, R. E. Morris, H. Chen, P. J. Sadler and D. I. Jodrell, *Br. J. Cancer*, 2002, **86**, 1652.
4) S. H. van Rijt, A. Mukherjee, A. M. Pizarro and P. J. Sadler, *J. Med. Chem.*, 2010, **53**, 840.

Chapter 6
Experimental Details

6.1 General remarks

All reactions were performed under an inert atmosphere using a dual vacuum/nitrogen line and standard Schlenk-line techniques. All reaction solvents were dried by refluxing under an inert atmosphere over the appropriate drying agent and all samples were dried under vacuum.

2-pyridinecarboxaldehyde, 4-pyridinecarboxaldehyde, salicylaldehyde, *n*-propylamine, 1,4-diaminobutane poly(propyleneimine) tetraamine (DAB-*dendr*-$(NH_2)_4$-**G1**) and hexamethylbenzene were purchased from Aldrich; α-Phellandrene was purchased from Fluka; 1,4-diaminobutane poly(propyleneimine) octaamine (DAB-*dendr*-$(NH_2)_8$-**G2**) was purchased from SyMO Chem and used without further purification. Ruthenium(III) trichloride trihydrate was obtained as a generous donation from Johnson Matthey/Anglo Platinum. $[(p\text{-cymene})RuCl_2]_2$,[1] and $[(hexamethylbenzene)RuCl_2]_2$,[2] were prepared according to literature methods. Deuterated solvents were purchased from Aldrich.

Nuclear magnetic resonance (NMR) spectra were recorded on a Varian Unity XR400 spectrometer (^1H: 399.95 MHz, $^{13}C\{^1H\}$: 100.58 MHz) or Varian Mercury XR300 spectrometer (^1H: 300.08 MHz, $^{13}C\{^1H\}$: 75.46 MHz) or Bruker Ultrashield 400 Plus spectrometer (^1H: 400.20 MHz, $^{13}C\{^1H\}$: 100.60 MHz) at ambient temperature with tetramethylsilane as an internal standard.

Infrared (IR) absorptions were measured on a Perkin-Elmer Spectrum One FT-IR spectrometer as KBr pellets or in NaCl solution cells in dichloromethane. Microanalysis for carbon, hydrogen and nitrogen were carried out using a Fisions EA 1108 CHNS elemental analyser. For certain metallodendrimers, the analyses are outside acceptable limits, and are ascribed to the encapsulation of solvent molecules and other inorganic salts by dendritic compounds. Melting points were determined using a Kofler hot stage microscope (Riechart Thermover) and are corrected.

Mass spectrometry was carried out at the University of Stellenbosch on a Waters API Quattro Micro triple quadrupole mass spectrometer. Data were recorded using Electrospray Ionisation (ESI) mass spectrometry in the positive-ion mode. Fast Atom Bombardment (FAB) and Matrix-Assisted Laser Desorption/Ionization-Time Of Flight (MALDI-TOF) mass spectrometry experiments were obtained from the Tokyo Institute of Technology. FAB data were obtained on the JEOL JMS-700 (3-nitrobenzyl alcohol) and MALDI-TOF analyses were carried out on a Bruker Ultraflex TOF/TOF mass spectrometer (Fluka 87884 trans-2-[3-(4-tert-Butylphenyl)-2-methyl-2-propenylidene]malonitrile, DCTB), equipped with a nitrogen laser and operated at an accelerating voltage of 25 kV.

6.2. Synthesis and experimental data of pyridyl-imine ligands (L1 - L6)

6.2.1 Preparation of monomeric ligand L1[3]

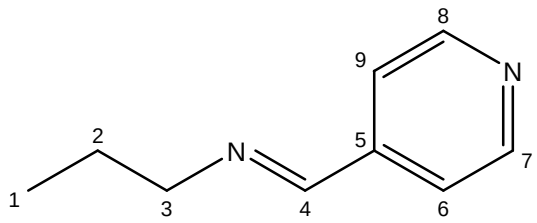

n-Propylamine (1.69 mL, 22.0 mmol) was added dropwise to an ice-cooled, solution of 4-pyridinecarboxaldehyde (2.00 mL, 21.0 mmol) in dry diethyl ether (50.0 mL) with stirring. Anhydrous $MgSO_4$ (~ 10 g) was added and the reaction mixture was allowed to stir for 24 hours at room temperature. The solution was filtered by gravity and the solvent removed under reduced pressure, resulting in a crude residue (**L1**). The residue was dissolved in hexane (20.0 mL) and washed with distilled H_2O (3 x 20.0 mL). The organic layer was dried over anhydrous $MgSO_4$ (~10 g), filtered by gravity and the solvent evaporated, yielding a pale-yellow oil (2.20 g, 70.7 %), which was dried *in vacuo*.

IR: NaCl cells, CH_2Cl_2, ν/cm^{-1}: 1647 (s, imine, C═N) and 1599 (s, pyridyl, C=N). **^{1}H NMR** (400 MHz, $CDCl_3$): δ (ppm) = 0.94 (t, ^3J = 7.4 Hz, 3H, $\underline{H}_1$), 1.56 (m, 2H, $\underline{H}_2$), 3.73 (t, 2H, $\underline{H}_3$), 7.45 (d, ^3J = 6.0 Hz, 2H, $\underline{H}_6$, $\underline{H}_9$), 8.09 (s, 1H, $\underline{H}_4$), 8.66 (d, ^3J = 6.0 Hz, 2H, $\underline{H}_7$, $\underline{H}_8$). **^{13}C{^{1}H} NMR** (100 MHz, $CDCl_3$): δ (ppm) = 11.8 (**C**H_3); 23.8, 63.6 (**C**H_2); 121.9, 150.4 (**C**H $_{pyr}$); 143.1 (**C** $_{pyr}$); 158.8 (**C**H $_{imine}$). **Elemental Analysis** (%): Calc. For $C_9H_{12}N_2$: C, 72.94; H, 8.16; N, 18.90; Found: C, 71.43; H, 7.19; N, 18.47. **MS** (ESI, m/z): 149 $[M+H]^+$.

6.2.2 Preparation of monomeric ligand L2[4]

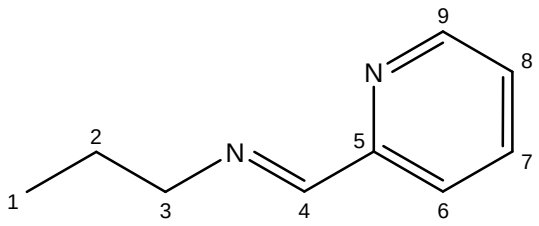

A solution of *n*-propylamine (1.82 mL, 22.0 mmol) in dry diethyl ether (20.0 mL) was added dropwise to an ice-cooled solution of 2-pyridinecarboxaldehyde (2.00 mL, 21.0 mmol) in dry diethyl ether (20.0 mL). To the reaction mixture anhydrous $MgSO_4$ (~ 10 g) was added and stirred at room temperature for 24 hours. The drying agent was filtered by gravity and the solvent removed under reduced pressure. The remaining yellow residue (**L2**) was dissolved in dichloromethane (20.0 mL) and washed copiously with distilled H_2O (3 x 20 mL). The organic layer was collected, dried over $MgSO_4$ (~10 g), filtered by gravity and the solvent removed by rotary evaporation, yielding a yellow oil (1.08 g, 34.8 %), which was dried *in vacuo*.

IR: NaCl cells, CH_2Cl_2, ν/cm^{-1}: 1650 (s, imine, C=N) and 1589 (s, pyridyl, C=N). **^{1}H NMR** (400 MHz, $(CD_3)_2CO$): δ (ppm) = 0.96 (t, ^3J = 7.4 Hz, 3H, $\underline{H}_1$), 1.75 (m, 2H, $\underline{H}_2$), 3.63 (t, ^3J = 6.9 Hz, 2H, $\underline{H}_3$), 7.28 (m, 1H, $\underline{H}_7$), 7.72 (t, ^3J = 7.7 Hz, 1H, $\underline{H}_8$), 7.98 (d, ^3J = 7.9 Hz, 1H, $\underline{H}_6$), 8.36 (s, 1H, $\underline{H}_4$), 8.63 (d, ^3J = 4.8 Hz, 1H, $\underline{H}_9$). **^{13}C{^{1}H} NMR** (100 MHz, $(CD_3)_2CO$): δ (ppm) = 11.7 (**C**H_3); 23.8, 63.2 (**C**H_2); 121.1, 124.4, 136.4, 149.3 (**C**H $_{pyr}$); 154.8 (**C** $_{pyr}$); 161.7 (**C**H $_{imine}$). **Elemental Analysis** (%): Calc. For $C_9H_{12}N_2$: C, 72.93; H, 8.16; N, 18.90; Found: C, 71.76; H, 10.97; N, 18.59. **MS** (ESI, m/z): 119 $[M–CH_3CH_2]^+$.

6.2.3 Preparation of dendritic ligand L3[5]

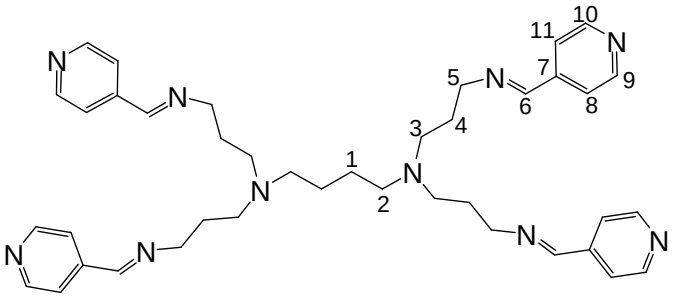

4-pyridinecarboxaldehyde (1.23 mL, 12.9 mmol) in dry toluene (5.00 mL) was added dropwise to an ice-cooled solution of DAB-*dendr*-$(NH_2)_4$ (1.01 g, 3.18 mmol) in dry toluene (50.0 mL). Anhydrous $MgSO_4$ (~ 10 g) was added and the resulting slurry was allowed to stir at room temperature for 24 hours. The $MgSO_4$ was filtered off and the solvent removed by rotary evaporation leaving behind a dark-brown crude product. The crude product (**L3**) was dissolved in dichloromethane (20.0 mL), and washed copiously with H_2O (6 x 20.0 mL). The organic layer was collected and dried over anhydrous $MgSO_4$ (~10 g). The $MgSO_4$ was filtered and the solvent removed from the filtrate by rotary evaporation and dried *in vacuo*, yielding a dark-orange oil (1.48 g, 67.9 %).

IR: NaCl cells, CH_2Cl_2, ν/cm^{-1}: 1648 (s, imine, C═N) and 1699 (s, pyridyl, C=N). **^{1}H NMR** (400 MHz, $CDCl_3$): δ (ppm) = 1.42 (m, 4H, $\underline{H}_1$), 1.83 (m, 8H, $\underline{H}_4$), 2.38 (br t, 4H, $\underline{H}_2$), 2.52 (m, 8H, $\underline{H}_3$), 3.63 (t, ^3J = 7.5 Hz, 8H, $\underline{H}_5$), 7.52 (d, ^3J = 6.0 Hz, 8H, $\underline{H}_8$, $\underline{H}_{11}$), 8.23 (s, 4H, $\underline{H}_6$), 8.63 (d, ^3J = 6.0 Hz, 8H, $\underline{H}_9$, $\underline{H}_{10}$). **^{13}C{^{1}H} NMR** (100 MHz, $CDCl_3$): δ (ppm) = 25.3, 28.3, 51.7, 54.1, 59.8 (**C**H_2); 121.8, 150.4 (**C**H $_{pyr}$); 143.0 (**C** $_{pyr}$); 159.0 (**C**H $_{imine}$). **Elemental Analysis** (%): Calc. For $C_{40}H_{52}N_{10}.1CH_2Cl_2$: C, 68.00; H, 7.47; N, 19.58; Found: C, 68.52; H, 7.50; N, 20.82. **MS** (ESI, m/z): 673 $[M]^+$.

6.2.4 Preparation of dendritic ligand L4[5]

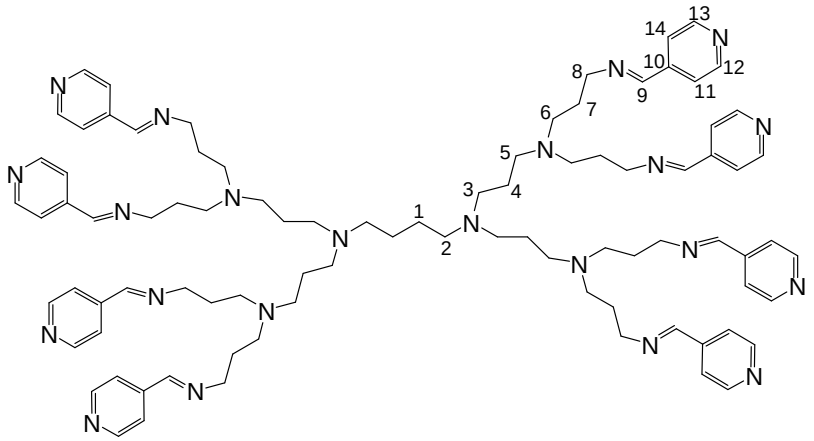

To a stirring solution of DAB-*dendr*-$(NH_2)_8$ (1.01 g, 1.30 mmol) in dry toluene (50.0 mL), 4-pyridinecarboxaldehyde (1.00 mL, 10.4 mmol) was added dropwise. The reaction mixture was cooled in ice and anhydrous $MgSO_4$ (~ 10 g) was added. The reaction mixture was allowed to stir for 24 hours at room temperature. The $MgSO_4$ was filtered by gravity and the solvent removed from the filtrate by rotary evaporation, resulting in a yellow residue (**L4**). The residue was dissolved in dichloromethane (20.0 mL) and washed with distilled H_2O (8 x 20.0 mL). The organic layer was dried over anhydrous $MgSO_4$ (~10 g), filtered by gravity and the solvent from the filtrate removed by rotary evaporation, yielding an orange-yellow oil (1.62 g, 84.0 %), which was dried *in vacuo*.

IR: NaCl cells, CH_2Cl_2, ν/cm^{-1}: 1648 (s, imine, C═N) and 1599 (s, pyridyl, C=N). **^{1}H NMR** (300 MHz, $CDCl_3$): δ (ppm) = 1.39 (br m, 4H, $\underline{H}_1$), 1.47 (br m, 8H, $\underline{H}_4$), 1.72 (m, 16H, $\underline{H}_7$), 1.94-2.44 (overlapping m, 36H, $\underline{H}_2$, $\underline{H}_3$, $\underline{H}_5$, $\underline{H}_6$), 3.56 (br t, ^3J = 6,5 Hz, 16H, $\underline{H}_8$), 7.48 (d, ^3J = 6.0 Hz, 16H, $\underline{H}_{11,}$ $\underline{H}_{14}$), 8.17 (s, 8H, $\underline{H}_9$), 8.57 (d, ^3J = 6.0 Hz, 16H, $\underline{H}_{12,}$ $\underline{H}_{13}$). **^{13}C{^{1}H} NMR** (75 MHz, $CDCl_3$): δ (ppm) = 24.8, 25.2, 28.3, 51.7, 52.2, 52.3, 54.3, 59.8 (**C**H_2); 121.8, 150.4 (**C**H *pyr*); 142.9 (**C** *pyr*); 159.0 (**C**H *imine*). **Elemental Analysis** (%): Calc. For $C_{88}H_{120}N_{22}.{}^1/_2CH_2Cl_2$: C, 69.54; H, 7.98; N, 20.16; Found: C, 68.93; H, 8.18; N, 20.69. **MS** (ESI, m/z): 1485 $[M]^+$.

6.2.5 Preparation of dendritic ligand L5[6]

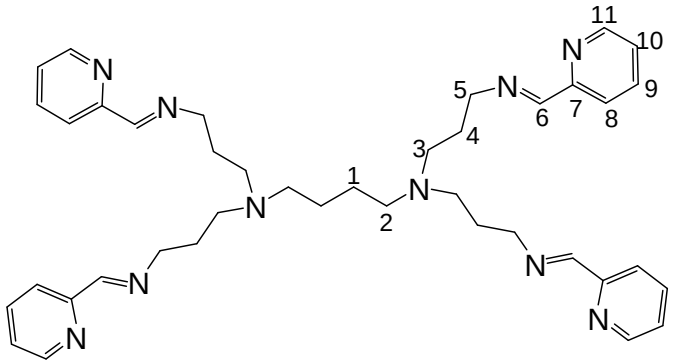

A solution of 2-pyridinecarboxaldehyde (1.24 mL, 13.0 mmol) in dry toluene (5 mL) was added dropwise to an ice-cooled solution of DAB-*dendr*-$(NH_2)_4$ (1.02 g, 3.21 mmol) in dry toluene (50.0 mL). Anhydrous $MgSO_4$ (~ 10 g) was added to the reaction mixture and the resulting slurry was stirred at room temperature for 24 hours. The solution was filtered by gravity and the solvent removed by rotary evaporation yielding a brown residue (**L5**). The residue was dissolved in dichloromethane (20.0 mL), and washed copiously with H_2O (6 x 20.0 mL). The organic layer was dried over anhydrous $MgSO_4$ (~10 g) and filtered by gravity, with the solvent removed by rotary evaporation and dried *in vacuo*, yielding a yellow-brown oil (1.54 g, 73.5 %).

IR: NaCl cells, CH_2Cl_2, ν/cm^{-1}: 1649 (s, imine, C═N) and 1588 (s, pyridyl, C=N). **^{1}H NMR** (300 MHz, $(CD_3)_2CO$): δ (ppm) = 1.47 (br s, 4H, $\underline{H}_1$), 1.87 (m, 8H, $\underline{H}_4$), 2.46 (m, 4H, $\underline{H}_2$), 2.56 (br t, 8H, $\underline{H}_3$), 3.69 (br t, 8H, $\underline{H}_5$), 7.42 (br t, 4H, $\underline{H}_9$), 7.85 (br t, 4H, $\underline{H}_{10}$) 7.96 (d, ^3J = 6.9 Hz, 4H, $\underline{H}_8$), 8.35 (s, 4H, $\underline{H}_6$), 8.58 (br d, 4H, $\underline{H}_{11}$). **^{13}C{^{1}H} NMR** (100 MHz, $(CD_3)_2CO$): δ (ppm) = 22.4, 27.6, 51.4, 53.9, 59.0 (**C**H_2); 121.4, 125.3, 137.4, 149.1 (**C**H $_{pyr}$); 154.1 (**C** $_{pyr}$); 162.1 (**C**H $_{imine}$). **Elemental Analysis** (%): Calc. For $C_{40}H_{52}N_{10}.^1/_2CH_2Cl_2$: C, 68.00; H, 7.47; N, 19.58; Found: C, 69.01; H, 8.60; N, 19.32. **MS** (FAB, m/z): 673 $[M]^+$.

6.2.6 Preparation of dendritic ligand L6[7]

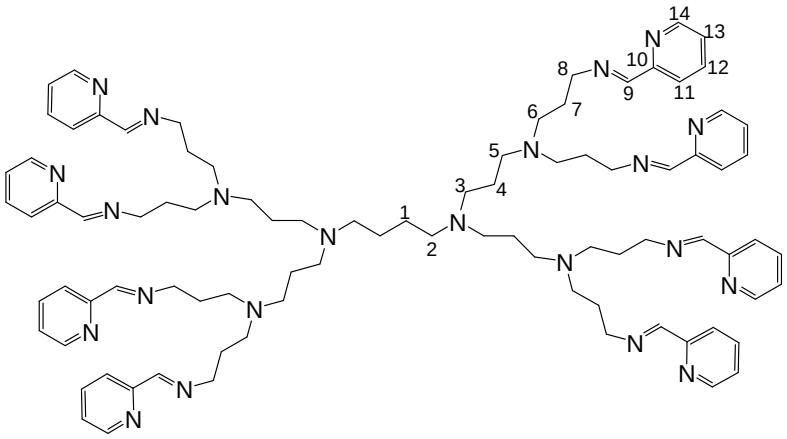

A slight excess of 2-pyridinecarboxaldehyde (1.00 mL, 10.5 mmol) in a solution of dry toluene (5.00 mL) was added dropwise to a stirring ice-cooled solution of DAB-*dendr*-$(NH_2)_8$ (1.01 g, 1.30 mmol) in dry toluene (50.0 mL). To the reaction mixture anhydrous $MgSO_4$ (~ 10 g) was added and the resulting slurry was stirred at room temperature for 24 hours. The solution was filtered by gravity to remove the drying agent and the solvent removed from the resulting filtrate by rotary evaporation resulting in a yellow residue (**L6**). The residue was taken up in dichloromethane (20.0 mL), and washed copiously with H_2O (8 x 20.0 mL). The organic layer was dried over anhydrous $MgSO_4$ (~10 g) and filtered by gravity, the solvent removed by rotary evaporation and dried *in vacuo*, yielding an orange-yellow oil (1.34 g, 69.2 %).
IR: NaCl cells, CH_2Cl_2, ν/cm^{-1}: 1649 (s, imine, C═N) and 1588 (s, pyridyl, C=N). **^{1}H NMR** (400 MHz, $(CD_3)_2CO$): δ (ppm) = 1.40 (br m, 4H, $\underline{H}_1$), 1.59 (br m, 8H, $\underline{H}_4$), 1.84 (br qn, 16H, $\underline{H}_7$), 2.43-2.53 (overlapping m, 36H, $\underline{H}_2$, $\underline{H}_3$, $\underline{H}_5$, $\underline{H}_6$), 3.66 (br t, 16H, $\underline{H}_8$), 7.39 (br t, 8H, $\underline{H}_{12}$), 7.82 (t, ^3J = 7.7 Hz, 8H, $\underline{H}_{13}$) 7.95 (d, ^3J = 7.9 Hz, 8H, $\underline{H}_{11}$), 8.33 (s, 8H, $\underline{H}_9$), 8.55 (d, ^3J = 4.9 Hz, 8H, $\underline{H}_{14}$).**^{13}C{^{1}H} NMR** (75 MHz, $(CD_3)_2CO$): δ (ppm) = 25.0, 25.8, 29.0, 52.7, 53.1, 53.3, 55.1, 60.2 (**C**H$_2$); 122.6, 126.5, 138.5, 150.3 (**C**H $_{pyr}$); 155.3 (**C** $_{pyr}$); 163.2 (**C**H $_{imine}$). **Elemental Analysis** (%): Calc. For $C_{88}H_{120}N_{22}.{}^1/_2CH_2Cl_2$: C, 69.54; H, 7.98; N, 20.16; Found: C, 69.51; H, 7.18; N, 21.16. **MS** (FAB, m/z): 1485 $[M]^+$.

6.3 Synthesis and experimental data of salicyldimine ligands (L7 - L9)

6.3.1 Preparation of monomeric ligand L7[8]

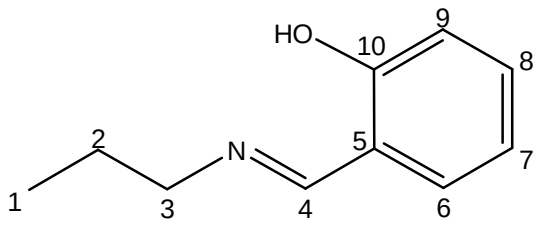

n-Propylamine (0.810 mL, 9.85 mmol) was added dropwise to a solution of salicyldehyde (1.00 mL, 9.38 mmol) in dry ethanol (20.0 mL). The reaction solution was gently heated (~ 40 ^{o}C) and stirred for 5 hours. The solvent was removed under reduced pressure, resulting in a crude yellow residue (**L7**). The residue was dissolved in dichloromethane (20.0 mL) and washed with distilled H_2O (10 x 50.0 mL). The organic layer was dried over anhydrous $MgSO_4$ (~10 g), filtered by gravity and the solvent evaporated, yielding an orange-yellow oil (1.10 g, 71.7 %), which was dried *in vacuo*.

IR: NaCl cells, CH_2Cl_2, ν/cm^{-1}: 1635 (s, imine, C=N). **^{1}H NMR** (400 MHz, $CDCl_3$): δ (ppm) = 1.00 (t, ^{3}J = 7.4 Hz, 3H, $\underline{H}_1$), 1.74 (m, 2H, $\underline{H}_2$), 3.56 (t, ^{3}J = 6.8 Hz, 2H, $\underline{H}_3$), 6.88 (t, ^{3}J = 7.4 Hz, 1H, $\underline{H}_7$), 6.97 (d, ^{3}J = 7.9 Hz, 1H, $\underline{H}_9$), 7.25 (d, ^{3}J = 7.6 Hz, 1H, $\underline{H}_6$), 7.31 (t, ^{3}J = 7.3 Hz, 1H, $\underline{H}_8$), 8.32 (s, 1H, $\underline{H}_4$), 13.66 (br s, 1H, O$\underline{H}$). **^{13}C{^{1}H} NMR** (100 MHz, $CDCl_3$): δ (ppm) = 11.5 (**C**H_3); 23.9, 61.0 (**C**H_2); 116.9, 118.1, 130.9, 131.9 (**C**H $_{Ar}$); 118.6, 161.3 (**C** $_{Ar}$); 164.4 (**C**H $_{imine}$). **Elemental Analysis** (%): Calc. For $C_{10}H_{13}NO$: C, 73.59; H, 8.03; N, 8.58; Found: C, 73.48; H, 7.90; N, 8.55. **MS** (ESI, m/z): 164 $[M+H]^+$.

6.3.2 Preparation of dendritic ligand L8[9]

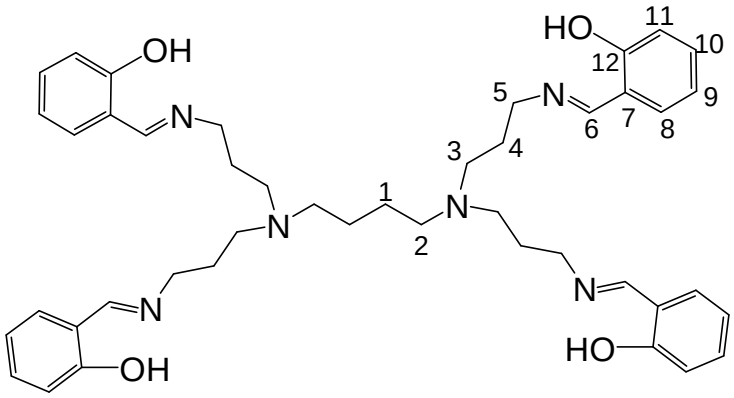

Salicyldehyde (1.37 mL, 12.9 mmol) was added dropwise to a solution of DAB-*dendr*-$(NH_2)_4$ (1.01 g, 3.18 mmol) in dry ethanol (20.0 mL). The reaction was allowed to stir overnight at 40 ^{o}C. The following day the reaction was allowed to cool to room temperature and the solvent was then removed by rotary evaporation leaving behind a yellow crude oil. The crude oil was dissolved in dichloromethane (10.0 mL), followed by the addition of hexane (30.0 mL) and placed in the freezer for 72 hours, to promote crystallisation. A yellow solid (**L8**) precipitated out of solution. This was isolated and dried *in vacuo*, yielding a yellow solid (1.19 g, 51.1 %).

IR: KBr pellets, ν/cm^{-1}: 1631 (s, imine, C=N). **^{1}H NMR** (300 MHz, $CDCl_3$): δ (ppm) = 1.40 (m, 4H, $\underline{H}_1$), 1.80 (m, 8H, $\underline{H}_4$), 2.39 (m, 4H, $\underline{H}_2$), 2.50 (t, ^{3}J = 7.2 Hz, 8H, $\underline{H}_3$), 3.60 (t, ^{3}J = 6.8 Hz, 8H, $\underline{H}_5$), 6.83 (t, ^{3}J = 7.5 Hz, 4H, $\underline{H}_9$), 6.93 (d, ^{3}J = 8.2 Hz, 4H, $\underline{H}_{11}$), 7.20 (d, ^{3}J = 7.7 Hz, 4H, $\underline{H}_8$), 7.27 (t, ^{3}J = 7.3 Hz, 4H, $\underline{H}_{10}$), 8.31 (s, 4H, $\underline{H}_6$), 13.54 (br s, 4H, O$\underline{H}$). **^{13}C{^{1}H} NMR** (75 MHz, $CDCl_3$): δ (ppm) = 25.1, 28.5, 51.4, 54.0, 57.3 (**C**H_2); 117.0, 118.4, 131.1, 132.0 (**C**H $_{Ar}$); 118.8, 161.3 (**C** $_{Ar}$); 164.8 (**C** $_{imine}$). **Elemental Analysis** (%): Calc. For $C_{44}H_{56}N_6O_4$: C, 72.10; H, 7.70; N, 11.47; Found: C, 71.66; H, 7.30; N, 10.89. **MS** (FAB, m/z): 733 $[M]^+$. **Melting Point**: 58-60 ^{o}C (**Lit. M.p.**: 66-68 ^{o}C)[9].

6.3.3 Preparation of dendritic ligand L9[9]

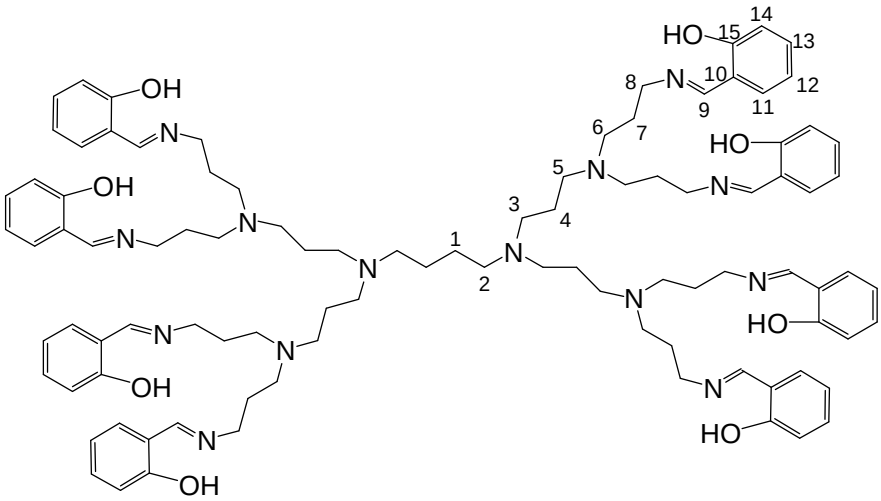

To a stirring solution of DAB-*dendr*-$(NH_2)_8$ (0.504 g, 0.652 mmol) in dry ethanol (30.0 mL), salicyldehyde (0.559 mL, 5.25 mmol) was added dropwise. The reaction mixture was allowed to stir for 48 hours at 40 ^oC. The solvent was removed by rotary evaporation, resulting in a orange residue (**L9**). The residue was dissolved in dichloromethane (20.0 mL) and washed with distilled H_2O (8 x 50.0 mL). The organic layer was dried over anhydrous $MgSO_4$ (~10 g), filtered by gravity and the solvent removed by rotary evaporation, yielding an orange oil (0.97 g, 92.2 %), which was dried *in vacuo*.

IR: NaCl cells, CH_2Cl_2, ν/cm^{-1}: 1635 (s, imine, C=N). **^{1}H NMR** (300 MHz, $CDCl_3$): δ (ppm) = 1.38 (br m, 4H, $\underline{H}_1$), 1.54 (br m, 8H, $\underline{H}_4$), 1.79 (m, 16H, $\underline{H}_7$), 2.35-2.40 (overlapping m, 20H, $\underline{H}_2$, $\underline{H}_3$, $\underline{H}_5$,), 2.49 (m, 16H, $\underline{H}_6$), 3.58 (t, ^3J = 6,6 Hz, 16H, $\underline{H}_8$), 6.82 (br t, ^3J = 7.3 Hz, 8H, $\underline{H}_{12}$), 6.92 (br d, ^3J = 8.3 Hz, 8H, $\underline{H}_{14}$), 7.19 (br d, ^3J = 7.7 Hz, 8H, $\underline{H}_{11}$), 7.26 (br t, ^3J = 6.7 Hz, 8H, $\underline{H}_{13}$), 8.29 (s, 8H, H_9), 13.49 (br s, 8H, O$\underline{H}$). **^{13}C{^{1}H} NMR** (100 MHz, $CDCl_3$): δ (ppm) = 24.6, 25.2, 28.6, 51.5, 52.2, 52.3, 54.2, 57.4 (**C**H_2); 117.0, 118.4, 131.1, 132.0 (**C**H $_{Ar}$); 118.7, 161.3 (**C** $_{Ar}$); 164.8 (**C**H $_{imine}$). **Elemental Analysis** (%): Calc. For. $C_{96}H_{128}N_{14}O_8$: C, 71.79; H, 8.03; N, 12.21; Found: C, 71.66; H, 8.35; N, 12.05. **MS** (FAB, m/z): 1607 $[M+H]^+$. **Melting Point:** 188 ^oC (decompose, without melting).

6.4 Synthesis and experimental data of ruthenium precursors

6.4.1 Synthesis of $[Ru(\eta^6\text{-}p\text{-}Pr^iC_6H_4Me)Cl_2]_2$[1]

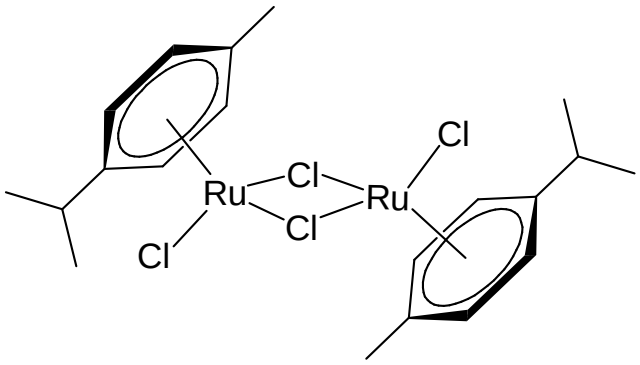

The procedure outlined by Bennett and Smith[4] was followed closely to synthesize the ruthenium dimer. To a Schlenk flask ruthenium(III) trichloride trihydrate (5.45 g, 20.4 mmol) was dissolved in dry ethanol (100 mL). α-Phellandrene (20.0 mL, 122.2 mmol) was added dropwise to this solution and the solution heated under reflux for 12 hours. The mixture was reduced and cooled on ice. The solution mixture was filtered and diethyl ether added to a reduced volume of the filtrate, to precipitate out the product. The precipitate was filtered on a Büchner filter funnel, washed with cold diethyl ether (3 x 20.0 mL) and dried under vacuum, yielding a dark red solid.

^{1}H NMR (300 MHz, $CDCl_3$): δ (ppm) = 1.27 (d, ^3J = 6.93 Hz, 12H, $CH(C\underline{H}_3)_2$), 1.64 (s, 6H, $C\underline{H}_3$), 2.91 (m, 2H, $C\underline{H}(CH_3)_2$), 5.32 (d, ^3J = 6.03 Hz, 4H, Ar $_{p\text{-cye}}$), 5.46 (d, ^3J = 6.03 Hz, 4H, Ar $_{p\text{-cye}}$). **Melting Point**: 201 - 204 ^{o}C (**Lit. M.p.**: 200 ^{o}C).[1]

6.4.2 Synthesis of $[Ru(\eta^6\text{-}C_6Me_6)Cl_2]_2$[2]

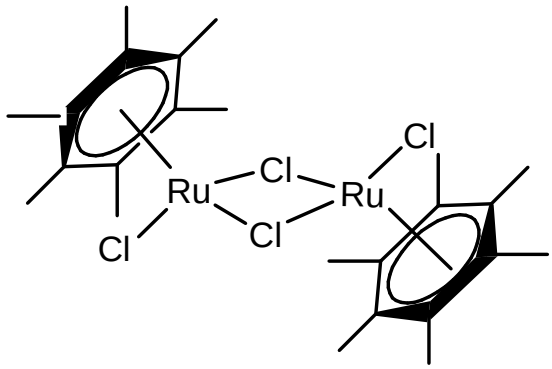

The $[Ru(\eta^6\text{-}p\text{-}Pr^iC_6H_4Me)Cl_2]_2$ dimer (1.50 g, 2.45 mmol) was stirred with molten hexamethylbenzene (ca. 7.00 g) for 3 days at 185 ^oC. The reaction vessel was allowed to cool to room temperature. Diethyl ether was added to extract any unreacted hexamethylbenzene. The reaction vessel was placed in an ultrasound bath to break up the large particles. The solution was filtered over Celite® and washed with excess ether. The red solid was extracted with chloroform and the solvent removed under vacuum to yield the product as a red crystalline solid.

^{1}H NMR (400 MHz, $CDCl_3$): δ (ppm) = 2.04 (s, 36H, C$\underline{H}_3$). **Melting Point**: 268-271 ^oC (**Lit. M.p.**: 270 ^oC).[2]

6.5 Synthesis and experimental data of neutral 4-pyridyl-imine mononuclear (1, 2) and multinuclear complexes (3 - 6)

6.5.1 Preparation of 1[5]

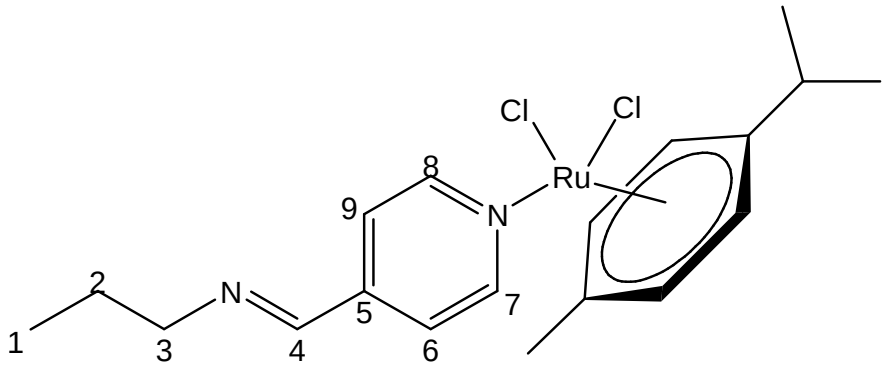

[Ru(η^6-*p*-Pr^{i}C$_6$H$_4$Me)Cl$_2$]$_2$ (0.223 g, 0.362 mmol) was dissolved in stirring dichloromethane (30.0 mL) and **L1** (0.107 g, 0.723 mmol) was added dropwise, the reaction mixture was stirred for 5 hours. The solvent was reduced to approximately 3.00 mL, and the product was precipitated with petroleum ether. This resulted in the formation of yellow precipitate, which was allowed to settle and the supernatant liquid removed. The precipitate was washed with petroleum ether (3 x 10.0 mL) and the mother liquor syringed off after each washing. The mustard-yellow solid **1** (0.15 g, 45.7 %) was dried *in vacuo*.

IR: NaCl cells, CH_2Cl_2, ν/cm^{-1}: 1647 (s, imine, C=N), 1615 (s, pyridyl, C=N). **^{1}H NMR** (400 MHz, $CDCl_3$): δ (ppm) = 0.97 (t, ^3J = 7.4 Hz, 3H, $\underline{H}_1$), 1.32 (d, ^3J = 7.0 Hz, 6H, CH(C$\underline{H}_3$)$_2$), 1.75 (m, 2H, $\underline{H}_2$), 2.11 (s, 3H, C$\underline{H}_3$), 3.00 (m, 1H, C$\underline{H}$(CH$_3$)$_2$), 3.66 (t, ^3J = 6.5 Hz, 2H, $\underline{H}_3$), 5.23 (d, ^3J = 5.9 Hz, 2H, Ar$_{p\text{-cye}}$), 5.45 (d, ^3J = 5.9 Hz, 2H, Ar$_{p\text{-cye}}$), 7.60 (d, ^3J = 6.5 Hz, 2H, $\underline{H}_6$, $\underline{H}_9$), 8.27 (s, 1H, $\underline{H}_4$), 9.10 (d, ^3J = 6.4 Hz, 2H, $\underline{H}_7$, $\underline{H}_8$). **^{13}C{^{1}H} NMR** (100 MHz, $CDCl_3$): δ (ppm) = 11.8 (**C**H$_3$); 18.2, 22.3 (**C**H$_{3\ p\text{-cye}}$); 23.8, 63.6 (**C**H$_2$); 30.7, 82.2, 83.1 (**C**H $_{p\text{-cye}}$); 97.3, 103.6 (**C** $_{p\text{-cye}}$); 122.5, 155.3 (**C**H $_{pyr}$); 144.6 (**C** $_{pyr}$); 157.3 (**C**H $_{imine}$). **Elemental Analysis** (%): Calc. For $C_{19}H_{26}N_2RuCl$: C, 50.22; H, 5.77; N, 6.16; Found: C, 49.96; H, 5.38; N, 5.99. **MS** (ESI, m/z): 419.1 [M-Cl]$^+$. **Melting Point:** 163 ^{o}C – 166 ^{o}C.

6.5.2 Preparation of 2[5]

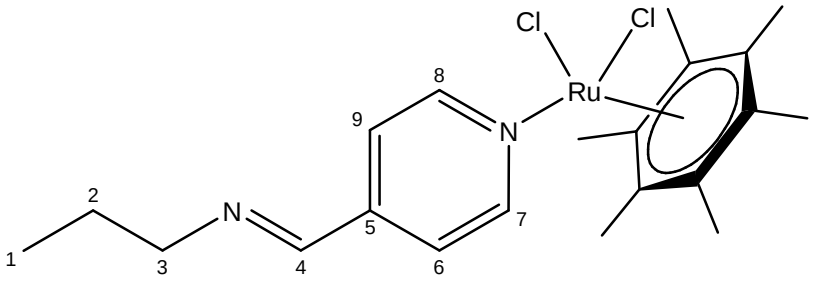

[Ru(η^6-C_6Me_6)Cl_2]$_2$ (0.069 g, 0.100 mmol) was dissolved in a stirring solution of dry dichloromethane (30.0 mL) in a Schlenk tube. A solution of ligand **L1** (0.0300 g, 0.200 mmol) in dry dichloromethane (5.00 mL) was added dropwise and the reaction mixture was allowed to stir for 2 hours. The solvent was reduced to approximately 3.00 mL, and the product (**2**) was precipitated after the addition of petroleum ether. This resulted in the formation of yellow-orange precipitate, which was allowed to settle and the supernatant liquid removed. The precipitate was further washed with petroleum ether (3 x 10.0 mL) and the mother liquor syringed after each washing. The yellow-orange solid (0.05 g, 50.1 %) was crystallized with slow diffusion of petroleum ether into dichloromethane and dried *in vacuo,* to yield orange crystals.
IR: NaCl cells, CH_2Cl_2, ν/cm^{-1}: 1646 (s, imine, C═N) and 1614 (s, pyridyl, C=N). **^{1}H NMR** (400 MHz, $CDCl_3$): δ (ppm) = 0.96 (t, ^3J = 7.4 Hz, 3H, $\underline{H}_1$), 1.74 (m, 2H, $\underline{H}_2$), 2.03 (s, 18H, C$\underline{H}_3$), 3.66 (t, ^3J = 6.9 Hz, 2H, $\underline{H}_3$), 7.57 (d, ^3J = 6.4 Hz, 2H, $\underline{H}_6$, $\underline{H}_9$), 8.26 (s, 1H, $\underline{H}_4$), 8.86 (d, ^3J = 6.2 Hz, 2H, $\underline{H}_7$, $\underline{H}_8$). **^{13}C{^{1}H} NMR** (100 MHz, $CDCl_3$): δ (ppm) = 11.8 (**C**H_3); 15.4 (**C**$H_{3\ HMB}$); 23.8, 63.6 (**C**H_2); 91.4 (**C** $_{HMB}$); 122.5, 155.1 (**C**H $_{pyr}$); 144.2 (**C** $_{pyr}$); 157.5 (**C**H $_{imine}$). **Elemental Analysis** (%): Calc. For $C_{21}H_{30}N_2RuCl_2$: C, 52.28; H, 6.27; N, 5.81; Found: C, 51.84; H, 5.94, N, 5.47. **MS** (ESI, m/z): 447 $[M\text{-}Cl]^+$. **Melting Point**: 139 ^{o}C (decompose, without melting).

6.5.3 Preparation of 3[5]

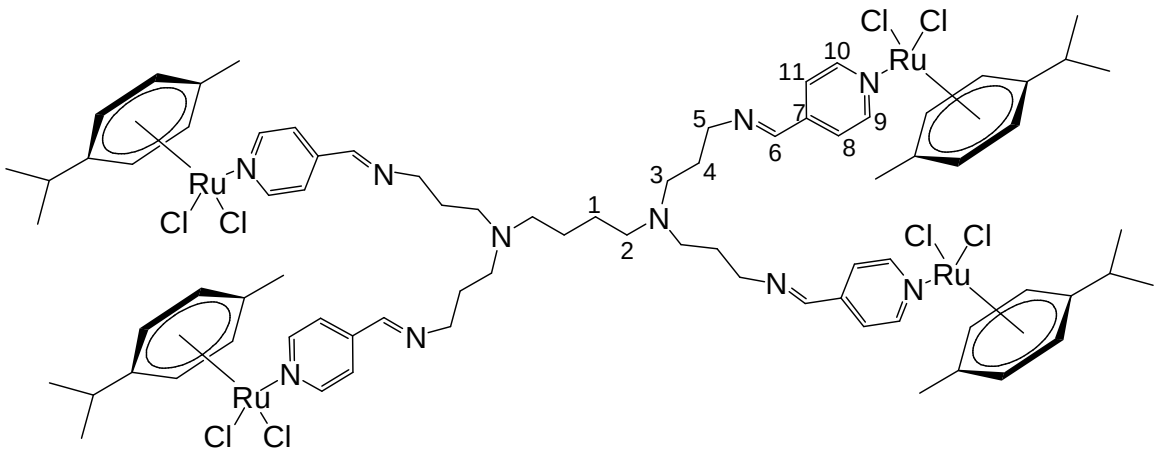

The dimer **[Ru(η^6-*p*-Pr^{i}C$_6$H$_4$Me)Cl$_2$]$_2$** (0.213 g, 0.346 mmol) and **L3** (0.117 g, 0.173 mmol) were dissolved together in dichloromethane (35.0 mL) and the mixture was then stirred at room temperature for 24 hours, with the red solution becoming darker over the stirring period. The solvent was reduced to 3.00 mL and the mustard-yellow product (**3**) was precipitated by the addition of an excess of petroleum ether. The solid (0.26 g, 79.1 %) was washed further with petroleum ether (6 x 10.0 mL) and then dried *in vacuo*.

IR: NaCl cells, CH_2Cl_2, ν/cm^{-1}: 1646 (s, imine, C═N), 1615 (s, pyridyl, C=N). **^{1}H NMR** (300 MHz, $CDCl_3$): δ (ppm) = 1.30 (d, ^3J = 6.9 Hz, 24H, CH(C$\underline{H}_3$)$_2$), 1.83 (br m, 4H, $\underline{H}_1$), 2.09 (s, 12H, C$\underline{H}_3$), 2.44 - 2.97 (overlapping m, 12H, $\underline{H}_2$, $\underline{H}_3$), 2.97 (m, 4H, C$\underline{H}$(CH$_3$)$_2$), 3.67 (br m, 4H, $\underline{H}_5$), 5.28 (d, ^3J = 5.7 Hz, 8H, Ar$_{p\text{-cye}}$), 5.70 (d, ^3J = 5.7 Hz, 8H, Ar$_{p\text{-cye}}$), 7.49 (d, ^3J = 6.2 Hz, 4H, $\underline{H}_8$, $\underline{H}_{11}$), 8.20 (s, 4H, $\underline{H}_6$), 9.06 (d, ^3J = 5.4 Hz, 4H, $\underline{H}_9$, $\underline{H}_{10}$). **^{13}C{^{1}H} NMR** (75 MHz, $CDCl_3$): δ (ppm) = 18.3, 22.3 (**C**H$_{3\ p\text{-}cye}$); 27.1, 31.5, 51.2, 53.7, 58.8 (**C**H$_2$); 30.7, 82.1, 83.3 (**C**H $_{p\text{-}cye}$); 97.5, 103.3 (**C** $_{p\text{-}cye}$); 122.5, 155.3 (**C**H $_{pyr}$); 139.8 (**C** $_{pyr}$), 158.4 (**C**H $_{imine}$). **Elemental Analysis** (%): Calc. For $C_{80}H_{108}N_{10}Ru_4Cl_8.1^1/_2CH_2Cl_2$: C, 48.34; H, 5.52; N, 6.92; Found: C, 48.22; H, 5.15; N, 6.74. **MS** (ESI, m/z): 565 [[M+4H+4CH_2Cl_2+H_2O]$^{4+}$. **Melting Point:** 165 ^{o}C (decompose, without melting).

6.5.4 Preparation of 4[5]

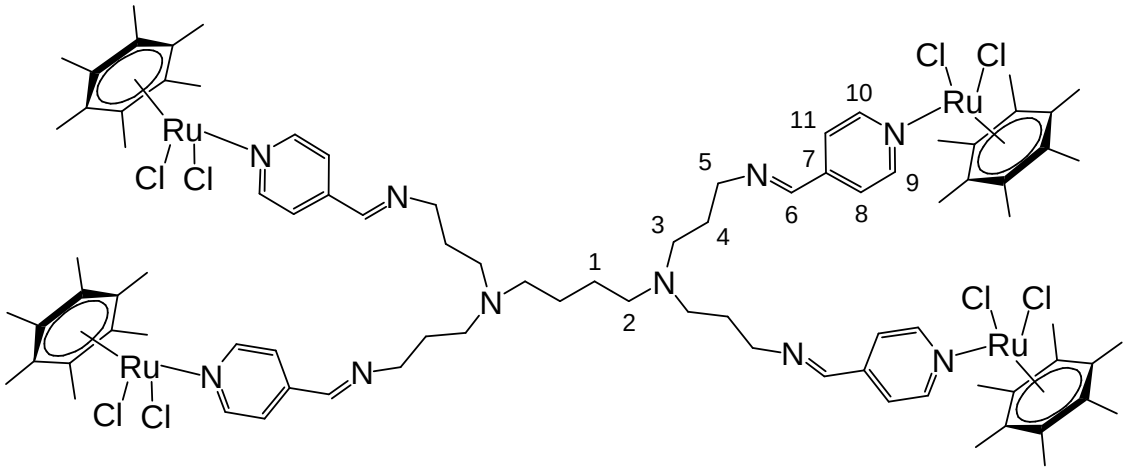

[Ru(η^6-C_6Me_6)Cl_2]$_2$ (0.056 g, 0.081 mmol) was dissolved in a stirring solution of dry dichloromethane (30.0 mL) in a Schlenk tube. A solution of ligand **L3** (0.027 g, 0.041 mmol) in dry dichloromethane (5.00 mL) was added dropwise and the reaction mixture was allowed to stir for 24 hours. The solvent was reduced to approximately 3.00 mL, and the product was precipitated with petroleum ether. This resulted in the formation of yellow-orange precipitate (**4**), which was allowed to settle and the supernatant liquid removed. The precipitate was further washed with petroleum ether (6 x 10.0 mL) and the mother liquor syringed after each washing. The yellow solid (0.05 g, 86.5 %) was dried *in vacuo*.

IR: NaCl cells, CH_2Cl_2, ν/cm^{-1}: 1646 (s, imine, C═N) and 1614 (s, pyridyl, C=N). **^{1}H NMR** (300 MHz, $CDCl_3$): δ (ppm) = 1.44 (br m, 4H, $\underline{H}_1$), 1.85 (br m, 8H, $\underline{H}_4$), 1.97 (s, 72H, C$\underline{H}_3$), 2.49-2.58 (overlapping m, 12H, $\underline{H}_2$, $\underline{H}_3$), 3.67 (m, 8H, $\underline{H}_5$), 7.51 (d, ^3J = 6.4 Hz, 8H, $\underline{H}_8$, $\underline{H}_{11}$), 8.23 (s, 4H, $\underline{H}_6$), 8.78 (d, ^3J = 6.3 Hz, 8H, $\underline{H}_9$, $\underline{H}_{10}$). **^{13}C{^{1}H} NMR** (75 MHz, $CDCl_3$): δ (ppm) = 15.4 (**C**H$_{3\ HMB}$); 24.2, 26.2, 51.0, 53.4, 58.2 (**C**H$_2$); 91.4 (**C** $_{HMB}$); 122.5, 155.0 (**C**H $_{pyr}$); 143.9 (**C** $_{pyr}$); 158.9 (**C**H $_{imine}$). **Elemental Analysis** (%): Calc. For $C_{88}H_{124}N_{10}Ru_4Cl_8.CH_2Cl_2$: C, 51.03; H, 6.06; N, 6.69; Found: C, 51.01; H, 5.85; N, 6.19. **MS** (ESI, m/z): 635 [M-3Cl]$^{3+}$. **Melting Point:** 188 ^{o}C (decompose, without melting).

6.5.5 Preparation of 5[5]

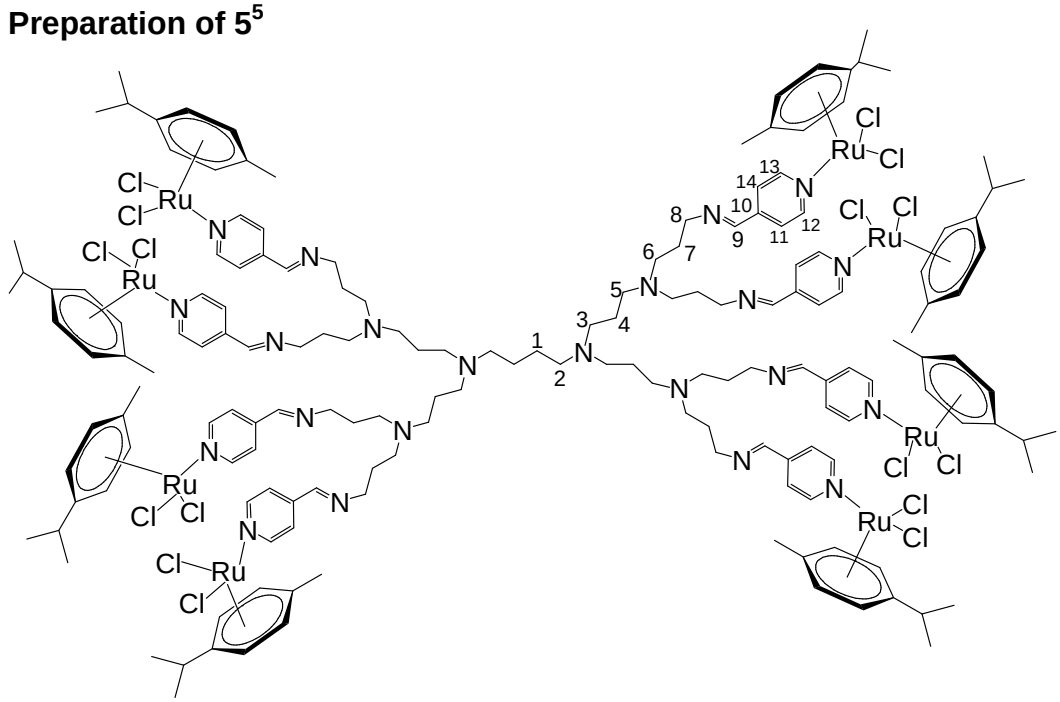

The dimer **[Ru(η^6-*p*-Pr^{i}C$_6$H$_4$Me)Cl$_2$]$_2$** (0.199 g, 0.307 mmol) and **L4** (0.114 g, 0.077 mmol) were dissolved together in dichloromethane (35.0 mL) and the reaction mixture was stirred at room temperature for 24 hours. The red solution turned darker in colour. The solvent was reduced to 3.00 mL, and the product precipitated with petroleum ether. This resulted in the formation of yellow-brown precipitate (**5**), which was allowed to settle and the supernatant liquid syringed off. The precipitate was further washed with petroleum ether (8 x 10.0 mL) and the supernatant syringed off after each washing. The mustard-yellow solid (0.30 g, 98.1 %) was dried *in vacuo.*

IR: NaCl cells, CH_2Cl_2, ν/cm^{-1}: 1646 (s, imine, C═N), 1614 (s, pyridyl, C═N). **^{1}H NMR** (300 MHz, $CDCl_3$): δ (ppm) = 1.32 (d, 48H, ^3J = 6.9 Hz, CH(C$\underline{H}_3$)$_2$), 1.35 – 1.48 (overlapping m, 12H, $\underline{H}_1$, $\underline{H}_4$), 1.78 (m, 16H, $\underline{H}_7$) 2.09 (s, 24H, C$\underline{H}_3$), 2.30 – 2.53 (overlapping m, 36H, $\underline{H}_2$, $\underline{H}_3$, $\underline{H}_5$, $\underline{H}_6$), 2.97 (br m, 8H, C$\underline{H}$(CH$_3$)$_2$), 3.67 (m, 16H, $\underline{H}_8$), 5.28 (d, ^3J = 6.0 Hz, 16H, Ar$_{p\text{-cye}}$), 5.49 (d, ^3J = 6.0 Hz, 16H, Ar$_{p\text{-cye}}$), 7.49 (d, 16H, ^3J = 6.6 Hz, $\underline{H}_{11,}$ $\underline{H}_{14}$), 8.19 (s, 8H, $\underline{H}_9$), 9.05 (d, 16H, ^3J = 6.5 Hz, $\underline{H}_{12,}$ $\underline{H}_{13}$). **^{13}C{^{1}H} NMR** (75 MHz, $CDCl_3$): δ (ppm) = 18.2, 22.2 (**C**H$_{3\ p\text{-}cye}$); 26.8, 27.1, 30.8, 38.8, 50.9, 51.4, 55.2, 58.8 (**C**H$_2$); 30.6, 82.0, 83.0 (**C**H $_{p\text{-}cye}$); 97.4, 103.2 (**C** $_{p\text{-}cye}$); 122.5, 155.3 (**C**H $_{pyr}$); 144.2 (**C** $_{pyr}$); 158.3 (**C**H $_{imine}$). **Elemental Analysis** (%): Calc. For $C_{168}H_{232}N_{22}Ru_8Cl_{16}.4CH_2Cl_2$: C, 48.32; H, 5.66; N, 7.21; Found: C, 48.37; H, 6.03; N, 6.61. **MS** (ESI, m/z): 569.0 [M-7Cl+3CH_2Cl_2+CH_3CN]$^{7+}$. **Melting Point:** 214 ^{o}C (decompose without melting).

6.5.6 Preparation of 6[5]

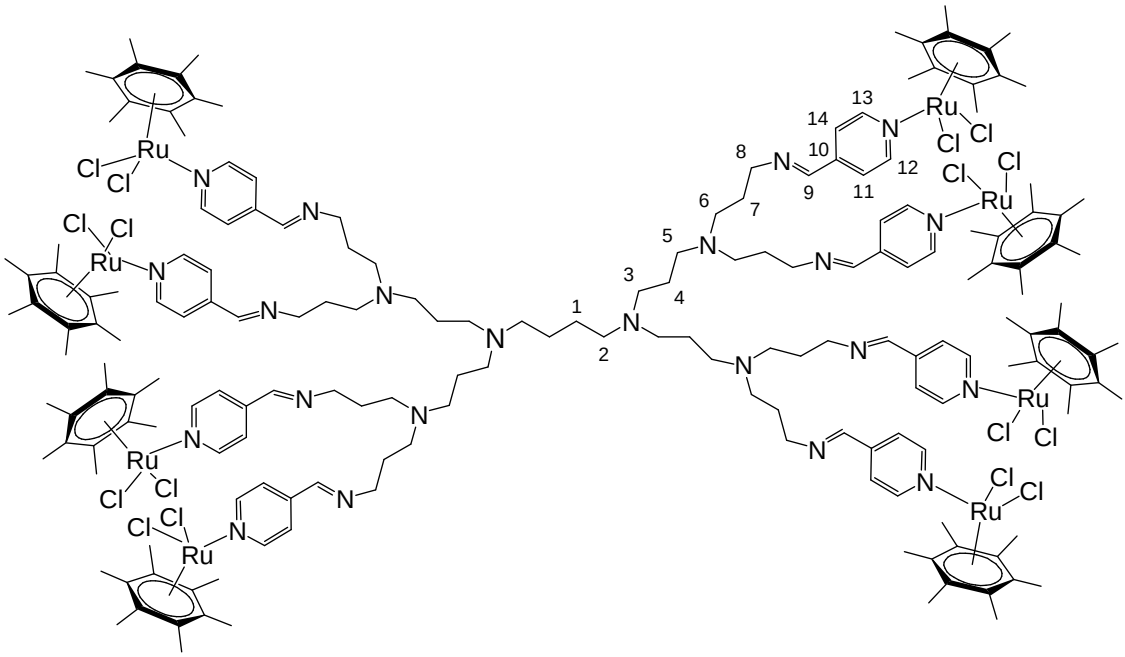

[Ru(η^6-C_6Me_6)Cl_2]$_2$ (0.168 g, 0.248 mmol) was dissolved in a stirring solution of dry dichloromethane (30.0 mL) in a Schlenk tube. A solution of ligand **L4** (0.062 g, 0.041 mmol) in dry dichloromethane (5.00 mL) was added dropwise and the reaction mixture was allowed to stir for 48 hours. The solvent was reduced to approximately 3.00 mL, and the product was precipitated with petroleum ether. This resulted in the formation of yellow-orange precipitate (**6**), which was allowed to settle and the supernatant liquid removed. The precipitate was further washed with petroleum ether (6 x 10.0 mL) and the mother liquor syringed after each washing. The yellow solid (0.23 g, 91.7 %) was dried *in vacuo*.

IR: NaCl cells, CH_2Cl_2, ν/cm^{-1}: 1646 (s, imine, C=N) and 1613 (s, pyridyl, C=N). **^{1}H NMR** (400 MHz, $CDCl_3$): δ (ppm) = 1.31 (br m, 4H, $\underline{H}_1$), 1.63 (br m, 8H, $\underline{H}_4$), 1.87 (m, 8H, $\underline{H}_5$), 1.99 (s, 144H, C$\underline{H}_3$), 2.15-2.38 (overlapping m, 24H, $\underline{H}_3$, $\underline{H}_7$), 2.50 (m, 4H, $\underline{H}_2$,), 2.60 (m, 16H, $\underline{H}_6$), 3.69 (m, 16H, $\underline{H}_8$), 7.54 (d, ^3J = 6.0 Hz, 16H, $\underline{H}_{11}$, $\underline{H}_{14}$), 8.23 (s, 8H, $\underline{H}_9$), 8.78 (d, ^3J = 5.6 Hz, 16H, $\underline{H}_{12}$, $\underline{H}_{13}$). **^{13}C{^{1}H} NMR** (100 MHz, $CDCl_3$): δ (ppm) = 15.4 (**C**H$_3$ *HMB*); 25.3 – 58.9 (**C**H$_2$); 91.4 (**C** *HMB*); 122.5, 155.0 (**C**H *pyr*); 143.9 (**C** *pyr*); 158.9 (**C** *imine*). **Elemental Analysis** (%): Calc. For $C_{184}H_{264}N_{22}Ru_8Cl_{16}.2CH_2Cl_2$: C, 51.60; H, 6.24; N, 7.12; Found: C, 51.69; H, 6.43, N, 6.82. **MS** (ESI, m/z): 631 [M-7Cl+5CH_2Cl_2+2CH_3CN]$^{7+}$. **Melting Point**: 194 ^{o}C (decompose, without melting).

6.6 Synthesis and experimental data of cationic 2-pyridyl-imine mononuclear (7, 8) and multinuclear complexes (9 - 12)

6.6.1 Preparation of 7

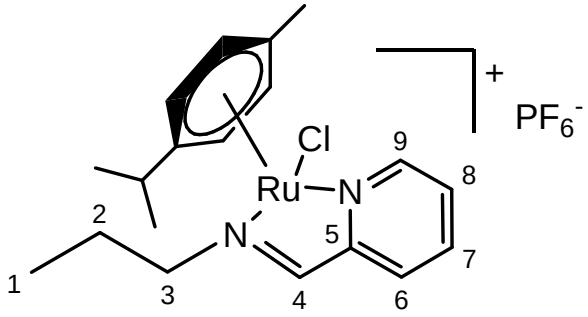

[Ru(η^6-*p*-Pr^{i}C$_6$H$_4$Me)Cl$_2$]$_2$ (0.230 g, 0.375 mmol) was added to a stirring solution of methanol (25.0 mL). The ligand **L2** (0.111 g, 0.750 mmol) was dissolved in methanol (5.0 mL) and added dropwise to the stirred solution. The solution was allowed to stir for 1 h at room temperature. The resulting solution was then filtered by gravity and the filtrate reduced to about 5 mL, where $NaPF_6$ (0.063 g, 0.375 mmol) was added and the reaction was allowed to stir at 0 ^oC for 3 h. This resulted in the formation of a yellow-orange precipitate (**7**), which was collected using a Hirsch filter funnel and dried under vacuum, to yield a yellow solid (0.16 g, 37.8 %).

IR: KBr pellets, ν/cm^{-1}: 1623 (s, imine, C=N), 1599 (s, pyridyl, C=N), 844 (s, P-F). **^{1}H NMR** (400 MHz, $(CD_3)_2CO$): δ (ppm) = 1.00 (t, ^3J = 7.4 Hz, 3H, $\underline{H}_1$), 1.09 & 1.16 (d, ^3J = 6.9 Hz, 6H, CH(C$\underline{H}_3$)$_2$), 1.99 & 2.05 (m, 2H, $\underline{H}_2$), 2.30 (s, 3H, CH_3), 2.79 (sep, 1H, C$\underline{H}$(CH$_3$)$_2$), 4.40 & 4.66 (m, 2H, $\underline{H}_3$), 5.94 (t, 2H, ^3J = 6.3 Hz, Ar$_{p\text{-cye}}$), 6.23 (dd, ^3J = 6.3 Hz, 2H, Ar$_{p\text{-cye}}$), 7.82 (t, ^3J = 5.7 Hz, 1H, $\underline{H}_7$), 8.23 (d, ^3J = 7.7 Hz, 1H, $\underline{H}_6$), 8.29 (t, ^3J = 7.7 Hz, 1H, $\underline{H}_8$), 8.79 (s, 1H, $\underline{H}_4$), 9.57 (d, ^3J = 5.6 Hz, 1H, $\underline{H}_9$). **^{13}C{^{1}H} NMR** (100 MHz, $(CD_3)_2CO$): δ (ppm) = 10.8 (**C**H$_3$); 21.3, 22.0, 23.0 (**C**H$_{3\ p\text{-}cye}$); 18.2, 68.9 (**C**H$_2$); 31.2, 84.8, 85.3, 85.7, 87.5 (**C**H $_{p\text{-}cye}$); 103.7, 106.1 (**C** $_{p\text{-}cye}$), 128.5, 128.9, 140.0, 156.0 (**C**H $_{pyr}$); 155.2 (**C** $_{pyr}$); 167.0 (**C**H $_{imine}$). **Elemental Analysis** (%): Calc. For $C_{19}H_{26}N_2RuClPF_6$: C, 40.47; H, 4.65; N, 4.97; Found: C, 40.40; H, 4.68; N, 4.87. **MS** (ESI, m/z): 419 $[M\text{-}PF_6]^+$. **Melting Point**: 186 ^oC – 187 ^oC.

6.6.2 Preparation of 8

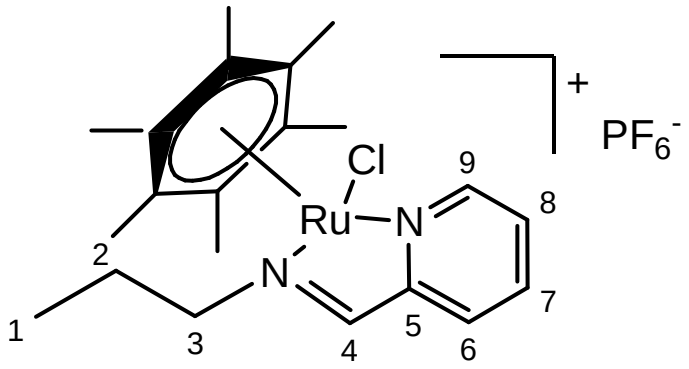

[Ru(η^6-C_6Me_6)Cl_2]$_2$ (0.248 g, 0.366 mmol) was added to stirring methanol (25.0 mL), resulting in a suspension of the dimer. The ligand **L2** (0.108 g, 0.731 mmol) was dissolved in methanol (5.0 mL) and added dropwise to the stirring solution. This solution was allowed to stir for 1.5 h at room temperature. This was filtered by gravity and the filtrate reduced to about 5 mL, followed by the addition of $NaPF_6$ (0.062 g, 0.366 mmol). The reaction was then stirred at 0 ^oC for a further 2 h, resulting in the formation of a yellow-orange precipitate. The solid was filtered using a Hirsch filter funnel and dried under vacuum, to yield the product (**8**) as an orange solid (0.22 g, 50.8 %).

IR: KBr pellets, ν/cm^{-1}: 1625 (s, imine, C=N), 1600 (s, pyridyl, C=N), 835 (s, P-F). **^{1}H NMR** (300 MHz, $(CD_3)_2CO$): δ (ppm) = 0.93 (t, ^3J = 7.4 Hz, 3H, $\underline{H}_1$), 1.82 & 1.98 (m, 2H, $\underline{H}_2$), 2.24 (s, 18H, C$\underline{H}_3$), 4.20 & 4.45 (m, 2H, $\underline{H}_3$), 7.84 (t, ^3J = 5.7 Hz, 1H, $\underline{H}_7$), 8.17 (d, ^3J = 7.8 Hz, 1H, $\underline{H}_6$), 8.22 (t, ^3J = 7.6 Hz, 1H, $\underline{H}_8$), 8.70 (s, 1H, $\underline{H}_4$), 9.07 (d, ^3J = 5.7 Hz, 1H, $\underline{H}_9$). **^{13}C{^{1}H} NMR** (75 MHz, $(CD_3)_2CO$): δ (ppm) = 10.8 (**C**H_3); 15.2 (**C**$H_{3\ HMB}$); 22.5, 65.7 (**C**H_2); 96.6 (**C** $_{HMB}$); 128.3, 128.4, 139.4, 153.6 (**C**H $_{pyr}$); 155.2 (**C** $_{pyr}$); 166.6 (**C**H $_{imine}$). **Elemental Analysis** (%): Calc. For $C_{21}H_{30}N_2RuClPF_6.{}^1/_2CH_3OH$: C, 42.47; H, 5.31; N, 4.61; Found: C, 42.47; H, 5.35; N, 4.58. **MS** (ESI, m/z): 447 $[M\text{-}PF_6]^+$. **Melting Point**: 239 ^oC – 241 ^oC.

6.6.3 Preparation of 9

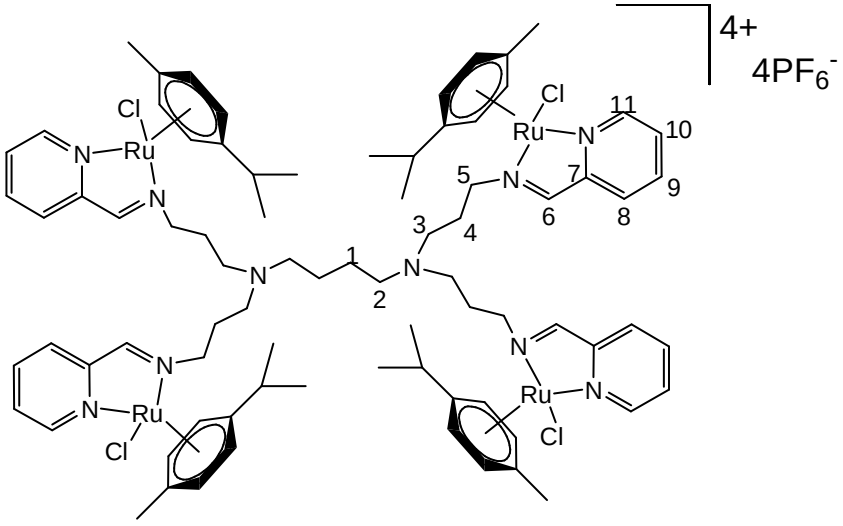

[Ru(η^6-*p*-Pr^{i}C$_6$H$_4$Me)Cl$_2$]$_2$ (0.191 g, 0.312 mmol) was added to a stirring solution of ethanol (25.0 mL). The ligand **L5** (0.103 g, 0.152 mmol) was dissolved in ethanol (5.0 mL) and added dropwise to the stirring solution. The solution was allowed to stir for 12 h at room temperature. The resulting solution was then filtered by gravity and the filtrate transferred into a round bottom flask. The filtrate was reduced to about 5 mL and was transferred to a round bottom flask, where $NaPF_6$ (0.061 g, 0.312 mmol) was added and the reaction was allowed to stir at 0 ^oC for 15 min. This resulted in the formation of a dark yellow precipitate (**9**), which was filtered using a Hirsch filter funnel and dried under vacuum, to yield a yellow-brown solid (0.17 g, 48.4 %).

IR: KBr pellets, ν/cm^{-1}: 1625 (s, imine, C=N), 1599 (s, pyridyl, C=N), 851 (s, P-F). **^{1}H NMR** (400 MHz, $(CD_3)_2CO$): δ (ppm) = 1.07 & 1.12 (br d, 24H, CH(C$\underline{H}_3$)$_2$), 1.29 (br m, 4H, $\underline{H}_1$), 1.81 (br m, 8H, $\underline{H}_4$), 2.30 (s, 12H, C$\underline{H}_3$), 2.46 (br m, 4H, $\underline{H}_2$), 2.76 (br s, 4H, C$\underline{H}$(CH$_3$)$_2$), 2.95 (br m, 8H, $\underline{H}_3$), 4.59 & 4.73 (br m, 8H, $\underline{H}_5$), 5.97 (br d, 8H, Ar$_{p\text{-cye}}$), 6.25 (br d, 8H, Ar$_{p\text{-cye}}$), 7.81 (br t, 4H, $\underline{H}_9$), 8.24 (br m, 8H, $\underline{H}_8$, $\underline{H}_{10}$), 8.98 (br s, 4H, $\underline{H}_6$), 9.57 (br d, 4H, $\underline{H}_{11}$). **^{13}C{^{1}H} NMR** (100 MHz, $(CD_3)_2CO$): δ (ppm) = 18.5, 21.4, 22.1 (**C**H$_{3\ p\text{-}cye}$); 24.2, 26.1, 51.3, 53.5, 64.9 (**C**H$_2$); 31.2, 84.8, 85.4, 85.8, 87.6 (**C**H $_{p\text{-}cye}$); 104.1, 106.1 (**C** $_{p\text{-}cye}$); 128.7, 129.4, 140.1, 156.1 (**C**H $_{pyr}$); 155.1 (**C** $_{pyr}$), 166.3 (**C**H $_{imine}$). **Elemental Analysis** (%): Calc. For $C_{80}H_{108}N_{10}Ru_4Cl_4P_4F_{24}$: C, 41.14; H, 4.66; N, 6.00; Found: C, 41.21; H, 4.70; N, 5.71. **MS** (MALDI-TOF, m/z): 2192 [M-PF$_6$]$^+$. **Melting Point:** 169 ^oC – 172 ^oC.

6.6.4 Preparation of 10

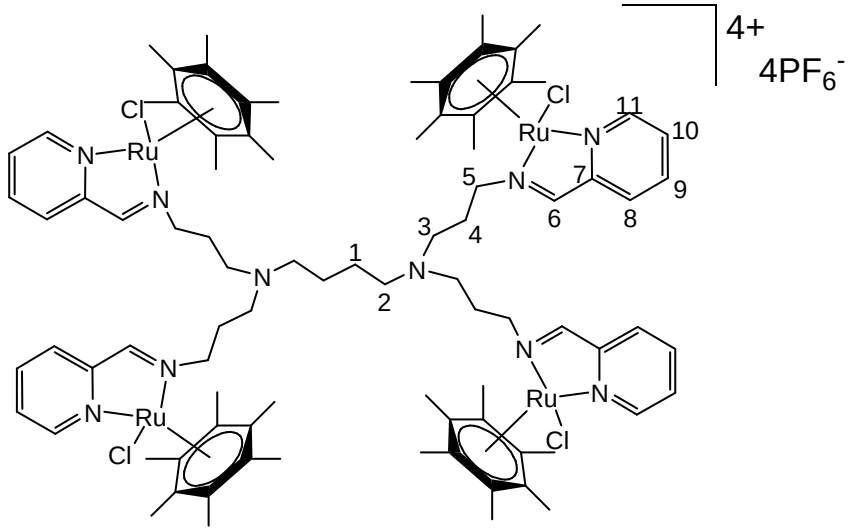

[Ru(η^6-C_6Me_6)Cl_2]$_2$ (0.211 g, 0.311 mmol) was added to a stirring solution of ethanol (25.0 mL). The ligand **L5** (0.102 g, 0.152 mmol) was dissolved in ethanol (5.0 mL) and added dropwise to the stirring solution. The solution was allowed to stir for 12 h at room temperature. The resulting solution was then filtered by gravity and the filtrate transferred into a round bottom flask. The filtrate was reduced to about 5 mL and was transferred to a round bottom flask, where $NaPF_6$ (0.053 g, 0.311 mmol) was added and the reaction was allowed to stir at 0 ^oC for 3 h. The flask was left in the freezer for 12 h. This resulted in the formation of a red-brown precipitate (**10**), which was filtered using a Hirsch filter funnel and first washed with ethanol and then further with diethyl ether. The product was dried under vacuum, to yield a red-brown solid (0.24 g, 65.9 %).

IR: KBr pellets, ν/cm^{-1}: 1624 (s, imine, C═N), 1598 (s, pyridyl, C=N), 839 (s, P-F). **^{1}H NMR** (300 MHz, $(CD_3)_2CO$): δ (ppm) = 1.28 (br m, 4H, $\underline{H}_1$), 1.50 (br m, 8H, $\underline{H}_4$), 2.21 (br s, 72H, C$\underline{H}_3$), 2.54 (br m, 4H, $\underline{H}_2$), 2.89 (br m, 8H, $\underline{H}_3$), 4.38 (br m, 8H, $\underline{H}_5$), 7.84 (br m, 4H, $\underline{H}_9$), 8.19 (br m, 8H, $\underline{H}_8$, $\underline{H}_{10}$), 8.76 (br s, 4H, $\underline{H}_6$), 9.08 (br m, 4H, $\underline{H}_{11}$). **^{13}C{^{1}H} NMR** (75 MHz, $(CD_3)_2CO$): δ (ppm) = 15.4 (**C**H$_{3\ HMB}$); 24.9, 26.5, 51.0, 53.6, 62.1 (**C**H$_2$); 96.6 (**C** $_{HMB}$); 128.4, 128.7, 139.5, 153.6 (**C**H $_{pyr}$); 155.1 (**C** $_{pyr}$); 167.3 (**C**H $_{imine}$). **Elemental Analysis** (%): Calc. For $C_{88}H_{124}N_{10}Ru_4Cl_4P_4F_{24}$: C, 43.18; H, 5.11; N, 5.72; Found: C, 42.92; H, 4.89; N, 5.44. **MS** (MALDI-TOF, m/z): 2304 [M-PF_6]$^+$. **Melting Point**: 232 ^oC – 236 ^oC.

6.6.5 Preparation of 11

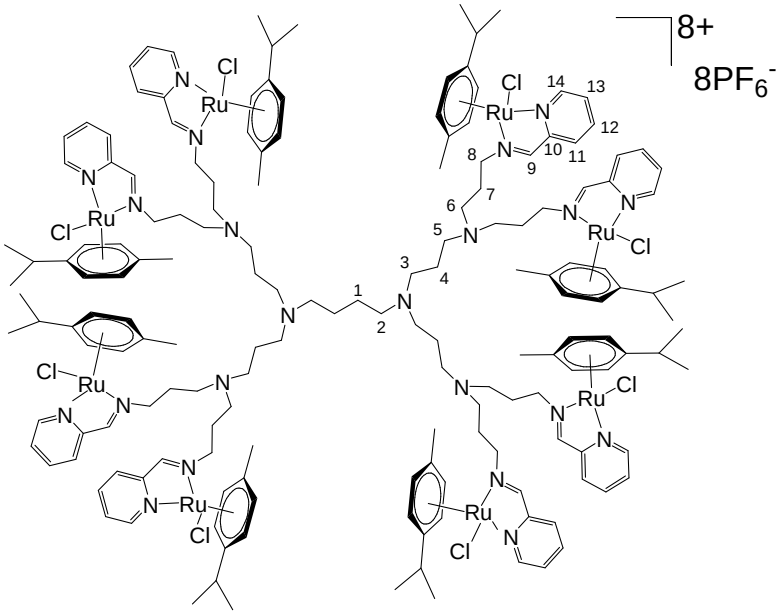

[Ru(η^6-*p*-Pr^{i}C$_6$H$_4$Me)Cl$_2$]$_2$ (0.169 g, 0.276 mmol) was added to a stirring solution of ethanol (25.0 mL). The ligand **L6** (0.101 g, 0.068 mmol) was dissolved in ethanol (5.0 mL) and added dropwise to the stirring solution. The solution was allowed to stir for 12 h at room temperature. The resulting solution was then filtered by gravity and the filtrate transferred into a round bottom flask. The filtrate was reduced to about 5 mL and was transferred to a round bottom flask, where $NaPF_6$ (0.048 g, 0.276 mmol) was added and the reaction was allowed to stir at 0 ^oC for 2 h. This resulted in the formation of a dark yellow precipitate (**11**), which was filtered using a Hirsch filter funnel and washed with ethanol. The product was dried under vacuum, to yield a yellow-brown solid (0.13 g, 39.8 %).

IR: KBr pellets, ν/cm^{-1}: 1623 (s, imine, C=N), 1598 (s, pyridyl, C=N), 847 (s, P-F). **^{1}H NMR** (400 MHz, $(CD_3)_2CO$): δ (ppm) = 1.06 & 1.11 (br d, 96H, CH(C$\underline{H}_3$)$_2$), 1.32 (br m, 4H, $\underline{H}_1$), 1.61 – 3.36 (overlapping m, 60H, $\underline{H}_2$, $\underline{H}_3$, $\underline{H}_4$, $\underline{H}_5$, $\underline{H}_6$, $\underline{H}_7$), 2.30 (s, 24H, C$\underline{H}_3$), 2.77 (br m, 8H, C$\underline{H}$(CH$_3$)$_2$), 4.75 (br m, 16H, $\underline{H}_8$), 5.97 (br m, 16H, Ar$_{p\text{-cye}}$), 6.29 (br m, 16H, Ar$_{p\text{-cye}}$), 7.80 (br m, 8H, $\underline{H}_{12}$), 8.28 (br m, 16H, $\underline{H}_{11}$, $\underline{H}_{13}$), 9.13 (br s, 8H, $\underline{H}_9$), 9.58 (br m, 8H, $\underline{H}_{14}$). **^{13}C{^{1}H} NMR** (100 MHz, $(CD_3)_2CO$): δ (ppm) = 18.7, 21.6, 22.3 (**C**H$_{3\ p\text{-}cye}$); 25.5-27.2, 50.5-52.0, 64.9 (**C**H$_2$); 31.3, 84.8, 85.6, 85.8, 87.7 (**C**H $_{p\text{-}cye}$); 104.3, 106.0 (**C** $_{p\text{-}cye}$); 128.7, 129.6, 140.1, 156.1 (**C**H $_{pyr}$); 155.1 (**C** $_{p\text{-}cye}$); 168.9 (**C**H $_{imine}$). **Elemental Analysis** (%): Calc. For $C_{168}H_{232}N_{22}Ru_8Cl_8P_8F_{48}$: C, 41.94; H, 4.86; N, 6.40; Found: C, 41.82; H, 5.02; N, 6.19. **MS** (MALDI-TOF, m/z): 4811 [M]$^+$. **Melting Point**: 175 ^oC – 179 ^oC.

6.6.6 Preparation of 12

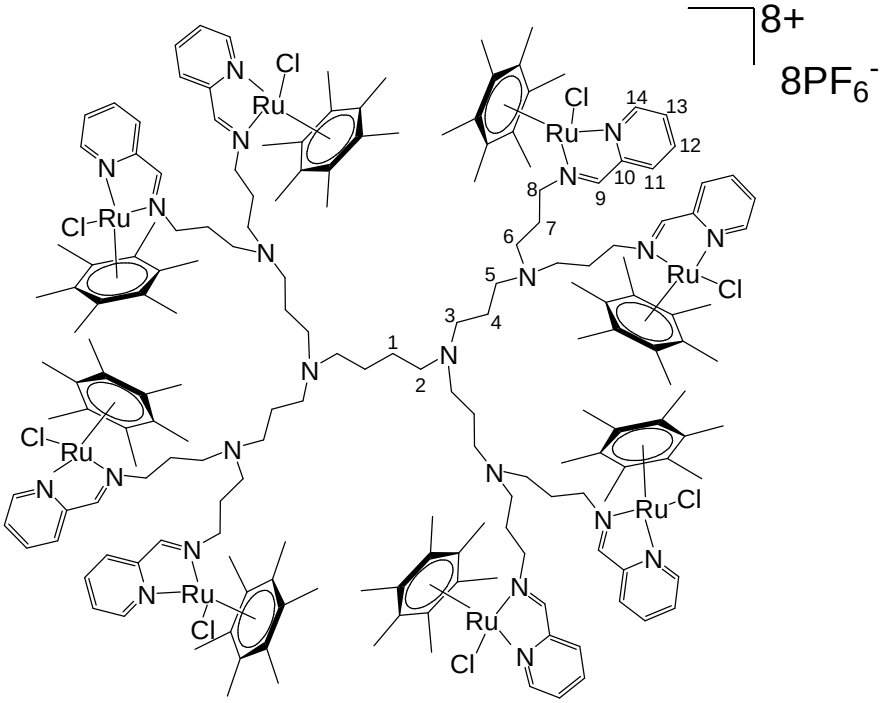

[Ru(η^6-C_6Me_6)Cl_2]$_2$ (0.200 g, 0.296 mmol) was added to a stirring solution of ethanol (25.0 mL). The ligand **L6** (0.109 g, 0.073 mmol) was dissolved in ethanol (5.0 mL) and added dropwise to the stirring solution. The solution was allowed to stir for 12 h at room temperature. The resulting solution was then filtered by gravity and the filtrate transferred into a round bottom flask. The filtrate was reduced to about 5 mL and was transferred to a round bottom flask, where $NaPF_6$ (0.055 g, 0.296 mmol) was added and the reaction was allowed to stir at 0 ^oC for 2 h. This resulted in the formation of a dark red precipitate (**12**), which was filtered using a Hirsch filter funnel and dried under vacuum, to yield a red-brown solid (0.18 g, 48.4 %).

IR: KBr pellets, ν/cm^{-1}: 1621 (s, imine, C=N), 1597 (s, pyridyl, C=N), 843 (s, P-F). **^{1}H NMR** (300 MHz, $(CD_3)_2CO$): δ (ppm) = 1.48 – 3.24 (overlapping m, 64H, $\underline{H}_1$, $\underline{H}_2$, $\underline{H}_3$, $\underline{H}_4$, $\underline{H}_5$, $\underline{H}_6$, $\underline{H}_7$), 2.20 (s, 144H, $C\underline{H}_3$), 4.39 (br m, 16H, $\underline{H}_8$), 7.83 (br m, 8H, $\underline{H}_{12}$), 8.18 (br m, 16H, $\underline{H}_{11}$, $\underline{H}_{13}$), 8.70 (br s, 8H, $\underline{H}_9$), 9.07 (br m, 8H, $\underline{H}_{14}$). **^{13}C{^{1}H} NMR** (75 MHz, $(CD_3)_2CO$): δ (ppm) = 15.4 (**C**$H_{3\ HMB}$); 24.0-24.8, 50.0-51.0, 51.1, 68.2 (**C**H_2); 96.6 (**C** $_{HMB}$); 128.4, 128.5, 139.4, 153.6 (**C**H $_{pyr}$); 155.1 (**C** $_{pyr}$); 167.0 (**C**H $_{imine}$). **Elemental Analysis** (%): Calc. For $C_{184}H_{264}N_{22}Ru_8Cl_8P_8F_{48}$: C, 43.88; H, 5.28; N, 6.12; Found: 43.57; H, 5.38; N, 6.22. **MS** (MALDI-TOF, m/z): 4891 $[M\text{-}PF_6]^+$. **Melting Point**: 210 ^oC – 212 ^oC.

6.7 Synthesis and experimental data of neutral salicylaldimine mononuclear (13, 14) and multinuclear complexes (15 - 18)

6.7.1 Preparation of 13

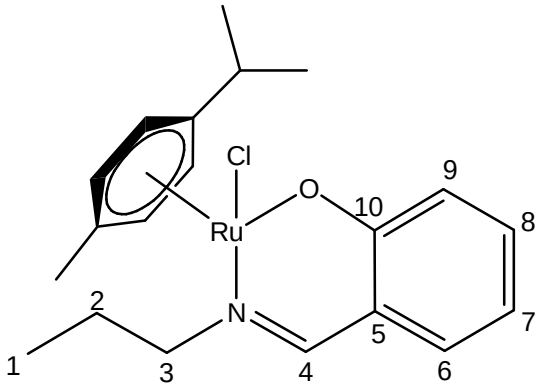

To a stirring solution of **L7** (0.105 g, 0.640 mmol), in dry ethanol, triethylamine (0.094 mL, 0.672 mmol) was added dropwise. The yellow suspension was allowed to stir at room temperature for 30 minutes. **$[Ru(\eta^6\text{-}p\text{-}Pr^iC_6H_4Me)Cl_2]_2$** (0.196 g, 0.320 mmol) was dissolved in dry ethanol (10.0 mL) and added drop wise to the reaction mixture. The reaction mixture was allowed to stir for 6 hours at room temperature. The reaction mixture was filtered by gravity and the solvent from the filtrate removed under reduced pressure, this resulted in an orange solid (**13**). The orange solid was dissolved in a minimum amount of toluene and placed in the freezer for 2 days. This resulted in the precipitation of a red-brown solid (0.12 g, 43.3 %) which was filtered and dried *in* vacuo.

IR: NaCl cells, CH_2Cl_2, ν/cm^{-1}: 1624 (s, imine, C=N). **^{1}H NMR** (300 MHz, $CDCl_3$): δ (ppm) = 1.01 (t, ^3J = 7.4 Hz, 3H, $\underline{H}_1$), 1.12 & 1.22 (d, ^3J = 6.9 Hz, 6H, $CH(C\underline{H}_3)_2$), 1.96 & 2.07 (m, 2H, $\underline{H}_2$), 1.88 (s, 3H, $C\underline{H}_3$), 2.76 (m, 1H, $C\underline{H}(CH_3)_2$), 3.97 & 4.19 (m, 2H, $\underline{H}_3$), 5.03 (d, ^3J = 5.6 Hz, 2H, $Ar_{p\text{-cye}}$), 5.39 (m, 2H, $Ar_{p\text{-cye}}$), 6.40 (t, ^3J = 6.9 Hz, 1H, $\underline{H}_7$), 6.91 (m, 2H, $\underline{H}_6$, $\underline{H}_9$), 7.14 (t, ^3J = 6.9 Hz, 1H, $\underline{H}_8$), 7.67 (s, 1H, $\underline{H}_4$). **^{13}C{^{1}H} NMR** (75 MHz, $CDCl_3$): δ (ppm) = 11.5 (**C**H_3); 18.5, 21.6, 22.7 (**C**$H_{3\ p\text{-}cye}$); 24.3, 71.1 (**C**H_2); 30.5, 80.2, 81.9, 83.1, 85.8 (**C**H $_{p\text{-}cye}$); 97.3, 101.5 (**C** $_{p\text{-}cye}$); 114.0, 122.3, 134.3, 134.5 (**C**H $_{Ar}$); 119.3, 165.0 (**C** $_{Ar}$); 163.5 (**C**H $_{imine}$). **Elemental Analysis** (%): Calc. For $C_{20}H_{26}NRuClO$: C, 55.48; H, 6.05; N, 3.24; Found: C, 55.40; H, 6.28, N, 3.03. **MS** (ESI, m/z): 430 $[C_{20}H_{23}NRuClO]^+$. **Melting Point**: 150 ^{o}C – 152 ^{o}C.

6.7.2 Preparation of 14

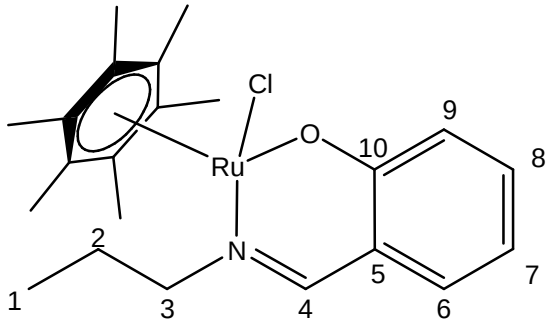

To a stirring solution of **L7** (0.109 g, 0.669 mmol), in dry ethanol, triethylamine (0.098 mL, 0.703 mmol) was added dropwise. The yellow suspension was allowed to stir at room temperature for 30 minutes. **$[Ru(\eta^6\text{-}C_6Me_6)Cl_2]_2$** (0.226 g, 0.335 mmol) was added to the reaction mixture. The reaction mixture was allowed to stir for 6 hours at room temperature. The reaction mixture was filtered by gravity and the solvent from the filtrate removed under reduced pressure, this resulted in a red solid. The red solid was dissolved in a minimum amount of tetrahydrofuran and filtered by gravity. The solvent was removed from the filtrate and the resulting residue dissolved in a minimum amount of toluene and placed in the freezer for 2 days. This resulted in the precipitation of a red-orange solid **14** (0.23 g, 74.4 %) which was filtered and dried *in* vacuo.

IR: NaCl cells, CH_2Cl_2, ν/cm^{-1}: 1624 (s, imine, C=N). **^{1}H NMR** (300 MHz, $CDCl_3$): δ (ppm) = 0.93 (t, ^3J = 7.4 Hz, 3H, $\underline{H}_1$), 1.70 (m, 1H, $\underline{H}_2$), 2.01 (m, 1H, $\underline{H}_2$), 1.96 (s, 18H, C$\underline{H}_3$), 3.96 (m, 1H, $\underline{H}_3$), 3.73 (m, 1H, $\underline{H}_3$), 6.38 (t, ^3J = 7.0 Hz, 1H, $\underline{H}_7$), 6.92 (m, 2H, $\underline{H}_6$, $\underline{H}_9$), 7.09 (t, ^3J = 6.9 Hz, 1H, $\underline{H}_8$), 7.70 (s, 1H, $\underline{H}_4$). **^{13}C{^{1}H} NMR** (100 MHz, $CDCl_3$): δ (ppm) = 11.4 (**C**H_3); 15.6 (**C**$H_{3\ HMB}$); 24.1, 66.4 (**C**H_2); 91.2 (**C** $_{HMB}$); 113.9, 124.0, 133.5, 133.6 (**C**H $_{Ar}$); 121.5, 166.3 (**C** $_{Ar}$); 161.8 (**C**H $_{imine}$). **Elemental Analysis** (%): Calc. For $C_{23}H_{30}NRuClO$: C, 57.32; H, 6.56; N, 3.04; Found: C, 57.19; H, 6.59; N, 2.94. **MS** (ESI, m/z): 426 $[M\text{-}Cl]^+$. **Melting Point:** 205 ^{o}C – 208 ^{o}C.

6.7.3 Preparation of 15

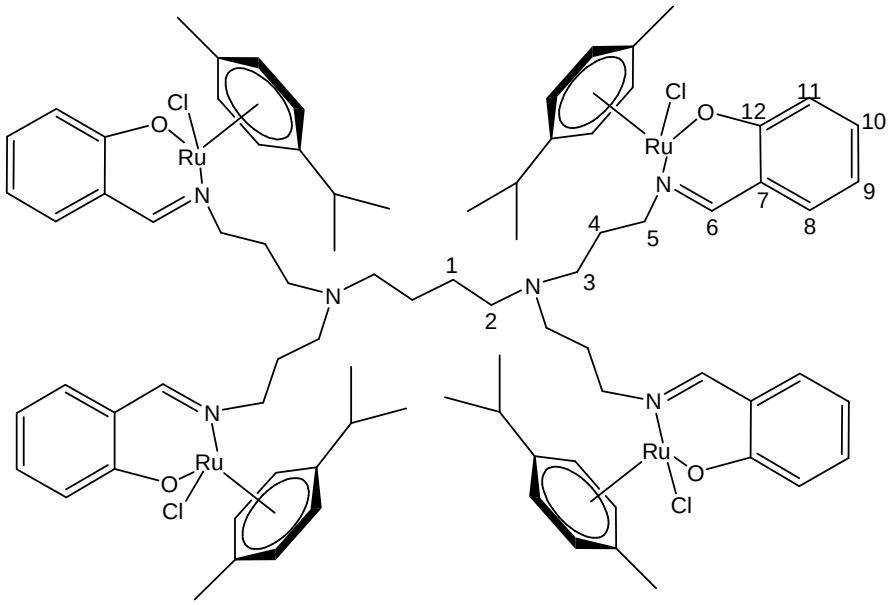

To a stirring solution of **L8** (0.205 g, 0.279 mmol) in dry ethanol, triethylamine (0.156 mL, 1.12 mmol) was added dropwise. The yellow suspension was allowed to stir at room temperature for 30 minutes. **[Ru(η^6-*p*-Pr^{i}C$_6$H$_4$Me)Cl$_2$]$_2$** (0.342 g, 0.558 mmol) was dissolved in dry ethanol (10.0 mL) and added dropwise to the reaction mixture. The reaction mixture was allowed to stir for 15 hours at room temperature. The reaction mixture was filtered by gravity and the solvent from the filtrate removed under reduced pressure, this resulted in an orange solid (**15**). The orange solid was dissolved in a minimum amount of dichloromethane and placed in the freezer for 2 days. This resulted in the precipitation of a orange-brown solid (0.12 g, 88.3 %) which was filtered and dried *in* vacuo.

IR: NaCl cells, CH_2Cl_2, ν/cm^{-1}: 1621 (s, imine, C=N). **^{1}H NMR** (400 MHz, $CDCl_3$): δ (ppm) = 1.06 & 1.16 (br m, 24H, CH(C$\underline{H}_3$)$_2$), 1.94 – 2.12 (overlapping m, 12H, $\underline{H}_1$, $\underline{H}_4$), 2.22 (s, 12H, C$\underline{H}_3$), 2.40 (m, 4H, $\underline{H}_2$), 2.64 (br m, 8H, $\underline{H}_3$), 3.19 (br m, 4H, C$\underline{H}$(CH$_3$)$_2$), 4.06 & 4.45 (br m, 4H, $\underline{H}_5$), 5.23 (br d, 8H, Ar$_{p\text{-cye}}$), 5.41 (br d, 8H, Ar$_{p\text{-cye}}$), 6.38 (br t, 4H, $\underline{H}_9$), 6.87 (br m, 4H, $\underline{H}_8$), 7.12 (br m, 8H, $\underline{H}_{10}$, $\underline{H}_{11}$), 7.96 (br m, 4H, $\underline{H}_6$). **^{13}C{^{1}H} NMR** (100 MHz, $CDCl_3$): δ (ppm) = 18.9, 21.7, 22.8 (**C**H$_{3\ p\text{-cye}}$); 21.1, 25.4, 51.4, 52.5, 67.2 (**C**H$_2$); 30.6, 46.0, 81.0, 81.5, 83.1, 87.8 (**C**H $_{p\text{-cye}}$); 99.1, 100.2 (**C** $_{p\text{-cye}}$); 114.1, 121.9, 134.8, 135.5 (**C**H $_{Ar}$); 118.9, 165.0 (**C** $_{Ar}$), 164.8 (**C**H $_{imine}$). **Elemental Analysis** (%): Calc. For $C_{84}H_{108}N_6Ru_4Cl_4O_4.4^1/_2CH_2Cl_2$: C, 48.45; H, 5.37; N, 3.83; Found: C, 48.15; H, 6.48; N, 3.99. **MS** (FAB, m/z): 1777 [M-Cl]$^+$. **Melting Point:** 161 ^{o}C – 164 ^{o}C.

6.7.4 Preparation of 16

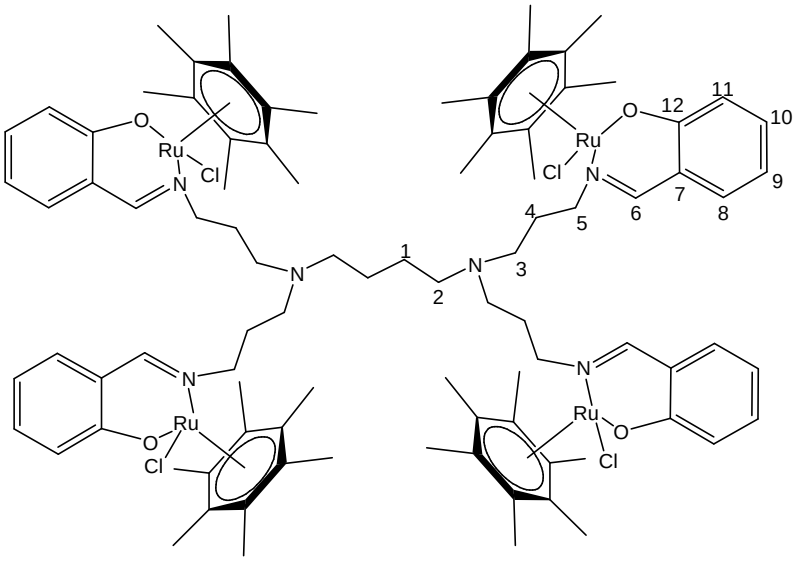

To a stirring solution of **L8** (0.203 g, 0.278 mmol), in dry ethanol, triethylamine (0.155 mL, 1.11 mmol) was added dropwise. The yellow suspension was allowed to stir at room temperature for 30 minutes. **[Ru(η^6-C_6Me_6)Cl_2]$_2$** (0.376 g, 0.555 mmol) was added to the reaction mixture. The reaction mixture was allowed to stir for 15 hours at room temperature. The reaction mixture was filtered by gravity and the solvent from the filtrate removed under reduced pressure, this resulted in a dark orange solid. The dark orange solid was dissolved in a minimum amount of tetrahydrofuran and filtered by gravity. The solvent was removed from the filtrate and the resulting residue dissolved in a minimum amount of dichloromethane. Diethyl ether was added to the dichloromethane solution, resulting in the precipitation of a solid. The precipitate was isolated by filtration and dried under reduced vacuum, to yield a dark orange solid **16** (0.46 g, 86.5 %).

IR: NaCl cells, CH_2Cl_2, ν/cm^{-1}: 1618 (s, imine, C=N). **^{1}H NMR** (400 MHz, $CDCl_3$): δ (ppm) = 1.28 (br m, 4H, $\underline{H}_1$), 1.71 (overlapping br s, 80H, $\underline{H}_4$, CH_3), 2.23 (br m, 4H, $\underline{H}_2$), 2.93 (br m, 8H, $\underline{H}_3$), 4.03 (br m, 8H, $\underline{H}_5$), 6.44 (br m, 4H, $\underline{H}_9$), 6.89 (br m, 4H, $\underline{H}_8$), 7.11 (br s, 8H, $\underline{H}_{10,}$ $\underline{H}_{11}$), 8.06 (br m, 4H, $\underline{H}_6$). **^{13}C{^{1}H} NMR** (100 MHz, $CDCl_3$): δ (ppm) = 15.7 (**C**H$_{3\ HMB}$); 21.7, 25.5, 50.2, 52.4, 62.7 (**C**H$_2$); 91.4 (**C** $_{HMB}$); 114.4, 123.7, 134.0, 134.7 (**C**H $_{Ar}$); 121.5, 166.1 (**C** $_{Ar}$); 164.8 (**C**H $_{imine}$). **Elemental Analysis** (%): Calc. For $C_{92}H_{124}N_6Ru_4O_4Cl_4.3^1/_2CH_2Cl_2$: C, 51.64; H, 5.94; N, 3.78; Found: C, 51.41; H, 6.36; N, 4.07. **MS** (FAB, m/z): 1888 [M-Cl]$^+$. **Melting Point:** 186 ^{o}C – 188 ^{o}C.

6.7.5 Preparation of 17

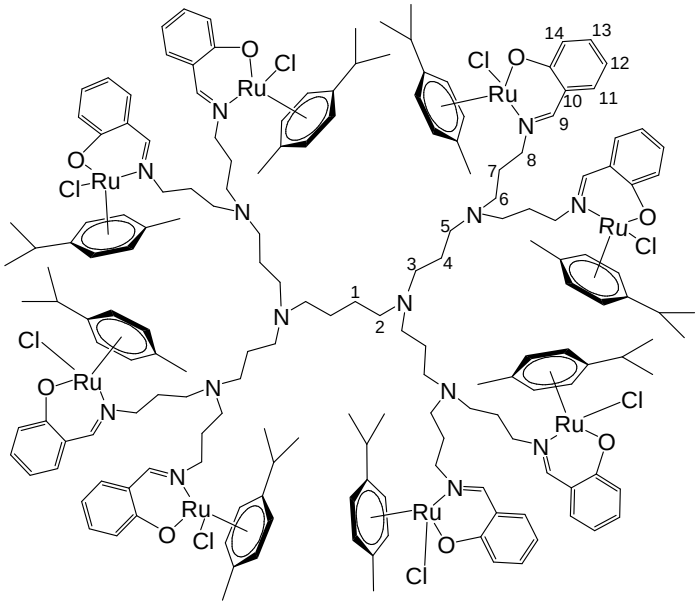

To a stirring solution of **L9** (0.136 g, 0.085 mmol) in dry tetrahydrofuran, triethylamine (0.100 mL, 0.715 mmol) was added dropwise. The yellow suspension was allowed to stir at room temperature for 30 minutes. **$[Ru(\eta^6\text{-}p\text{-}Pr^iC_6H_4Me)Cl_2]_2$** (0.208 g, 0.340 mmol) was dissolved in dry tetrahydrofuran (10.0 mL) and added dropwise to the reaction mixture. The reaction mixture was allowed to stir overnight at room temperature. The solvent was removed from the reaction mixture, resulting in a orange-red residue. The residue was dissolved in a minimal volume of dichloromethane. Diethyl ether was added to the dichloromethane solution, resulting in the precipitation of a red-orange solid (**17**). The solid (0.19 g, 60.3 %) was isolated by filtration and dried under reduced vacuum.

IR: NaCl cells, CH_2Cl_2, ν/cm^{-1}: 1621 (s, imine, C=N). **^{1}H NMR** (400 MHz, $CDCl_3$): δ (ppm) = 1.04 & 1.15 (br m, 48H, $CH(C\underline{H}_3)_2$), 1.84 – 2.76 (overlapping m, 64H, $\underline{H}_1$, $\underline{H}_2$, $\underline{H}_3$, $\underline{H}_4$, $\underline{H}_5$, $\underline{H}_6$, $\underline{H}_7$), 2.24 (s, 24H, $C\underline{H}_3$), 3.26 (br m, 8H, $C\underline{H}(CH_3)_2$), 4.20 & 4.48 (br m, 16H, $\underline{H}_8$), 5.26 (br d, 16H, $Ar_{p\text{-cye}}$), 5.45 (br d, 16H, $Ar_{p\text{-cye}}$), 6.39 (br m, 8H, $\underline{H}_{12}$), 6.81 (br m, 8H, $\underline{H}_{11}$), 7.11 (br m, 8H, $\underline{H}_{14}$), 7.18 (br m, 8H, $\underline{H}_{13}$), 8.10 (br m, 8H, $\underline{H}_9$). **^{13}C{^{1}H} NMR** (100 MHz, $CDCl_3$): δ (ppm) = 19.0, 21.7, 22.9 (**C**$H_{3\ p\text{-}cye}$); 22.3, 25.2, 30.8, 49.9, 51.1, 51.5, 53.2, 67.4 (**C**H_2); 30.5, 46.0, 80.6, 81.1, 83.4, 87.9 (**C**$H_{p\text{-}cye}$); 98.9, 99.8 (**C** $_{p\text{-}cye}$); 114.2, 121.8, 134.8, 135.7 (**C**H_{Ar}); 119.1, 165.1 (**C** $_{Ar}$); 164.5 (**C**H_{imine}). **Elemental Analysis** (%): Calc. For $C_{176}H_{232}N_{14}Ru_8Cl_8O_8.{}^1/_2CH_2Cl_2$: C, 55.69; H, 6.17; N, 5.15; Found: C, 55.59; H, 6.34; N, 4.89. **MS** (MALDI-TOF, m/z): 3765 $[M\text{-}Cl]^+$. **Melting Point:** 172 ^oC (decompose without melting).

6.7.6 Preparation of 18

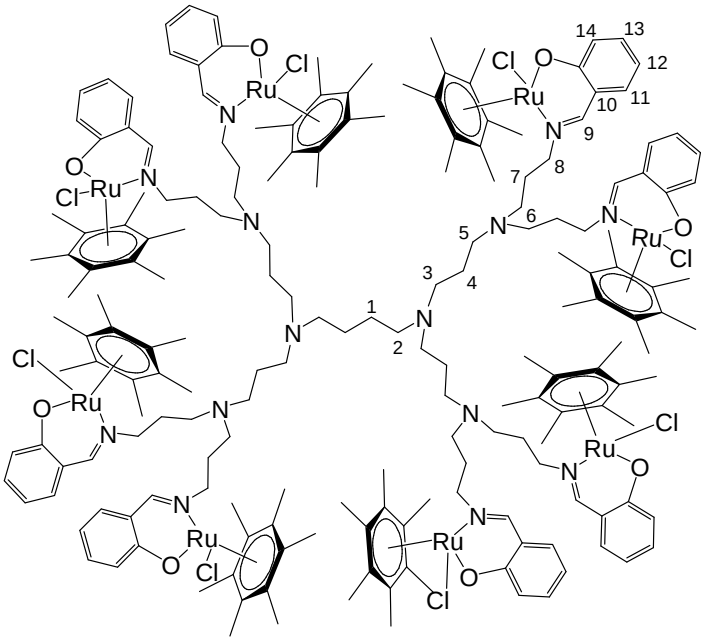

To a stirring solution of **L9** (0.121 g, 0.075 mmol) in dry tetrahydrofuran, triethylamine (0.084 mL, 0.603 mmol) was added dropwise. The yellow suspension was allowed to stir at room temperature for 30 minutes. **$[Ru(\eta^6\text{-}C_6Me_6)Cl_2]_2$** (0.204 g, 0.302 mmol) was dissolved in dry tetrahydrofuran (10.0 mL) and added drop wise to the reaction mixture. The reaction mixture was allowed to stir overnight at room temperature. The solvent was removed from the reaction mixture, resulting in an orange-red residue. The residue was dissolved in a minimal volume of dichloromethane. Diethyl ether was added to the solution, resulting in the precipitation of a solid (**18**). The precipitate was isolated by filtration and dried under reduced vacuum, to yield a mustard yellow solid (0.20 g, 65. 5 %).

IR: NaCl cells, CH_2Cl_2, ν/cm^{-1}: 1618 (s, imine, C=N). **^{1}H NMR** (400 MHz, $CDCl_3$): δ (ppm) = 1.60 – 3.00 (overlapping m, 64H, $\underline{H}_1$, $\underline{H}_2$, $\underline{H}_3$, $\underline{H}_4$, $\underline{H}_5$, $\underline{H}_6$, $\underline{H}_{7)}$, 1.94 (s, 144H, CH_3), 4.00 (br m, 8H, $\underline{H}_8$), 4.10 (br m, 8H, $\underline{H}_8$), 6.43 (br m, 8H, $\underline{H}_{12}$), 6.89 (br m, 8H, $\underline{H}_{11}$), 7.12 (overlapping m, 16H, $\underline{H}_{13}$, $\underline{H}_{14}$), 8.12 (br m, 8H, $\underline{H}_9$). **^{13}C{^{1}H} NMR** (100 MHz, $CDCl_3$): δ (ppm) = 15.8 (**C**$H_{3\ HMB}$); 21.2, 22.5, 25.6, 38.0, 50.6, 53.2, 56.3, 62.5 (**C**H_2); 91.3 (**C** $_{HMB}$); 114.2, 121.7, 134.0, 134.7 (**C**H $_{Ar}$); 121.7, 166.2 (**C** $_{Ar}$); 164.7 (**C**H $_{imine}$). **Elemental Analysis** (%): Calc. For $C_{192}H_{264}N_{14}Ru_8Cl_8O_8{}^1/_2.CH_2Cl_2$: C, 57.36; H, 6.63; N, 4.86; Found: C, 57.19; H, 7.03; N, 4.16. **MS** (ESI, m/z): 3955 $[M\text{-}Cl]^+$. **Melting Point**: 177 ^oC (decompose without melting).

6.8 X-ray crystallography

The crystal structures were solved by direct methods using the program SHELXS-97.[10] Refinement and all further calculations were carried out using SHELXL-97.[10] In all cases, the H-atoms were included in calculated positions and treated as riding atoms using the SHELXL default parameters. In all cases, the non-H atoms were refined anisotropically, using weighted full-matrix least-square on F^2. Crystallographic details of complexes were drawn with ORTEP[11] and/or MERCURY.[12]

6.9 Cell culture and inhibition of cell growth

The human A2780 and A2780cisR human ovarian cancer cell lines were obtained from the European Collection of Cell Cultures (Salisbury, UK). Cells were grown routinely in RPMI-1640 medium with 10 % foetal calf serum (FCS) and antibiotics at 37 ℃ and 5 % CO_2. Cytotoxicity was determined using the MTT assay (MTT = 3(4,5-dimethyl-2-thiazolyl)-2,5-diphenyl-2H-tetrazolium bromide). Cells were seeded in 96-well plates as monolayers with 100 μL of cell solution (approximately 20,000 cells) per well and pre-incubated for 24 hours in medium supplemented with 10 % FCS. Compounds were prepared as DMSO solution then dissolved in the culture medium and serially diluted to the appropriate concentration, to give a final DMSO concentration of 1 %. 100 μL of drug solution was added to each well and the plates were incubated for another 72 hours. Subsequently, MTT (5 mg/mL solution) was added to the cells and the plates were incubated for a further 2 hours. The culture medium was aspirated, and the purple formazan crystals formed by the mitochondrial dehydrogenase activity of vital cells were dissolved in DMSO. The optical density, directly proportional to the number of surviving cells, was quantified at 540 nm using a multiwell plate reader and the fraction of surviving cells was calculated from the absorbance of untreated control cells. Evaluation is based on means from three independent experiments, each comprising three microcultures per concentration level.

6.10 DNA binding study

Samples were prepared by mixing a solution of 75 ng/μL pBR322 plasmid DNA with the appropriate complex at the appropriate concentration to give the required r value (0.5, 0.25 and 0.125, r being the ratio of the metal center to DNA base pairs). The samples were incubated for 24 hours at 37 ℃. The m obility of the plasmid DNA was analyzed by gel electrophoresis on 0.8% agarose gels, at a constant voltage of 100 V for 1 hour in Tris-acetate-EDTA buffer. The gel was stained for 30 min in 0.5 μg/mL (w/v) ethidium bromide and the bands were then analyzed with an UVP gel scanner.

6.11 References

1) M. A. Bennett and A. K. Smith, *J. Chem. Soc. Dalton Trans.*, 1974, **2**, 233.
2) M. A. Bennett, T. W. Matheson, G. B. Robertson, A. K. Smith and P. A. Tucker, *Inorg. Chem.*, 1980, **19**, 1014.
3) P. Di Bernardo, P. L. Zanonato, S. Tamburini and P. A. Vigato, *Inorg. Chim. Acta*, 2007, **360**, 1083.
4) J. Cloete and S. F. Mapolie, *J. Mol. Catal. A: Chem.*, 2006, **243**, 221.
5) P. Govender, N. C. Antonels, J. Mattsson, A. K. Renfrew, P. J. Dyson, J. R. Moss, B. Therrien and G. S. Smith, *J. Organomet. Chem.*, 2009, **694**, 3470.
6) G. Smith, R. Chen and S. Mapolie, *J. Organomet. Chem.*, 2003, **673**, 111.
7) G. S. Smith and S. F. Mapolie, *J. Mol. Catal. A: Chem.*, 2004, **213**, 187.
8) M. A. Torzilli, S. Colquhoun, D. Doucet and R. H. Beer, *Polyhedron,* 2002, **21**, 697.
9) R. Malgas, S. F. Mapolie, S. O. Ojwach, G. S. Smith and J. Darkwa, *Cat. Comm.*, 2008, **9**, 1612.
10) G. M. Sheldrick, *Acta Cryst.*, 2008, **A64**, 112.
11) L. J. Farrugia, *J. Appl. Cryst.*, 1997, **30**, 565.
12) I. J. Bruno, J. C. Cole, P. R. Edgington, M. Kessler, C. F. Macrae, P. McCabe, J. Pearson and R. Taylor, *Acta Cryst*., 2002, **B58**, 389.